ISBN 978-82-326-7694-1 (printed ver.)
ISBN 978-82-326-7693-4 (electronic ver.)
ISSN 1503-8181 (printed ver.)
ISSN 2703-8084 (electronic ver.)

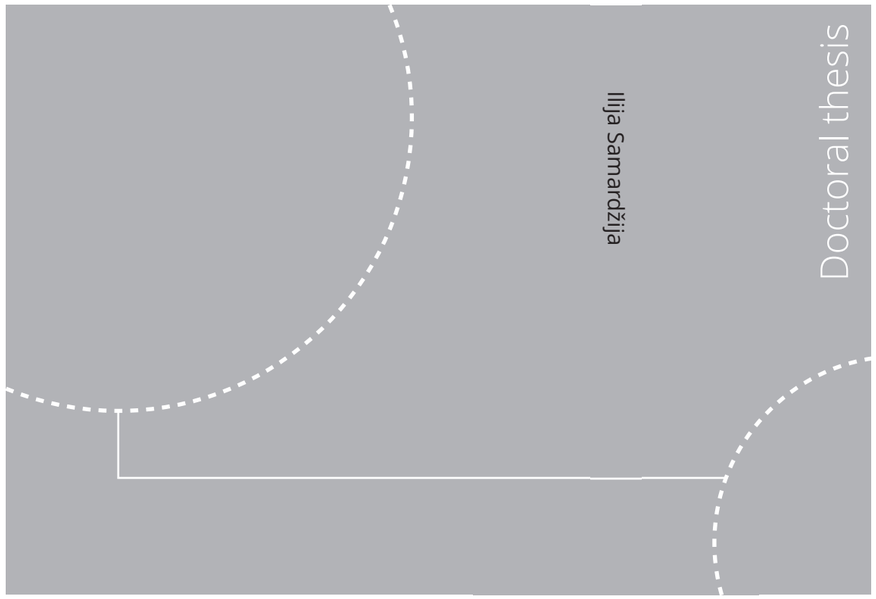

Doctoral theses at NTNU, 2024:45

Ilija Samardžija

Probabilistic assessment of first-year ice ridge loads on offshore structures

Doctoral theses at NTNU, 2024:45

NTNU
Norwegian University of Science and Technology

NTNU
Norwegian University of Science and Technology
Thesis for the degree of Philosophiae Doctor
Faculty of Engineering
Department of Civil and Environmental Engineering

NTNU

NTNU
Norwegian University of Science and Technology

Ilija Samardžija

Probabilistic assessment of first-year ice ridge loads on offshore structures

Thesis for the degree of Philosophiae Doctor

Trondheim, January 2024

Norwegian University of Science and Technology
Faculty of Engineering
Department of Civil and Environmental Engineering

NTNU
Norwegian University of
Science and Technology

NTNU
Norwegian University of Science and Technology

Thesis for the degree of Philosophiae Doctor

Faculty of Engineering
Department of Civil and Environmental Engineering

ISBN 978-82-326-7694-1 (printed ver.)
ISBN 978-82-326-7693-4 (electronic ver.)
ISSN 1503-8181 (printed ver.)
ISSN 2703-8084 (electronic ver.)

Doctoral theses at NTNU, 2024:45

PRINTED IN NORWAY
NO - 1598

NORDIC SWAN ECOLABEL
Printed matter
2041 0731

Printed by Skipnes Kommunikasjon AS

Abstract

Advancements in technological capabilities, growing energy demands, and climate change are making offshore regions with floating sea ice increasingly attractive for infrastructure development. Notable examples include the potential for hydrocarbon retrieval in the Barents Sea and offshore wind initiatives in the Bothnian Sea. In ice-covered seas, first-year ice ridges frequently impose the most significant loads on offshore infrastructure. Structures must be designed to withstand these loads with satisfactory reliability, while avoiding excessive conservatism to maintain the economic feasibility of the infrastructure projects.

Deterministic approaches for assessing ice ridge loads often result in overestimation of the design loads due to the necessity of assuming extreme values for several crucial input parameters, especially when data is sparse. In contrast, probabilistic methods present an opportunity for a less conservative assessment of ridge loads. The primary aim of this thesis is to lay the foundational framework, from both a scientific and engineering perspective, for methodologies that determine the structural reliability of offshore infrastructure in cold regions utilizing existing data. The focus is specifically on creating a probabilistic framework for modelling the loads of first-year ice ridges on fixed offshore structures.

This thesis explores the development of a method for the probabilistic simulation of input variables for ridge load calculations, ensuring the preservation of their significant correlations. The simulated variables should be unbiased and accurately represent the entire population of ice ridges over a season. Additionally, the research addresses the challenges of implementing this in regions with limited available data.

The study first focuses on long-term measurements of ice draft from the Beaufort Sea. From this data, individual ridge keel drafts, level ice thickness, and ridge frequency are extracted, and statistical analysis is used to establish relationships between these parameters. As anticipated from other studies, a positive relationship was found between level ice thickness and both ridge keel draft and ridge frequency. This study quantified these relationships in a way that is optimized for the probabilistic simulation of all ridges throughout a season while maintaining these relationships.

The study further combines ridge frequency data and theoretical analysis to simulate ridge creation and consolidated layer growth and to analyse the relationship between consolidated layer thickness and ridge keel draft. A negative relationship was observed between consolidated layer thickness and ridge keel draft, indicating that deeper ridges tend to have thinner consolidated layers.

The proposed probabilistic simulation model offers the advantage of requiring only annual maximum level ice thickness and information on the duration of the season and sea ice presence as input parameters, eliminating the need for data on ridge keel draft or consolidated layer thickness. As additional data is collected, the model can be further refined. This adaptability to diverse data availabilities enhances its applicability across various design stages, with the model's reliability increasing with more available data.

However, the model’s reliance on correlations from Beaufort Sea studies may limit its applicability to other seas, such as the Baltic Sea. Thus, for more accurate results, collecting long-term ice draft measurements and organizing field campaigns for consolidated layer thickness data are advisable. Future studies should explore recalibrating the established correlations between input variables for different regions.

Acknowledgement

I would like to express my deepest appreciation and sincere gratitude to my supervisor, Knut Vilhelm Høyland. Your guidance through the intricate paths of this research, along with your patience and insightful perspectives, have been invaluable. Your steadfast belief in my capabilities propelled me towards this achievement, particularly during a critical moment a year ago when I was on the verge of giving up. Your motivational boost was instrumental in steering this thesis to completion.

Sincere thanks to my co-supervisors, Bernt Johan Leira, and Arvid Næss, for their invaluable guidance, engaging discussions, and consistent support throughout this journey.

I am indebted to the Norwegian University of Science and Technology for furnishing the essential resources, facilities, and research-conducive environment. The dedication and assistance of the support staff and administration have been pivotal, and I extend my gratitude to them.

A warm thank you to Dennis Monteban for the refreshing discussions, steadfast friendship, and willingness to always lend a helping hand. Your companionship has been a source of joy and fulfilment in this journey. Our joint "productive" procrastination marathons, debating the finer points of plot aesthetics and chasing that elusive perfect color scheme, will forever be carved in my 'fond' memories.

I express my gratitude to Equinor for organizing the Station Keeping Trials in the Baltic Sea and allowing me the privilege to participate in a unique scientific measurement and trial experience aboard an icebreaker. Witnessing and understanding sea ice from such a vantage point has enriched my perspective on Arctic engineering.

I also wish to acknowledge Sveinung Løset and Raed Lubbad for affording me the opportunity to momentarily step away from PhD research and immerse myself in a real-case industrial project. This experience was enlightening and greatly appreciated.

I reserve my most heartfelt thanks for my in-house fan club: my wife Vera and superstar daughters, Teodora, and Anna. Juggling the mad scientist life with dad duties had its moments, but your unwavering support (and occasional reality checks) made the tightrope walk feel like a dance. Thank you for being my anchor, even when I almost floated away with my head in the clouds.

Lastly, I owe an immeasurable debt of gratitude to my brave mother. Single-handedly navigating the turbulent landscape of war-torn Yugoslavia, she built our lives from the ashes, all the while steering me towards a brighter future. Her resilience, persistence, and unwavering faith are the bedrock upon which this thesis stands. This achievement is as much hers as it is mine – this thesis is a testament to her victory![1]

[1] Translation in Serbian: Na kraju, dugujem neizmernu zahvalnost mojoj hrabroj majci. Samostalno se probijajući kroz burno okruženje ratom razorene Jugoslavije, izgradila je naš život iz pepela, sve vreme usmeravajući me ka svetlijoj budućnosti. Njena otpornost, upornost i nepokolebljiva vera su temelj na kojem ova teza stoji. Ovo postignuće je jednako njeno koliko i moje - ova teza je dokaz njene pobede!

Publication list and declaration of authorship

List of appended papers

The papers listed below form an integral part of this thesis and are appended. The summary provided in Sections 1-7 draws from the research presented in these papers.

Paper 1: Samardžija, I., Høyland, K. V., Leira, B. J., & Næss, A. (2018). Probabilistic Assessment of Ice Environment and Ridge Loads for the Norströmsgrund Lighthouse. *24th IAHR Symposium on Ice*, Vladivostok, Russia.

The first and second authors were responsible for the conceptualization and development of the study's methodology. Additionally, the first author handled coding of the calculations, formal analysis, investigation, validation, visualization and writing of the manuscript. The co-authors, who also served as the PhD mentors, were engaged in revising the manuscript and providing mentorship throughout the project.

Paper 2: Samardžija, I., & Høyland, K. V. (2019). Initial results of a study into the relationship between level ice draft and ridge keel draft. *25th International Conference on Port and Ocean Engineering under Arctic Conditions*, Delft, The Netherlands.

The first and second authors were responsible for the conceptualization and development of the study's methodology. Additionally, the first author handled coding of the calculations, formal analysis, investigation, validation, visualization and writing of the manuscript. The co-author, who also served as the PhD mentor, was engaged in revising the manuscript and providing mentorship throughout the project.

Paper 3: Samardžija, I., & Høyland, K. V. (2023). Analysis of the relationship between level ice draft, ridge frequency and ridge keel draft for use in the probabilistic assessment of ice ridge loads on offshore structures. *Ocean Engineering*, *270*, 113593. https://doi.org/10.1016/j.oceaneng.2022.113593

The first and second authors were responsible for the conceptualization and development of the study's methodology. Additionally, the first author handled coding of the calculations, formal analysis, investigation, validation, visualization and writing of the manuscript. The co-author, who also served as the PhD mentor, was engaged in revising the manuscript and providing mentorship throughout the project.

Paper 4: Samardžija, I., Høyland, K. V., Leira, B. J., & Næss, A. (2023a). Consolidated layer thickness in probabilistic simulation of first-year ice ridges. *Cold Regions Science and Technology, 216,* 104021. https://doi.org/10.1016/j.coldregions.2023.104021

The first and second authors were responsible for the conceptualization and development of the study's methodology. Additionally, the first author handled coding of the calculations, formal analysis, investigation, validation, visualization and writing of the manuscript. The co-authors, who also served as the PhD mentors, were engaged in revising the manuscript and providing mentorship throughout the project.

Paper 5: Samardžija, I., Høyland, K. V., Leira, B. J., & Næss, A. (2023b). Probabilistic assessment of first-year ice ridge action on offshore structures. *Cold Regions Science and Technology*. [Paper under peer review]

The first and second authors were responsible for the conceptualization and development of the study's methodology. Additionally, the first author handled coding of the calculations, formal analysis, investigation, validation, visualization and writing the manuscript. The co-authors, who also served as the PhD mentors, were engaged in revising the manuscript and providing mentorship throughout the project.

List of additional papers

The papers listed below are not included in this thesis because they are not related to its research topic. However, they were completed during the course of the PhD project.

Paper 1: Samardžija, I. (2018). Two applications of a cross-correlation based ice drift tracking algorithm; Ship-based marine radar images and camera images from a fixed structure. *24th IAHR Symposium on Ice*, Vladivostok, Russia.

Paper 2: Nord, T. S., Samardžija, I., Hendrikse, H., Bjerkås, M., Høyland, K. V., & Li, H. (2018). Ice-induced vibrations of the Norströmsgrund lighthouse. *Cold Regions Science and Technology*, *155*, 237-251. https://doi.org/10.1016/j.coldregions.2018.08.005

Paper 3: Teigen, S. H., Lindvall, J. K., Samardžija, I., & Hansen, R. I. (2018). Station-Keeping Trials in Ice: Ice and Metocean Conditions. *37th International Conference on Ocean, Offshore and Arctic Engineering, OMAE*, Madrid, Spain. https://doi.org/10.1115/OMAE2018-78620

Paper 4: Ervik, Å., Nord, T. S., Høyland, K. V., Samardzija, I., & Li, H. (2019). Ice-ridge interactions with the Norströmsgrund lighthouse: Global forces and interaction modes. *Cold Regions Science and Technology*, *158*, 195-220. https://doi.org/10.1016/j.coldregions.2018.08.020

Paper 5: Monteban, D., Lubbad, R., Samardzija, I., & Løset, S. (2020). Enhanced iceberg drift modelling in the Barents Sea with estimates of the release rates and size characteristics at the major glacial sources using Sentinel-1 and Sentinel-2. *Cold Regions Science and Technology*, *175*, 103084. https://doi.org/10.1016/j.coldregions.2020.103084

Contents

List of figures

1. Introduction

1.1. Background and motivation

Melting sea ice and technological advancements are making the offshore regions of the Arctic more attractive for infrastructural development. As global energy demand continues to grow, the petroleum industry has been paying increased attention to hydrocarbon reserves in Arctic and sub-Arctic regions. The US Geological Survey (USGS) estimates that the Arctic contains 16% of the world's undiscovered conventional oil and 25% of the world's undiscovered natural gas (Bird et al., 2008). Russia is estimated to hold 58% of Arctic resources, followed by the United States with 18%, Greenland with 12%, and Norway with 12%. The development of offshore petroleum is crucial to the economic development of the Arctic areas in all these countries. Although there have been reports of a 'race for resources' since potential hydrocarbon reserves were discovered in Arctic waters, the region remains relatively undeveloped at present (Shapovalova & Stephen, 2019). However, while the development of petroleum seems to have slowed in many Arctic countries, Norway and Russia are showing signs of accelerated progress in the development of Arctic offshore petroleum potential. Currently there are three offshore fields producing hydrocarbons in the Arctic offshore: two in Norway and one in Russia.

Despite being economically attractive, petroleum exploration in Arctic waters poses significant environmental risks. The unique features of Arctic ecosystems as well as the remoteness, climate conditions, and lack of infrastructure exacerbate these risks greatly. While global temperatures are rising, Arctic offshore production is still less cost-effective than production in most of other petroleum regions. Extraction of petroleum resources in the Arctic offshore may require technological breakthroughs in several areas to be economically viable. Further prerequisites for the development of Arctic petroleum are favourable market conditions and political support. The development of petroleum in this sensitive region could also be hindered by environmental risks and opposition from the public.

While the future of Arctic offshore petroleum is uncertain at present, the development of offshore wind energy is fuelling the need for technological breakthroughs needed for the installation of wind farms in cold offshore regions. The majority of the operating wind farms in sea ice prone regions are in the Baltic Sea. Two of these wind farms are in Finland: Pori and Kemi. During the winter, wind turbines at these locations need to withstand the actions imposed by the moving sea ice and if needed be halted to avoid instabilities and structural damage.

Over 22 GW of offshore wind power is currently installed in Europe, including 77% of it in the North Sea. ENTSOE (2020) estimates that the capacity will reach 70 GW by 2030 and 112 GW by 2040. Because of the greater wind resources far from shore and the exhaustion of near-shore sites, future wind farms will be placed farther offshore and in deeper waters. In the Baltic Sea, offshore wind energy sources could generate 93 GW by 2050, up from 2.2 GW today. Baltic Sea offshore wind is likely to grow significantly over the coming decades (WindEurope, 2021). The Baltic Sea exhibits a diverse range of sea ice environments, spanning from southern areas with intermittent thin ice to northern regions where severe ice conditions occur annually. A better understanding of the ice-structure interaction phenomenon and a better set of engineering tools are needed for future projects to be feasible, sustainable, and economically viable.

Sea ice in the offshore Arctic region is proving to be one of the most challenging issues for both wind and petroleum energy projects, as well as for ship traffic in ice-covered waters. A significant cost reduction opportunity arises from enhancing knowledge regarding risks caused

by sea ice. Despite a number of significant improvements in the last couple of decades, there is still a great deal of unresolved questions surrounding the ice-structure interaction phenomenon (Jordaan, 2015; Kellner et al., 2017; von Bock und Polach et al., 2019). Furthermore, the reliability of currently available empirical formulas used for estimating ice loads is somewhat restricted due to their foundation on a limited set of full-scale measurements.

Reliable ice load assessments are often hindered by insufficient data. The remoteness of Arctic offshore projects often results in scarce or incompatible data. Therefore, conducting a thorough data collection campaign is a critical part of any project. Despite these limitations, early-stage assessments can be achieved by extrapolating or interpolating the existing data, using information from regions with similar characteristics.

In the prediction of ice loads on offshore structures, a high level of uncertainty exists, which often leads to the use of conservative assumptions. As a result, the design solutions for offshore structures can become inefficient and expensive. The main source of conservatism arises from deterministic calculations of ridge loads, which involve making overly conservative assumptions about input variables and applying unlikely combinations of extreme values. Probabilistic methods, however, present an opportunity to avoid such pitfalls and provide fewer conservative estimates of extreme ice loads. This, in turn, can lead to the development of more cost-efficient offshore structures.

1.2. Objectives and scope

This thesis aims to address the challenge of ensuring adequate safety levels for offshore structures in Arctic environments. The principal objective is to establish a solid scientific and engineering foundation for estimating structural reliability, utilizing existing long-term data. The specific goal of the research is to formulate a probabilistic modelling framework to calculate the loads exerted on fixed offshore structures by first-year ice ridges. A pivotal challenge here is the quantification of aleatory uncertainty in estimating ridge loads through the analysis of the statistical characteristics of relevant variables (such as statistical distributions and correlations). Moreover, this research seeks to mitigate epistemic uncertainties by introducing new insights drawn from data analysis. Ultimately, the goal is to facilitate more precise ridge load estimations, potentially leading to cost efficiencies in constructing offshore structures in the Arctic.

The thesis primarily focuses on the input parameters employed for calculating ridge loads, such as ridge keel draft, consolidated layer thickness, and ridge occurrence rate. However, it does not contribute to a deeper understanding of ice-structure interaction processes. Even though the input parameters and resulting ridge load distributions of the Monte Carlo experiments are analysed, they are not extensively compared with reported full-scale ridge loads. Hence, this study does not enhance the existing formulation for calculating ridge loads.

The central focus is on fixed offshore installations. Yet, the findings of this study can be adapted to calculate ridge loads on floating installations and could be beneficial for ship design calculations and offshore operations. For instance, the analysis of ridge occurrence rate and seasonality of ridge loads could prove vital for offshore operations such as well exploration. Additionally, the frequency of ridge occurrence is significant for optimizing routes for vessels navigating Arctic waters.

This research is exclusively focused on first-year ridges. Old ridges undergo complex thermo-mechanical processes that drastically alter the ridge's geometry and mechanical properties (Shestov et al., 2018), which are not accounted for in this thesis.

A considerable part of this research is dedicated to enhancing the understanding of the correlations between critical variables in ridge load calculations. The objective of quantifying these correlations is to incorporate them into probabilistic ridge load calculations and to prevent overestimation by using realistic combinations of input parameters. While understanding the causal nature of the correlations could assist in better synchronization of input parameters, this is not the immediate focus of this research. Rather, the goal is to identify the most crucial correlations that can be calibrated for specific projects with minimal data collection, thus offering a pragmatic approach for estimating ridge loads.

The primary objective is to construct a probabilistic model using the Monte Carlo simulation technique to estimate probability distributions for ridge loads. This thesis introduces a framework for such a simulation model, which involves a statistical analysis of the ridge keel draft data obtained from ice profiling sonars (IPS) to prepare input parameters for the model, including ridge keel draft, level ice thickness, and ridge occurrence frequency. Moreover, a probabilistic simulation technique for generating consolidated layer thickness for a ridge population is proposed. This technique is rooted in an analytical analysis of ridge population development throughout the winter season and a thermodynamic formulation of ice growth to simulate consolidated layer growth.

1.3. Research approach

During the initial stages of the research, the focus was on conducting a comprehensive review of the relevant literature and gaining a thorough understanding of the state-of-the-art techniques related to structural reliability in the context of arctic offshore engineering. In order to gain further knowledge and insights, several workshops and seminars were organized, involving both academia and industry experts. Throughout the course of the doctoral study, I had the opportunity to serve as a teaching assistant at The University Centre in Svalbard (UNIS) where laboratory and field experiments were conducted. These activities provided valuable insights into ice mechanics and ice engineering measurement techniques. In addition, I also participated in the "Station Keeping Trials - SKT" research expedition, organized by Equinor, with the main objective of obtaining full-scale measurements for station keeping operations supported by ice management. While this expedition and the data collected were not directly utilized in the primary aspect of the PhD research, it provided valuable insights into sea ice and Arctic engineering.

After the early phases of the research, the primary objective was defined: establish a framework for probabilistic modelling of ridge loads. The first step was to identify the shortcomings of the current state-of-the-art in this area and to find a suitable modelling technique. Various methods of probabilistic modelling of ice loads on offshore structures were considered as part of a literature review. It was concluded that the Monte Carlo simulation technique is best suited for capturing the complexity of ice-structure interaction. This is because the interaction is characterized by a large number of variables being involved. Furthermore, Monte Carlo simulation is well suited for capturing the seasonal variability of the ice environment. The main advantages are that the method is versatile, clear, and well understood. The most prominent disadvantage of the method is computational unaffordability. However, the computational framework described in this thesis shows that this is not a problem for the simulation of ice ridge loads even with a desktop computer. Other probabilistic methods, such as the First Order Reliability Method (FORM) and Second Order Reliability Method (SORM), are not well suited for handling processes that involve a large number of variables and that are characterized by nonlinearities (Melchers & Beck, 2018).

The Monte Carlo simulation of loads follows a relatively straightforward procedure. The simulation technique involves sampling the input variables and combining them in the load expression in a large number of experiments and observing the results. The challenge of performing a simulation lies in finding suitable data for stochastic variables and accurately modelling them with appropriate probability distribution functions. For the best approximation of the tails of the distributions, long-term data should be used. There should be a natural connection between the variables (e.g., obtained in the same measurement campaign), so that the eventual correlations between the variables are well captured. Along with the variables used in the load expression, data for the frequency of occurrence of load events should be processed because this has a significant effect on the resulting load distribution (Jordaan, 2005).

To explore the challenges associated with probabilistic simulations of ridge loads, an initial set of numerical experiments was conducted. Samardžija et al. (2018) established a simplistic Monte Carlo simulation to model ridge loads affecting the Norströmsgrund lighthouse. The study highlighted a number of limitations with such simulations. For example, obtaining the necessary data to establish probabilistic distribution functions for input variables proved challenging due to the lack of connectivity between data used for different variables, as well as incompatibility in spatial and temporal scales. Additionally, important correlations were not taken into consideration, and the frequency of load events was inadequate and not connected to other variables. Lastly, the simulation of the consolidation layer thickness was incomplete.

The next step in the research was to identify and analyse a suitable dataset that includes important variables for ridge load calculations. It has been determined that ice profiling sonars are a good option to achieve this goal. This measurement technique offers data at a suitable temporal and spatial scale for engineering purposes. The data is long-term and spans whole seasons without sampling biases. It is also very accurate. By processing the data, one can obtain important variables for ridge load calculations: ridge keel draft, level ice thickness and ridge occurrence frequency. A suitable dataset with ice-profiling measurements spanning 15 years was found in the Beaufort Gyre Exploration Project, a project whose primary objective was to investigate basin-scale mechanisms that regulate anomalies in freshwater content in the Beaufort Gyre. Using this data, an optimized approach was developed for establishing the probability density function of the variables critical for the probabilistic calculation of ridge loads (ridge keel draft, level ice draft and ridge frequency) (Samardžija & Høyland, 2023). The advantage of the proposed approach is that it incorporates seasonality into the model as well as correlations between variables.

Next, the study explored how the thickness of the consolidated layer could be incorporated into a probabilistic model for ridge loads (Samardžija et al., 2023a). Lack of data makes it difficult to establish reliable probability density functions for this variable. There are currently no existing measurement techniques that could be used to measure the thickness of consolidated layers in a continuous manner on a large scale. Typically, this is measured by costly and time-consuming field expeditions. Consequently, datasets are collected sporadically and there is a risk of biased sampling. To combine such data with, for example, unbiased data for ridge keel draft, one of the two variables must be adjusted to account for the bias caused by the incomplete data for the consolidated layer thickness. However, the growth of the consolidated layer is a predictable process and ratios that compare its growth to that of the adjacent level ice are well established. An issue arises from the fact that the age of a ridge that impacts a structure during a simulation cannot be determined. Predicting (simulating) the age of the impacting ridge can give us a good reference for making a solid estimate of the consolidated layer thickness. In the article cited above, a method for achieving this is outlined. The proposed method uses data from the above-mentioned Beaufort Gyre dataset to analyse the increasing population of ridges

throughout a season and makes an estimate of the ridge creation rate. Then, consolidated layer thickness is simulated using probabilistic simulation of ridge creation timing (and thereby the age of impacting ridges) and formulations of consolidated layer growth.

The final phase of the study was dedicated to establishing a framework for the probabilistic simulation of ridge loads. Utilizing the methods developed in the earlier phases of this PhD, it investigates a case study involving numerical experiments conducted by means of Monte Carlo simulations (Samardžija et al., 2023b).

1.4. Structure of the thesis

This thesis is comprised of a collection of international journal and conference papers. Five papers serve as the foundation of this work and are included in Appendix A for reference. The summary section of the thesis is divided into seven chapters:

- **Chapters 1-3** provide a general introduction, a brief overview of structural reliability topics, and discussions related to first-year ice ridge loads on offshore structures.
- **Chapters 4-6** provide a summary and connect the contents of papers 3-5. (Refer to the "Publication List and Declaration of Authorship" section for paper numbering.)
- **Chapter 7** presents the conclusions drawn from this research and provides recommendations for future studies.

2. Structural reliability

Reliability analysis and probabilistic design have become increasingly important in civil engineering, primarily due to the complex, uncertain, and inherently variable nature of engineering systems and environmental conditions. This chapter provides a concise introduction to some fundamental concepts of reliability analysis and probabilistic design methods in civil engineering. Its primary objective is to provide a refresher on the core theory, including safety, uncertainty, probability, reliability, and stochasticity, and their relevance to engineering analysis and design. For more detailed information on the theory and calculation methods presented in this chapter, readers are encouraged to consult the following textbooks: Ditlevsen and Madsen (1996), Jonkman et al. (2015) and Melchers (1999).

2.1. Risk

Response of an engineering structure under load is determined by its structural strength and stiffness, as well as the type and magnitude of the applied load. Whether the response is satisfactory depends on the criteria set forth by the designer and authorities, such as standards or codes. These criteria may include the structure's safety against collapse, limitations on damage and deflection. A limit state occurs when a structure ceases to meet the relevant design criteria (CEN, 2001).

Buildings and structures should be safe for occupants, users, and those in their immediate surroundings. Stakeholders rely on the professional care and expertise of individuals involved in the planning, design, analysis, detailing, construction, and maintenance of structures. Structural collapses are extremely rare, but they do occur, and no structure can be entirely safe from collapse. Risks are inherent in any project. Designers and other stakeholders need to recognize and minimize these risks while taking care to balance economy and safety.

The notion of *risk* is often used interchangeably with terms like *chance*, *likelihood*, and *probability* when there is uncertainty about the state of an issue under consideration. For example, one might say: "Smoking increases the *chances* for developing lung cancer." or "Smoking increases the *risk* of developing lung cancer." Nonetheless, it is imperative, particularly in the context of engineering decision-making, to establish a precise definition of risk, despite the apparent synonymity among these terms. In this regard, the most prevalent definition of risk in the engineering and insurance industries is that of expected value:

Risk is the probability of an undesired event multiplied by the consequences.

The following equation can be used to express the risk of an activity governed by a single adverse event with a consequence C and probability of occurrence P:

$$R = P\ C \tag{2.1}$$

An example of this is the failure risk for an offshore structure. Failures of offshore structures can be caused by various causing events (e.g., structural damage, collision, blowout, etc.). Figure 2.1 shows an example for the distribution of initiating events for failures of fixed offshore structures.

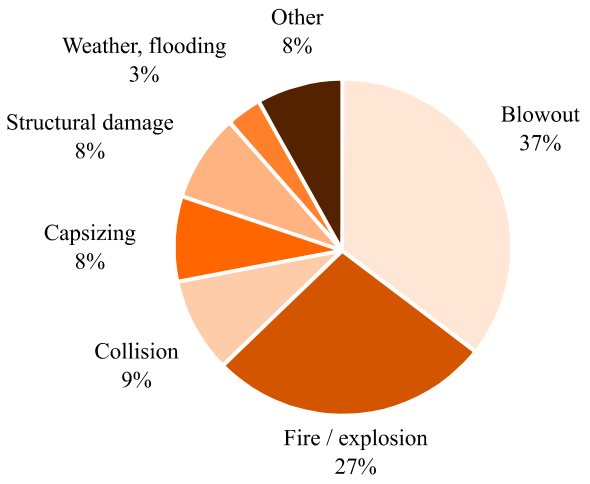

Figure 2.1 Percentage of type of accident for fixed platforms (Bertrand & Escoffier, 1989)

For a system with multiple uncorrelated risk sources, the total risk can be expressed as the sum of individual risks, each with its own consequences C_i and occurrence probabilities P_i :

$$R = \sum_{i=1}^{n} P_i \; C_i \tag{2.2}$$

The unit for the risk, then, depends on the units used for the probability (e.g., per year, per operation, per lifetime) and for the consequence (e.g., economical loss, human fatalities, environmental damage).

Risk quantification is an integral part of *risk assessment*. The remaining components of risk analysis include system definition, qualitative analysis, and risk evaluation. In addition to the steps of risk assessment for a given system, *risk management* also includes the reduction and control of risks. Figure 2.2 shows a schematic representation of these components.

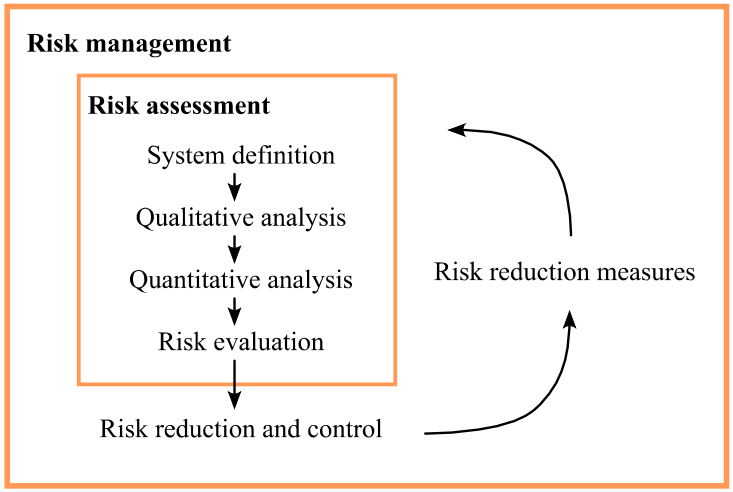

Figure 2.2 Schematic view of steps in risk management (Jonkman et al., 2015)

Depending on the results of the risk assessment, steps can be taken to mitigate the risks, and the risk assessment is then repeated for the reconfigured system. These steps are often repeated several times to reach the desired and/or optimal design.

System definition includes defining the scope and objectives of the analysis as well as describing the system. It is common for a system to be divided into components and subsystems. With internal relationships between these components and subsystems, the total system is formed. *Qualitative analysis* involves identifying and describing undesirable events, potential hazards, failure mechanisms, and scenarios. In this phase, the goal is to obtain a comprehensive understanding of the potential undesired events and their consequences. This phase is where the limit states are defined, such as the ultimate limit state (ULS) and the serviceability limit state (SLS). It is important to understand the various undesired events and failures that may occur before conducting a quantitative analysis in a risk analysis. The failure to recognize failure modes is a cause of many accidents in practice.

Quantitative analysis is evaluating the probabilities and consequences of components and subsystems, as well as of the system as a whole. Consequences considered typically include economic losses, fatalities, and environmental damage. Based on the type of component/subsystem and the availability of failure data, the probabilities of failure can be assessed in two ways. If a system has a large number of failure records, the failure probability can be estimated empirically based on observed failure rates (e.g., in electrical systems). However, this approach is not adequate for systems such as engineering structures, where failures are rare. The assessment of failure probabilities in these situations requires methods from structural reliability theory.

The breakdown of risk management is given here to show how the research in this thesis fits into the broader context of risk management. Most of the research presented in this thesis focuses on structural reliability. It is concerning *quantitative analysis* as it is aimed at quantifying the probabilities of ridge loads on offshore structures. The structural reliability analysis estimates the structural failure probability by considering random variations in material properties, geometric measures, and loads. It is worth noting that material properties and geometric measures of the structure itself (i.e., resistance) are not considered in this thesis.

2.2. Probability

Most of the processes in nature are characterized by uncertainty. These processes are not predictable in advance. *Random* processes can be reproduced to a certain extent, but their outcomes are uncertain. *Probability* is the degree to which one outcome of a random process is more likely than any other possible outcome. An example would be the probability that an iceberg will collide with an offshore structure during a period of one year. It is not possible to predict with certainty whether this will happen or not. Further, it is not possible to make a completely accurate estimate of the probability that such an event will take place. However, we can be certain that iceberg collision is more probable in the Arctic than in the Caribbean Sea. Offshore structures in the Caribbean Sea have a practically non-existent probability of failure (p_f) due to iceberg collision. Due to the possibility of iceberg collision, offshore structures in the Arctic have only a small but not negligible probability of failure, and therefore inherited risks need to be addressed for such projects.

In the field of structural reliability, *reliability* is commonly defined as the complement of failure probability (= 1 - pf). It is the probability of a structure's safety (or intended performance) over a given period of time.

The concept of probability can be interpreted in diverse ways depending on how much information is available and depending on the practical application of the probability. Further, the interpretation of the concept of probability is a philosophical problem. The following three interpretations are mostly used: classical interpretation, frequentist interpretation, and Bayesian interpretation.

The *classical interpretation* originates from the early work in mathematical probability theory dating back to the seventeenth century. It defines probability as the ratio between the number of outcomes in which an event occurs and the total number of possible outcomes. For example, the probability of drawing a diamond-faced card from a standard 52-card deck would be equal to $\frac{13}{52} = \frac{1}{4}$. In this example there are 13 outcomes in which the event of drawing a diamond-faced card occurs out of total of 52 possible events. The use of classical interpretations is limited to systems for which outcomes are equally likely or for which the system can be decomposed into such subsystems.

The *frequentist interpretation* of probability was developed in the latter part of the nineteenth and first half of the twentieth century. This interpretation defines the probability as the relative frequency of occurrence of an event *A* in an experiment with *n* trials. The probability is expressed as the number of events where event *A* occurred divided by the number of trials *n*. For the example of drawing a diamond-faced card, an experimentalist would repeat the experiment of drawing a card from a standard 52-card deck many times (e.g., 4000 trials) and count the number of times when the diamond-faced card was drawn. If "diamonds" had occurred 987 times, the probability of this event would be estimated to be 987/4000 = 0.24675. However, with an increased number of experiments the resulting probability estimate would converge to 0.25. According to this interpretation, probability is a characteristic of nature.

The *Bayesian interpretation* is named after Thomas Bayes, who initiated the theory in the eighteenth century. In this interpretation, frequency is not the same as probability. The frequencies are used to estimate probabilities. Probability is defined as the degree of belief an individual has that an event will occur. According to experience, expertise, and preferences, the degree of belief reflects the state of mind of the individual. Contrary to frequentist interpretations, probability is not considered a natural characteristic. In this interpretation, probability is subjective, meaning that two persons can assign varying probabilities to the same event. The Bayesian approach employs both frequentist and classical interpretations as tools to obtain subjective estimates of probabilities where information can be obtained from experiments as well as analytical considerations (e.g., symmetry).

A structure's failure probability cannot be estimated solely based on the frequentist interpretation. In most cases, structures have unique configurations, and failures are extremely rare. Therefore, failure probability cannot be calculated using "experiments." The Bayesian interpretation of probability is more appropriate in the case of structure failure probability estimation. Instead of constructing a random experiment, we can instead use a "thought-experiment" or simulations to construct a theory using frequency. This is the approach used in this thesis, where frequencies are analysed for relevant variables, probability distributions are created, and these are then combined in numerical experiments using the Monte Carlo technique to make an estimate of probabilities for extreme ridge loads.

2.3. Risk acceptance

Societal risk acceptance can vary significantly depending on the nature of the risk. The difference can correspond to orders of magnitude between so-called "voluntary" risks and

"involuntary" risks (e.g., the typical risk of death for alpine climbing is about 2×10^{-3}, while for structural failure the risk of death is about 1×10^{-7}) (Melchers & Beck, 2018). Cultural and political factors can also change the perception of risk. Further, society tends to be more risk-averse in the case of catastrophic events with a small probability and large consequences, such as nuclear catastrophes, even though the risk is smaller compared to less catastrophic accidents such as traffic fatalities. Therefore, risk evaluation is not strictly technical process, but also encompasses many subjective components.

Risk can be viewed as an unwanted side effect of otherwise beneficial and legitimate activities, such as production or transportation. Managing risk is concerned with achieving a balance between economic and social activities on one hand, and the maintenance of a sufficiently safe society on the other. Risks may be evaluated using the following three criteria (Jonkman et al., 2015; Vrijling et al., 1998):

- To limit the *individual risk* so that no person is exposed to risks that may be disproportionally large.
- To limit the *societal risk* of large-scale accidents which cause many fatalities.
- To optimise investments in risk reduction from an economic perspective in an *economic optimization* analysis.

Individual risk refers to the probability of death caused by an accident. This criterion has a variety of related definitions. Based on statistics, it is possible to derive the "average individual risk" for a certain activity. Individual risk due to an accident can be calculated as follows:

$$IR = P_f P_{d|f} \tag{2.3}$$

Where IR is the individual risk (per year), P_f is the probability that the accident will occur (per year) and $P_{d|f}$ is the conditional probability of death given the accident. An infrastructure project, for instance, may use this measure to analyse whether the project (e.g., an airport) increases the risk of death among nearby residents.

An accident that results in multiple fatalities is considered a *societal risk*. Using this criterion, accidents that result in many fatalities can be given higher weight. One way to represent risk for fatalities for multiple events is with an FN-curve. FN-curves are graphs that illustrate the probability of exceeding potential numbers of fatalities ($P(N > n)$) on a double-log scale. A schematic example is given in Figure 2.3. A crucial component of the curve is the α parameter that determines the steepness of the limit curve. A limiting FN curve with $\alpha > 1$ puts a higher weight on accidents with many fatalities. Other parameters include the base point C that depicts the exceedance probability of one fatality, and cut-off parameters A and B that dictate the limited acceptable upper limit for the accident probability and highest acceptable number of fatalities, respectively.

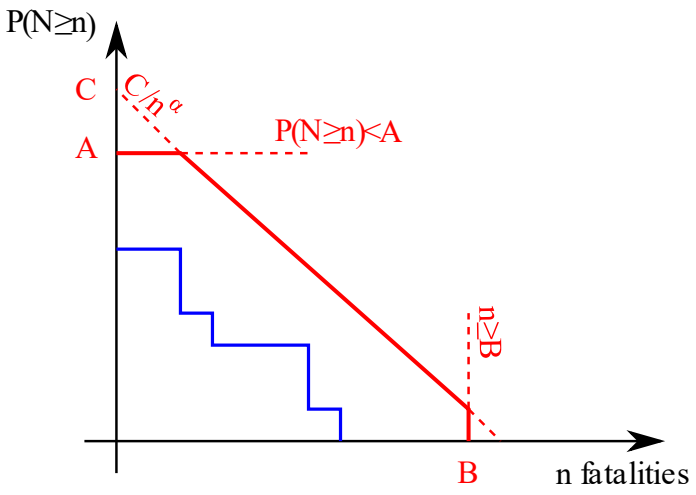

Figure 2.3 Schematic example of a calculated FN curve (blue line) and the limit criterion FN curve (red line).

Individual risk assessments and societal risk assessments are governed by regulatory institutions and standards, while *economic optimization* analyses are typically conducted by stakeholders evaluating the utility of proposed activities or investments, such as infrastructure projects. The goal of economic optimization is to derive an optimal level of safety by considering the costs involved in increasing the level of safety and reducing the risks. An economic optimization analysis is commonly employed when deciding on the failure probability level for a system that has yet to be designed, with an infinite number of design options. Such analysis may suggest that a lower risk than the one prescribed by the regulations may be economically advantageous.

An example of this type of decision problem is the hull design for an icebreaker ship. The hull needs to be strong (thick) enough to withstand the impacts of floating ice features. A thin hull design would be associated with lower initial costs, but the high expected value of risks (future maintenance costs or ship sinking) would make the total costs large. An overly thick hull design would be associated with high initial costs that would also make the total costs large, despite the negligibly low expected value of risks. An optimal design can be found between these two boundary situations where both initial costs and expected value of risks are reasonably low.

In a simplistic economic optimization, the procedure can be undertaken by calculating the total costs (C_{tot}) that consists of initial costs (I) and the present value of risks (R):

$$C_{tot} = I + R \tag{2.4}$$

The present value of risks is given as:

$$R = \frac{E(D)}{r} = \frac{P_f D}{r} \tag{2.5}$$

Where $E(D)$ is the expected value of risk (expected economic damage) [€/yr], P_f is the probability of failure per year, D is the damage in case of failure, and r is the discount rate that transfers future costs into present value.

The expected value of risks can be reduced either by limiting the potential damage (smaller D) or by designing a safer system (reduced P_f). Reduction in failure probability can be achieved by increasing the initial costs and thereby the initial cost can be presented as a function of failure probability:

$$I = I(P_f) \tag{2.6}$$

The economically optimal design is found by finding the minimum of the total costs. Mathematically, the problem can be solved by finding the following situation:

$$\frac{dC_{tot}}{dP_f} = 0 \tag{2.7}$$

The problem is illustrated in Figure 2.4.

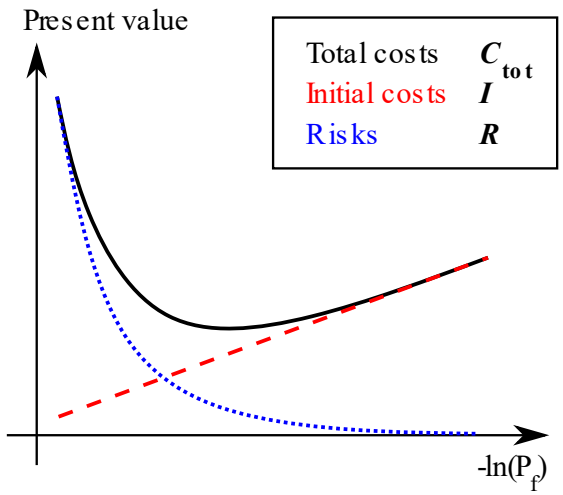

Figure 2.4 Schematic illustration of economic optimization showing the total costs, initial costs, and risks as a function of the failure probability.

For offshore structures in Arctic regions, the risk acceptance level is regulated by the ISO 19906 standard, as well the ISO 19902 and ISO 19903 standards. Depending on the exposure level (a measure describing the life-safety and consequence category of a structure), the upper bound for the yearly probability of failure (reliability target) is ranging from 1×10^{-5} to 1×10^{-3}. The framework for probabilistic calculation of ridge loads presented in this thesis is one component in the quantitative analysis of risk assessment. To meet the required reliability target, loads with a specific return period are calculated and used in the design procedure in accordance with the relevant regulations.

2.4. The basic structural reliability problem

An example of a structural reliability problem is the calculation of the failure probability for a structural component. This analysis considers only one load effect, S, resisted by one resistance, R. The load effect S is obtained from the acting load Q by means of structural analysis. This can be either a direct deterministic transformation or some sort of probabilistic transformation. Probability density functions are allocated both for the load effect, f_S, and for the resistance, f_R. The failure probability is then equal the probability that the load effect S is larger than the resistance R:

$$P_f = P[S \geq R] \tag{2.8}$$

Other criteria for failure can be chosen, and for this reason, it is practical to introduce the limit state function Z, which expresses the criteria of failure. In the simple case given above, the limit state function is expressed as $Z = R - S$, and failure occurs when $Z < 0$. The failure probability equals $P_f = P(Z \leq 0)$.

In Figure 2.5, we can see the marginal density functions for R and S, denoted as f_R and f_S, respectively. Additionally, the joint bivariate density function $f_{RS}(r,s)$ is depicted. This function describes the probability of R taking a value between r and $r + \Delta r$, and S taking a value between s and $s + \Delta s$, where Δr and Δs approach zero. For any infinitesimal element ($\Delta r\ \Delta s$), the value of $f_{RS}(r,s)$ represents the probability of this occurrence. The hatched failure domain D in Figure 2.5 represents Equations (2.8), allowing us to express the failure probability as:

$$P_f = P[S \geq R] = \iint_D f_{RS}(r,s)\ dr\ \ ds \tag{2.9}$$

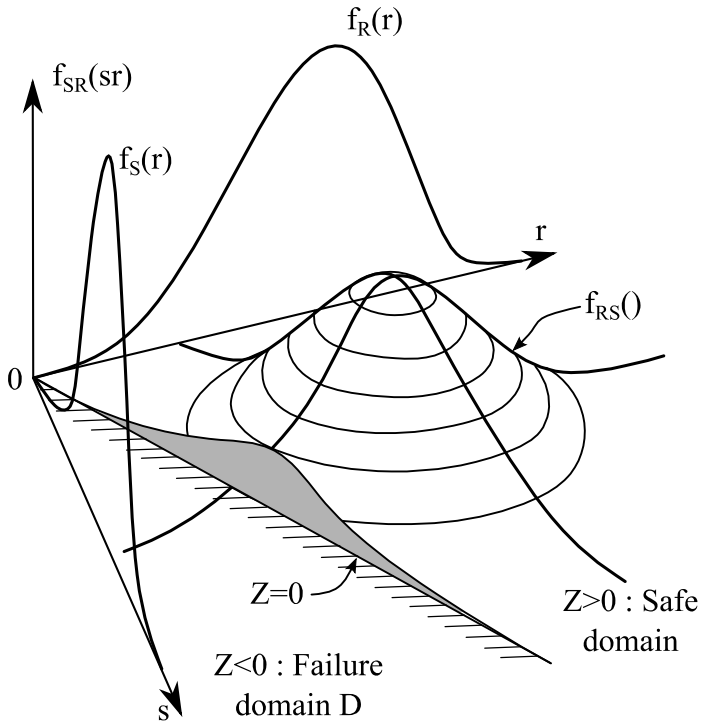

Figure 2.5 Space of the two random variable (r, s) and the joint density function $f_{RS}(r,s)$, the marginal density functions f_R and f_S and the failure domain D (adopted from Melchers and Beck (2018)).

The task of calculating the failure probability in fundamental structural reliability problems can be accomplished using a variety of methods. These can be divided into three main groups (Jonkman et al., 2015):

Level III methods provide the most accurate estimation of failure probability, achieved through the utilization of precise analytical computations, numerical integration, or the application of Monte Carlo simulations. While the analytical approach is limited to simple cases, numerical

integration is only feasible with a small number of variables. Monte Carlo simulations, on the other hand, offer a flexible alternative that generates precise results, even in complex scenarios.

Level II methods primarily leverage the means, first, and second moments of variables. They typically involve approximation of the limit state function at the so-called design point, usually through linearization. A common approximation in this category involves choosing the point on the limit state function ($Z = 0$) that corresponds to the minimum distance in a normalized space. This approach is often referred to as the first-order approximation or first-order second-moment approximation (FOSM).

Level I methods are also known as semi-probabilistic methods. These methods use characteristic values to represent the relevant variables of a problem. The upper percentile represents actions while the lower percentile represents strength. These characteristic values are combined with partial factors that are already calibrated using either level II or level III methods.

In addition to the Level I, II, and III methods, there are two other methodologies. **Level 0** methods are related to deterministic calculations, while **Level IV** methods go beyond reliability measures by considering consequences, including costs, thus offering a more comprehensive risk assessment.

When utilizing reliability methods for design purposes, it is essential to calibrate these methods to ensure that consistent reliability levels are achieved. For instance, Level I methods may be calibrated by employing Level II methods, while Level II methods may be calibrated by employing Level III methods, and so on.

This thesis proposes a probabilistic framework for calculating ice ridge loads, which can be classified as a Level III method when ice ridge loading is treated as an isolated subsystem in an offshore structure reliability assessment. The approach involves estimating the marginal probability distribution of the load effect f_S. On the other hand, when the complete system, rather than just the isolated ice ridge loading subsystem, is considered, the method can be categorized as a Level I method. The probabilistic model is used to estimate the characteristic values of the ice ridge load that correspond to a certain return period, such as the 100-year load. These characteristic values are then combined with partial load factors that are previously calibrated using Level III methods and readily available in the ISO 19906 standard (OGP Report 422, 2010; Thomas, 2014).

Alternatively, the model proposed in this thesis can be utilized in a fully probabilistic assessment of offshore structure reliability and for the calibration of partial safety factors using Level III methods.

3. First-year ice ridge loads on offshore structures

3.1. Ice ridges

Sea ice ridges are a natural occurrence commonly found in Arctic seas. They form when level ice floes collide or shear, causing the ice to break into smaller pieces, which then accumulate to form large piles of broken ice. Ridges usually form during stormy events when ice floes are pushed by the wind, but ocean currents can also contribute to their formation. In some cases, ridges can form in calm conditions when weaker but persistent winds push ice floes over longer periods. In temperate regions, such as the Baltic Sea, large ridges are typically about 15 m thick (Leppäranta, 2023), but significantly deeper ridges have also been measured with a record value for the Baltic Sea of 31.5 m (Palosuo, 1975). In the Arctic, ridges may be thicker than 50 m (Timco et al., 2000).

While ridges often manifest as elongated, linear structures with triangular or trapezoidal cross-sections, they can also form in more intricate geometries (Jordaan, 2015). Figure 3.1 illustrates a schematic cross-sectional view of an ice ridge. The submerged ice pieces constitute the keel of the ridge, while the protruding ice pieces above the water surface form the sail. Once the ridge is formed, the broken ice pieces near the water surface freeze together to create a consolidated layer of solid ice, which tends to grow thicker than the surrounding level ice, assuming sufficient time is available for growth. The rate of growth of the consolidated layer is up to twice as fast as that of the surrounding level ice (Høyland, 2002; Leppäranta & Hakala, 1992; Timco & Goodrich, 1988). Knowledge of the thickness of this layer is particularly crucial for ice engineering applications, as the consolidated layer frequently exerts the most significant forces on offshore structures during a ridge/structure interaction.

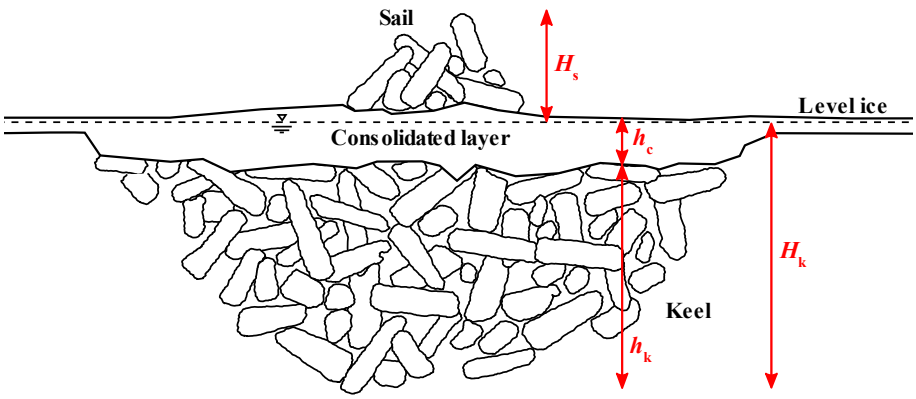

Figure 3.1 Characteristic cross section of an ice ridge. H_s – sail height, H_s – keel draft, h_c – consolidated layer thickness, h_k – thickness of the unconsolidated rubble.

First-year (FY) ridges are those that are not older than one winter season, while second-year ridges are those that survive one summer season. Old ridges are those that have survived one or more summer seasons. First-year ridges can also occur in more moderate climate conditions, such as in the Baltic Sea. The thickness and geometry of a ridge can provide clues about its age and formation. For example, first-year ridges typically have a lower consolidated layer thickness and simpler geometry compared to old ridges, which may have a more complex internal structure due to repeated deformation and refreezing.

Ridges demonstrate a remarkable variety in their form and magnitude. Zubov (1943) introduced a simple triangular model for first-year ridges while examining the buoyancy of hummocks/ridges. Typically, the keel base is not triangular, but rather irregular, and the cross-section can be approximated with a trapezoidal shape. The ISO 19906 (2019) standard suggests that the keel bottom width can vary from 0 to five times the sail height. The sail height is typically utilized as a defining parameter for other geometric characteristics, coupled with level ice thickness, owing to its simplicity in measurement through either manual field observations or aerial surveys. The customary practice of determining ratios between the maximum keel depth, maximum sail height, keel width, and keel depth, is well-documented in the literature (Strub-Klein & Sudom, 2012; Sudom et al., 2011; Timco & Burden, 1997). This information is particularly helpful in guiding the design process for offshore structures and floating vessels.

Sea ice ridges are instrumental in defining design loads in Arctic marine regions devoid of icebergs (Blanchet, 1998). Ideally, precise modelling and computations require inputs such as ridge dimensions, macroporosity, and an array of physical and mechanical properties. However, in practice, gathering all this data concurrently presents a formidable challenge, attributed to the limited time and extreme environmental conditions encountered during fieldwork in cold regions.

3.2. Ice loads from first year ice ridges on offshore structures

Understanding the characteristics of ice ridges and the forces they can generate requires a combination of theoretical analysis and full-scale measurements. Despite progress in recent years, the prediction of ice forces remains a challenging task due to the complex and variable nature of the ice environment. In this context, the use of simplified models and upper limit estimations is often necessary to ensure the safety and reliability of offshore structures in ice-covered waters. An upper limit estimation of the horizontal force exerted by a first-year ridge can be obtained by summing the individual contributions from the consolidated layer and the keel rubble, Eq. (3.1). This method of calculation is recommended by the ISO 19906 standard and is described further in this subchapter.

$$F_{\mathrm{R}} = F_{\mathrm{c}} + F_{\mathrm{k}} \tag{3.1}$$

where F_c is the action component due to the consolidated part of the ridge and F_k is the action component due to keel rubble. The contribution of the sail to the total ridge action is typically neglected as its volume is insignificant compared to the keel volume.

To obtain an approximation of the consolidated layer action component, F_c, one can use the equation for the global pressure of level ice provided in Eq. (3.2):

$$F_{\mathrm{c}} = p_{\mathrm{G}} \cdot h_{\mathrm{c}} \cdot w \tag{3.2}$$

where p_G is the ice pressure averaged over the nominal contact area, h_c is the consolidated layer thickness and w is the width of the structure.

The pressure p_G can be determined by utilizing the equation provided in Eq. (3.3). This equation is derived from full-scale measurements conducted in various regions, such as Cook Inlet, the Beaufort Sea, Baltic Sea, and Bohai Sea, to determine the maximum ice pressure values during events where first-year (FY) or multi-year (MY) ice collides with a vertical structure. ISO 19906 also provides formulae for estimating level ice action on inclined structures and this can be used for approximation of the consolidated layer action component on inclined structures (not included here).

$$p_{\mathrm{G}} = C_{\mathrm{R}}\left[\left(\frac{h_{\mathrm{c}}}{h_1}\right)^{n}\left(\frac{w}{h_{\mathrm{c}}}\right)^{m} + f_{\mathrm{AR}}\right] \tag{3.3}$$

In Eq. (3.3), $p_{\mathrm{G}}[\mathrm{MPa}]$ is the global average consolidated layer ice pressure, $w[m]$ is the projected width of the structure, $h_{\mathrm{c}}[m]$ is the average consolidated layer thickness, $h_1[m]$ is a reference thickness of 1 m, $m[-]$ is an empirical coefficient equal to $-0{,}16$, $n[-]$ is an empirical coefficient ($-0{,}50 + h/5$ for $h < 1{,}0m$, and $-0{,}30$ for $h \geq 1m$), $C_{\mathrm{R}}[\mathrm{MPa}]$ is the ice strength coefficient, and f_{AR} is a factor that accounts for the aspect ratio effect that is given in Eq. (3.4):

$$f_{\mathrm{AR}} = e^{\frac{-w}{3h_{\mathrm{c}}}}\sqrt{1 + 5\frac{h_{\mathrm{c}}}{w}} \tag{3.4}$$

The ISO 19906 standard's approach to determining the ridge keel rubble action component draws upon the research of Dolgopolov et al. (1975) and incorporates adjustments made by Kärnä and Nykänen (2004):

$$F_{\mathrm{k}} = \mu_{\phi} h_{\mathrm{k}} w\left(\frac{h_{\mathrm{k}}\mu_{\phi}\gamma_{\mathrm{e}}}{2} + 2c\right)\left(1 + \frac{h_{\mathrm{k}}}{6w}\right) \tag{3.5}$$

$$\mu_{\phi} = tan\left(45° + \frac{\phi}{2}\right) \tag{3.6}$$

$$\gamma_{\mathrm{e}} = (1 - e)(\rho_{\mathrm{w}} - \rho_{\mathrm{i}})g \tag{3.7}$$

where μ_{ϕ} is the passive pressure coefficient, ϕ is the angle of internal friction, c is the apparent keel cohesion, w is the width of the structure, γ_{e} is the effective buoyancy, e is the keel porosity, ρ_{w} is the water density, and ρ_{i} is the ice density.

The outlined formulation pertains to the scenario where a ridge, under the intense environmental stress induced by wind and currents, collapses against a structure – a situation referred to as the limit stress scenario. Conversely, during periods of limited environmental stress, a ridge halts in front of the structure, with the resulting ridge action being confined by the available forces within the surrounding level ice. This situation is termed the limit force scenario. It is important to highlight that even in instances of strong wind and currents, the ridge building action can still be restrained by the limited thickness of the surrounding level ice. When the thin level ice is incapable of transferring the stress, it fails, and the load imposed on the structure is then confined by the ridge building action. For a comprehensive analysis of the limiting conditions for ice actions, please refer to Croasdale (1984), Croasdale (2009) and Timco et al. (2017).

This formulation is primarily influenced by three key parameters when determining the load of first year ice ridges, namely the coefficient C_{R}, consolidated layer thickness h_{c}, and the thickness of the unconsolidated portion of the keel h_{k} (or keel draft H_{k}, which can be used in conjunction with h_{c} to calculate h_{k}). In addition, including the limit force in the scenario necessitates accurate knowledge of the thickness of the surrounding level ice to effectively estimate the ridge building action.

Understanding the technique that was used for measuring the ridge properties such as the consolidated layer and the ridge draft is crucial in accurately predicting ice loads on offshore structures. This is because the measurements directly influence the calculated forces exerted by the ice structure. Without knowledge of the measurement technique, inaccuracies in the data can lead to inaccurate force calculations and consequently, inadequate design of offshore structures. Therefore, it is imperative to ensure that the measurement techniques used are reliable, consistent, and well-documented, and that the data collected is carefully analysed and

interpreted. This factor becomes especially significant in probabilistic evaluation of ice ridge loads. For instance, understanding whether the data was exclusively collected at the end of a winter season is crucial. Any such bias could cause discrepancies when simulating ridges over the course of an entire season, potentially compromising load calculations.

3.3. Probabilistic assessment of ice loads on offshore structures

The ISO 19906 standard recognizes the necessity for a probabilistic treatment of ice loads. A comprehensive account of the standard's design methodology is found in Thomas et al. (2011). The standard adopts the limit states design approach and mandates that characteristic ice loads, with their corresponding annual exceedance probability, be determined and used in load combinations. To achieve the required reliability targets, the action (load) factors in the load combination are calibrated. The calibration process for the ice load factors itself is probabilistic in nature and is explained in a report prepared by OGP Report 422 (2010) and summarized in Fuglem et al. (2011) and Maes and Thomas (2011).

The subsequent paragraphs offer a brief chronological literature review of probabilistic ice load assessment. It is noteworthy to acknowledge that significant advancements have also been made in the field of probabilistic assessment of ice-ship interaction. However, this aspect is beyond the scope of the present review and the focus is on the probabilistic assessment of ice-structure interactions.

Bercha et al. (1978) were among the first to attempt a probabilistic ice-structure interaction analysis. Wheeler (1981) employed Monte Carlo simulation to estimate the statistical distribution of ice loads on a conical offshore structure. Jordaan (1983) stressed the significance of probabilistic approaches for risk and safety assessment in Arctic offshore projects. Vivatrat and Slomski (1983, 1984) presented a comprehensive Monte Carlo simulation with a sensitivity analysis of ice-structure interaction. Dunwoody (1991) conducted a Monte Carlo simulation analysis of ice loads and suggested that the probability distributions of ice feature characteristics should adhere to the log-normal family. While log-normal distributions can provide a satisfactory fit around the mean value, the heavy tail of the distribution often leads to an overestimation of loads. Nessim and Jordaan (1991) and Nevel (1991) are two landmark papers that demonstrated the state-of-the-art in probabilistic ice load assessment at that time. These two papers marked the end of the initial development period, followed by two distinct periods, as described below.

During the first period, publicly available research papers suggest limited interest and scattered publications without significant structured progress. This period culminated in the introduction of the ISO 19906 draft version in 2007. Kato (1992) proposed a system based on a Monte Carlo simulation for evaluating ice loads for various ice features and offshore structure types. He later presented more specific examples of how this system could be applied (two publications mentioned below). Comfort et al. (1998) employed Monte Carlo simulation to analyse the influence of limit-stress and limit-force loading scenarios. Kato (1998) performed a Monte Carlo simulation of ice loads on a caisson structure for offshore Sakhalin. Brown et al. (2001) described a comprehensive Monte Carlo simulation of ice loads for the Confederation Bridge and elaborated on the implications of choosing the parent distribution for extreme loads. Specifically, they demonstrated how the use of a log-normal distribution could lead to overestimates of extreme loads. Spencer and Masterson (2002) conducted a Monte Carlo simulation for a multi-legged offshore platform interacting with first-year ice ridges. Timco and Frederking (2004) used a Monte Carlo simulation to perform a probabilistic analysis of the seasonal ice loads, which can have operational applications, unlike most publications where

extreme loads were analysed. Kato (2006) conducted a Monte Carlo simulation of first-year ridge loads with sensitivity analysis and concluded that the consolidated layer thickness and the encounter rate of ridges are the most dominant input parameters for the resulting probability distribution of ice loads. Finally, Bercha et al. (2006) addressed the reliability of offshore structures in the Arctic in general.

The introduction of ISO 19906 has marked a second period in the field of probabilistic ice loads assessment, resulting in a more focused and systematic advancement in this field. Various authors and groups have since published their approaches, focusing on implementing the probabilistic framework in connection with ISO 19906. Several publications address issues concerning multi-year sea ice, including works by Fuglem, Richard and Thijssen (2014), Thijssen et al. (2016) and Thijssen and Fuglem (2015). Other scholarly works explore concerns related to risk and structural reliability for offshore Arctic structures, both generally and in conjunction with ISO 19906, such as those presented by Fuglem, Richard and King (2014), Fuglem et al. (2011), McKenna et al. (2014), Moslet et al. (2011), Thomas (2014, 2015) and Thomas et al. (2011).

Cammaert et al. (2008) thoroughly discuss significant aspects of probabilistic assessments of ice loads, such as the importance of incorporating correlations between relevant parameters, seasonal variation of parameters, the influence of climate change on ice loads, and the uncertainty of the formulation of ice loads. Onishchenko (2009) presented an analytical approach for calculating design values of loads associated with discrete ice features in Arctic conditions, distinguishing itself from most of the publications discussed here, which predominantly rely on the Monte Carlo simulation technique. Eik and Gudmestad (2010) provide an example of how probabilistic analysis can contribute to the assessment of iceberg design loads and the efficiency of various components of iceberg management. Jordaan et al. (2011) present an intriguing simulation methodology for modelling the seasonal development of the ice environment during winter in the Caspian Sea. Wang et al. (2011) compare the First-Order Reliability Method (FORM) and the Monte Carlo simulation approach in the scope of probabilistic ice loads analysis. Walter et al. (2013) describe how an ice environmental model can be developed using the contour methodology. Bekker et al. (2012) analyse ice data from the Gulf of Bothnia and describe a method of developing a probabilistic ice environment model. The study's interesting results include nomograms showing the inter-seasonal development of the ice parameters' probability distributions. The same leading author published more work on the topic of probabilistic ice load assessment in Bekker et al. (2013a), Bekker et al. (2013b), and Bekker et al. (2009). Thijssen and Fuglem (2015) provide a probabilistic treatment of ice loads for seasonal operations.

Charlebois et al. (2018) evaluated different approaches for describing pack ice pressure, including the ridge-building equation in the ISO 19906 standard, in a probabilistic model for ice forces on a caisson platform in the Beaufort Sea. Chai and Leira (2018) and Chai et al. (2020) examine the concept of environmental contours in relation to the assessment of first-year ice ridge statistics. Taylor and Jordaan (2015) developed a probabilistic fracture mechanics model to investigate spalling during edge indentation in ice, generating estimates of mean pressure required to trigger fracture events and confirming the interplay between fracture and crushing during compressive ice failure. Taylor et al. (2019) proposed a probabilistic approach for modelling ice loads from high-pressure zones on local and global areas, with a focus on thin, first-year sea ice interacting with a bottom-founded structure. This study is continued in Hossain et al. (2021) where a probabilistic modelling framework for dynamic ice-structure interaction based on the mechanics of high-pressure zones is presented. Sinsabvarodom et al. (2020) used Monte Carlo simulations to investigate uncertainties in ice

loads on vertical and sloping structures, considering the effect of correlation between ice strength and thickness. Sinsabvarodom et al. (2021) conducted a probabilistic fatigue evaluation of a mooring line, considering the loads that arise from the station-keeping of a ship. Valenti et al. (2021) presented a probabilistic description of pressure ridge width, spacing, and keel depth for the Chukchi and Beaufort seas based on IPS and ADCP observations.

In summary, the literature review provides an overview of the progress in probabilistic evaluation of ice loads on offshore structures. It presents a chronological summary of the research conducted from the early stages to the current developments, including the introduction of ISO 19906 and the latest advancements. Although the review is not exhaustive, it covers significant contributions and emphasizes the importance of probabilistic approaches in ensuring the safety and reliability of offshore structures exposed to Arctic conditions.

This thesis introduces a probabilistic framework that utilizes Monte Carlo simulation to incorporate crucial aspects of ice ridge load characteristics. While the Monte Carlo simulation technique itself is not novel in reliability theory, this research focuses on identifying the most appropriate distribution functions for relevant parameters to accurately reflect the variables utilized in ridge load formulas. The probabilistic framework is subject to several requirements and limitations, outlined as follows:

- Only first-year ridges are considered.
- The simulation must include all ridges deeper than 5 meters that impact the structure.
- The simulation should accurately reflect the seasonality of all parameters exhibiting substantial inter-seasonal variability.
- Relationships (correlations) between the most critical parameters must be reflected in the simulation.
- The framework must be flexible enough to accommodate varying degrees of data availability, such as scenarios with only level ice thickness information, and scenarios with several years of ULS ice draft measurements, possibly supplemented by additional field measurement campaigns.

4. Relationship between level ice draft, ridge frequency and ridge keel draft

One of the main focuses of this thesis is to establish relationships between the key ice ridge variables used for ridge load calculation. One way to establish relationships between these variables is by analysing the phenomenology of the creation process and morphological evolution of ridges throughout a season. However, this approach is complex, and understanding just one relationship, such as the correlation between level ice thickness and ridge keel draft, would require significant research efforts. Therefore, instead of this approach, this thesis focuses on extracting relationships (correlations) between the relevant variables directly from the available data.

Accurate estimates of these values are sufficient for calculating ice ridge loads, even if we do not have knowledge of the phenomenological nature of the variables and their interrelationships. Therefore, understanding the causal relationship between these variables is of secondary relevance in this study. It is important to note that the new discoveries in this thesis regarding the relationships between the ridge parameters are relevant for their use in the probabilistic evaluation of ice ridge loads. Inferences on causality are limited, requiring further research to draw definitive conclusions. Where necessary, relevant explanations and connections to existing literature are provided.

This chapter centres around the investigation conducted in Samardžija and Høyland (2023), which examines the relationship between level ice draft, ridge frequency, and ridge keel draft by utilizing sonar ice draft data from the Beaufort Sea. Prior research by other scholars has established a positive correlation between ridge frequency and ridge keel draft with level ice thickness (Amundrud et al., 2004; Hibler III et al., 1972). However, the approach employed in Samardžija and Høyland (2023) differs from previous methods by optimizing these correlations for use in the probabilistic evaluation of ice ridge loads. As such, the study offers a more specific analysis of these relationships compared to earlier works.

The motivation for the study in Samardžija and Høyland (2023) stemmed from the inadequacy of the relationships between key ridge variables reported in the literature for use in probabilistic ice ridge load simulations, as identified in our previous work (Samardžija et al., 2018). Furthermore, the inter-seasonal variations of these key variables were not sufficiently documented for their application in a probabilistic simulation.

The initial challenge was that statistics related to ridge keel draft were typically presented as a single distribution, covering multiple seasons for a specific region. This kind of distribution is insufficient for simulating the inter-seasonal variability associated with ridge keels and their corresponding loads.

The difficulty of estimating the ridge frequency was the second challenge. Spatial frequency (e.g., in ridges/km) was typically used in the literature to represent this. However, this required converting the spatial distribution into a temporal distribution, which involved multiplying the spatial ridge frequency with ice drift speed and ice concentration. The challenge was that measurements of ridge spatial frequency were usually obtained only in the late periods of the winter season, so the inter-seasonal variation of ridge frequency could not be accurately reflected in the simulation using this data.

The third challenge involved introducing the relationship between the parameters in the probabilistic simulation. Gathering data on ridge properties can be difficult, as it often comes

from various sources with different scales, filters, and biases. In an attempt to incorporate the correlation between the surrounding level ice thickness and ridge keel draft, we have tried to utilize the findings presented in Amundrud et al. (2004). The level ice thickness in Amundrud et al. (2004) refers to the nearby level ice thickness found in the vicinity of a ridge. However, it is important to note that this nearby level ice thickness is not the same as the level ice thickness used in ridging force formulae. In these formulae, level ice thickness estimates the limit forcing or the surrounding ice's capacity to push the ridge against a structure. Using the level ice thickness from Amundrud et al. (2004) could lead to an underestimation of the limit forcing since the immediate vicinity's level ice thickness could initially fail, and a thicker ice floe could push the ridge to fail against the structure. Furthermore, the ridge keel draft in Amundrud et al. (2004) represents the deepest ridges on transects of approximately 50 km. This indicates that the correlation is incompatible for use in the simulation of all ridges. It is important to note that the deepest ridges do not necessarily cause the highest loads, as the consolidated layer plays a significant role.

The study presented in Samardžija and Høyland (2023) outlines a probabilistic simulation methodology and an analysis of the correlation between level ice draft, ridge frequency, and ridge keel draft. The presented approach can be replicated in other regions where sonar data on ice draft is available, offering an effective means to recalibrate correlations based on local conditions. In addition, the proposed simulation method has demonstrated potential for application in areas where only level ice thickness data is available or can be derived from temperature data. By utilizing these established correlations, it would be possible to simulate ridge draft and frequency using only level ice thickness data. Replication of the analysis conducted in Samardžija and Høyland (2023) in other regions could offer insights into the extent to which correlations vary and how they might be adapted for areas lacking ice ridge data.

The remainder of this chapter provides a description of the upward looking sonar measurement technique, followed by a discussion of the relationship between level ice thickness, ridge frequency, and ridge keel draft. It is worth noting that the probabilistic simulation technique for these parameters will be discussed in Chapter 6.

4.1. Ice ridge geometry from upward looking sonar data

Obtaining simultaneous geometrical measurements of both the sail and the keel of an ice ridge necessitates profiling the ridge. This typically involves field measurement campaigns, using techniques such as drilling or other discrete measurement methods. These methods are time demanding and expensive. Discrete measurements of ridges have accounted for only about 500 ridges in the past 50 years (Bonath et al., 2018; Ervik, 2015; Guzenko et al., 2021; Strub-Klein & Sudom, 2012; Timco & Burden, 1997). This type of measurement is essential for establishing the relationship between different geometrical parameters, such as sail height and ridge keel draft. The drawback is that the available data is geographically spread and is biased toward certain parts of the season. This makes the data less capable of establishing statistical distributions for ridge parameters that can capture the extremes and the interannual variability.

Alternative measuring techniques that can be used for extracting ice ridge geometrical parameters include continuous scanning methods. These methods are restricted to measurement of either the top or bottom surface of the ice. Top surface measurement techniques include aerial photogrammetry, satellite altimetry and LiDAR. Data from such surface measurements can be used to extract sail heights and ridge frequency, which in turn can be used in combination with established relationships to estimate keel draft statistics.

Traditionally, the bottom surface of ice was measured using upward-looking sonars, but recently a multi-beam sonar was used to map the bottom surface in three dimensions (Wadhams & Doble, 2008). Initially, ice bottom surface measurements were performed with sonars mounted on submarines (Hibler III et al., 1972) and later with stationary bottom moored sonars (Melling et al., 1995; Pilkington & Wright, 1991).

The upward looking sonars (ULSs) that measure the ice draft are specialized sonars also known as ice profiling sonars (IPSs). These instruments emit acoustic signals that reflect off the bottom surface of the ice and are then detected by the instrument. The time it takes for the signal to return is used to calculate the distance, while the speed of sound in the water above the instrument is used to convert time to distance. In addition to this, pressure sensors are utilized to measure the distance to the water surface. By subtracting the distance to the water surface from the distance to the ice bottom surface, the ice draft can be accurately calculated. Such measurements can be done continuously for one or several seasons at a time, resulting in time series of ice draft. A conversion to spatial series is possible where ice drift speed is known (typically obtained from Acoustic Doppler Current Profiler - ADCP). Davis and Wadhams (1995), Marcellus et al. (2011), Melling and Riedel (1995), Melling and Riedel (1996), Ekeberg et al. (2015); Obert and Brown (2011); Wadhams (2000) all reported on the identification and analysis of ridges from ULS data. ULS data has primarily been analysed for the purpose of monitoring and estimating changes in the probability density function for ice thickness.

Ice ridges are commonly identified in ULS ice draft data using the Rayleigh criterion, which specifies that an independent ridge is present when the troughs on either side of the keel crest descend halfway to the local level ice surface (Wadhams & Horne, 1980). This criterion helps to distinguish large ridges with multiple local peaks from multiple individual ridges. Prior to conducting further analysis on the identified ridges, it is customary to exclude ridges with more shallow drafts to ensure that only mechanically grown ice is included in the ridge identification process.

Probabilistic estimation of extreme ridge keel draft can be achieved by fitting a probability distribution function to the extracted ridge keel draft data. Previous studies of ridges from ULS data suggest that the exponential distribution is well-suited for representing the distribution of ridge keel drafts (Melling et al., 1995; Wadhams, 1983, 2000). Alternative distributions, such as the Weibull distribution (Ross et al., 2012) and the generalized Pareto distribution (GPD) (Ekeberg et al., 2013), have also been used. However, research by Ross et al. (2012) showed that the Weibull distribution's shape parameter is close to 1, which makes it equivalent to the exponential distribution. Similarly, the study by Ekeberg et al. (2013) found that the GPD's shape parameter is nearly zero, which results in the GPD being equivalent to the exponential distribution. The advantage of the exponential distribution is that it requires only one parameter, making it useful for establishing relationships with other parameters, such as level ice thickness. This is the primary reason the exponential distribution is favoured in the research of this thesis, alongside its good fit to the ridge draft distribution.

4.2. Ridge frequency

The ridge frequency is a key parameter that characterizes the number of ridges in an ice field, and it is typically quantified in the spatial domain. However, it can also be expressed in terms of ridge spacing, which is the distance between two adjacent ridges. Alternatively, assuming the availability of ice drift speed and ice concentration data, ridge frequency can be transformed from the spatial to the temporal domain. Ridge frequency in the temporal domain can also be directly obtained from stationary sonar measurements. In the context of probabilistic

assessment of ridge loads, temporal-domain ridge frequency is particularly important because it is a crucial input for simulations. Specifically, a higher number of ridges interacting with a structure result in a deeper ridge for a fixed return period. Therefore, accurate estimation of the temporal-domain ridge frequency is essential for predicting the extreme ridge loads that a structure may encounter.

Ridge frequency in seasonal ice is influenced by numerous factors, including time, wind, currents, and local conditions. During the initial stages of ice formation, no ridges are present. However, as the season progresses, ridges begin to form due to deformation caused by the combined effects of wind and currents. The number of ridges generally increases over time, but the rate of increase varies depending on location and prevailing environmental conditions. For example, in areas with stronger winds and frequent storms, more ridges may form at a faster rate. Ridge frequency is site-specific and can be influenced by factors such as the dynamics of ice motion and boundary conditions (e.g., proximity to shore or other obstacles).

Early research on the distribution of ice ridge spacing showed that a negative exponential distribution was a suitable model (Mock et al., 1972). However, subsequent studies revealed that a two-parameter log-normal distribution provides a better fit (Lensu, 2003; Lewis et al., 1993; Wadhams & Davy, 1986). The relationship between ridge frequency and other ridge parameters has also been studied, primarily focusing on the relationship between ridge frequency and ridge keel draft or sail height. Dierking (1995) reported a linear relationship between mean ridge height and ridge frequency, whereas Tan et al. (2012) indicated that a logarithmic relationship could also be appropriate in some cases. For ridge load calculations, the relationship between ridge frequency and keel draft is more critical. Hibler III et al. (1972) observed a linear relationship between these two parameters and suggested that the positive correlation is stronger in offshore regions than in the central Arctic basin. This positive correlation was confirmed by Wadhams et al. (2011).

As stated earlier, the ridge count in an ice field tends to rise throughout the season. An example of such seasonal development was reported in Samardžija and Høyland (2023), where the weekly number of ridges passing above sonars in the Beaufort Sea is reported (Figure 4.1). It should be noted that the data shown in this figure encompasses both first-year and multi-year ice, which explains the presence of datapoints with a high number of ridges in the early winter season. Additionally, it is worth noting that the high variability in the data is mainly caused by the variation in ice drift speed.

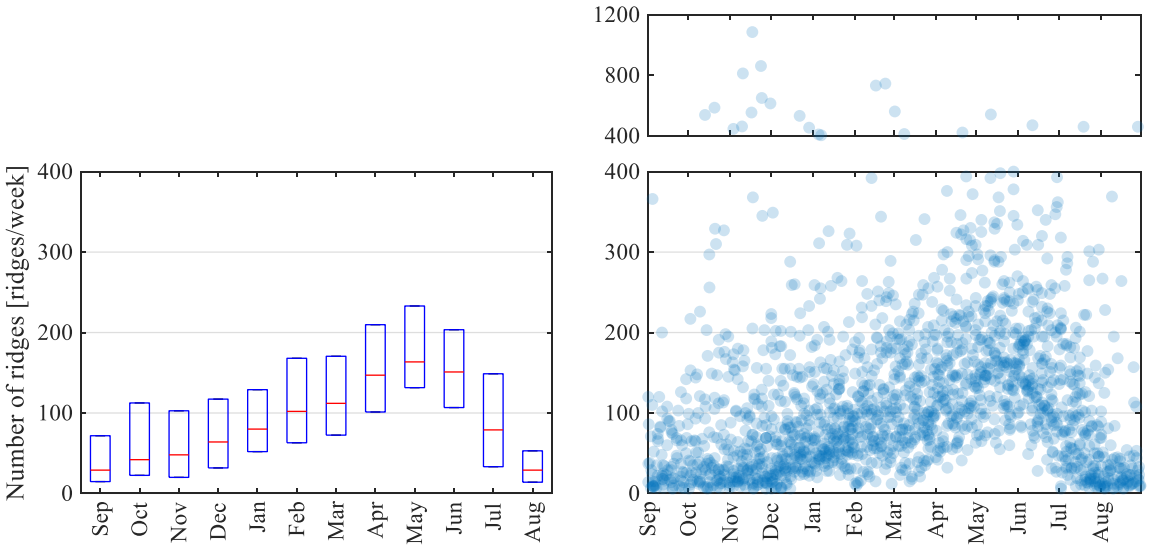

Figure 4.1 From Samardžija and Høyland (2023): Seasonal development of the weekly number of ridges. The left panel shows the median indicated with red lines, with the 25th and 75th percentile indicated with the bottom and top edges of the boxes, respectively. The right panel shows a scatter plot, where each analysed week is represented with an individual circle. The right panel is divided into two parts, allowing for a more detailed inspection of the seasonal development.

The fact that level ice also grows throughout the season makes the ridge frequency indirectly correlated to the level ice thickness. A direct causal relationship between level ice thickness and ridge frequency is less obvious, and, to the author's knowledge, not reported in the literature. While there may be a causal relationship between ice thickness and ridge frequency, it is complex and multifaceted, requiring further study and investigation for full understanding. One potential explanation is that thicker ice, which is more variable due to the opening and refreezing of leads, exerts greater pressure on surrounding ice as it moves, resulting in more frequent formation of ice ridges. In contrast, thinner ice exerts less pressure and may produce fewer or less pronounced ridges.

In Samardžija and Høyland (2023), a probabilistic simulation technique is given where temporal ridge frequency and ridge keel draft are simulated directly from level ice thickness. For this purpose, the relationship between level ice draft (closely related to level ice thickness) and ridge frequency is analysed (Figure 4.2). As in the case of Figure 4.1, the primary cause of variability in the weekly ridge count is due to differences in ice drift speed. A positive correlation is found, and a power function is fitted that is of practical use in the probabilistic simulation of ridge frequency. The simulation is further elaborated in Chapter 6.

It is important to note that alternative simulation techniques are possible. For example, one could establish a relationship between level ice thickness and spatial ridge frequency, then transform the spatial frequency into temporal frequency using ice drift speed and ice concentration. Another approach would be to use the relationship between keel draft and spatial ridge frequency, which is a relationship that is commonly studied and has a more direct causal relationship. However, the authors found that these alternative simulation techniques resulted in substantially less accurate results, with the seasonality of important variables critically impaired.

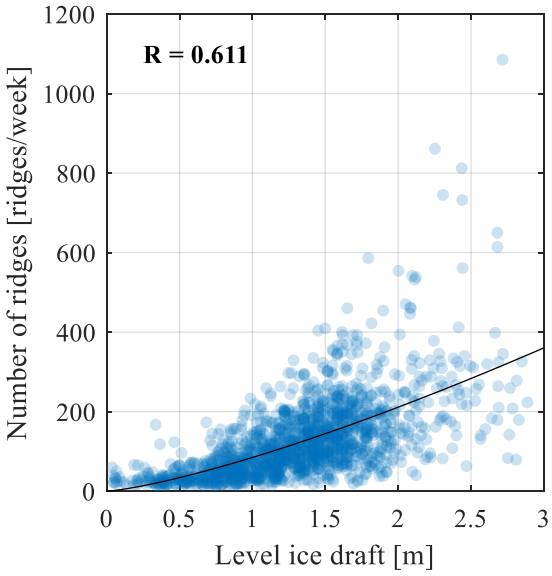

Figure 4.2 From Samardžija and Høyland (2023): Relationship between level ice draft and the weekly number of ridges. The solid line represents a fitted power function of the type $y = a_3 \cdot x^{b_3}$ ($a_3 = 84.69$; $b_3 = 1.318$). R is the Pearson correlation coefficient for the two parameters.

4.3. Ridge keel draft

The calculation of the rubble component of the total ridge load requires determining the thickness of the rubble layer beneath the consolidated layer. This is obtained by subtracting the consolidated layer thickness from the ridge keel draft. It has been customary practice in the past to analyse the extreme keel drafts by fitting probability distribution functions to data from stationary sonar measurements or submarine sonar measurements over extended periods of time or over long distances (e.g., Ekeberg et al. (2012); Wadhams (2012)). In the study of this thesis, however, the focus is on simulating the keel draft for all ridges, not just estimating the deepest ones. In addition, the simulated ridge keel draft should maintain its relationship to other key variables. Therefore, it is of interest to investigate the relationship between the level ice thickness and the ridge keel draft.

Researchers have found a correlation between level ice thickness and ridge keel draft, with ice strength and level ice thickness being key factors governing this relationship between the two variables. A physical modelling study by Parmerter and Coon (1972) confirmed this relationship. Tucker and Govoni (1981) reported in a field study of 30 ridges that sail heights scale with the square root of level ice thickness. Furthermore, it is worth noting that sail height is closely related to the keel draft (Strub-Klein & Sudom, 2012; Timco & Burden, 1997)

In his work, Hopkins (1998) used a two-dimensional particle model to illustrate the ridging pressure of ice. This model subdivides the ridging process into four distinct stages, derived from the results of the simulation. The first stage begins with an intact sheet of relatively thinner lead ice impacting a thicker floe and ends when the maximum sail volume is reached. The second stage involves the deepening and broadening of the ridge keel, which ends when the maximum keel draft is reached. The third stage involves leadward growth, creating a rubble field of approximately uniform thickness, which ends when the intact sheet of lead ice is depleted. The fourth stage involves the compression of the rubble field between floes.

The formation of a deep ridge requires the fulfilment of certain conditions, including an adequate supply of contiguous level ice, wind, and current stresses strong enough to cause failure of the ice, and a critical stress duration that is sufficient to complete the ridge-building process. It is uncommon for all these conditions to be met. As a result, a ridge typically fails to achieve its full size for the given level of ice thickness consumed during its construction. Assuming that the mentioned conditions are met, the maximum keel draft will be governed by the buckling strength of the level ice, which has a square-root relationship with the thickness of the level ice.

Empirical relationships between ridge keels and adjacent level ice have been established in studies by other authors, but they are inadequate for use in probabilistic simulations where all ridges need to be simulated. Amundrud et al. (2004) report an upper bound to the keel draft that can be modelled with a square-root function of the adjacent level ice thickness. Hibler (1980), Hopkins (1994, 1998), Melling and Riedel (1996) and Mudge et al. (2013) proposed a similar truncation curve.

Metzger et al. (2021) suggest that the maximum draft of a ridge is not necessarily limited by the parent ice thickness, and keels of any size may be possible if there is sufficient convergence to create enough rubble. This view is based on the analysis of ridge geometry from sonar ice draft data. This contradiction, compared to other studies mentioned above, highlights the difficulty in establishing the relationship between the two parameters solely through phenomenological studies and supports the need for establishing an empirical relationship from direct data analysis.

The most natural approach to analysing these parameters is to examine them as they arrive at a specific location (above a sonar), since this is the same as what the structure experiences. By doing so, probability distributions and relationships derived from the analysis can be directly implemented in a probabilistic simulation without additional transformation that may introduce errors.

In our study (Samardžija & Høyland, 2023), we conducted a similar analysis to that in Amundrud et al. (2004)-Figure 5, comparing the relationship between the level ice draft and the weekly deepest keel draft (Figure 4.3). However, it is important to note the differences between our study and Amundrud's. Firstly, there is an obvious difference in the keel draft, with ours being the deepest keel of one week, while Amundrud's is the deepest keel of 50 km transects. Although the mean length of weekly transects was longer at 61.8 km in our study, the transect lengths exhibited significant variability due to variations in ice drift speed, resulting in a wider scatter in the vertical direction (keel draft). Shorter transects would result in a shallower weekly deepest ridge and deeper ridges for the longer transects. Secondly, in Amundrud's study, the level ice draft was the adjacent level ice, while in ours, it represented the deepest level ice thickness mode present in the field, typically representing the level ice growing from the start of the season or occasionally multi-year ice. Therefore, the level ice draft in our study is typically equal to or greater than the adjacent level ice, leading to points being shifted towards the right when compared to Amundrud's study.

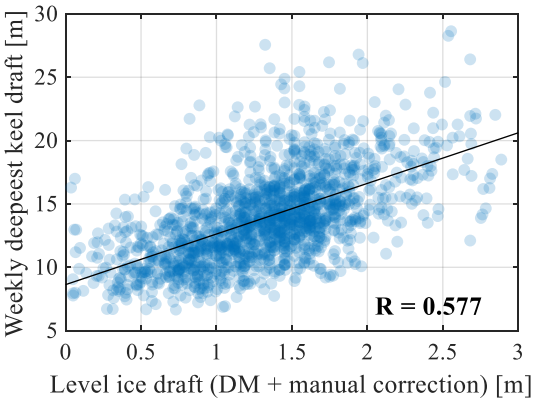

Figure 4.3 From Samardžija and Høyland (2023): Relationship between level ice and weekly deepest keel draft. The solid line represents a regression obtained by least-squares approximation (intercept $a_1 = 8.63$; slope $b_1 = 3.99$). *R* is the Pearson correlation coefficient for the two parameters.

In the Samardžija and Høyland (2023) study, we analysed the relationship between the weekly deepest keels and level ice draft to simulate only the deep ridges (not all ridges). This simulation is particularly useful for designing seabed installations that may be susceptible to damage from deep ridges. Additionally, to simulate all ridges, we investigated the relationship between level ice draft and the mean ridge keel draft, as shown in Figure 4.4.

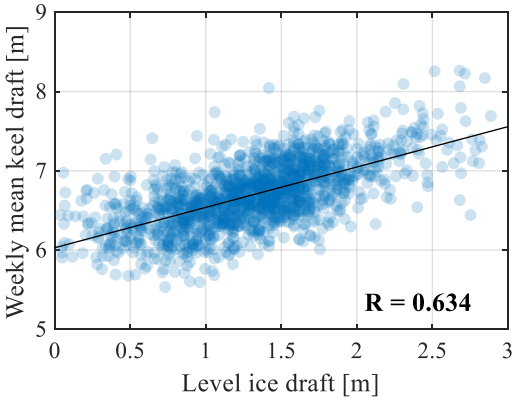

Figure 4.4 From Samardžija and Høyland (2023): Relationship between level ice and weekly mean keel draft. The solid line represents a linear regression obtained by least-squares approximation (intercept $a_2 = 6.03$; slope $b_2 = 0.51$). *R* is the Pearson correlation coefficient for the two parameters.

It is crucial to note the caveat regarding the relationship between level ice and keel draft presented in the study by Samardžija and Høyland (2023). The relationship found is between present level ice and present ridges, not between the level ice that formed the ridges, making the causal relationship in this study unclear. Although thicker level ice is expected to create deeper ridges due to the mechanical principles of ridge building processes, it is also true that level ice is thicker towards the end of the ice growth period, allowing more time for deep ridges to form. However, it should be noted that the mean ridge keel draft of present ridges does

increase during the season (Figure 4.5), indicating that the mean keel draft of newly-formed ridges must also increase. Further elaboration on this aspect can be found in Chapter 5 of the thesis.

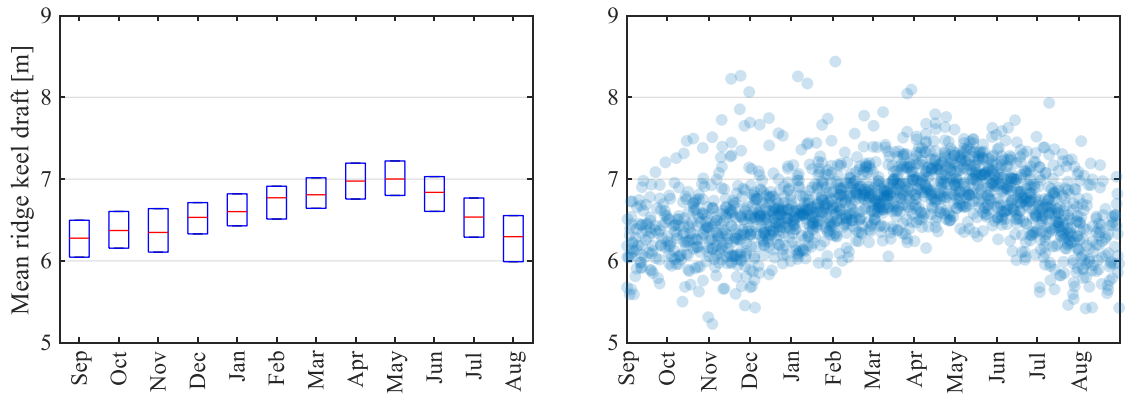

Figure 4.5 From Samardžija and Høyland (2023): Seasonal development of weekly mean keel draft. Left panel: Monthly median indicated with red lines with 25th and 75th percentiles indicated with the bottom and top edges of the boxes, respectively. The right panel shows a scatter plot where each analysed week is represented with an individual circle.

Our analysis of the relationship between level ice draft and weekly ridge keel draft employs a temporal sampling technique, where each data point represents a subsample determined by a week-long time unit. This approach contrasts with the more commonly used spatial subsampling technique, where each data point represents a subsample defined by a spatial unit, such as a 50 km long profile. The choice of sampling technique results in subtle but significant qualitative differences in the relationship between level ice and ridge keel draft. For instance, with spatial sampling, the general relationship between maximum keel draft and surrounding level ice thickness typically exhibits a square root shape. In contrast, our temporal sampling approach reveals a linear relationship between mean keel draft and surrounding level ice thickness(Figure 4.4). When performing a probabilistic simulation of ridge keel draft, where the correlation with the level ice draft is retained, it is essential to be aware of this difference. Careful interpretation of this correlation is essential when applying it to probabilistic simulation.

This chapter has elucidated the correlation analysis between the thickness of level ice and ridge statistics, including their draft and frequency. Based on these correlations, it becomes feasible to simulate the evolution of all ridges over the course of a season. The relationship between the thickness of level ice and both keel draft and ridge frequency can be directly maintained in the simulation. Additionally, the indirect relationship between keel draft and ridge frequency can also be preserved. Chapter 6 provides details on the simulation technique. Prior to this, Chapter 5 delves into a study on how the inner-seasonal development of ridge statistics can be used to draw conclusions about the seasonal evolution of the consolidated layer thickness.

5. Consolidated layer thickness in probabilistic simulation of first-year ice ridges

Gathering data on the thickness of consolidated layer in first-year ice ridges is challenging due to the significant expenses and complexities of field measurements. The current data pool is confined to specific regions and is primarily collected at the end of the season. This may introduce a bias towards older and larger ridges. This chapter introduces a method for incorporating consolidated layer thickness into a probabilistic simulation framework for first-year ice ridges. This method, detailed in Samardžija et al. (2023a), is presented here in a more comprehensible manner, simplifying the mathematical explanations. For further details, the reader is referred to the original paper.

The primary objective of this study was to examine the potential correlation between consolidated layer thickness and ridge keel draft, which has traditionally been assumed to be uncorrelated (ISO 19906, 2019, p. 217; Løset et al., 2006, p. 115; Timco and Burden, 1997).

The research focuses exclusively on first-year ice ridges. The characterization and mathematical modelling of the consolidation process in older ridges are considerably more intricate than for first-year ice ridges. This complexity arises from a less comprehensive understanding of the decay phase during the transition from a first-year ridge to a second-year ridge (Shestov et al., 2018; Shestov & Marchenko, 2016).

To simulate all ridges interacting with a structure during a season, one can use the relationship between level ice thickness and ridge keel draft and frequency described in the previous chapter. However, the challenge is to simulate the consolidated layer for these ridges. This requires making certain assumptions about the growth of the consolidated layer, and ultimately determining the age of the ridges and the start of the consolidation process.

In the following subchapters, we will explore how to construct a probability distribution function (PDF) for ridge formation time, which can be transferred to the ridge age for any ridge in a simulation, given its draft and time of arrival at a structure. Initially, we assume that the PDF is entirely random (uniform).Then, we will analyse how the seasonality of ridge creation rate and the mean draft of created ridges individually influence this PDF. Finally, we will examine the combined effect of both factors.

5.1. Statistical features of ridge creation time

Assuming a specific ridge keel draft and a predetermined interaction time with a structure during the season, one might initially presume that the probability of ridge formation is equally distributed from the season's onset until the interaction time. This assumption would be valid if both the ridge creation rate and the probability distribution of the ridge keel draft for the created ridges remained constant throughout the season. Consequently, in such a scenario, the probability distribution for ridge formation would closely resemble the pattern illustrated in Figure 5.1. By leveraging this function, one could simulate the thickness of the consolidated layers by probabilistically sampling the creation time (i.e., age) of the ridges. Thereafter, the thickness could be approximated by implementing a growth formula for the consolidated layer.

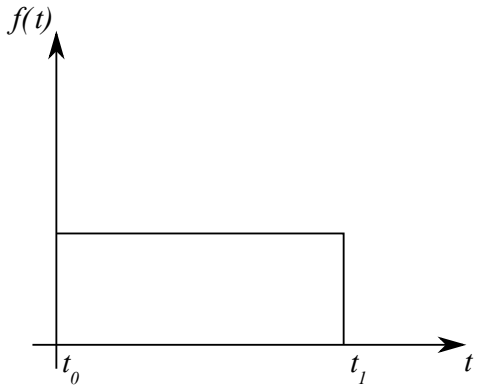

Figure 5.1 Qualitative illustration of a uniform probability density function for ridge creation time. The horizontal axis represents time during a winter season.

However, it is important to note that neither the ridge creation rate nor the probability distribution of the draft for the newly formed ridges remains constant throughout the season.

5.2. Seasonality of ridge formation and the implications for ridge creation probability

First, let us consider the rate of ridge creation. At the beginning of a season, the ice is too thin to support ridging. However, as time progresses, ridge production intensifies, reaching a peak within the season. After this peak in production, ridge creation starts to slow down and eventually stops as the winter ends, marked by the ice breaking up. It is important to note that these observations reflect average trends over multiple seasons. In any particular season, the pattern can differ significantly, with peak production occurring at unpredictable times, often following storm events.

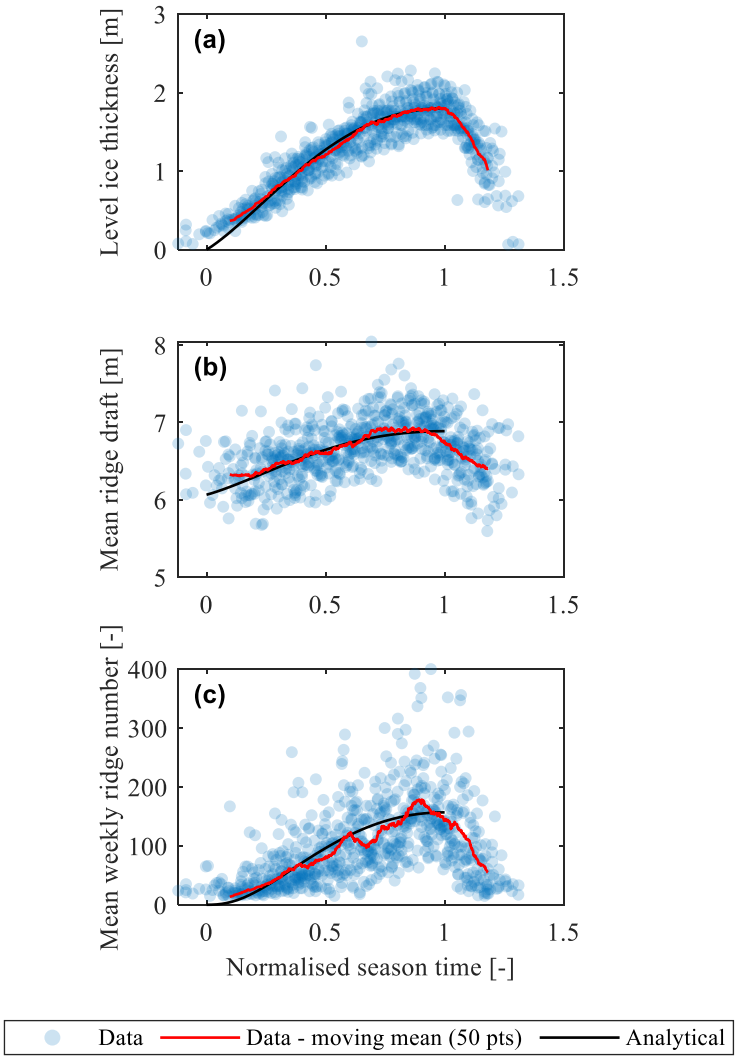

Figure 5.2 From Samardžija et al. (2023a): Blue points represent the weekly measured level ice thickness, mean ridge keel draft and mean weekly number of ridges passing a sonar. A detailed derivation of the analytical curves represented by the black lines is given in the referenced paper.

To gather insights into the inter-seasonal variations of ridge production rates, it is beneficial to analyse the weekly count of ridges passing above a sonar throughout a season. This aspect is demonstrated in Figure 5.2-c, utilizing data from the Beaufort Sea. It is noteworthy that only those seasons characterized predominantly by first-year ice are considered, while those with a noticeable presence of multi-year ice have been filtered out.

By calculating the time derivative of the weekly ridge count, we can estimate the ridge creation rate, as depicted in Figure 5.3. It is important to note that the number of ridges passing a sonar is directly linked to the ice drift speed, which is not uniform throughout a season. This aspect has been neglected in the derivation for the sake of simplification.

Additionally, it is worth highlighting that the ridge production rate, as presented in this figure, lacks a spatial dimension, i.e., it does not specify how many ridges are created within a particular area during a week. Nevertheless, this metric proves valuable in our pursuit to understand the relative variations in ridge production at different points in the season.

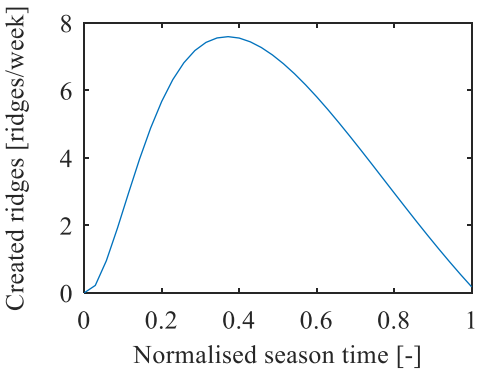

Figure 5.3 From Samardžija et al. (2023a): Seasonal development of the weekly ridge creation rate.

Let us observe how the ridge creation rate influences the initially presumed uniform probability density function (PDF) of the ridge creation time. The probability of a ridge being created is directly related to the ridge creation rate. This is a reasonable assumption, as it is more likely for a ridge to be created during the part of the season when more ridges are created. In the following example, we will examine a scenario where a ridge interacts with a structure at a normalized season time $t = 0.6$. Here, the normalization of season time is relative to the commencement of ice melting, where the onset of ice growth is denoted as zero, and the initiation of ice melting as one.

In qualitative terms, the PDF for the time of ridge creation would resemble the curve shown in Figure 5.4 (directly proportional to the ridge creation rate shown in Figure 5.3). The probability of ridge formation increases in the first part of a season. This gradual increase, rather than a sudden spike, can be rationalized by the previously discussed averaging over multiple seasons. The probability of ridge formation reaches a peak at some point in the season and then gradually decreases to zero towards the end of the season.

It should be noted that the function's characteristics bear the imprint of previous assumptions and mathematical formulations. A notable outcome is the ridge creation rate hitting zero at the season's end, which contradicts reality, as ridges can form towards the latter part of the ice growth season and even after the onset of ice melting. This effect is a consequence of the analytical model choice for the seasonal development of level ice thickness (Figure 5.2-a). The analytical model for the weekly average ridge count (Figure 5.2-c) is derived from the level ice thickness model, building on the correlation between these two parameters. This transformation leads to a model for the weekly average ridge count that, much like the model for the level ice thickness, reaches a first derivative equal to zero at the season's end, resulting in a zero ridge production rate. This aspect highlights a potential area for enhancement in the current model. A possible improvement would involve conducting a direct evaluation of the ridge creation rate for each individual season, rather than deriving the ridge creation rate based on the averaged seasonal curve for the ridge numbers. Alternatively, modelling the seasonal evolution of level ice thickness with a function that does not have a first derivative equal to zero at the end of the season could solve this problem.

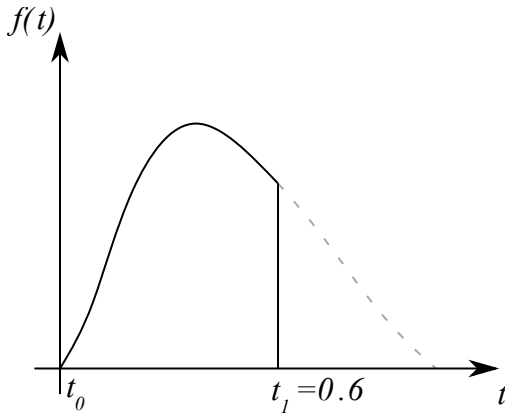

Figure 5.4 Qualitative illustration of a PDF for ridge creation time that is proportional to the ridge creation rate. The horizontal axis represents time during a winter season. The solid line represents a PDF for a ridge created at normalized season time $t_1 = 0.6$. The dashed line illustrates what the function would look like over the entire season.

5.3. Seasonality of ridge keel draft and the implications ridge creation probability

Let us now examine the impact of seasonal variations in average keel draft on the timing of ridge formation. As shown in Figure 5.2-b, there is a notable increase in the average keel draft of the present ridges throughout the season. This suggests that the average keel draft of the newly formed ridges must also follow a similar upward trend. The average keel draft of the ridge population can only increase if ridges deeper than the existing ones are incorporated. With the knowledge of the evolving average keel draft of current ridges and the rate of ridge production, we can quantify the seasonal progression of the average keel draft for the created ridges. This concept is illustrated in Figure 5.5.

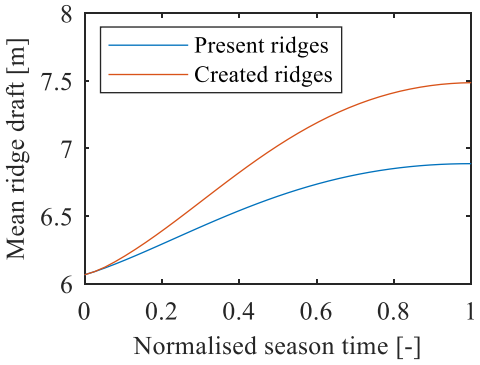

Figure 5.5 From Samardžija et al. (2023a): Comparison of the seasonal development of the mean ridge keel draft of ridges present in the ice field and newly created ridges.

In the forthcoming example, we will study two ridges that arrive at the structure at a standardized seasonal time of $t = 0.6$. The two ridges have respective ridge keel drafts of $H_{k,1} = 5.5$ m and $H_{k,2} = 8.0$ m. Figure 5.6-a depicts how the mean ridge keel draft of created ridges evolves during a season. Furthermore, Figure 5.6-b presents three examples of keel draft PDFs for ridges created at various seasonal stages. Focusing on the ridge with a keel draft of $H_{k,1} = 5.5$ m, reveals that the probability of a newly formed ridge having this draft diminishes as the season progresses (Figure 5.6-c). In contrast, the probability increases for the ridge with

a keel draft of $H_{k,2} = 8.0$ m. The overall pattern suggests that ridges with a deeper draft have a relatively higher probability of formation during the later parts of the season. Functions presented in Figure 5.6-c answer the question "What is the probability for a ridge to be created with a ridge draft $H = x$ at time $t = y$?"

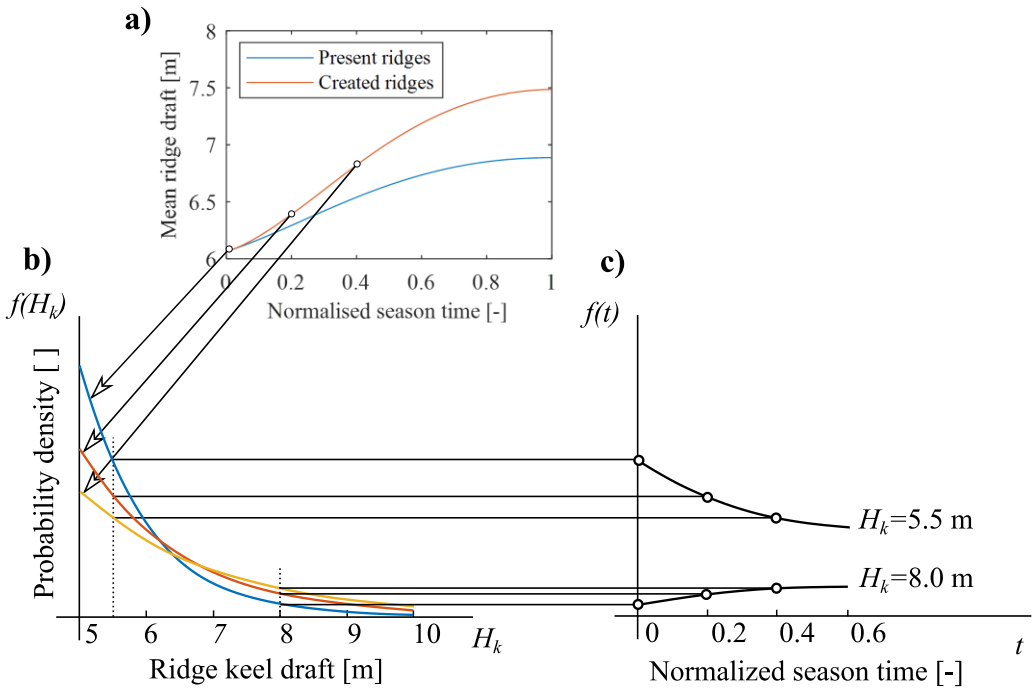

Figure 5.6 **a)** Comparison of the seasonal development of the mean ridge keel draft of ridges present in the ice field and newly created ridges for one week. **b)** Probability density functions for the keel draft of a ridge formed at three distinct periods within a season, with corresponding mean keel drafts indicated as $f(H_k(t = 0) = 6.1)$, $f(H_k(t = 0.2) = 6.4)$ and $f(H_k(t = 0.6) = 6.8)$. **c)** Shape of the probability density function for ridge creation time for two ridges that interact with a structure at season normalized time $t = 0.6$ with keel drafts equal of $H_{k,1} = 5.5\ m$ and $H_{k,2} = 8.0\ m$.

5.4. Combined implications of ridge formation rate and keel draft seasonality on the ridge creation probability

We now turn our attention to the cumulative effect of the ridge formation rate and the mean keel draft seasonality on the ridge creation probability. Figure 5.7 depicts the relative likelihood functions associated with ridges of diverse drafts. All ridges reach their structure by the end of the season, denoted as t=1.0. These functions are normalized based on their respective maximum likelihood peaks. Alternatively, the functions can be normalized such that the area under the curve equals one. In doing so, we derive a formal Probability Density Function (PDF) for the ridge formation time, which can subsequently be employed for probabilistic modelling of ridge formation time.

This PDF can be generated for any ridge based on its given draft and time of arrival at the structure. The PDF can then be utilized to simulate both the ridge creation time and the ridge's age. The ridge age can subsequently be incorporated into a consolidated layer growth formula to determine the consolidated layer thickness. In Samardžija et al. (2023a), a simple expression

was adopted, assuming a growth rate double that of the level ice. More sophisticated formulations can also be implemented.

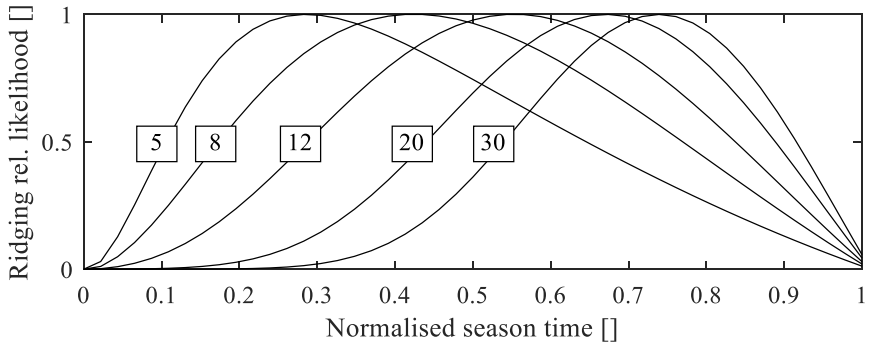

Figure 5.7 From Samardžija et al. (2023a): Relative ridging likelihood functions for five distinct ridges that approach a structure at time $t_a = 1$, coinciding with the peak of ice growth. Drafts of these ridges are denoted by numerals within the squares. The depicted trend reveals that ridges with shallower keels tend to originate in the early phases, while ridges characterized by deeper keels predominantly form during the latter portions of the season.

5.5. Results

Figure 5.8 showcases the results of a simulation implementing the methodology described above for simulating consolidated layer thickness (Samardzija et al., 2023). This simulation spanned 10,000 seasons and incorporated a total of 30,375,508 ridges. As anticipated, the simulation results demonstrated a negative correlation between the consolidated layer thickness and ridge keel draft: an increase in consolidated layer thickness was associated with a reduction in ridge keel draft. Ridges that form earlier in the season, being shallower, have more time to develop a consolidated layer. In contrast, deeper ridges, which form later in the season, may not have sufficient time for this process, elucidating the observed negative correlation. This line of thought echoes the findings of Brown et al. (2001), who identified two 'typical' classes of extreme ridges: those with deep keels paired with a relatively thin consolidated layer, and those with shallow keels coupled with a more substantial consolidated layer.

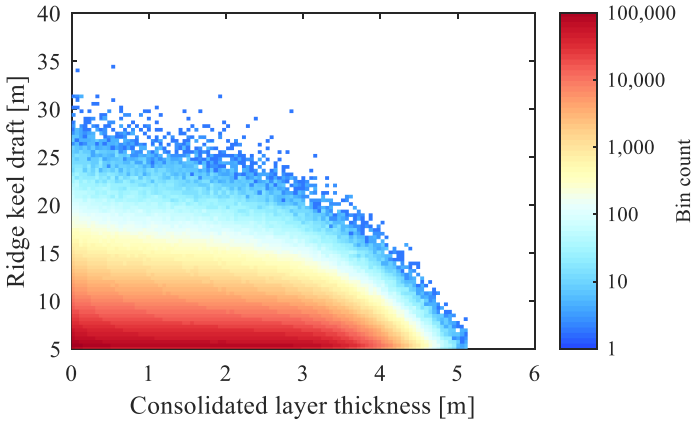

Figure 5.8 From Samardžija et al. (2023a): Bivariate intensity plot illustrating the relationship between consolidated layer thickness and ridge keel draft. It is important to note that the ridges depicted in this plot represent all simulated ridges that reached the specified location over the course of the simulated winter seasons.

Figure 5.9 aims to clarify the negative correlation between consolidated layer thickness and keel draft using two example ridges. Ridge "A", which forms early in the season, has a shallow keel. This is attributed to the positive relationship between the thickness of the surrounding level ice and the mean keel draft of the ridges that form. By the season's end, Ridge "A" develops a thick consolidated layer due to its early formation. Conversely, Ridge "B" forms mid-season and has a deeper keel because the surrounding level ice is thicker at that time. However, it has a thinner consolidated layer than Ridge "A" due to its later formation and the shorter time available for consolidation.

An important observation is that, when averaged over all ridges at the end of the season, both the consolidated layer and keel draft reach their maximum values However, when examining individual ridges, those with deeper drafts tend to have thinner consolidated layers.

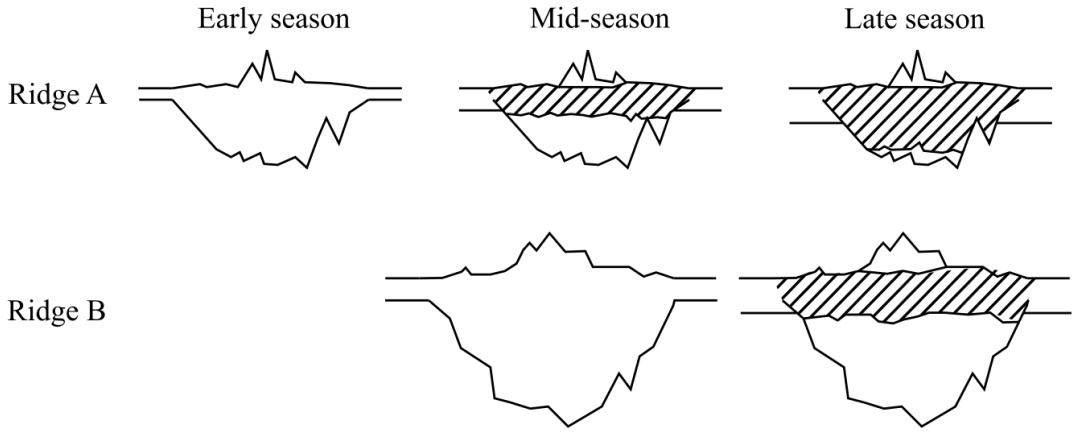

Figure 5.9 From Samardžija et al. (2023a): Comparison of ridges based on formation time: early-season (Ridge A) and mid-season (Ridge B). The hatched section indicates the consolidated layer. Ridge A showcases an older first-year ridge with a thick consolidated layer and a shallow keel. In contrast, Ridge B represents a younger first-year ridge, characterized by a thinner consolidated layer and a deeper keel.

In this study, a central assumption is that the ridge keel draft remains constant after formation. However, two key phenomena can modify the keel draft after its creation.

Firstly, re-ridging can deepen the keel. The existing literature provides limited insights on this, leaving questions about its occurrence frequency and the extent of the subsequent depth increase. If re-ridging is common, it could weaken the observed negative correlation between consolidated layer thickness and ridge keel draft. For example, a shallow ridge initially forms, it develops a significant consolidated layer, and then undergoes late-season re-ridging, resulting in a deeper keel. This dynamic mechanism might account for deep ridges with thick consolidated layers.

The second factor is the reduction in ridge keel draft due to thermal degradation influenced by oceanic heat flux, rubble packing, and the mechanical breakdown of rubble, as discussed in Ervik et al. (2018) and Leppäranta et al. (1995). Increased oceanic heat flux, particularly in warmer regions or those experiencing oceanic warming, could intensify this degradation. Consequently, the negative correlation between the thickness of the consolidated layer and ridge keel draft becomes more pronounced, as a deep ridge arriving late in the season would be less likely to have developed early. Figure 17 illustrates the impact of the presumed ridge keel reduction rate on the relative likelihood function of the ridging.

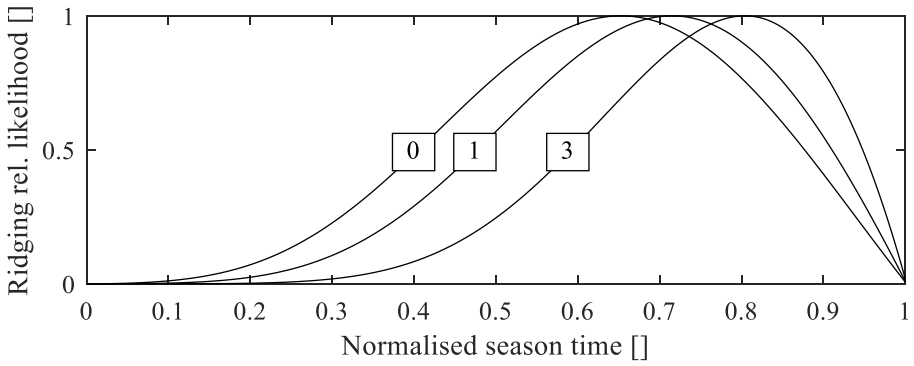

Figure 5.10 From Samardžija et al. (2023a): Comparison of ridging likelihood for a 20 m draft ridge arriving at time $t_a = 1$ (ice growth peak). The three distinct lines represent varied ridge keel reduction rates, as denoted by the values within the squares (0, 1, and 3 cm/day). These rates can mimic differences in oceanic heat flux, with elevated rates reflecting greater heat flux scenarios.

This study indicates a negative relationship between the consolidated layer thickness and the keel draft. Nonetheless, these findings warrant additional verification. The lack of comprehensive and unbiased data covering entire seasons restricts definitive validation. Emerging tools, such as satellite measurements, may offer the extensive datasets required for this purpose. Currently, conclusions drawn from this research can only be validated to a limited extent by expert judgment.

It is important to note that the analyses in this and the preceding chapter rely on measurements taken from the Beaufort Sea. The recommended methodology necessitates validation and recalibration when applied to other locations. However, it is suitable for preliminary evaluations of ice ridge loads, even in areas lacking data. The subsequent chapter will illustrate this through a probabilistic simulation of ice loads on a hypothetical structure in the Baltic Sea.

6. Probabilistic assessment of first-year ice ridge loads on offshore structures

There exists a variety of methodologies for the probabilistic simulation of ice actions, as exemplified by the works of Nessim and Jordaan (1991), Timco and Frederking (2004), Jordaan et al. (2011), and Thijssen et al. (2014). The choice of a specific approach often depends on factors such as data availability, the type of offshore structure, ice feature characteristics, the formula used for calculating ice action, and the desired results. Given a consistent set of these conditions, a designer has numerous options when formulating a probabilistic simulation scheme for ice actions. It is essential to understand that the probabilistic model for ridge actions proposed in this chapter represents one of many potential approaches.

This chapter provides an overview of the probabilistic model designed for estimating first-year ice ridge loads on a fixed structure, as detailed in Samardzija et al. (2023b). Key elements of this model are rooted in methodologies introduced in Chapters 4 and 5:

- Chapter 4 (Samardžija & Høyland, 2023): Simulation technique for ice ridge frequency and ridge keel draft based on the level ice thickness data.
- Chapter 5 (Samardžija et al., 2023a): Simulation technique for the consolidated layer thickness.

The present chapter, which is a summary of the research presented in Samardžija et al. (2023b), combines these prior studies and provides the necessary details for the probabilistic model of ice ridge loads. It should be noted that this model does not introduce novel innovations as such; rather, it serves as a demonstration of how prior research findings can be integrated into a probabilistic ridge load model.

The hypothetical case study utilizes a structure inspired by the Norströmsgrund lighthouse located in the Baltic Sea. While the actual lighthouse features a stepwise widening cylindrical shape, the hypothetical structure in the case study retains a consistent diameter of 7.2 m. Its location is identical to the coordinates of the Norströmsgrund lighthouse (65° 6' N, 22 ° 19' E), with environmental inputs derived from the same.

6.1. Simulation procedure

Ridge loads are calculated based on the ISO 19906 standard approach. The formulas can be found in both Samardžija et al. (2023b) and Section 3.2 of this thesis; hence, they are not reiterated in this section.

Table 6.1 provides an overview of the input variables for the calculation. These input variables can be categorized into three types: deterministic, uncorrelated random, and correlated random variables. Those labelled as "PDF" in the table are uncorrelated random variables, signifying that they are sourced directly from probability distribution functions. On the other hand, variables labelled as "Simulated" are correlated random variables, which involve more intricate simulation processes. The simulation methods for these variables have been outlined in Chapters 4 and 5 and are described in detail in Samardžija and Høyland (2023) and Samardžija et al. (2023a).

Table 6.1. Overview of the input variables.

Variable			Type	Information
Structure width	w	[m]	Deterministic	7.2
Water density	ρ_{w}	[kg/m^3]	Deterministic	1005
Ice density	ρ_{i}	[kg/m^3]	Deterministic	910
Apparent keel cohesion	c	[kPa]	PDF	Uniform dist. [5; 7]
Angle of internal friction	ϕ	[°].	PDF	Uniform dist. [20; 40]
Keel macroporosity	e	[-]	PDF	Uniform dist. [0.2; 0.5]
Coefficient	C_{R}	[MPa]	PDF	Gamma dist. [10.1; 0.07]
Level ice thickness	h	[m]	Simulated	
Ridge keel draft	H_{k}	[m]	Simulated	Unconsolidated keel layer: $h_{\mathrm{k}} = H_{\mathrm{k}} - h_{\mathrm{c}}$
Consolidated layer thickness	h_{c}	[m]	Simulated	
Ice ridge width	D	[m]	Simulated	
Season length		[weeks]	Simulated	

For a comprehensive understanding of the simulation procedure, it is beneficial to visualize the process. The flowchart presented in Figure 6.1 summarizes this procedure, delineating each step to offer a clearer perspective of how the variables interrelate and shape the results. In addition to the flowchart, the simulation procedure is described in a step-by-step manner presented below.

Simulation procedure steps:

1. **Annual maximum level ice thickness simulation:** The process begins by simulating the maximum annual level ice thickness. This variable serves a dual purpose – it not only provides a value for ice thickness but also acts as an indicator of the severity of the ice season.
2. **Weekly ice thickness simulation:** Once the annual thickness is simulated, the simulation further refines this variable, deducing the level ice thickness for each week of the ice season.
3. **Simulating ridge parameters based on weekly level ice thickness:**
    - For every week, the procedure simulates the mean ridge keel draft, denoted by $\bar{H}_{\mathrm{k,i}}$, and the weekly number of ridges, N_{i}. These are determined by accounting for correlation to the respective week's level ice thickness.

- For each week, ridges are generated, equalling the number N_i. The simulation of ridge drafts follows an exponential distribution, where the mean parameter is $\bar{H}_{k,i}$.

4. **Consolidated layer thickness calculation:** Every ridge's time of arrival and its keel are used as inputs in the simulation of its age. Based on the simulated age of the ridge, the thickness of the consolidated layer is calculated.
5. **Variable implementation:** Three sets of variables come into play at this step:
   - **Deterministic variables:** These variables remain consistent for all individual ridges.
   - **Uncorrelated variables:** These are variables which, for every individual ridge, are simulated directly from the associated PDFs.
   - **Correlated variables:** These variables are simulated with more advanced simulation techniques where more steps are taken in the simulation.
6. **Calculation of ridge action:** Employing all the variables and information derived from the preceding steps, the ridge action for each individual ridge is computed using the ridge action formulation.

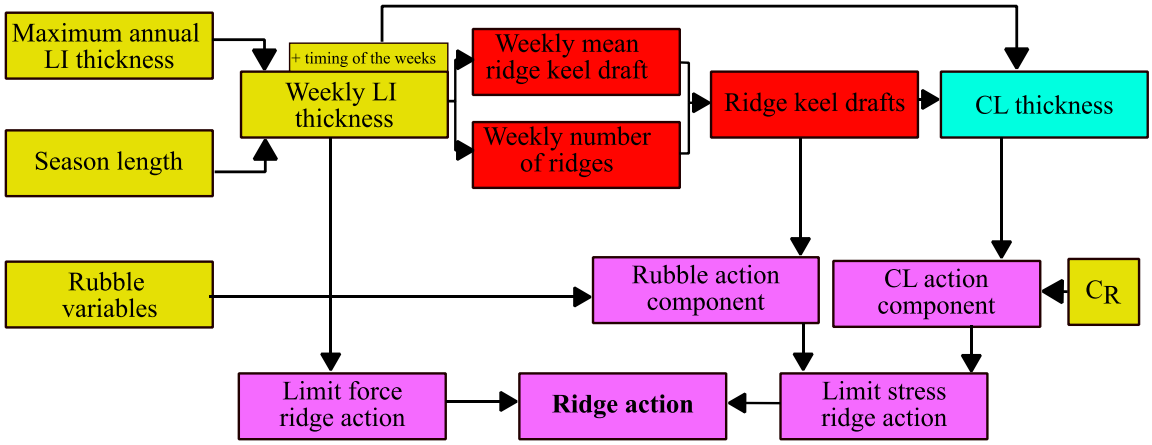

Figure 6.1 Monte Carlo simulation framework. Red shading indicates procedures that are established in Samardžija and Høyland (2023). Cyan shading indicates procedures established in Samardžija et al. (2023a). Yellow shading indicates procedures described in Samardžija et al. (2023b). Purple shading indicates the implementation of simulated variables in the ridge action calculation formulae (also described in Samardžija et al. (2023b)).

Various aspects of the simulation are discussed in the following subsections.

6.1.1. Level ice thickness and season length

The core methodology of the level ice simulation mirrors that of Samardžija and Høyland (2023), but with the added consideration of season length and ice presence in this study. Data on annual maximum level ice thickness and season length are obtained for the location of the Kemi lighthouse from Ronkainen (2013). Ice in the Bothnian Bay can drift to Norströmsgrund, making the Kemi data a conservative reference. The annual maximum ice thickness follows a

log-normal distribution (mean: 0.72, standard deviation: 0.12), and season length follows a normal distribution (mean: 27, standard deviation: 2.3) (Figure 3). The low correlation coefficient (0.13) indicates no strong relationship between these parameters. Figure 6.2 showcases a sample of the simulated annual maximum ice thickness and season duration.

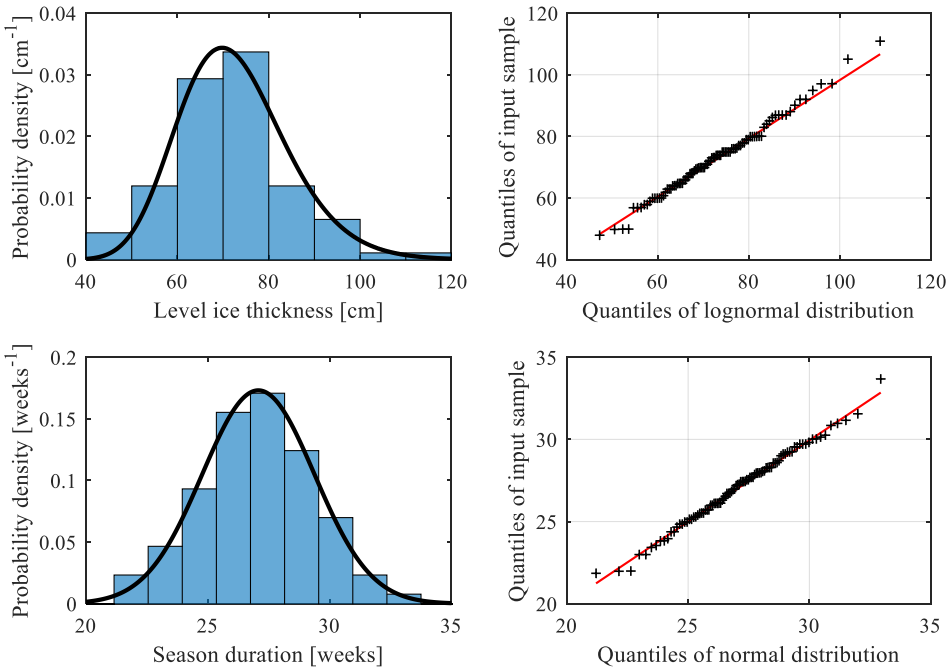

Figure 6.2 From Samardžija et al. (2023b): On the left, histograms display the measured data distributions. Solid lines represent the log-normal PDF for annual maximum ice thickness and the normal PDF for season duration. On the right, Q-Q plots assess the adequacy of the fitted distributions.

Once the annual maximum ice thickness is simulated, we proceed to simulate the weekly ice thickness for each season. This is achieved through an expression representing the typical curve of level ice growth:

$$h_{\mathrm{i}} = \bar{t}^{(1-\bar{t})} \cdot h_{\mathrm{i,AM}} \tag{3.8}$$

where h_{i} is the weekly level ice thickness, $\bar{t}$ is the normalized season time (with $\bar{t} = 0$ marking the start of the ice growth season and $\bar{t} = 1$ marking the onset of the ice melt), and $h_{\mathrm{i,AM}}$ denotes the season's maximum annual level ice thickness.

In the Bay of Bothnia, sea ice presence varies due to wind-driven patterns. Using statistics on ice concentration, we have simulated conditions to reflect periods when ice is absent. After determining weekly ice thicknesses, these statistics help eliminate certain weeks to simulate the open water or low ice concentration periods. Figure 6.3 displays an example of level ice thickness simulation across 20 seasons.

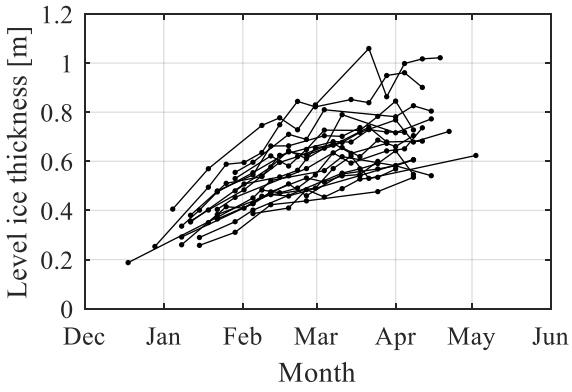

Figure 6.3 From Samardžija et al. (2023b): An illustration of level ice thickness simulated over 20 seasons.

6.1.2. Weekly mean ridge keel draft and weekly number of ridges

The simulation of weekly values for the mean keel draft and the count of ridges is based on their relationship with the level ice thickness, as outlined in Chapter 4. A more comprehensive analysis of this relationship can be found in Samardžija and Høyland (2023).

Traditionally, ridge keels are simulated by fitting a negative exponential distribution to keel draft data and employing this in a Monte Carlo simulation. This method overlooks the correlation between keel and level ice draft. In contrast, our methodology maintains this connection. Furthermore, our technique is adaptable for modelling the seasonal variance of ridge statistics, facilitating a probabilistic examination of the seasonal progression of ridge loads.

The simulated weekly level ice thickness allows us to determine the weekly mean ridge keel draft, $\bar{H}_{\mathrm{k,i}}$, using the expression:

$$\bar{H}_{\mathrm{k,i}} = (a_1 + b_1 \cdot h_i)\bar{R}_{\mathrm{i}} \tag{3.9}$$

Parameters a_1 and b_1 are derived from the linear relationship between level ice thickness and weekly mean ridge keel draft as established in Samardžija and Høyland (2023) – (Figure 4.3 in this thesis). $\bar{R}_{\mathrm{i}}$ is a normalized weekly mean keel draft ratio (randomly sampled from a normal distribution with a mean of 1.0 and standard deviation of 0.05). The equation connects level ice thickness with mean ridge keel draft, integrating both a direct linear relationship and a randomness factor, $\bar{R}_{\mathrm{i}}$, to capture natural variations. Thicker level ice correlates with deeper ridges, a relationship supported by multiple studies.

The weekly ridge count is simulated similarly to mean keel draft, but uses a power function to relate it to the level ice thickness:

$$N_{\mathrm{i}} = a_2 \cdot {h_{\mathrm{i}}}^{b_2} \cdot R_{\mathrm{N,i}} \cdot r \tag{3.10}$$

where a_2 and b_2 are coefficients from Samardžija and Høyland (2023) – (Figure 4.2 in this thesis); $R_{\mathrm{N,i}}$ is a ratio, sampled from a gamma distribution with a scale parameter of 0.28 and a shape parameter of 3.52. This ratio simulates the scatter of the simulated ridge count around the fitted power function that describes the relation between the ridge count and level ice thickness. The factor $r = 0.25$ adjusts for the difference in ice drift speeds between the

Beaufort Sea and the Bay of Bothnia. As ice drift in the Bay is slower (0.025 m/s versus 0.1 m/s), the ridge count is four times less.

Figure 6.4 displays the simulated weekly values for the mean ridge keel draft and the weekly ridge count, based on the input of the simulated level ice thickness used for their calculations.

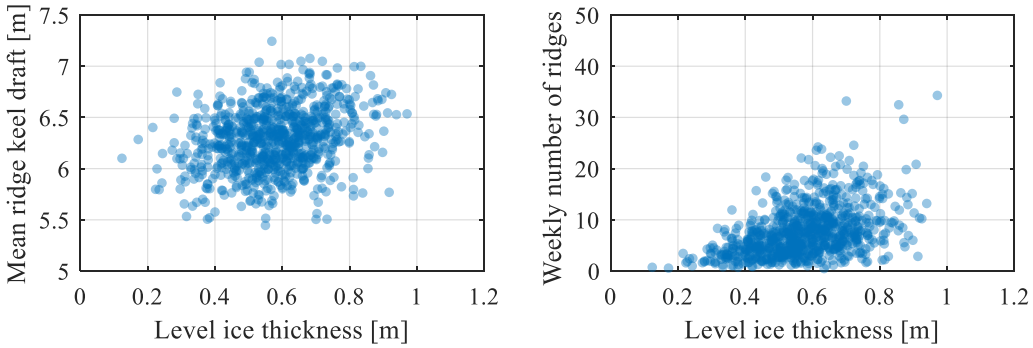

Figure 6.4 From Samardžija et al. (2023b): On the left, the relationship between the simulated level ice thickness and mean ridge keel draft is shown. The right side depicts the relationship between the simulated level ice thickness and the weekly ridge count. Every data point represents a simulated week.

The interaction rate, quantified as the number of ridge impacts per time unit, is a crucial parameter that should correlate with the statistical distributions of other input variables we are considering. It is synonymous with the temporal ridge frequency (ridges/week) assessed in our study. The interaction rate measures a structure's exposure to the ice environment, as highlighted by Jordaan et al. (2010).

We have chosen to measure ridge frequency temporally (number of ridges per week) for its relevance in probabilistic simulation of ridge loads. While it is feasible to determine ridge frequency spatially (e.g., ridges per kilometre), in probabilistic simulation of ridge loads, there is an inevitable necessity to convert spatial frequencies to temporal ones, given that simulations operate in the time domain. Such a conversion demands the incorporation of ice drift speed and concentration. We have experienced that this introduces unnecessary complexity, diminishing the precision of correlations between crucial variables for ridge load computation, and compromising the reliability of load predictions.

To elucidate our approach, we offer two flowcharts: Figure 6.5 outlines our preferred simulation method, while Figure 6.6 showcases a potential method using spatial ridge frequency. Our adopted strategy emphasizes simplicity, focusing solely on parameters needed for ridge load predictions as outlined in ISO 19906: level ice draft, mean ridge keel draft, and temporal ridge frequency. Conversely, the alternative illustrated in Figure 6.6 requires the simulation of ice concentration and drift speed to translate spatial ridge frequencies to temporal ones. Beginning with level ice drift, this method demands multiple intermediary steps (either two or three, depending on choosing path A or B) to derive the temporal ridge frequency. These intermediary steps inadvertently introduce errors. As these errors accumulate, they distort the relationship between level ice draft and temporal ridge frequency. Moreover, from our observation, this methodology disrupts the seasonality inherent to the temporal ridge frequency, making it unfit for the probabilistic assessment of seasonal ridge loads.

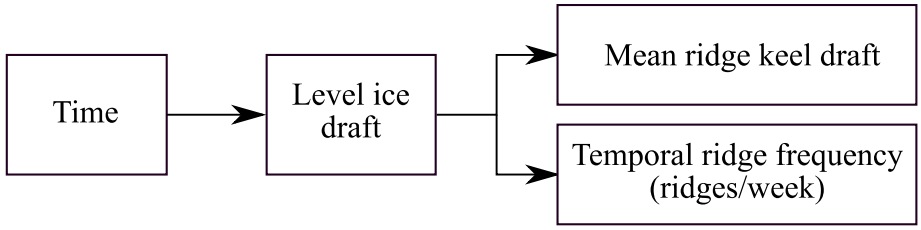

Figure 6.5 From Samardžija and Høyland (2023): Flowchart illustrating the proposed probabilistic simulation approach for ridge load variable calculation.

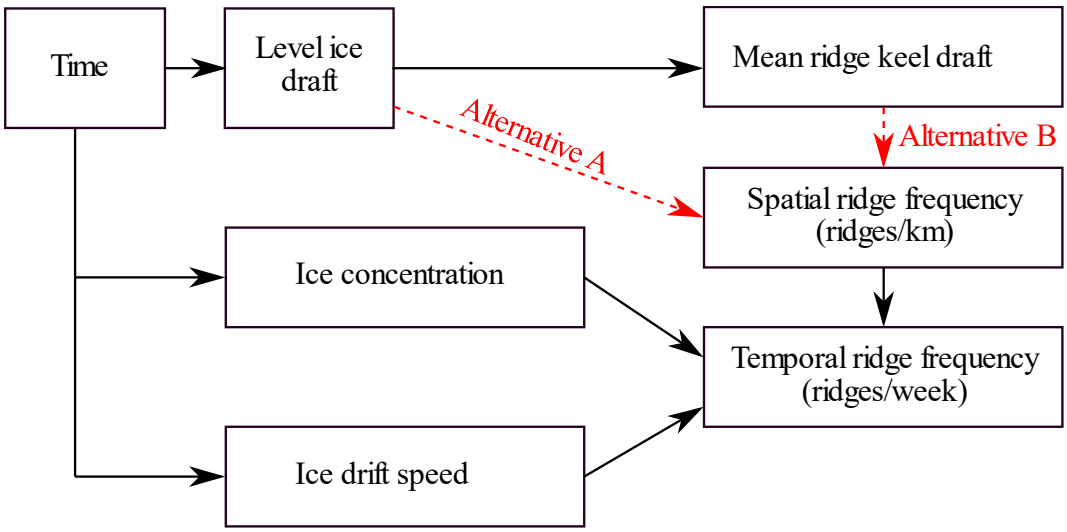

Figure 6.6 From Samardžija and Høyland (2023): Flowchart displaying a possible probabilistic simulation method incorporating spatial ridge frequency.

After simulating the weekly mean keel drafts and the weekly ridge counts for all weeks, for each specified i-th week, N_{i} number of ridges can be modeled using a negative exponential distribution with a mean parameter of $\bar{H}_{\mathrm{k,i}}$. In this manner, the entire population of ice ridges, those deeper than 5 m, is simulated.

6.1.3. Consolidated layer thickness

To simulate the consolidated layer thickness for ridges, the probabilistic approach from Chapter 5 (described in detail in Samardžija et al. (2023a)) is employed. This method factors in ridge arrival timing and keel draft. By modelling the ridge creation time and utilizing established consolidated layer growth formulas, the consolidated layer thickness is determined. For each individual ridge, a probability density function for ridge creation timing is created based on its draft and time of arrival. These PDFs rely on the seasonal progression of the mean ridge keel draft and the weekly ridge count, indicative of the ridge production rate.

Illustrative PDFs for two ridges are depicted in Figure 7. For instance, a ridge with an 8 m keel draft sees its highest creation probability just before the mid-season, tapering off subsequently. Conversely, ridges with deeper keels (e.g., 20 m), exhibit their formation likelihood peaking closer to the season's end, as deeper ridges predominantly form during this phase.

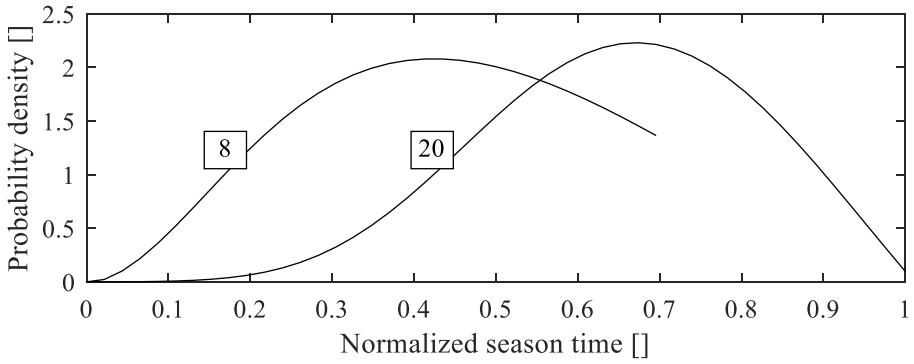

Figure 6.7 From Samardžija et al. (2023a): This illustrates the probability density functions for the creation timing of ridges with keel drafts of 8 m and 20 m, arriving at normalized season times of 0.7 and 1.0 respectively. The ridge drafts are highlighted with squares.

6.1.4. C_R coefficient

In line with ISO 19906, the global ice pressure equation, Eq. (3.3), can be applied in a probabilistic manner by first establishing PDFs for both ice thickness and the C_{R} coefficient. While ice thickness modelling has been discussed earlier, modelling the strength coefficient poses more challenges as it is rooted in comprehensive statistical analysis of full-scale data. It is imperative to note that the PDF of this coefficient is strictly tied to the specific data and statistical techniques used to create the initial formulation. Because it is not a tangible physical entity but rather an amalgamation of auxiliary statistical constructs, it is challenging to formulate without direct statistical analysis of the data it originated from. A shortcoming of ISO 19906 is its lack of clarity on deriving a PDF for this coefficient, providing only deterministic values for certain return periods.

For our purposes, we need a more generalized PDF, one that reflects the coefficient's probability for any given ridge event, termed the parent distribution. ISO 19906 sets forth the characteristic values for this coefficient for the Baltic Sea at 1.8 MPa and 1.3 MPa for 100-year and 1-year return periods, respectively. Our ridge keel simulations suggest an average of 69 ridge interactions annually. We postulate that the parent distribution for the C_{R} coefficient aligns with a Gamma distribution. If the yearly ridge interactions average at n, then the probability for a 1-year event is $1/n$, while a 100-year event is $1/(100n)$. These probabilities, combined with their characteristic values, allow us to calculate the Gamma distribution's parameters, yielding a shape parameter of 10.1 and a scale parameter of 0.0704. The ISO 19906 also prescribes a 10,000-year characteristic value at 2.3 MPa, which aligns with our Gamma distribution (see Figure 6.8). Alternative distribution models, such as log-normal, Gumbel, and Weibull, do not fit well with all three points.

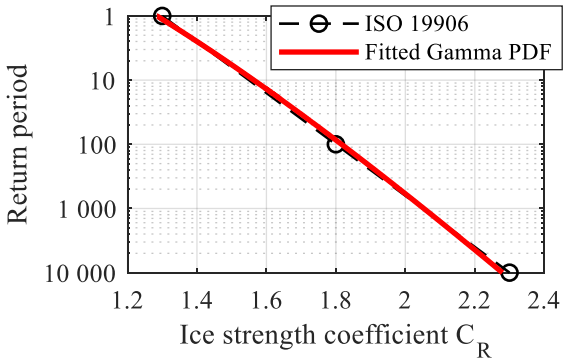

Figure 6.8 From Samardžija et al. (2023b): Exceedance probability plot comparing the Gamma distribution of the C_R coefficient with ISO 19906 values.

6.1.5. Limit force

The calculation of the limit ridge building action follows ISO 19906 as outlined below:

$$F_B = p_D D \tag{3.11}$$

Here, D represents the width of the ice feature interacting with the structure, and p_D signifies the ridge building action line load calculated as:

$$p_D = Rh^{1.25}D^{-0.54} \tag{3.12}$$

where h denotes the thickness of the surrounding level ice, and R is a coefficient distributed uniformly between 2 and 10 as advised by ISO 19906.

In the case of ridges, the ice feature width can be considered the distance along an ice ridge's spine. This distance accumulates the force exerted by surrounding ice and conveys it to the structure. There is a positive correlation between the ridge width across the spine, W, and the ridge keel draft. To achieve this, we use the mean and standard deviation from Strub-Klein and Sudom (2012) to simulate ridge width:

$$W_i = R_{D/d,i}\ H_{k,i} \tag{3.13}$$

Here, $R_{D/d,i}$ is the ratio between ridge width and keel draft from a log-normal distribution with a mean of 4.85 and a standard deviation of 2.65; $H_{k,i}$ represents ridge keel draft.

A constraint is needed on the maximum distance along an ice ridge's spine, to estimate its force accumulation from surrounding ice and transmission to a structure. Guidance for this is lacking. We assume a 45° force travel angle through the ridge, as in Figure 9. This allows width calculation via Eq. (3.14).

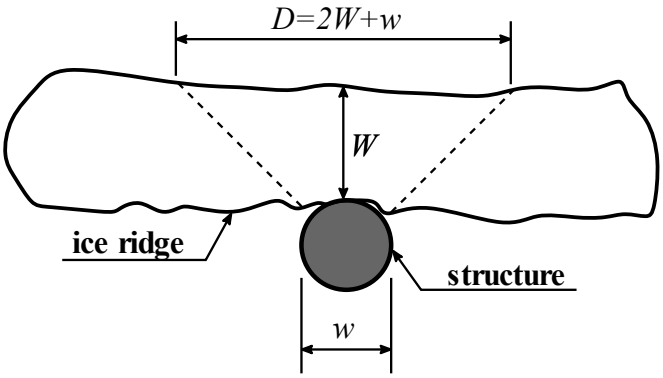

Figure 6.9 From Samardžija et al. (2023b): Relationship between the width of the ridge across its spine and the corresponding portion of this width along the spine. It is assumed that this specific portion is responsible for transmitting the force exerted by the surrounding level ice to the structure.

$$D = 2W + w \tag{3.14}$$

In our simulations, the limit force scenario occurred in only 0.12% of events. The inclusion of the limit force did not affect the distribution of annual maximum ridge actions. The structure's narrowness means minimal action is needed for ridge failure. Surrounding ice typically provides a sufficient driving force. Although it could be omitted for this particular structure, including the limit force showcases the technique in our probabilistic model.

6.2. Results

The primary outcome of the simulation is the distribution of the yearly peak ridge actions, which is showcased in Figure 10 through an exceedance probability chart and a histogram. The exceedance probability chart efficiently determines values for specific return periods, such as the 100-year action with a 0.01 annual exceedance probability. These figures can be integrated into design load combinations as per the ISO 19906 standard.

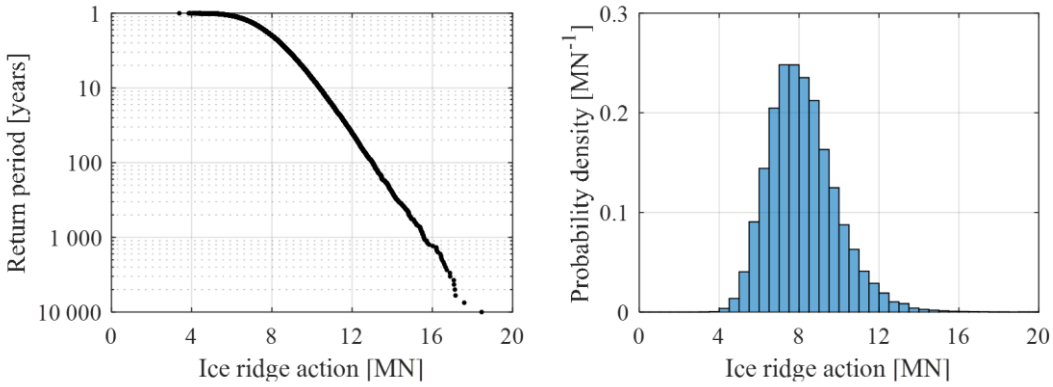

Figure 6.10 From Samardžija et al. (2023b): Exceedance probability plot (left) and distribution (right) of the annual maximum ridge actions.

Figure 6.11 illustrates the relationship between the consolidated layer and the rubble action components for the subset of annual peak actions. A significant 90.90% of these events showed that the consolidated layer action exceeded the rubble action. There is a clear negative

correlation between the two components, highlighting the rarity of simultaneous extreme values for both. The consolidated layer is a predominant contributor to the total ridge action, overshadowing the keel rubble. However, it is notable that extreme actions may occasionally occur where the rubble component plays a dominant role. It should be noted that the hypothetical structure in this study is assumed to have infinite depth, allowing every ridge to interact with it, regardless of its keel draft. In contrast, for this specific location, the deepest ridges would ground before reaching the structure.

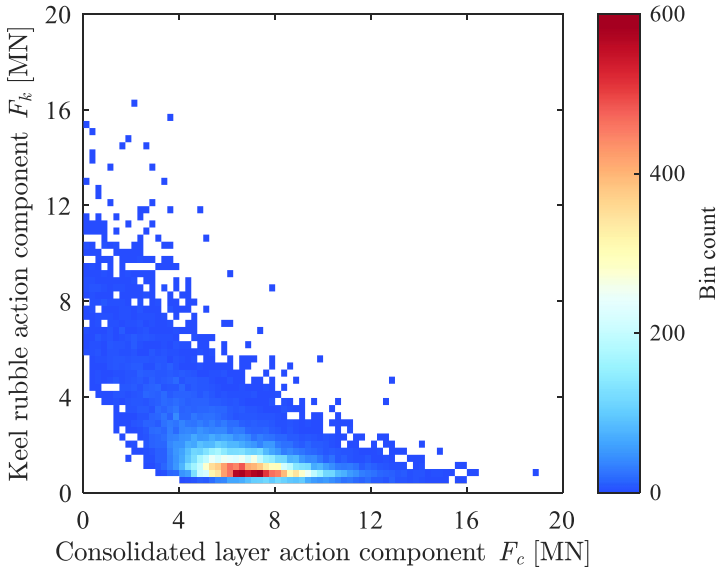

Figure 6.11 From Samardžija et al. (2023b): Bivariate histogram illustrating the relationship between consolidated layer and keel rubble actions during annual maximum events.

Figure 6.12 showcases the interplay between the thickness of the consolidated layer and the keel draft of ridges responsible for annual maximum actions. To construct this plot, all events with maximum annual actions ($F > 0$) were initially plotted. From these, three subsets were derived based on the intensity of the actions. These subsets represent events deviating by ± 0.5 MN from the action intensities with 10, 100, and 1,000-year return periods. Specifically, they represent annual maximum action events within the intensity ranges of $9.9 > F > 10.9$, $12.5 > F > 13.5$ and $14.8 > F > 15.8$. The intensities for the specific return periods were obtained from Figure 6.10. By examining Figure 6.12, one can determine the typical combinations of consolidated layer thickness and keel draft for extreme action events. This information can guide the selection of a "representative ridge" scenario, assisting in a more detailed physical or computational study of ridge-structure dynamics.

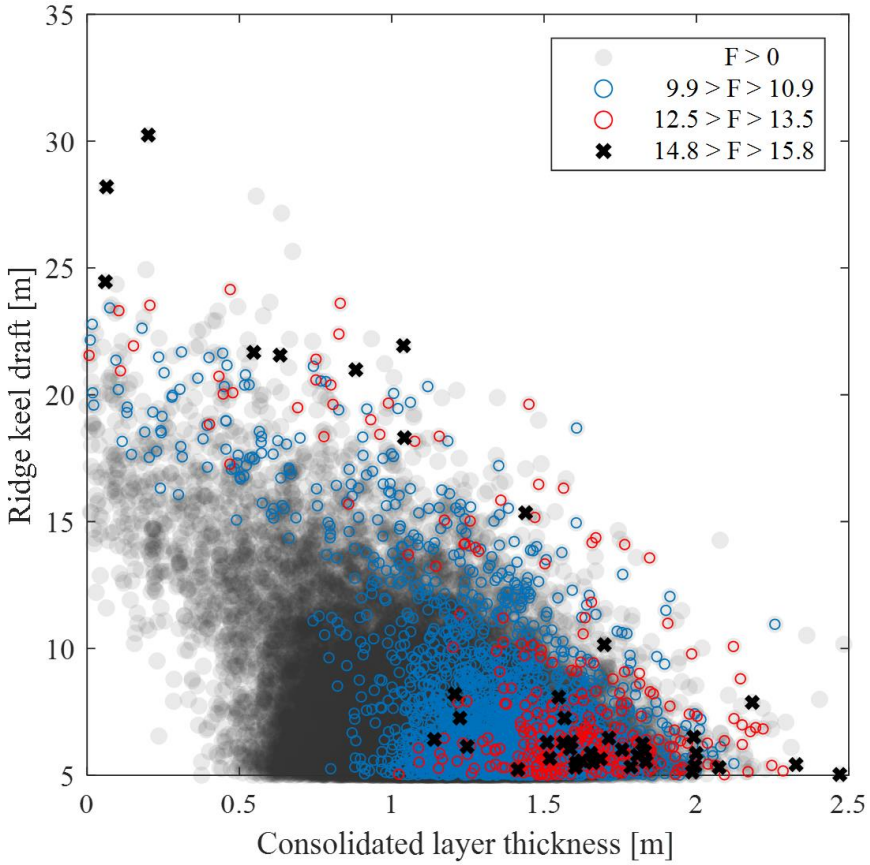

Figure 6.12 From Samardžija et al. (2023b): Illustration of the relationship between consolidated layer thickness and ridge keel draft for annual maximum action events (grey shading), along with events of intensity ± 0.5 MN relative to actions with 10 (blue circles), 100 (red circles), and 1,000-year (black crosses) return periods.

Figure 6.13 provides a depiction of the seasonality in ridge actions. It illustrates a bivariate distribution concerning the temporal progression within the season and the corresponding ridge action intensity. Superimposed on this distribution are the projected weekly mean and maximum ridge actions as functions of time. The resulting seasonality of the ridge action offers useful insights for strategic offshore operation scheduling within distinct seasonal windows.

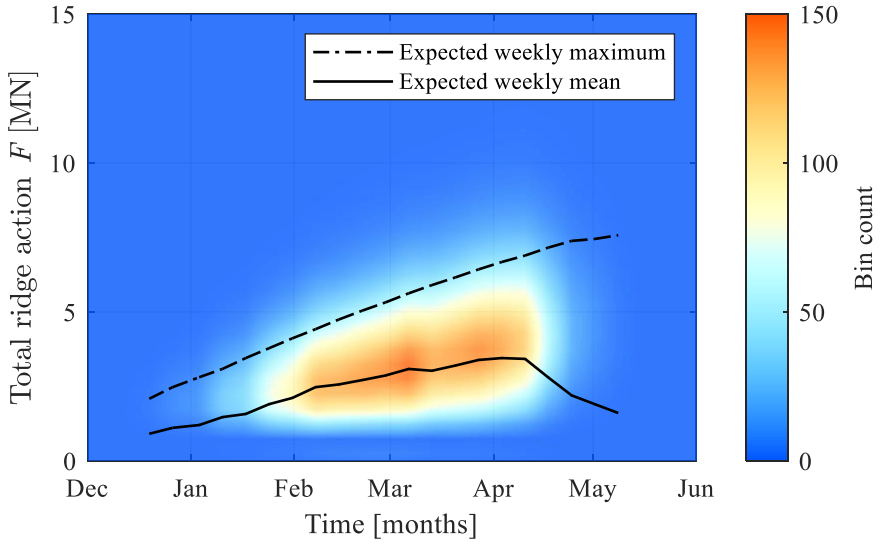

Figure 6.13 From Samardžija et al. (2023b): Seasonality of ridge actions illustrated with a bivariate histogram.

7. Conclusions and recommendations for further work

7.1. Conclusions

This thesis primarily seeks to establish a probabilistic framework for simulating ridge actions using a minimum number of input variables. The model presented in Chapter 6 requires only the annual maximum level ice thickness and data on the length of the season and sea ice presence. Conveniently, level ice thickness data is relatively easy to obtain and can be modelled accurately. Moreover, information on the length of the season and ice presence is now readily accessible through satellite remote sensing. Notably absent from our model's input requirements are ridge keel draft and consolidated layer thickness data.

However, this minimal data input is not without its constraints. While our model does not require ridge keel draft and consolidated layer thickness data, it compensates by utilizing correlations from our studies ice draft data from the Beaufort Sea. This raises concerns about the applicability of these correlations to other seas, such as the Baltic Sea, both qualitatively and quantitatively. Thus, the simulated ridge actions, at best, are suitable for preliminary design stages. For more reliable outcomes, location-specific data is crucial. It would be sensible to collect long-term sonar ice draft measurements and organize field campaigns to collect data on consolidated layer thickness. While our model can operate with limited data, its reliability remains questionable in such conditions. The objective of a fully reliable model with limited input data remains elusive.

Predictably, the reliability of a probabilistic simulation increases with greater data availability. Our model's strength lies in its adaptability to various levels of data availability. Its applicability spans various design stages, from preliminary phases with limited data to later stages enriched with years of data. The model also allows for updates of the probabilistic ridge load assessment after construction, facilitating reassessment of structural reliability and safety enhancements.

A point of contention within our model is the use of C_{R} coefficient for determining the consolidated layer action component, which introduces inherent uncertainties. The distribution of this coefficient has been derived from specific reported values, but the methodology remains questionable, given the lack of practical guidelines on its implementation in probabilistic ridge action simulations. More research on this is needed, but the cost implications of acquiring full-scale ridge action measurements make this unlikely in the near future.

Another highlight of our model is its ability to maintain critical correlations among key variables (e.g., consolidated layer thickness and ridge keel draft). This results in realistic combinations of variables, leading to less conservative ridge action estimates. Furthermore, it acknowledges the dynamic nature of key variables throughout the winter season.

7.2. Recommendations for further work

- **Re-evaluation of ice thickness and ridge parameters for other regions**: Building upon the work of Samardzija and Høyland (2023), there is an imperative need to analyse the relationship between level ice thickness, ridge keel draft, and ridge frequency in locations other than the Beaufort Sea. It would be interesting to investigate how these relationships can be applied to regions with limited data. While it is hypothesized that ridge frequency scales linearly with ice drift speed, it is also important to assess this variable with different ridging conditions.

- **Advancement in ridge load measurements**: An unfortunate gap in our understanding of ridge loads is the lack of contemporary full-scale measurements. This is exemplified in the shortage of description for a probability distribution function of the C_{R} coefficient for use in probabilistic ridge load modelling. Given the advancements in technology, it is crucial to use new measurement techniques that harness the latest developments in sensor and data acquisition technologies. Such measurements could provide a more detailed understanding of ice-structure interactions, potentially leading to improvements in ridge load calculation methodologies.

- **Refining ridge production rate modelling**: Our current model has a limitation, particularly when it suggests a null ridge production rate at the end of the season due to the predetermined seasonal development of level ice thickness. A more detailed examination of the ridge production rate, bypassing mean value computations, may yield more accurate insights.

- **Spatial ridge simulation for navigation optimalisation**: The concept of simulating ridges based on level ice thickness can be expanded to generate spatial representations, such as ridges per kilometre. Combined with geometric data such as keel draft and consolidated layer thickness, this could be a valuable tool for icebreakers. A thorough spatial understanding of ridge distributions can significantly aid in effective route risk assessment, leading to more optimized navigation strategies in challenging Arctic conditions.

- **Integration of remote sensing technologies**: Building upon the methodologies presented in our study, there is significant potential in employing advanced satellite remote sensing to refine our understanding of ridge formations. Incorporating these technologies could provide more detailed data on ice thickness and ridge frequency, complementing the current methods of simulating ridges based on level ice thickness. This would not only refine the accuracy of our simulations but also reinforce real-time navigation and infrastructure decision-making in Arctic regions.

- **Field measurement campaign for consolidated layer thickness:** A more comprehensive field measurement campaign is pivotal to our understanding of consolidated layer thickness in ridges. Future efforts should strive for random selection of ridges, avoiding the bias towards larger or more prominent formations. Moreover, measurements should not be limited to the end of the season alone. By adopting a consistent and unbiased approach to measurements throughout different times of the season, we could enhance the validation process and refine the consolidated layer simulation model described in this study.

References

Amundrud, T. L., Melling, H., & Ingram, R. G. (2004). Geometrical constraints on the evolution of ridged sea ice. *Journal of Geophysical Research, 109*(C6) https://doi.org/10.1029/2003JC002251

Bekker, A. T., Sabodash, O. A., & Kovalenko, R. G. (2013a). Modeling and analysis of probabilistic distributions of ice loads on lighthouse structures in the Gulf of Bothnia. *23rd International Offshore and Polar Engineering Conference, ISOPE*, Anchorage, Alaska, USA

Bekker, A. T., Sabodash, O. A., & Kovalenko, R. G. (2013b). Probabilistic modeling of extreme value distributions of ice loads on "Molikpaq" platform for Sakhalin-II project. *32nd International Conference on Ocean, Offshore and Arctic Engineering, OMAE* Nantes, France. https://doi.org/10.1115/OMAE2013-10008

Bekker, A. T., Sabodash, O. A., Kovalenko, R. G., & Rusakov, D. S. (2012). Probabilistic modeling of ice environment from lighthouses zone in the Gulf of Bothnia. *22nd International Offshore and Polar Engineering Conference, ISOPE*, Rhodes, Greece

Bekker, A. T., Sabodash, O. A., Seliverstov, V. I., Koff, G. L., & Pipko, E. N. (2009). Estimation of Limit Ice Loads On Engineering Offshore Structures In the Sea of Okhotsk. *9th International Offshore and Polar Engineering Conference, ISOPE*, Osaka, Japan

Bercha, F. G., Danys, J. V., & Rokne, J. G. (1978). Probabilistic ice-structure interaction theory. *5th IAHR Symposium on Ice*, Lulea, Sweden

Bercha, F. G., Gudmestad, O. T., Nevel, D., Foschi, R., Sliggers, F., & Nikitina, N. (2006). Reliability of arctic offshore installations. *7th International Conference and Exhibition on Performance of Ships and Structures in Ice, ICETECH*, Banff, AB, Canada. https://doi.org/10.5957/ICETECH-2006-113

Bertrand, A., & Escoffier, L. (1989). IFP databanks on offshore accidents. In *Reliability Data Collection and Use in Risk and Availability Assessment* (pp. 115-128). Springer.

Bird, K. J., Charpentier, R. R., Gautier, D. L., Houseknecht, D. W., Klett, T. R., Pitman, J. K., Moore, T. E., Schenk, C. J., Tennyson, M. E., & Wandrey, C. R. (2008). Circum-Arctic resource appraisal: Estimates of undiscovered oil and gas north of the Arctic Circle (2327-6932). https://doi.org/10.3133/fs20083049

Blanchet, D. (1998). Ice loads from first-year ice ridges and rubble fields. *Canadian Journal of Civil Engineering, 25*(2), 206-219. https://doi.org/10.1139/l97-073

Bonath, V., Petrich, C., Sand, B., Fransson, L., & Cwirzen, A. (2018). Morphology, internal structure and formation of ice ridges in the sea around Svalbard. *Cold Regions Science and Technology, 155*, 263-279. https://doi.org/10.1016/j.coldregions.2018.08.011

Brown, T. G., Jordaan, I. J., & Croasdale, K. R. (2001). A probabilistic approach to analysis of ice loads for the Confederation Bridge. *Canadian Journal of Civil Engineering, 28*(4), 562-573. https://doi.org/10.1139/cjce-28-4-562

Cammaert, A. B., Trumars, J., & Eide, L. I. (2008). A probabilistic approach to design ice loads for an Arctic jack-up drilling platform. *27th International Conference on Offshore Mechanics and Arctic Engineering, OMAE*, Berlin, Germany. https://doi.org/10.1115/OMAE2008-57519

CEN. (2001). EN 1990:2002, Eurocode - Basis of Structural Design.

Chai, W., & Leira, B. J. (2018). Environmental contours based on inverse SORM. *Marine Structures*, *60*, 34-51. https://doi.org/10.1016/j.marstruc.2018.03.007

Chai, W., Leira, B. J., Naess, A., Høyland, K., & Ehlers, S. (2020). Development of environmental contours for first-year ice ridge statistics. *Structural Safety*, *87*, 101996. https://doi.org/10.1016/j.strusafe.2020.101996

Charlebois, L., Frederking, R., Timco, G. W., Watson, D., & Richard, M. (2018). Evaluation of pack ice pressure approaches and engineering implications for offshore structure design. *Cold Regions Science and Technology*, *149*, 71-82. https://doi.org/10.1016/j.coldregions.2018.01.020

Comfort, G., Singh, S., & Dinovitzer, A. (1998). Limit-force ice loads and their significance to offshore structures in the Beaufort Sea. *International Journal of Offshore and Polar Engineering*, *8*(1), 16-21.

Croasdale, K. R. (1984). The limiting driving force approach to ice loads. *16th Offshore Technology Conference, OTC*, Houston, TX, USA. https://doi.org/10.4043/4716-MS

Croasdale, K. R. (2009). Limit force ice loads - An update. *20th International Conference on Port and Ocean Engineering under Arctic Conditions, POAC*, Lulea, Sweden

Davis, N., & Wadhams, P. (1995). A statistical analysis of Arctic pressure ridge morphology. *Journal of Geophysical Research: Oceans*, *100*(C6), 10915-10925. https://doi.org/10.1029/95JC00007

Dierking, W. (1995). Laser profiling of the ice surface topography during the Winter Weddell Gyre Study 1992. *Journal of Geophysical Research: Oceans*, *100*(C3), 4807-4820. https://doi.org/10.1029/94JC01938

Ditlevsen, O., & Madsen, H. O. (1996). *Structural reliability methods* (Vol. 178). Wiley New York.

Dolgopolov, Y. V., Afanasiev, V. P., Koren'kov, V. A., & Panfilov, D. F. (1975). Effect of hummocked ice on the piers of marine hydraulic structures. *3rd IAHR Symposium on Ice Problems*, Hanover, NH, USA

Dunwoody, A. B. (1991). Reliability against drifting ice. An adjunct to Monte Carlo simulation. *Journal of Offshore Mechanics and Arctic Engineering*, *113*(3), 253-259. https://doi.org/10.1115/1.2919928

Eik, K., & Gudmestad, O. T. (2010). Iceberg management and impact on design of offshore structures. *Cold Regions Science and Technology*, *63*(1-2), 15-28. https://doi.org/10.1016/j.coldregions.2010.04.008

Ekeberg, O., Høyland, K., & Hansen, E. (2012). Ice ridge identification methods and analysis of upward looking sonar data from Fram Strait 2006-2010. *21st IAHR Symposium on Ice*, Dalian, China

Ekeberg, O.-C., Hoyland, K., & Hansen, E. (2013). Extreme keel drafts in the Fram Strait 2006-2011. *22nd International Conference on Port and Ocean Engineering under Arctic Conditions, POAC*, Espoo, Finland

Ekeberg, O.-C., Høyland, K., & Hansen, E. (2015). Ice ridge keel geometry and shape derived from one year of upward looking sonar data in the Fram Strait. *Cold Regions Science and Technology*, *109*, 78-86. https://doi.org/10.1016/j.coldregions.2014.10.003

ENTSOE. (2020). *Regional investment plan 2020-Northern Seas*. Retrieved 30.09.2023 from https://eepublicdownloads.blob.core.windows.net/public-cdn-container/tyndp-documents/IoSN2020/200810_RegIP2020_NS_beforeconsultation.pdf

Ervik, A. (2015). Full scale actions from first year ridge interactions with fixed structures. *23rd International Conference on Port and Ocean Engineering under Arctic Conditions, POAC*, Trondheim, Norway

Ervik, Å., Høyland, K. V., Shestov, A., & Nord, T. S. (2018). On the decay of first-year ice ridges: Measurements and evolution of rubble macroporosity, ridge drilling resistance and consolidated layer strength. *Cold Regions Science and Technology*, *151*, 196-207. https://doi.org/10.1016/j.coldregions.2018.03.024

Ervik, Å., Nord, T. S., Høyland, K. V., Samardzija, I., & Li, H. (2019). Ice-ridge interactions with the Norströmsgrund lighthouse: Global forces and interaction modes. *Cold Regions Science and Technology*, *158*, 195-220. https://doi.org/10.1016/j.coldregions.2018.08.020

Fuglem, M., Richard, M., & King, T. (2014). An implementation of ISO 19906 formulae for global sea ice loads within a probabilistic framework. *Arctic Technology Conference*, Houston, TX, USA. https://doi.org/10.4043/24548-MS

Fuglem, M., Richard, M., & Thijssen, J. (2014). Challenges Implementing ISO 19906 for Probabilistic Assessment of Multi-year Sea Ice Loads on Sloping Structures. *11th International Conference and Exhibition on Ships and Structures in Ice*, Alberta, Canada. https://doi.org/10.5957/ICETECH-2014-154

Fuglem, M., Stuckey, P., & Jordaan, I. (2011). Probabilistic ice loads assessments for arctic regions: Inputs for calibration of ISO 19906. *Arctic Technology Conference*, Houston, TX, USA. https://doi.org/10.4043/22070-MS

Guzenko, R. B., Mironov, Y. U., May, R. I., Porubaev, V. S., Kornishin, K., & Efimov, Y. O. (2021). Morphometric particularities of ice ridges with the greatest thickness of the consolidated layer and other statistical patterns of morphometry of first-year ice ridges. *31st International Ocean and Polar Engineering Conference*, Rhodes, Greece

Hibler III, W. D., Weeks, W. F., & Mock, S. J. (1972). Statistical aspects of sea-ice ridge distributions. *Journal of Geophysical Research*, *77*(30), 5954-5970. https://doi.org/10.1029/JC077i030p05954

Hopkins, M. A. (1994). On the ridging of intact lead ice. *Journal of Geophysical Research*, *99*(C8), 16351-16360. https://doi.org/10.1029/94JC00996

Hopkins, M. A. (1998). Four stages of pressure ridging. *Journal of Geophysical Research*, *103*(C10), 21883-21891. https://doi.org/10.1029/98JC01257

Hossain, R., Taylor, R., & Moro, L. (2021). A Probabilistic High-Pressure Zone Model of Dynamic Ice Structure Interactions and Associated Ice-Induced Vibrations. *40th International Conference on Ocean, Offshore and Arctic Engineering, OMAE*, Virtual, Online. https://doi.org/10.1115/omae2021-62966

Høyland, K. V. (2002). Consolidation of first-year sea ice ridges. *Journal of Geophysical Research*, *107*(C6), 15-11. https://doi.org/10.1029/2000JC000526

ISO 19906. (2019). *Petroleum and natural gas industries - Arctic offshore structures*.

Jonkman, S. N., Steenbergen, R. D. J. M., Morales-Nápoles, O., Vrouwenvelder, A. C. W. M., & Vrijling, J. K. (2015). *Probabilistic Design: Risk and Reliability Analysis in Civil Engineering*. Department of Hydraulic Engineering. Faculty of Civil Engineering and Geosciences. Delft University of Technology.

Jordaan, I. (1983). Risk and Safety Assessment for Arctic Offshore Projects. *2nd Massachusetts Institute of Technology Sea Grant College Program Lecture and Seminar*,

Jordaan, I. (2005). *Decisions under uncertainty: probabilistic analysis for engineering decisions*. Cambridge University Press.

Jordaan, I. (2015). Some issues in ice mechanics. *34th International Conference on Ocean, Offshore and Arctic Engineering, OMAE*, St. John's, NL, Canada. https://doi.org/10.1115/OMAE2015-42042

Jordaan, I., Bruce, J., Masterson, D., & Frederking, R. (2010). Local ice pressures for multiyear ice accounting for exposure. *Cold Regions Science and Technology*, *61*(2-3), 97-106. https://doi.org/10.1016/j.coldregions.2009.12.008

Jordaan, I., Stuckey, P., Bruce, J., Croasdale, K., & Verlaan, P. (2011). Probabilistic modelling of the ice environment in the northeast Caspian sea and associated structural loads. *21st International Conference on Port and Ocean Engineering under Arctic Conditions, POAC*, Montreal, QC, Canada

Kärnä, T., & Nykänen, E. (2004). An approach for ridge load determination in probabilistic design. *17th IAHR Symposium on Ice*, Saint Petersburg, Russia

Kato, K. (1992). Design ice force estimating system. *2nd International Offshore and Polar Engineering Conference, ISOPE*, San Francisco, CA, USA

Kato, K. (1998). Trial calculation of design ice loads on an arctic structure for offshore Sakhalin. *8th International Offshore and Polar Engineering Conference, ISOPE*, Montreal, Canada

Kato, K. (2006). Morphology of a first-year ridge and its influences on design ice load in the Sea of Okhotsk. *18th IAHR Symposium on Ice*, Sapporo, Japan

Kellner, L., Herrnring, H., & Ring, M. (2017). Review of ice load standards and comparison with measurements. *36th International Conference on Ocean, Offshore and Arctic Engineering, OMAE*, Trondheim, Norway. https://doi.org/10.1115/OMAE2017-61735

Lensu, M. (2003). *The evolution of ridged ice fields*. Helsinki University of Technology.

Leppäranta, M. (2023). History and Future of Snow and Sea Ice in the Baltic Sea. In *Oxford Research Encyclopedia of Climate Science*.

Leppäranta, M., & Hakala, R. (1992). Structure and strength of first-year ice ridges in the Baltic sea. *Cold Regions Science and Technology*, *20*(3), 295-311. https://doi.org/10.1016/0165-232X(92)90036-T

Leppäranta, M., Lensu, M., Kosloff, P., & Veitch, B. (1995). The life story of a first-year sea ice ridge. *Cold Regions Science and Technology*, *23*(3), 279-290. https://doi.org/10.1016/0165-232x(94)00019-t

Lewis, J. E., Lepparanta, M., & Granberg, H. B. (1993). Statistical properties of sea ice surface topography in the Baltic Sea. *Tellus, Series A (Dynamic Meteorology and Oceanography)*, *45A*(2), 127-142. https://doi.org/10.1034/j.1600-0870.1993.t01-1-00004.x

Maes, M. A., & Thomas, G. A. N. (2011). Risk-based calibration of action factors in the new ISO 19906 Arctic Offshore Structures Standard. *Arctic Technology Conference*, Houston, TX, USA. https://doi.org/10.4043/22071-MS

Marcellus, B., McKenna, R., McGonigal, D., & Pilkington, R. (2011). Old Ice Floe and Ridge Statistics from Submarine Upward Looking Sonar Data for the Beaufort Chukchi and Arctic Seas. *21st International Conference on Port and Ocean Engineering under Arctic Conditions, POAC*, Montreal, QC, Canada

McKenna, R., Fuglem, M., & Croocker, G. (2014). Uncertainty in 100 and 10,000 Year Ice Loads on Offshore Structures. *11th International Conference and Exhibition on Ships and Structures in Ice*, Alberta, Canada. https://doi.org/10.5957/ICETECH-2014-167

Melchers, R. E. (1999). *Structural reliability analysis and prediction* (2nd ed. ed.). Wiley.

Melchers, R. E., & Beck, A. T. (2018). *Structural reliability analysis and prediction*. John wiley & sons.

Melling, H., Johnson, P. H., & Riedel, D. A. (1995). Measurements of the underside topography of sea ice by moored subsea sonar. *Journal of Atmospheric and Oceanic Technology*, *12*(3), 589-602. https://doi.org/10.1175/1520-0426(1995)012<0589:MOTUTO>2.0.CO;2

Melling, H., & Riedel, D. A. (1995). The underside topography of sea ice over the continental shelf of the Beaufort Sea in the winter of 1990. *Journal of Geophysical Research*, *100*(C7), 13641-13653. https://doi.org/10.1029/95JC00309

Melling, H., & Riedel, D. A. (1996). Development of seasonal pack ice in the Beaufort Sea during the winter of 1991-1992: a view from below. *Journal of Geophysical Research*, *101*(C5), 11975-11991. https://doi.org/10.1029/96JC00284

Metzger, A. T., Mahoney, A. R., & Roberts, A. F. (2021). The Average Shape of Sea Ice Ridge Keels. *Geophysical Research Letters*, *48*(24), e2021GL095100. https://doi.org/10.1029/2021GL095100

Mock, S. J., Hartwell, A. D., & Hibler, W. D., III. (1972). Spatial aspects of pressure ridge statistics. *Journal of Geophysical Research*, *77*(30), 5945-5953. https://doi.org/10.1029/JC077i030p05945

Monteban, D., Lubbad, R., Samardzija, I., & Løset, S. (2020). Enhanced iceberg drift modelling in the Barents Sea with estimates of the release rates and size characteristics at the major glacial sources using Sentinel-1 and Sentinel-2. *Cold Regions Science and Technology*, *175*, 103084. https://doi.org/10.1016/j.coldregions.2020.103084

Moslet, P. O., Gudmestad, O. T., Sildnes, T., & Saebo, E. (2011). The new ISO19906 standard and related arctic activities at DNV. *21st International Conference on Port and Ocean Engineering under Arctic Conditions, POAC*, Montreal, QC, Canada

Mudge, T. D., Ross, E., Fissel, D. B., & Marko, J. R. (2013). Further improvements to understandings of extreme arctic sea ice thickness derived from upward looking sonar ice data. *22nd International Conference on Port and Ocean Engineering under Arctic Conditions, POAC*, Espoo

Nessim, M., & Jordaan, I. (1991). The Selection of Design Ice Loads and Design Ice Features for Fixed Structures in the Beaufort Sea. In *Ice-Structure Interaction* (pp. 483-506). Springer. https://doi.org/10.1007/978-3-642-84100-2_24

Nevel, D. E. (1991). Probabilistic Ice Forces on Offshore Structures. In *Ice-Structure Interaction* (pp. 541-557). Springer. https://doi.org/10.1007/978-3-642-84100-2_26

Nord, T. S., Samardžija, I., Hendrikse, H., Bjerkås, M., Høyland, K. V., & Li, H. (2018). Ice-induced vibrations of the Norströmsgrund lighthouse. *Cold Regions Science and Technology*, *155*, 237-251. https://doi.org/10.1016/j.coldregions.2018.08.005

Obert, K. M., & Brown, T. G. (2011). Ice ridge keel characteristics and distribution in the Northumberland Strait. *Cold Regions Science and Technology*, *66*(2-3), 53-64. https://doi.org/10.1016/j.coldregions.2011.01.004

OGP Report 422. (2010). Calibration of action factors for ISO 19906 Arctic offshore structures.

Onishchenko, D. A. (2009). Analytical approach to the calculation of the design values of the loads associated with discrete ice features. *20th International Conference on Port and Ocean Engineering under Arctic Conditions, POAC*, Lulea, Sweden

Palosuo, E. (1975). *The formation and structure of ice ridges in the Baltic* (9514615093).

Parmerter, R. R., & Coon, M. D. (1972). Model of pressure ridge formation in sea ice. *Journal of Geophysical Research, 77*(33), 6565-6575. https://doi.org/10.1029/JC077i033p06565

Pilkington, G. R., & Wright, B. (1991). Beaufort Sea ice thickness measurements from an acoustic, under ice, upward looking ice keel profiler. *1st International Offshore and Polar Engineering Conference, ISOPE*, Edinburgh, United Kingdom

Ronkainen, I. (2013). *Long-term changes in Baltic Sea ice conditions* [Master, University of Helsinki]. Helsinki, Finland.

Ross, E., Fissel, D., Marko, J., & Reitsma, J. (2012). An improved method of extremal value analysis of arctic sea ice thickness derived from upward looking sonar ice data. *Arctic Technology Conference*, Houston, TX, USA. https://doi.org/10.4043/23811-MS

Samardžija, I. (2018). Two applications of a cross-correlation based ice drift tracking algorithm; Ship-based marine radar images and camera images from a fixed structure. *24th IAHR Symposium on Ice*, Vladivostok, Russia

Samardžija, I., & Høyland, K. V. (2019). Initial results of a study into the relationship between level ice draft and ridge keel draft. *25th International Conference on Port and Ocean Engineering under Arctic Conditions*, Delft, The Netherlands

Samardžija, I., & Høyland, K. V. (2023). Analysis of the relationship between level ice draft, ridge frequency and ridge keel draft for use in the probabilistic assessment of ice ridge loads on offshore structures. *Ocean Engineering, 270*, 113593. https://doi.org/10.1016/j.oceaneng.2022.113593

Samardžija, I., Høyland, K. V., Leira, B. J., & Næss, A. (2018). Probabilistic Assessment of Ice Environment and Ridge Loads for the Norströmsgrund Lighthouse. *24th IAHR Symposium on Ice*, Vladivostok, Russia

Samardžija, I., Høyland, K. V., Leira, B. J., & Næss, A. (2023a). Consolidated layer thickness in probabilistic simulation of first-year ice ridges. *Cold Regions Science and Technology, 216*, 104021. https://doi.org/10.1016/j.coldregions.2023.104021

Samardžija, I., Høyland, K. V., Leira, B. J., & Næss, A. (2023b). Probabilistic assessment of first-year ice ridge action on offshore structures. *Cold Regions Science and Technology*. [Paper under peer review]

Shapovalova, D., & Stephen, K. (2019). No race for the Arctic? Examination of interconnections between legal regimes for offshore petroleum licensing and level of industry activity. *Energy policy, 129*, 907-917. https://doi.org/10.1016/j.enpol.2019.01.045

Shestov, A., Høyland, K., & Ervik, Å. (2018). Decay phase thermodynamics of ice ridges in the Arctic Ocean. *Cold Regions Science and Technology, 152*, 23-34. https://doi.org/10.1016/j.coldregions.2018.04.005

Sinsabvarodom, C., Chai, W., Leira, B. J., Høyland, K. V., & Naess, A. (2020). Uncertainty assessments of structural loading due to first year ice based on the ISO standard by using

Monte-Carlo simulation. *Ocean Engineering*, *198*, 106935. https://doi.org/10.1016/j.oceaneng.2020.106935

Sinsabvarodom, C., Leira, B. J., Chai, W., & Naess, A. (2021). Probabilistic Fatigue Assessment of a Mooring Line Based on Station-Keeping Trials in Ice. *40th International Conference on Ocean, Offshore and Arctic Engineering, OMAE*, Virtual, Online. https://doi.org/10.1115/OMAE2021-62924

Spencer, P., & Masterson, D. (2002). A Monte-Carlo simulator for calculating ice loads on multi-legged offshore structures. *16th IAHR Symposium on Ice*, Dunedin, New Zealand

Strub-Klein, L., & Sudom, D. (2012). A comprehensive analysis of the morphology of first-year sea ice ridges. *Cold Regions Science and Technology*, *82*, 94-109. https://doi.org/10.1016/j.coldregions.2012.05.014

Sudom, D., Timco, G., Sand, B., & Fransson, L. (2011). Analysis of first-year and old ice ridge characteristics. *21st International Conference on Port and Ocean Engineering under Arctic Conditions, POAC*, Montreal, QC, Canada

Tan, B., Li, Z. j., Lu, P., Haas, C., & Nicolaus, M. (2012). Morphology of sea ice pressure ridges in the northwestern Weddell Sea in winter. *Journal of Geophysical Research: Oceans*, *117*(C6). https://doi.org/10.1029/2011JC007800

Taylor, R. S., & Jordaan, I. J. (2015). Probabilistic fracture mechanics analysis of spalling during edge indentation in ice. *Engineering Fracture Mechanics*, *134*, 242-266. https://doi.org/10.1016/j.engfracmech.2014.10.021

Taylor, R. S., Richard, M., & Hossain, R. (2019). A Probabilistic High-Pressure Zone Model for Local and Global Loads During Ice-Structure Interactions. *Journal of Offshore Mechanics and Arctic Engineering*, *141*(5). https://doi.org/10.1115/1.4042386

Teigen, S. H., Lindvall, J. K., Samardžija, I., & Hansen, R. I. (2018). Station-Keeping Trials in Ice: Ice and Metocean Conditions. *37th International Conference on Ocean, Offshore and Arctic Engineering, OMAE*, Madrid, Spain. https://doi.org/10.1115/OMAE2018-78620

Thijssen, J., & Fuglem, M. (2015). Methodology to evaluate sea ice loads for seasonal operations. *34th International Conference on Ocean, Offshore and Arctic Engineering, OMAE*, St. John's, NL, Canada. https://doi.org/10.1115/OMAE2015-42194

Thijssen, J., Fuglem, M., & Croasdale, K. (2016). Probabilistic Assessment of Multi-Year Sea Ice Loads on Upward Sloping Arctic Structures. *Arctic Technology Conference*, St. John's, Newfoundland and Labrador, Canada. https://doi.org/10.4043/27364-MS

Thijssen, J., Fuglem, M., Richard, M., & King, T. (2014). Implementation of ISO 19906 for probabilistic assessment of global sea ice loads on offshore structures encountering first-year sea ice. *OCEANS 2014*, Piscataway, NJ, USA. https://doi.org/10.1109/OCEANS.2014.7003190

Thomas, G. A. N. (2014). Design method for ISO 19906 Arctic offshore structures. *Arctic Technology Conference*, Houston, TX, USA. https://doi.org/10.4043/24546-MS

Thomas, G. A. N. (2015). Risk and reliability in the design of arctic offshore structures. *23rd International Conference on Port and Ocean Engineering under Arctic Conditions, POAC*, Trondheim, Norway

Thomas, G. A. N., Bercha, F. G., & Jordaan, I. (2011). Reliability, limit states and action factors for ISO 19906. *Arctic Technology Conference*, Houston, TX, USA. https://doi.org/10.4043/22072-MS

Timco, G., & Burden, R. (1997). An analysis of the shapes of sea ice ridges. *Cold Regions Science and Technology*, *25*(1), 65-77. https://doi.org/10.1016/S0165-232X(96)00017-1

Timco, G., & Goodrich, L. E. (1988). Ice rubble consolidation. *9th IAHR Symposium on Ice*, Sapporo, Japan

Timco, G. W., Croasdale, K., & Wright, B. (2000). *An overview of first-year sea ice ridges* (NRC Report HYD-TR-047).

Timco, G. W., & Frederking, R. (2004). Probabilistic analysis of seasonal ice loads on the Molikpaq. *17th IAHR Symposium on Ice*, Saint Petersburg, Russia

Timco, G. W., Sudom, D., Frederking, R., Barker, A., & Wright, B. D. (2017). A critical review of Arctic pack ice driving forces: New sources of data. *Cold Regions Science and Technology*, *138*, 1-17. https://doi.org/10.1016/j.coldregions.2017.02.010

Tucker, W. B., & Govoni, J. W. (1981). Morphological investigations of first-year sea ice pressure ridge sails. *Cold Regions Science and Technology*, *5*(1), 1-12. https://doi.org/10.1016/0165-232X(81)90036-7

Valenti, V., Mahoney, A., & Metzger, A. (2021). A probabilistic description of pressure ridge width, spacing, and keel depth for the Chukchi and Beaufort seas based on IPS and ADCP observations. *Cold Regions Science and Technology*, *182*, 103171. https://doi.org/10.1016/j.coldregions.2020.103171

Vivatrat, V., & Slomski, S. (1983). A Probabilistic Basis for Selecting Design Ice Pressures and Ice Loads for Arctic Offshore Structures. *15th Offshore Technology Conference, OTC*, Houston, TX, USA. https://doi.org/10.4043/4457-MS

Vivatrat, V., & Slomski, S. (1984). Probabilistic selection of ice loads and pressures. *Journal of waterway, port, coastal, and ocean engineering*, *110*(4), 375-391. https://doi.org/10.1061/(ASCE)0733-950X(1984)110:4(375)

von Bock und Polach, R. F., Klein, M., Kubiczek, J., Kellner, L., Braun, M., & Herrnring, H. (2019). State of the art and knowledge gaps on modelling structures in cold regions. *International Conference on Offshore Mechanics and Arctic Engineering, OMAE*, Glasgow, Scotland, UK. https://doi.org/10.1115/OMAE2019-95085

Vrijling, J. K., van Hengel, W., & Houben, R. J. (1998). Acceptable risk as a basis for design. *Reliability Engineering & System Safety*, *59*(1), 141-150. https://doi.org/10.1016/S0951-8320(97)00135-X

Wadhams, P. (1983). The prediction of extreme keel depths from sea ice profiles. *Cold Regions Science and Technology*, *6*(3), 257-266. https://doi.org/10.1016/0165-232X(83)90046-0

Wadhams, P. (2000). *Ice in the Ocean*. CRC Press.

Wadhams, P. (2012). New predictions of extreme keel depths and scour frequencies for the Beaufort Sea using ice thickness statistics. *Cold Regions Science and Technology*, *76-77*, 77-82. https://doi.org/10.1016/j.coldregions.2011.12.002

Wadhams, P., & Davy, T. (1986). On the spacing and draft distributions for pressure ridge keels. *Journal of Geophysical Research*, *91*(C9), 10-697. https://doi.org/10.1029/JC091iC09p10697

Wadhams, P., & Doble, M. J. (2008). Digital terrain mapping of the underside of sea ice from a small AUV. *Geophysical Research Letters*, *35*(1), 01501-01501. https://doi.org/10.1029/2007GL031921

Wadhams, P., & Horne, R. J. (1980). An analysis of ice profiles obtained by submarine sonar in the Beaufort Sea. *Journal of Glaciology*, *25*(93), 401-424. https://doi.org/10.3189/s0022143000015264

Wadhams, P., Hughes, N., & Rodrigues, J. (2011). Arctic sea ice thickness characteristics in winter 2004 and 2007 from submarine sonar transects. *Journal of Geophysical Research: Oceans*, *116*(C8). https://doi.org/10.1029/2011JC006982

Walter, E. L., Stole-Hentschel, S., & Moslet, P. O. (2013). Estimating characteristic load effects on floating structures in ice. *32nd International Conference on Ocean, Offshore and Arctic Engineering, OMAE*, Nantes, France. https://doi.org/10.1115/OMAE2013-11400

Wang, B., Basu, R., Jha, A., & Winterstein, S. (2011). Reliability analysis of ice loads on arctic offshore structures. *21st International Conference on Port and Ocean Engineering under Arctic Conditions, POAC*, Montreal, QC, Canada

Wheeler, J. D. (1981). Probabilistic force calculations for structures in ice-covered seas. *Engineering Structures*, *3*(1), 45-51. https://doi.org/10.1016/0141-0296(81)90017-1

WindEurope. (2021). *Significant developments on offshore wind in the Baltic Sea*. Retrieved 30.09.2023 from https://windeurope.org/newsroom/significant-developments-on-offshore-wind-in-the-baltic-sea/

Zubov, N. (1943). *Arctic ice*. Izdatel'stvo Glavsevmorputi.

A Appended papers

A.1 Paper 1

Paper 1:

Samardžija, I., Høyland, K. V., Leira, B. J., & Næss, A. (2018). Probabilistic Assessment of Ice Environment and Ridge Loads for the Norströmsgrund Lighthouse. *24th IAHR Symposium on Ice,* Vladivostok, Russia.

International Association for Hydro-Environment Engineering and Research
Supported by Spain Water and IWHR, China

24th IAHR International Symposium on Ice
Vladivostok, Russia, June 4 to 9, 2018

Probabilistic Assessment of Ice Environment and Ridge Loads for the Norströmsgrund Lighthouse

Ilija Samardžija[1], Knut V. Høyland[1], Bernt J. Leira[2], Arvid Næss[3]
[1] *Sustainable Arctic Marine and Coastal Technology (SAMCoT)*
Norwegian University of Science and Technology, Høgskoleringen 7A, 7491 Trondheim, Norway
ilija.samardzija@ntnu.no
[2] *Department of Marine Technology Norwegian University of Science and Technology*
Otto Nielsens veg 10, Marine Technology Centre, 7491 Trondheim, Norway
[3] *Centre for Ships and Ocean Structures (CeSOS) Norwegian University of Science and Technology*
Otto Nielsens veg 10, Marine Technology Centre, 7491 Trondheim, Norway

Structural reliability analysis requires statistical distribution of the loads. One such case is ice load calculation for offshore structures. Ice-structure interaction is a highly stochastic phenomenon due to the natural variability of sea ice (aleatory uncertainties) and lack of knowledge about the processes that are taking place and long-term data needed for ice load calculation (epistemic uncertainties). Ice ridges are typically the ice features that govern the quasi-static ice load calculations in areas without icebergs. This is the case for Gulf of Bothnia, where Norströmsgrund lighthouse is located. This paper investigates how to utilize a Monte Carlo simulation for probabilistic assessment of ice environment and ice loads on the Norströmsgrund lighthouse. Information found in literature about sea ice growth, ridge formation and ice drift in Gulf of Bothnia (and in general) are used to simulate the ice environment parameters (e.g., ice ridge frequency of occurrence, ridge keel depth, consolidated layer thickness). Simple and generally accepted load models are used to avoid involving additional uncertainties that arise with more advanced models. The final result of the simulation is the probability distribution of the ridge horizontal load acting on Norströmsgrund lighthouse, from which loads with specific return period can be extracted (e.g., 100-year load).

1. Introduction

Modelling an uncertain phenomenon can be fully described only by using a probabilistic approach, where one needs to capture both aleatory uncertainties of the natural variability and epistemic uncertainties inherited by the lack of knowledge. Using a deterministic approach often results in excessively conservative design and overlook of important information. In order to analyze the reliability of an offshore structure it is necessary to assess the probability distributions of the extreme loads. For a structure located in ice-infested waters, sea ice will most likely govern the extreme horizontal loads. In areas where icebergs are not present, ice ridges are expected to govern the loads. Sea ice has a large natural variability spanning small and large spatial and temporal scales. Uncertainties in describing the ice-structure interaction are immense. Phenomena of ice-structure interaction has been researched extensively in the past couple of decades. However, there are gaps in knowledge that are still puzzling scientists and engineers. Examples of these difficulties are given by Jordaan (2015), where the author points out some of the issues concerning the mechanical behavior of ice, full-scale data analysis and crude idealizations of ice features in load models. This paper examines how a Monte Carlo simulation (MCS) can be utilized to simulate individual ice ridge loading events on the Norströmsgrund lighthouse. By simulating many seasons, a set of annual maximum loads is created from which statistical conclusions can be made.

The need for probabilistic treatment of ice loads acknowledged by the ISO 19906 Arctic offshore structures standard. A summary about the design methodology given in the ISO 19906 can be found in Thomas et al. (2011). The standard uses the limit states design approach and specifies that characteristic ice loads with associated annual exceedance probability shall be determined and used in load combinations. The action (load) factors in the load combination are calibrated in order to meet the required reliability targets. Background of the calibration for the ice loads factors, that itself is done using a probabilistic approach, can be found in the report made by C-CORE (2010) and summarized in Fuglem et al. (2011); Maes and Thomas (2011).

The accuracy of parameters and types of input probability distributions greatly depends on the quality and quantity of available data. In this work, we use readily available sources to establish statistical distributions for the needed input parameters. The accuracy of the adopted statistical distribution types and parameters is secondary in this paper and the methods are the primary focus. Some of the assumptions are too simplistic and several important correlations are neglected. This is done deliberately to make a simplistic probabilistic model that will lay a foundation for a more advanced model that will be developed in our future studies. This way, it will be possible to evaluate the implications of including more subtle details of the ice-structure interaction phenomena.

In the following few paragraphs, we try to give a short literature review in a chronological order and regarding the field of probabilistic ice loads assessment. To the authors knowledge, the first attempt to make a probabilistic ice-structure interaction analysis was done by Bercha et al. (1978). Another pioneering attempt was done by Wheeler (1981), where a MCS is used to estimate the ice load statistical distribution for a conical offshore structure. From the same period, it is worth mentioning the work by Jordaan (1983), where the author emphasizes the importance of probabilistic methodologies for decision-making in risk and safety assessment for

arctic offshore projects. A comprehensive ice-structure MCS with a sensitivity analysis is given in Vivatrat and Slomski (1983, 1984). Dunwoody (1991) performs an MCS of ice loads, but makes a questionable claim that the probability distributions of the ice feature characteristics must be from the log-normal family (in our experience, a lognormal type of distribution can have a good fit around the mean value, but the heavy tail of the distribution usually causes overestimation of the loads). Nessim and Jordaan (1991); Nevel (1991) are two landmark papers that show the state-of-the art (at the time) of the probabilistic ice load assessment. These two landmark papers conclude the initial development in the field. In the view of the authors of this paper, the initial period is followed by two distinct periods.

The first period is marked by somewhat reduced interest in the field and mostly scattered publications without noticeable structured progress. The period ends with introduction of the ISO 19906 draft version in the year 2007. Kato (1992) proposes a MCS based system for evaluating the ice loads for various ice features and offshore structure types. He later gives more specified examples of how this system can be used (two publications mentioned below). Comfort et al. (1998) use a MCS to analyze the influence of the limit-stress and limit-force loading scenarios. Kato (1998) performs a MCS of ice loads on a caisson structure for offshore Sakhalin. A comprehensive MCS of the ice loads for the Confederation Bridge is described by Brown et al. (2001), where they elaborately discuss the implications of choice of the parent distribution to the extreme loads. Specifically, it is described how usage of a lognormal distribution can lead to overestimates of the extreme loads. Spencer and Masterson (2002) perform a MCS for a multi-legged offshore platform interacting with first-year ice ridges. Timco and Frederking (2004) utilize a MCS to make a probabilistic analysis of the seasonal ice loads that can have operational applications, unlike the most of the publications where extreme loads were analyzed. Kato (2006) performs a MCS of first-year ridge loads with some sensitivity analysis and concludes that the consolidated layer thickness and the encounter rate of ridges are the most dominating input parameters for the resulting probability distribution of ice loads. Finally, it is worth noting the publication of Bercha et al. (2006), where the reliability of offshore structures in Arctic is addressed in general.

After the provision of the ISO 19906, one can track more structured development in the field, where particular authors (or groups) develop their approach through several publications. All of the publications address the issues and possibilities of implementing the probabilistic framework in connection to the ISO 19906. First in the series of publications is work done by Cammaert et al. (2008), where several important aspects of ice loads probabilistic assessments are discussed (e.g., the importance of including the correlations between the relevant parameters, seasonal variation of the parameters, influence of climate change on ice loads and model uncertainty). Onishchenko (2009) presents an analytical approach to the problem, unlike the most of the publications mentioned here, where MCS simulation technique is the primary method of choice. Eik and Gudmestad (2010) shows an example of how a probabilistic analysis can contribute to assessment of the iceberg design loads and the efficiency of the various components of iceberg management. Fuglem et al. (2015) give another publication addressing the iceberg design loads, where also the companion wave loads are considered. Jordaan et al. (2011) show an interesting possibility of simulating the ice environment development during a winter seasons in the Caspian Sea. Wang et al. (2011) make a comparison of the First-Order Reliability Method (FORM) and the MCS in scope of probabilistic ice loads analysis. Walter et al. (2013) describes how an ice

environmental model can be developed using the contour methodology. Bekker et al. (2012) analyze ice data from Gulf of Bothnia and describes a method of developing a probabilistic ice environment model. Interesting result in this study are the nomograms showing the inner-seasonal development of the ice parameters probability distributions. More work on the topic of probabilistic ice loads assessment by the same leading author can be found in Bekker et al. (2013a); Bekker et al. (2013b); Bekker et al. (2009). Thijssen and Fuglem (2015) give a probabilistic treatment of the ice loads for seasonal operations. Several publications are addressing the issues concerning with multi-year sea ice, Fuglem et al. (2014b); Thijssen et al. (2016); Thijssen et al. (2015). Most recent publication by Charlebois et al. (2018) uses a probabilistic model for ice forces on a caisson structure in Beaufort Sea. Finally, we list the remaining publications that are discussing issues of risk and structural reliability for offshore arctic structures in general and in connection to the ISO 19906: Fuglem et al. (2014a); Fuglem et al. (2011); McKenna et al. (2014); Moslet et al. (2011); Thijssen et al. (2014); Thomas (2014, 2015); Thomas et al. (2011).

Probabilistic ice loads assessment using a MCS can be performed in various ways, mostly depending on the ice-structure interaction considered, as well as the quality and quantity of available data. Even for a same problem of interest and identical data available, one can take different paths in order to evaluate the probability distribution of the ice loads. The work presented here does not represent any significant advancement in the field, but shows an example of a probabilistic assessment of ice environment and ridge loads. The methodology presented here will serve as a base case study for further development of a probabilistic ice loads model that we intend to develop in our future research.

2. Methods

2.1 First-year ridge load calculation formulae

Formulation given in ISO 19906 (section *A.8.2.4.5.1 First-year ridges*) is used to estimate the horizontal ridge load for the individual events. Upper bound estimate for FY ridges horizontal global load, F_R, can be done by separately taking into account contribution from consolidated layer and keel rubble load component (Eq. [1]). We assume that there is enough forcing in the surrounding ice so that the ridge is always failing against the structure (limit stress). This is a conservative assumption, as some of the strongest ridges might not fail against the structure. For further details on limiting mechanisms, see Croasdale (2009); Timco et al. (2017). Total ice ridge load can be estimated as follows:

$$F_R = F_C + F_K \,, \qquad \textbf{[1]}$$

where F_C is the load component due to the ridge consolidated layer and F_K is the load component due to the keel rubble of the ridge.

Ice load from consolidated component can be estimated using the formulation for the ice crushing global load calculation, same to that of level ice. Other than the ice crushing failure mode, there are other failure modes for the consolidated layer and ice ridge in general, such as splitting, shearing (plug failure) and spine failure (Timco et al., 2000). However, these are

considered to result in less severe loads compared to the crushing failure mode (Bjerkås & Bonnemaire, 2004). The level ice (or consolidated layer) load in case of crushing failure can be estimated as:

$$F_C = F_G = p_G \, w \, h, \qquad \textbf{[2]}$$

where p_G is the average ice pressure over the nominal contact area; w is the width of the of the contact area (structure width – 7.2 m in our case); h is the level ice thickness.

Equation for estimating the upper bound global average ice pressure given in ISO 19906 is based on the work by Kärnä and Qu (2006). The expression reads:

$$p_G = C_R \left(\frac{h}{h_1} \right)^n \left(\frac{w}{h} \right)^m \qquad \begin{array}{l} m = -0.16 \\ n = -0.5 + h/5 \;\; h < 1\text{m} \;\; ; n = -0.3 \;\; h \geq 1\text{m} \end{array}, \qquad \textbf{[3]}$$

where p_G is the global average ice pressure, in megapascals; h is the level ice thickness, in meters; h_1 is a reference thickness of 1 m; m and n is are empirical coefficients; C_R is the ice strength coefficient, in megapascals.

The adopted model for the load component of keel rubble is based on the approach used in soil mechanics for estimating the passive failure of granular material. The formulae are based on work of Dolgopolov et al. (1975), with modifications by Kärnä and Nykänen (2004):

$$F_K = \mu \, h_k \, w \left(\frac{h_k \, \mu_\phi \, \gamma_e}{2} + 2c \right) \left(1 + \frac{h_k}{6w} \right), \qquad \textbf{[4]}$$

$$\mu_\phi = \tan\left(45° + \frac{\phi}{2} \right), \qquad \textbf{[5]}$$

where h_k is the rubble thickness measured from bottom of consolidated layer; μ_ϕ is the passive pressure coefficient; ϕ is the angle of internal friction; c is the apparent keel cohesion (average value over the keel volume); γ_e is the effective buoyancy. The effective buoyancy is calculated as follows:

$$\gamma_e = \; 1 - e \quad \rho_w - \rho_i \;\; g \, , \qquad \textbf{[6]}$$

where e is the keel macroporosity; ρ_w is the water density (1005 kg/m^3 – deterministic value in our simulation); ρ_i is the ice density (910 kg/m^3 – deterministic value in our simulation).

2.2 Monte Carlo simulation

Monte Carlo simulation is performed for 1,000,000 seasons, with number of ridge-structure interaction events set to 1200 for each season. The number of events (interaction rate) is a key

component in probabilistic analysis. The number is estimated by taking into account average season duration, percentage of time when ice is failing in crushing mode and mean ice drift speed when ice is crushing as given in Kärnä and Qu (2006), as well as the ice ridge occurrence frequency as given in Lewis et al. (1993). This rough estimate is too simplistic and uncoupled from the statistical distributions of ice parameters. This issue is discussed further in the discussion section of this paper.

To reflect the seasonal variability of winter severity we use data about the maximum level ice thickness. The idea is that the ice thickness will be proportional in some way to the maximum level ice thickness throughout a season. The maximum annual level ice thickness is modeled using a normal distribution with a mean of 0.72 m and a standard deviation of 0.12 m. The parameters of the distribution are based on data from Kemi measurement station and we assume that this is a good representative for Northern Bay of Bothnia (Ronkainen, 2013). Note that this location is further north from our location and in landfast ice zone. Therefore, this statistics might somewhat overestimate the ice thickness.

Simulation of one season starts by generating a maximum level ice thickness for that season from the distribution described above. Assuming that a ridge interaction event can occur at any point in time during the season with equal probability, we generate interaction times for all of the N number of events. Interaction times, t_n, are given in normalized values of season length. Knowing the interaction time, we can estimate the level ice for the given event. This is done using a normalized ice growth curve that was developed based on the average ice growth trend obtained from Saloranta (2000), where average ice growth of seasons 1979-90 for a location in Gulf of Bothnia is given. It is assumed that ice grows in similar manner in our location as well. Similar type of ice growth curve was also used in probabilistic ice loads assessment by Timco and Frederking (2004) for a structure in Beaufort Sea. The normalized ice growth equation adopted here is approximate and used as an example to point out the importance of inner-seasonal ice thickness variation in probabilistic simulation. The equation can be expressed as:

$$\begin{aligned} h_n\ t_n &= \sqrt{\frac{t_n}{0.8}} && \text{for} \quad 0 \le t_n \le 0.8, \\ h_n\ t_n &= 5 - 5t_n && \text{for} \quad 0.8 < t_n \le 1, \end{aligned} \qquad \textbf{[7]}$$

where h_n is the normalized ice thickness and t_n is the normalized time of ridge interaction in the given winter season. Graphical illustration of the Eq. [7] is shown in Fig. 1. The approach assumes that the ice is growing to its maximum thickness in the first 80% of the season proportional to square root of time. In addition to the field measurements and numerical simulations (Saloranta, 2000), this assumption is supported by analytical ice growth models (Leppäranta, 1993; Stefan, 1891). In summary, for a given season's maximum ice thickness, normalized time of ridge interaction and assuming the above described ice growth nature, level ice thickness for an event will have the following value:

$$h_{LI,i} = h_{y,AM} \times h_n\ t_n\ , \qquad \textbf{[8]}$$

where $h_{y,AM}$ is the simulated maximum level ice thickness (annual maximum – AM).

We have established a method for generating the surrounding level ice thickness for events, but we need the consolidated layer thickness. ISO 19906 recommends that in absence of data, the consolidated layer thickness can be assumed to be twice as the surrounding ice. Immediately after a ridging event, the surrounding level ice will have a certain thickness, while the consolidated layer is about to develop from the loose rubble. The consolidated layer will grow with a faster rate than the nearby level ice because only the voids in the rubble need to be frozen. Based on the field measurements reported in literature, it can be deducted that the ratio between consolidated layer and level ice will not get greater than two (FY ridges). We assume that age of a ridge (time since it was created) when the ridge is hitting the structure completely random. Thereby, the ratio between the consolidated layer and the level ice will be random too. It is assumed that this ratio for a given ridge interaction event has a uniform distribution with bounds [1, 2]. In summary, after simulating level ice thickness, we multiply it with a randomly simulated ratio to get the consolidated layer thickness. Fig. 2 illustrates the input level ice annual maximum (AM) level ice thickness and the results of the ice thicknesses simulation (level ice thickness for a given event (GAE), consolidated layer thickness for a given event and annual maximum consolidated layer thickness).

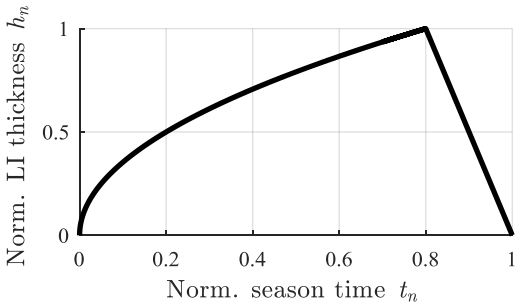

Fig. 1. Eq. [7] – Normalized ice growth function.

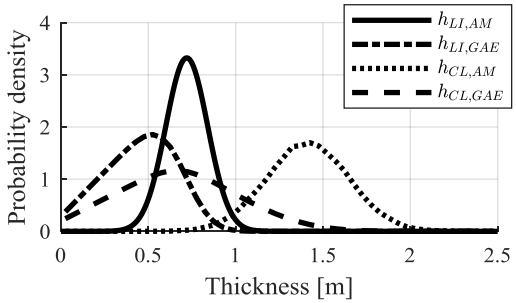

Fig. 2. Ice thicknesses probability distributions.

Next step is to simulate the strength coefficient C_R. ISO 19906 instructs that PDF should be estimated for this parameter when probabilistic approach is used. Unfortunately, no guidance is given on how to establish this probability distribution. Only the characteristic values with a certain return period are given. In our probabilistic simulation, we need distributions with probabilities for a given event (parent distributions). ISO 19906 recommends characteristic value of the strength coefficient with 100-year return period for Baltic Sea (1.8 MPa). Figure 10 in paper by Kärnä and Masterson (2011) summarizes the results from an extreme value analysis of both local and global ice pressures that was previously performed by Kärnä and Qu (2005); Kärnä et al. (2006). The figure shows how ice strength coefficient varies with the return period. Line from the figure that corresponds to the global pressure is recreated in the Fig. 3 (dashed line). Using these results, we can read the ratio between the characteristic values with 100-year and 1-year return periods. From this, we calculate that the characteristic value associated with 1-year is 1.2 MPa. We assume that the parent distribution of strength coefficient can be described with a two-parameter Weibull distribution. By knowing the average number of events per season n, we know that the probability (in the parent distribution) of the 1-year event is equal to $1/n$ and for the 100-year event it is equal to $1/\,100\times n$. This gives us enough information to calibrate the shape parameter α (1.234) and the scale parameter β (0.245) of the assumed

Weibull distribution. Full line in Fig. 3 shows how this artificially created distribution gives us variation of the strength coefficient with the return period. When comparing this to the original variation as given in Kärnä and Masterson (2011), one can see that characteristic values for 1-year and 100-year return period are equal (these were our calibration points), and for the rest it is reasonably accurate. Fig. 4 illustrates the given an event (GAE) distribution of the adopted Weibull distribution for the strength coefficient with the above stated parameters and the resulting annual maximum (AM) distribution given the number of events per season.

It is important to note that the above-mentioned recommendations for the strength coefficient are valid for level ice, but we use it for consolidated layer. Due to the higher homogeneity of level ice thickness in comparison to the consolidated layer and possibly the same relation in local strength properties, one would expect that level ice would give higher global loads than the consolidated layer of a same average thickness. In our simulations, we neglect this effect. For further details on this topic, reader is referred to the discussions on the subject given in Høyland (2007); Høyland et al. (2000); Shafrova and Høyland (2008).

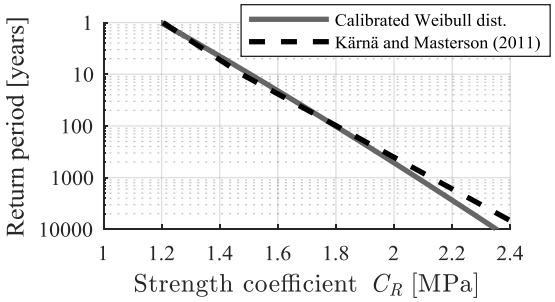

Fig. 3. Characteristic values for associated return periods of strength parameter.

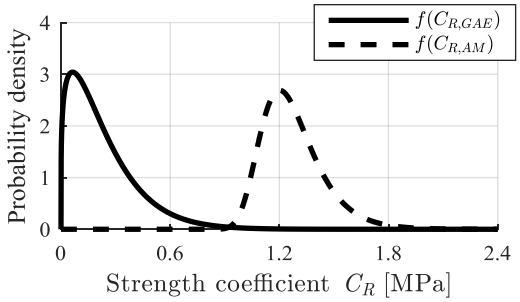

Fig. 4. Given an event (GAE) and annual maximum (AM) PDF of the strength coefficient C_R.

Having established the simulation methodology for both ice thickness and strength coefficient (for a given event in a given season), we can now simulate the consolidated layer component of the total ridge load. To complete the total ridge load simulation, we need to simulate the rubble component. No correlation between the parameters of the consolidated layer and parameters of the rubble is assumed. Implications of this assumption is discussed later in the text. The following parameters are used for describing the probability distributions of the parameters needed for the rubble load component. Uniform distributions (with bounds given in brackets) are used for keel macroporosity [20 % – 40 %], apparent cohesion [5 kPa – 7 kPa] and angle of friction [20° – 40°]. The bounds are adopted from the recommendations given in the ISO 19906. The most important parameter, the keel depth, is modelled using an exponential distribution. The exponential type of distribution for this parameter was used because previous studies show considerable evidence that ridge keel depths obey this type of distribution (Wadhams & Davy, 1986). The only parameter of the distribution, the mean, was calculated using the mean sail height measured by helicopter-borne laser profiling (Lewis et al., 1993) and multiplied by the ratio of maximum keel depth to maximum sail height (Strub-Klein & Sudom, 2012). This calculation gives us a mean keel depth of 4.2 m. We use this approach in absence of upward looking sonar data for the Baltic Sea, which would be the best source of data for this parameter. The used exponential distribution is shifted by 2 m and with a mean of 2.2 m. Note that it is assumed that any ridge deeper than the water depth cannot approach the structure.

3. Results and discussion

Fig. 5 summarizes the results of the MCS performed in this paper. It shows the probability distribution of total horizontal ridge load, as well as the probability distributions two load components (consolidated layer and rubble). The characteristic loads with 100-year and 10000-year return periods are 11.7 MN and 16.1 MN, respectively. It is interesting to note that the design line load for the Norströmsgrund lighthouse was 2.2 MN/m (Bjerkås & Nord, 2016). This means that the design ice load was 15.84 MN.

The rubble load component does not increase significantly with higher return periods because of the depth limitations. Although the consolidated layer gives higher loads for a same return period when the two components are analyzed independently, the rubble component still contributes significantly to the total load. For 54% of the maximum annual load events, the rubble component was higher than the consolidated layer component. Further clues about the importance of rubble can be seen on Fig. 6 with a bivariate distribution of consolidated layer thickness and keel depth for the events of annual maximum loads. It can be seen that there are two concentrations of these events. One is located towards the limiting water depth and modal consolidated layer thickness (0.68 m). Second is located towards the minimum value of keel depth as previously defined in the keel distribution (2 m) and close to the modal maximum annual consolidated layer thickness (1.41 m).

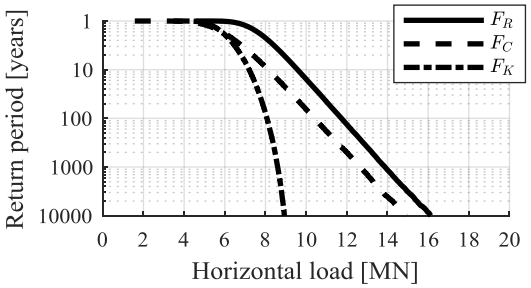

Fig. 5. Probability of exceedance for ridge loads and its components given in terms of return periods.

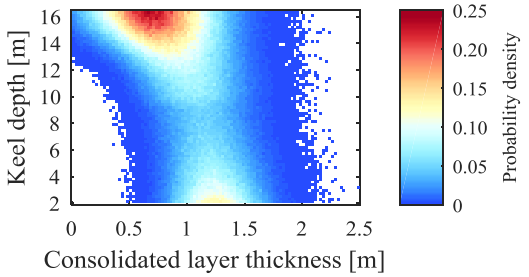

Fig. 6. Bivariate probability distribution for the annual extreme loads.

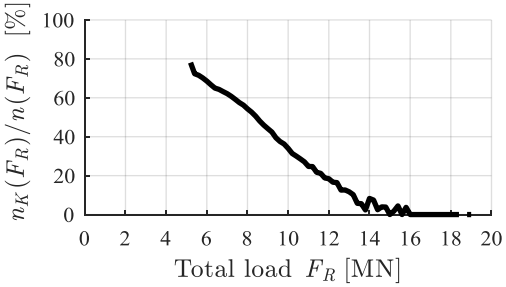

Fig. 7. Percentage of annual extreme events where rubble gives a higher load than the consolidated layer.

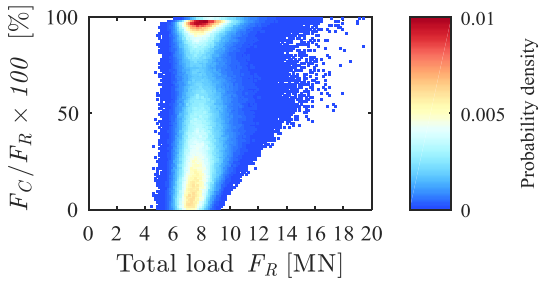

Fig. 8. Consolidated layer load component contribution to the total load.

To give a complete description, we need to show the relative importance of the two load components. First, we subsample all of the annual extreme events in intervals of 0.2 MN of the total load F_R. In each of these intervals there will be a certain number of extreme events $n\ F_R$. For each interval, we count the extreme load events where the rubble load was the dominating component $n_K\ F_R$ (contributing to the total load with more than 50%). By dividing

$n_K\ F_R\ /n\ F_R$ we get the percentage of the extreme events that were dominated by rubble load for each interval (Fig. 7). It can be seen that more events are dominated by consolidated layer component as the total load increases. This is caused by the assumption that the consolidated layer probability distribution varies from year to year, while the keel depth has the same probability distribution for all years. This means that for those years where the consolidated layer thickness is small, the keel rubble is governing the loads. This still does not mean that the rubble is not important for the higher extreme loads. We can see this on Fig. 8 that illustrates the probability distribution of the annual maximum load events with respect both to the total load F_R and the consolidated layer contribution to the total load $F_C/F_R \times 100$. Although for the higher total loads the consolidated layer component contribution is usually higher than 50%, the rubble component is often contributing with a significant percentage.

4. Conclusion and outlook

The approach described is aimed at development of probabilistic assessment of ice environment and ice ridge loads. Case study was performed using a Monte Carlo simulation for the Norströmsgrund lighthouse. This structure was chosen for the case study because a great deal of knowledge about the full scale ice-structure interaction originates from the measurements done on this structure. Still, it was not a trivial task to setup the simulation. Difficulties arise when probability distributions of relevant parameters need to be established. For example, the strength coefficient is an empirical parameter. Therefore, only full-scale measurements can serve as a basis for establishing the probability distribution of the parameter. A method to back-calculate the parent distribution of this coefficient is proposed in this paper. In addition, a way to simulate the consolidated layer thickness for the individual events is described.

We emphasize the importance of establishing the probability distribution in accordance to what is simulated. Adopting a probability distribution from data of annual extremes when simulating individual events is one example where a crude error can be made. More subtle errors are made when distributions are based on data that comes from field measurements at the end of the season, while the simulation is performed throughout a season. This error is present in this paper, where we take measurements of ridge sails that represent the state at one point in time and we use the same distribution for all the seasons and throughout a season. Having same ridge keel depth statistics for all season will not cause a big error. However, assumption that the ridges are statistically equally deep throughout a season will cause overestimated keel depths early in the season because it can be expected that level ice thickness and keel depths are positively correlated (i.e., deep keels are produced towards the end of the season when level ice is sufficiently thick) (Amundrud et al., 2004; Hopkins, 1998).

Another error is hidden in the assumption of uniform distribution of interaction times in the season. To a smaller extent, this is not true due to the fact that ice mobility can change during the season. To a larger extend, a more subtle effect influences the distribution of the number of events in different parts of a season. Ridge statistics is commonly obtained from Upward Looking Sonar instruments and Rayleigh criterion is used to identify the individual ridges. Thresholds used in Rayleigh criterion will influence the number of ridges (Ekeberg et al., 2015). Early in the season the number of ridges identified by the method will be much smaller due to the fact that most of the ridges are below the threshold. Appropriate way to account for this would be to use a keel depth probability distribution that develops throughout a season and

number of events that must be coupled to the used probability distribution of keel depths (and thereby also developing throughout a season). One way to do this is to quantify the correlation of level ice and ridge keel depth statistics and then simulate ridges accordingly to the surrounding level ice. We hope that this will be possible in our future research. Furthermore, we will explore the possibilities of simulating the consolidation of rubble more accurately by taking the physics of the phenomena into account. Among other details of ice-structure interaction that were not included in our simulation and not discussed here, we highlight the importance of including the limiting scenarios in the simulation (limit-stress and limit force).

The presented case study clearly has some limitations. The first is the limited data on which the probability distributions of the input parameters were established. The second is negligence of important correlations, such as level ice and keel depth correlation. The third is rather simplified treatment of interaction rate. The final, forth, is the negligence of some of the important aspects of ice-structure interaction, such as limiting scenarios. Furthermore, sensitivity analysis was not performed and this is the main reason why the results need to be interpreted with caution. It is easy to expect that characteristic loads would change with adjusted input parameters, but more importantly, the qualitative conclusions about the relative contributions of the two load components could completely alter with adjusted relative weights between inputs related to the consolidated layer and to the keel rubble. Despite the limitations of our method, the approach shows some important aspects of probabilistic assessment of ice loads and ice environment and provides a framework for further improvements. We have shown how relative importance of consolidated layer and rubble in ridge loads calculations can be analyzed. This is one example of how probabilistic analysis can be beneficial in enhancing our understanding of ice-structure interaction and possibly give us guidance about what should be the focus of future studies in ice engineering and/or future full-scale measurements.

Let us end this paper by concluding that a better treatment of strength coefficient, C_R, need to be made. This parameter contains a great deal of aleatory uncertainty owing to the natural variability of ice environment. This part of the uncertainty is not fully quantified yet. In addition, there is epistemic uncertainty built into this parameter as well, as we still cannot fully understand the ice-structure interaction phenomena. Increasing the reliability of offshore structures in arctic areas can be done most effectively with a better characterization of ice-structure interaction. In example of ridge loads, this would be reflected in better description of the strength coefficient uncertainty by quantifying the aleatory and reducing the epistemic part of the uncertainty that are combined in this coefficient. It is our recommendation that this can be best done by comprehensive long-term full-scale measurements of ice-structure interaction.

Acknowledgements

The authors wish to acknowledge the support of the Research Council of Norway through the Centre of Research-based Innovation, SAMCoT, and the support of the SAMCoT partners. This work has been carried out within the NTNU Oceans Pilot project "Risk, reliability and ice data in arctic marine environment".

References

Amundrud, T. L., Melling, H., and Ingram, R. G. (2004). Geometrical constraints on the evolution of ridged sea ice. *Journal of Geophysical Research, 109*(C6), 12 pp.

Bekker, A. T., Sabodash, O. A., and Kovalenko, R. G. (2013a). Modeling and analysis of probabilistic distributions of ice loads on lighthouse structures in the Gulf of Bothnia. Proc. 23rd International Offshore and Polar Engineering Conference. International Society of Offshore and Polar Engineers, Anchorage, Alaska, USA.

Bekker, A. T., Sabodash, O. A., and Kovalenko, R. G. (2013b). Probabilistic modeling of extreme value distributions of ice loads on "Molikpaq" platform for Sakhalin-II project. Proc. 32nd International Conference on Ocean, Offshore and Arctic Engineering, OMAE Nantes, France.

Bekker, A. T., Sabodash, O. A., Kovalenko, R. G., and Rusakov, D. S. (2012). Probabilistic modeling of ice environment from lighthouses zone in the Gulf of Bothnia. Proc. 22nd International Offshore and Polar Engineering Conference, ISOPE, Rhodes, Greece.

Bekker, A. T., Sabodash, O. A., Seliverstov, V. I., Koff, G. L., and Pipko, E. N. (2009). Estimation of Limit Ice Loads On Engineering Offshore Structures In the Sea of Okhotsk. Proc. 9th International Offshore and Polar Engineering Conference, Osaka, Japan.

Bercha, F. G., Danys, J. V., and Rokne, J. G. (1978). Probabilistic ice-structure interaction theory. *5th IAHR Symposium on Ice, v*(1), 77-95.

Bercha, F. G., Gudmestad, O. T., Nevel, D., Foschi, R., Sliggers, F., and Nikitina, N. (2006). Reliability of arctic offshore installations. Proc. 7th International Conference and Exhibition on Performance of Ships and Structures in Ice, ICETECH, Banff, AB, Canada.

Bjerkås, M., and Bonnemaire, B. (2004). Ice ridge-structure interaction Part II: Loads from firstyear ice ridges and their surrounding ice sheets. Proc. 17th IAHR Symposium on Ice, St. Petersburg, Russia.

Bjerkås, M., and Nord, T. S. (2016). Ice action on Swedish lighthouses revisited. Proc. 23rd IAHR Symposium on Ice, Ann Arbor, Michigan, USA.

Brown, T. G., Jordaan, I. J., and Croasdale, K. R. (2001). A probabilistic approach to analysis of ice loads for the Confederation Bridge. *Canadian Journal of Civil Engineering, 28*(4), 562-573.

C-CORE. (2010). Calibration of action factors for ISO 19906 Arctic offshore structures.

Cammaert, A. B., Trumars, J., and Eide, L. I. (2008). A probabilistic approach to design ice loads for an Arctic jack-up drilling platform. Proc. 27th International Conference on Offshore Mechanics and Arctic Engineering, OMAE, Berlin, Germany.

Charlebois, L., Frederking, R., Timco, G. W., Watson, D., and Richard, M. (2018). Evaluation of pack ice pressure approaches and engineering implications for offshore structure design. *Cold Regions Science and Technology, 149*, 71-82.

Comfort, G., Singh, S., and Dinovitzer, A. (1998). Limit-force ice loads and their significance to offshore structures in the Beaufort Sea. *International Journal of Offshore and Polar Engineering, 8*(1), 16-21.

Croasdale, K. R. (2009). Limit force ice loads - An update. Proc. 20th International Conference on Port and Ocean Engineering under Arctic Conditions, POAC, Lulea, Sweden.

Dolgopolov, Y. V., Afanasiev, V. P., Koren'kov, V. A., and Panfilov, D. F. (1975). Effect of hummocked ice on the piers of marine hydraulic structures. Proc. 3rd IAHR Symposium on Ice Problems, Hanover, W Ger.

Dunwoody, A. B. (1991). Reliability against drifting ice. An adjunct to Monte Carlo simulation. *Journal of Offshore Mechanics and Arctic Engineering, 113*(3), 253-259.

Eik, K., and Gudmestad, O. T. (2010). Iceberg management and impact on design of offshore structures. *Cold Regions Science and Technology, 63*(1-2), 15-28.

Ekeberg, O.-C., Høyland, K., and Hansen, E. (2015). Ice ridge keel geometry and shape derived from one year of upward looking sonar data in the Fram Strait. *Cold Regions Science and Technology, 109*, 78-86.

Fuglem, M., Richard, M., and King, T. (2014a). An implementation of ISO 19906 formulae for global sea ice loads within a probabilistic framework. Proc. Arctic Technology Conference, Houston, TX, United states.

Fuglem, M., Richard, M., and Thijssen, J. (2014b). Challenges Implementing ISO 19906 for Probabilistic Assessment of Multi-year Sea Ice Loads on Sloping Structures. Proc. 11th International Conference and Exhibition on Ships and Structures in Ice, Alberta, Canada.

Fuglem, M., Stuckey, P., and Jordaan, I. (2011). Probabilistic ice loads assessments for arctic regions: Inputs for calibration of ISO 19906. Proc. Arctic Technology Conference, Houston, TX, United states.

Fuglem, M., Stuckey, P., and Suwan, S. (2015). Estimating iceberg-wave companion loads using probabilistic methods. Proc. 34th International Conference on Ocean, Offshore and Arctic Engineering, OMAE, St. John's, NL, Canada.

Hopkins, M. A. (1998). Four stages of pressure ridging. *Journal of Geophysical Research, 103*(C10), 21883-21891.

Høyland, K. V. (2007). Morphology and small-scale strength of ridges in the North-western Barents Sea. *Cold Regions Science and Technology, 48*(3), 169-187.

Høyland, K. V., Kjestveit, G., Heinonen, J., and Määttänen, M. (2000). LOLEIF ridge experiments at Marjaniemi; The size and strength of the consolidated layer. Proc. 15th IAHR Symposium on Ice, Gdansk, Poland.

ISO 19906. (2010). Arctic offshore structures. *Petroleum and natural gas industries*.

Jordaan, I. (1983). Risk and Safety Assessment for Arctic Offshore Projects. Proc. 2nd Massachusetts Institute of Technology Sea Grant College Program Lecture and Seminar.

Jordaan, I. (2015). Some issues in ice mechanics. Proc. 34th International Conference on Ocean, Offshore and Arctic Engineering, OMAE, St. John's, NL, Canada.

Jordaan, I., Stuckey, P., Bruce, J., Croasdale, K., and Verlaan, P. (2011). Probabilistic modelling of the ice environment in the northeast Caspian sea and associated structural loads. Proc. 21st International Conference on Port and Ocean Engineering under Arctic Conditions, POAC, Montreal, QC, Canada.

Kärnä, T., and Masterson, D. M. (2011). Data for crushing formula. Proc. 21st International Conference on Port and Ocean Engineering under Arctic Conditions, POAC, Montreal, QC, Canada.

Kärnä, T., and Nykänen, E. (2004). An approach for ridge load determination in probabilistic design. Proc. 17th IAHR Symposium on Ice, Saint Petersburg, Russia.

Kärnä, T., and Qu, Y. (2005). Analysis of the Size Effect in Ice Crushing – edition 2. In: VTT Technical Research Centre of Finland, Internal Rep. No. RTE-IR-6/2005, Version.

Kärnä, T., and Qu, Y. (2006). Extended Baltic model of global ice forces. Proc. 18th IAHR Symposium on Ice, Sapporo, Japan.

Kärnä, T., Qu, Y., and Yue, Q. (2006). An extreme value analysis of local ice pressures. Proc. 7th International Conference and Exhibition on Performance of Ships and Structures in Ice, ICETECH Banff, AB, Canada.

Kato, K. (1992). Design ice force estimating system. Proc. 2nd International Offshore and Polar Engineering Conference, San Francisco, CA, USA.

Kato, K. (1998). Trial calculation of design ice loads on an arctic structure for offshore Sakhalin. Proc. 8th International Offshore and Polar Engineering Conference, Montreal, Canada.

Kato, K. (2006). Morphology of a first-year ridge and its influences on design ice load in the Sea of Okhotsk. Proc. 18th IAHR Symposium on Ice, Sapporo, Japan.

Leppäranta, M. (1993). A review of analytical models of sea‐ice growth. *Atmosphere-Ocean, 31*(1), 123-138.

Lewis, J. E., Lepparanta, M., and Granberg, H. B. (1993). Statistical properties of sea ice surface topography in the Baltic Sea. *Tellus, Series A (Dynamic Meteorology and Oceanography), 45A*(2), 127-142.

Maes, M. A., and Thomas, G. A. N. (2011). Risk-based calibration of action factors in the new ISO 19906 Arctic Offshore Structures Standard. Proc. Arctic Technology Conference, Houston, TX, United states.

McKenna, R., Fuglem, M., and Croocker, G. (2014). Uncertainty in 100 and 10,000 Year Ice Loads on Offshore Structures. Proc. 11th International Conference and Exhibition on Ships and Structures in Ice, Alberta, Canada.

Moslet, P. O., Gudmestad, O. T., Sildnes, T., and Saebo, E. (2011). The new ISO19906 standard and related arctic activities at DNV. Proc. 21st International Conference on Port and Ocean Engineering under Arctic Conditions, POAC, Montreal, QC, Canada.

Nessim, M., and Jordaan, I. (1991). The Selection of Design Ice Loads and Design Ice Features for Fixed Structures in the Beaufort Sea. In *Ice-Structure Interaction* (pp. 483-506): Springer.

Nevel, D. E. (1991). Probabilistic Ice Forces on Offshore Structures. In *Ice-Structure Interaction* (pp. 541-557): Springer.

Onishchenko, D. A. (2009). Analytical approach to the calculation of the design values of the loads associated with discrete ice features. Proc. 20th International Conference on Port and Ocean Engineering under Arctic Conditions, POAC, Lulea, Sweden.

Ronkainen, I. (2013). *Long-term changes in Baltic Sea ice conditions.* (Master thesis). University of Helsinki, Helsinki, Finland.

Saloranta, T. M. (2000). Modeling the evolution of snow, snow ice and ice in the Baltic Sea. *Tellus, 52A*, 93-108.

Shafrova, S., and Høyland, K. V. (2008). Morphology and 2D spatial strength distribution in two Arctic first-year sea ice ridges. *Cold Regions Science and Technology, 51*(1), 38-55.

Spencer, P., and Masterson, D. (2002). A Monte-Carlo simulator for calculating ice loads on multi-legged offshore structures. Proc. 16th IAHR Symposium on Ice, Dunedin, New Zealand.

Stefan, J. (1891). Über die Theorie der Eisbildung, insbesondere über die Eisbildung im Polarmeere. *Annalen der Physik, 278*(2), 269-286.

Strub-Klein, L., and Sudom, D. (2012). A comprehensive analysis of the morphology of first-year sea ice ridges. *Cold Regions Science and Technology, 82*, 94-109.

Thijssen, J., and Fuglem, M. (2015). Methodology to evaluate sea ice loads for seasonal operations. Proc. 34th International Conference on Ocean, Offshore and Arctic Engineering, OMAE, St. John's, NL, Canada.

Thijssen, J., Fuglem, M., and Croasdale, K. (2016). Probabilistic Assessment of Multi-Year Sea Ice Loads on Upward Sloping Arctic Structures. Proc. Arctic Technology Conference, St. John's, Newfoundland and Labrador, Canada.

Thijssen, J., Fuglem, M., Muggeridge, K., Morrison, T., and Spencer, P. (2015). Update on Probabilistic Assessment of Multi-year Sea Ice Loads on Vertical-faced Structures. Proc. Arctic Technology Conference, Copenhagen, Denmark.

Thijssen, J., Fuglem, M., Richard, M., and King, T. (2014). Implementation of ISO 19906 for probabilistic assessment of global sea ice loads on offshore structures encountering first-year sea ice. Proc. OCEANS 2014, Piscataway, NJ, USA.

Thomas, G. A. N. (2014). Design method for ISO 19906 Arctic offshore structures. Proc. Arctic Technology Conference, Houston, TX, United states.

Thomas, G. A. N. (2015). Risk and reliability in the design of arctic offshore structures. Proc. 23rd International Conference on Port and Ocean Engineering under Arctic Conditions, POAC, Trondheim, Norway.

Thomas, G. A. N., Bercha, F. G., and Jordaan, I. (2011). Reliability, limit states and action factors for ISO 19906. Proc. Arctic Technology Conference, Houston, TX, United states.

Timco, G. W., Croasdale, K., and Wright, B. (2000). An overview of first-year sea ice ridges. NRC Report HYD-TR-047. Ottawa, Ont., Canada.

Timco, G. W., and Frederking, R. (2004). Probabilistic analysis of seasonal ice loads on the Molikpaq. Proc. 17th IAHR Symposium on Ice, Saint Petersburg, Russia.

Timco, G. W., Sudom, D., Frederking, R., Barker, A., and Wright, B. D. (2017). A critical review of Arctic pack ice driving forces: New sources of data. *Cold Regions Science and Technology*, *138*, 1-17.

Vivatrat, V., and Slomski, S. (1983). A Probabilistic Basis for Selecting Design Ice Pressures and Ice Loads for Arctic Offshore Structures. Proc. 15th Offshore Technology Conference, Houston, TX, USA.

Vivatrat, V., and Slomski, S. (1984). Probabilistic selection of ice loads and pressures. *Journal of waterway, port, coastal, and ocean engineering, 110*(4), 375-391.

Wadhams, P., and Davy, T. (1986). On the spacing and draft distributions for pressure ridge keels. *Journal of Geophysical Research, 91*(C9), 10-697.

Walter, E. L., Stole-Hentschel, S., and Moslet, P. O. (2013). Estimating characteristic load effects on floating structures in ice. Proc. 32nd International Conference on Ocean, Offshore and Arctic Engineering, OMAE, Nantes, France.

Wang, B., Basu, R., Jha, A., and Winterstein, S. (2011). Reliability analysis of ice loads on arctic offshore structures. Proc. 21st International Conference on Port and Ocean Engineering under Arctic Conditions, POAC, Montreal, QC, Canada.

Wheeler, J. D. (1981). Probabilistic force calculations for structures in ice-covered seas. *Engineering Structures, 3*(1), 45-51.

A.2 Paper 2

Paper 2:

Samardžija, I., & Høyland, K. V. (2019). Initial results of a study into the relationship between level ice draft and ridge keel draft. *25th International Conference on Port and Ocean Engineering under Arctic Conditions*, Delft, The Netherlands.

Proceedings of the 25th International Conference on
Port and Ocean Engineering under Arctic Conditions
June 9-13, 2019, Delft, The Netherlands

Initial results of a study into the relationship between level ice draft and ridge keel draft

Ilija Samardžija[1], Knut V. Høyland[1]
[1] Sustainable Arctic Marine and Coastal Technology (SAMCoT), Norwegian University of Science and Technology, Trondheim, Norway

ABSTRACT

Probabilistic assessment of global ice actions on offshore structures must include correlations between relevant input variables. The most important geometrical properties of ice ridges are the consolidated layer thickness and the ridge keel draft. However, an estimate of the surrounding level ice thickness is also needed for calculating the limit force mechanism (the force giving ice ridging a distance away from the ridge instead of crushing at the structure surface). It is, therefore, important to understand the correlation between level ice thickness and ridge keel draft. This paper is focused on quantifying the correlation between level ice draft (convertible to level ice thickness) and ridge keel draft for later use in probabilistic ice load calculations. This is done by analyzing ice draft data obtained by upward looking sonars in the Beaufort Sea. A positive linear correlation is found between level ice draft and extreme keel draft. An approach is proposed for probabilistic simulation of these two variables.

KEY WORDS: Sea ice; Ridge keel; Draft; Thickness, Probabilistic ice actions.

NOMENCLATURE:

ADCP – Acoustic Doppler Current Profiler

ULS – Upward-Looking Sonar.

FYI – First-Year Ice.

MYI – Multi-Year Ice.

PDF – Probability Density Function.

LI – Level Ice.

INTRODUCTION

Sea ice is characterized by high natural variability with respect to its physical properties. Due to this variability, but also due to the incomplete understanding of phenomena and limited environmental data, ice-structure interaction is associated with large uncertainties. This requires a probabilistic treatment of the problem, where ice environment is replicated in procedures such as Monte Carlo simulation. Deterministic approach typically requires an estimate of extreme values for the input variables and often results in overly conservative design due to unlikely combinations of conservative assumptions. Probabilistic approach

accounts for this fact and characterizes each variable with a probability density function. Given that the variables are not positively correlated, combinations of extremes are unlikely. Unlike other environmental actions such as wind and waves, where the number of environmental variables is relatively small, a proper description of ice actions depends on many environmental variables. Surely, some of these variables are correlated and neglecting them represents a serious pitfall that can cause underestimation (or overestimation) of ice actions.

One such correlation, often being neglected, is the relationship between the surrounding level ice (LI) thickness and the ridge keel draft. Considering a scenario where an ice ridge is hitting a structure, an isolated ridge rarely causes extreme loads and more often it is a ridge that is pushed by the surrounding ice pack. Therefore, to estimate the load exerted on a structure, both limit force and limit stress scenarios must be considered (Croasdale, 1984). Limit force represents the maximum loading that the surrounding ice can transfer to a structure through an ice ridge in front of the structure. Limit stress represents the maximum loading that a ridge can exert on the structure while failing immediately in front of the structure. The lower of the two conditions will limit the maximum loading for a given event. State of the knowledge regarding the limit force condition was summarized by Croasdale (2009, 2012a, 2012b) and adopted in the informative section of the 19906 ISO Arctic Offshore Structures Standard (ISO 19906, 2010). More recently, Timco et al. (2017) contributed to further understanding of pack ice driving forces by analyzing various sources of full-scale data and proposed a new approach that uses a probability exceedance function for the pack ice driving force calculation (limit force scenario). Charlebois et al. (2018) compare this new approach to the one given in the ISO 19906 (2010) and discuss engineering implications from a probabilistic design perspective. In all above-mentioned publications, authors have acknowledged the importance of the LI thickness in limit force calculations. Most of the formulations indicate a dependence of pack ice pressure on the LI thickness. Furthermore, LI thickness is important even if pack ice pressure is not a function of the LI ice thickness because the limit force will still be linearly proportional to the LI thickness (relation of force to the nominal area). This raises the following question: how should we simulate the surrounding LI thickness in probabilistic simulations of ice ridge loads on an offshore structure?

To further describe the importance of the LI thickness in relation to probabilistic ridge load assessment, let us discuss the implications of the correlation between the surrounding LI thickness and ridge keel draft. If the two variables are uncorrelated in a probabilistic simulation, extreme events with deep ridges will not be associated with thick surrounding LI. In this scenario, the maximum loading will often be governed by the limit force condition because the thin surrounding LI will not be able to produce high enough forcing to fail the ridge against the structure (the limit force will be smaller than the limit stress). If, however, the two variables are positively correlated, extreme events with deep ridges will be associated with thick surrounding LI. This means that, relative to the uncorrelated scenario, it will be more likely that the maximum loading will be governed by the limit stress scenario. An extreme load with a given return period will be higher in case of correlated variables (e.g., extreme load with 100-years return period) and ignoring this can run a risk of underestimation of the extreme load.

There is considerable evidence indicating that deep ridges are associated with thicker surrounding LI. Numerical models of ridge building processes conclude that limited draft of ridge keels is a function of LI strength and thickness (Parmerter and Coon, 1972, Hopkins, 1998). This relation was also confirmed in physical tests on a laboratory scale (Tuhkuri and Lensu, 2002). In addition, the relation has been observed in full-scale measurement (Amundrud et al., 2004, Melling and Riedel, 1996, Ross et al., 2012, Mudge et al., 2013). Numerical and physical models give a good insight into the physical background of ridge creation, but do not provide readily available statistical information that could be used in probabilistic simulations. Full-scale measurements offer an opportunity to quantify the relation, but publicly available literature (e.g., full-scale measurement in the publications listed above) are focused on showing

the existence of the correlation and estimating the upper limits of keel draft with respect to the surrounding LI thickness.

The aim of our work is to analyze the correlation between LI draft (convertible to LI thickness) and ridge keel draft in a way that will be suitable for later use in probabilistic assessments of ice ridge loads on offshore structures. This is done by dividing the ice draft records into weekly segments, estimating the representative LI draft, finding the deepest ridge and comparing the two variables. This paper is divided into six sections. The second section describes the upward-looking sonar data used in this paper. The third section describes the methodology for estimating the LI draft from ice draft data. The fourth section examines the relationship between LI draft and ridge keel draft and presents an approach for probabilistic simulation of the two variables. Finally, the fifth and sixth sections are devoted to discussion and conclusions, respectively.

DATA

In this study, we use long-term measurements of ice draft from ULS moorings from the Beaufort Sea. The data were collected and made available by the Beaufort Gyre Exploration Program based at the Woods Hole Oceanographic Institution (http://www.whoi.edu/beaufortgyre) in collaboration with researchers from Fisheries and Oceans Canada at the Institute of Ocean Sciences. Beginning in August 2003, ULS models IPS-4 or IPS-5 (manufactured by ASL Environmental Sciences in Canada) were deployed on bottom-tethered moorings in the Beaufort Sea on either 3 or 4 locations (Figure 1) to obtain ice draft measurements. All the moorings were in water depths deeper than 3500 m and the ULS instrumentation was attached to the top flotation sphere positioned between 50 and 85 m beneath the ice cover. The ULS instrument measures the ice draft by emitting signals and recording the travel time as they get reflected from the bottom surface of the ice. The footprint of the beam is estimated to be about 2 m for a nominal depth of 50 m. Most of the seasons had sampling rate set to 2 s and starting with season 2014-2015, the last two seasons had sampling rate set to 1 s. For more details about the instrumentation, see Krishfield et al. (2014) and the above-mentioned website of the Beaufort Gyre project.

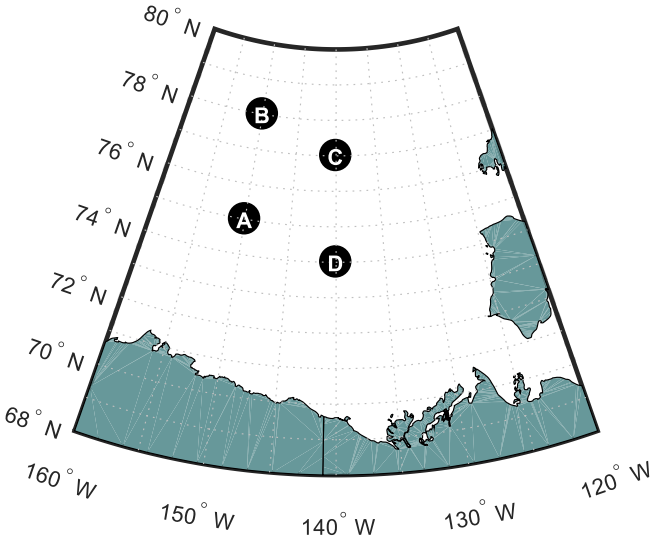

Figure 1. Locations of moorings with upward-looking sonars.

Table 1 gives an overview of the available datasets and indicates datasets that are not included in our analysis. The reason for omitting some of the datasets is that on several occasions there were evident measurement errors in form of unrealistically steep and narrow (spike) features. These errors would impair the keel identification procedure and the overall analysis. Although it is possible to remove these spikes form signals, we decided not to use these datasets

altogether because there is enough data to make firm conclusions using rest of the datasets only.

Table 1. Overview of datasets. Available datasets are depicted with green and unavailable datasets are depicted with red. Crosses mark datasets excluded from analysis due to measurement errors.

Season / Location	2003 - 2004	2004 - 2005	2005 - 2006	2006 - 2007	2007 - 2008	2008 - 2009	2009 - 2010	2010 - 2011	2011 - 2012	2012 - 2013	2013 - 2014	2014 - 2015	2015 - 2016
A							×						
B			×		×				×			×	
C				×									
D									×				×

LEVEL ICE DRAFT

This section describes how LI draft is estimated from the ULS ice draft records. LI draft cannot be readily extracted from the draft records due to the large draft variability. The variability is a result of thermodynamic and dynamic processes such as rafting, ridging, lead opening and refreezing. To analyze this variability, it is practical to examine the probability distribution of the ice draft by means of a histogram and/or probability density function (PDF). Draft probability distributions are commonly characterized by one or multiple modes that point to most frequently occurring draft classes. Typically, these modes indicate the draft of level ice, as this draft class is spatially most frequent for any sea ice environment (Haas, 2010). For the first-year ice (FYI) environment, a distinct sharp mode is a typical feature in ice draft distributions. Towards the later stage of a season, secondary modes can occur due to events of lead opening and refreezing. Multi-year ice (MYI) environment is somewhat more complicated, as older ice goes through extensive processes of melting, refreezing and deformation. In addition, presence of MYI is often characterized by a combination of floes of different age. This results in modes that are less distinct in comparison to the FYI environment. The following paragraphs of this section describe a mathematical formulation for finding the modes of ice draft distribution and outlines a classification of modes in case of multi-modal distributions. The classification of different modes is used in later sections for choosing a representative mode for the context of our study.

Estimating the mode of a distribution from a histogram is a seemingly simple procedure of finding the peak of the histogram. However, one needs to define a bin with to create the histogram and this parameter has implications on the mode's location. Overly narrow bins can produce spurious modes and overly wide bins reduce the resolution of the mode estimate. Bin width can be manually optimized, but it is not possible to allocate one bin width that is optimal for all possible ice environments (e.g., start of the winter season vs end of the winter season; FYI vs MYI). Improvements are possible, such as done by Mudge et al. (2013), where authors find the initial mode with somewhat wider bins and subsequently further precise the LI draft by calculating the median from the data contained in the modal bin and two neighboring bins.

We utilize a non-parametric estimate of PDF to approximate the ice draft probability distribution and to find the modes. This approach approximates the PDF with a smooth line, which offers an approach for systematic identification of the mode(s) that is universal for all possible ice environments. The method demonstrates its effectiveness particularly well in cases with MYI multimodal distributions. Kernel density estimation with normal kernel function (Bowman and Azzalini, 1997) is used. The kernel estimator is given in the following form:

$$\hat{f}(y) = \frac{1}{n}\sum_{i=1}^{n} w(y - y_i; h), \quad (1)$$

where w is the kernel function, which is itself a probability density. y is the variable of interest (ice draft in our case) and n is the total number of observations. We use the normal density function for w:

$$w(y - y_i; h) = \phi(y - y_i; h), \tag{2}$$

where $\phi(z; h)$ denotes the normal density function in z with a mean 0 and standard deviation h, in this context called bandwidth.

Similarly to the subjective allocation of the bin width for histograms, kernel density estimation suffers a drawback in the form of subjective allocation of the bandwidth parameter. This parameter, also called the smoothing parameter, determines the manner in which the probability associated with each observation is spread over the surrounding sample space (Bowman and Azzalini, 1997). Overly small bandwidth parameter will cause undesirable variations in the approximated PDF that are associated with individual observations. This can cause appearance of spurious modes that do not reflect the LI draft. Overly large bandwidth parameter is smoothing the data too much and often to an extent that allows merging of two distinct modes that represent two separate level ice drafts present in the area. We have experienced that the parameter can be optimized manually by trial and error procedures. However, to limit the subjectiveness of the procedure, we use the rule of thumb as proposed by Silverman (1986) that allocates the bandwidth parameter as follows:

$$h_{opt} = 1.06 \sigma n^{-1/5}, \tag{3}$$

where σ is the standard deviation and n is the number of observations in the data sample. Using this procedure is simple and it showed satisfactory results.

Figure 2 illustrates an example of an estimate of the LI draft for a weeklong ice draft record. This example is from January 2013 where the ice environment consists only of FYI. It represents a simple case where the draft distribution is unimodal and there is no ambiguity in finding the level ice draft. Note that this case was most frequent in our analysis.

Figure 3 illustrates an example from March 2013 with FYI environment where the draft distribution is bimodal. Absolute mode (AM) is the mode with highest probability density. Deepest mode (DM) is the mode with deepest draft. The AM mode, in this case, has a shallower draft. It was formed in an event of large-scale divergent deformation of ice that created open water leads and subsequently new ice has grown. The DM mode, in this case, represents the ice that has been growing since the start of the winter season.

Figure 4 illustrates an example from November 2013 with MYI environment where the draft distribution is bimodal. In this case, AM and DM are in the same position. MYI nature of the level ice can be concluded by observing relatively larger roughness of the ice bottom surface. Furthermore, the ice is too thick for the early part of the winter season to be FYI.

We have presented a method for identifying the modes of draft distributions that reflect LI thickness and differentiated between the absolute and the deepest mode of multimodal distributions. In the analysis of the correlation between LI draft and ridge keel draft, we must choose which of these two modes is representative and practical for later use in probabilistic assessments of ridge loads. This will be discussed in the next section of this paper.

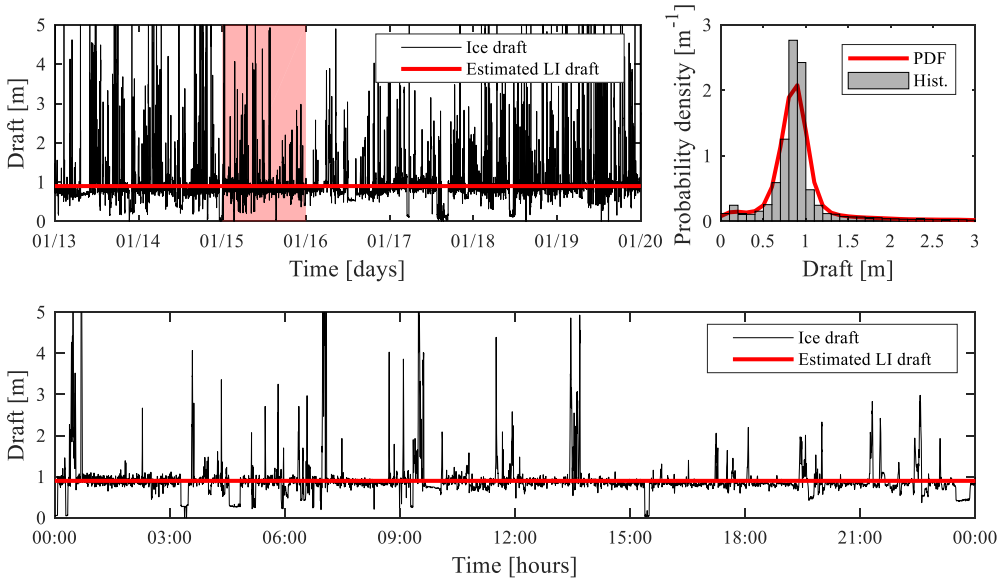

Figure 2. Example of level ice estimation for a weeklong draft record in FYI environment. The top left panel shows ice draft as recorded by the ULS and the estimated LI draft. The top right panel shows a histogram of the LI draft and a non-parametric estimate of the PDF. The bottom panel shows a 24-hour sample (shaded with red in top right panel) for more detailed inspection.

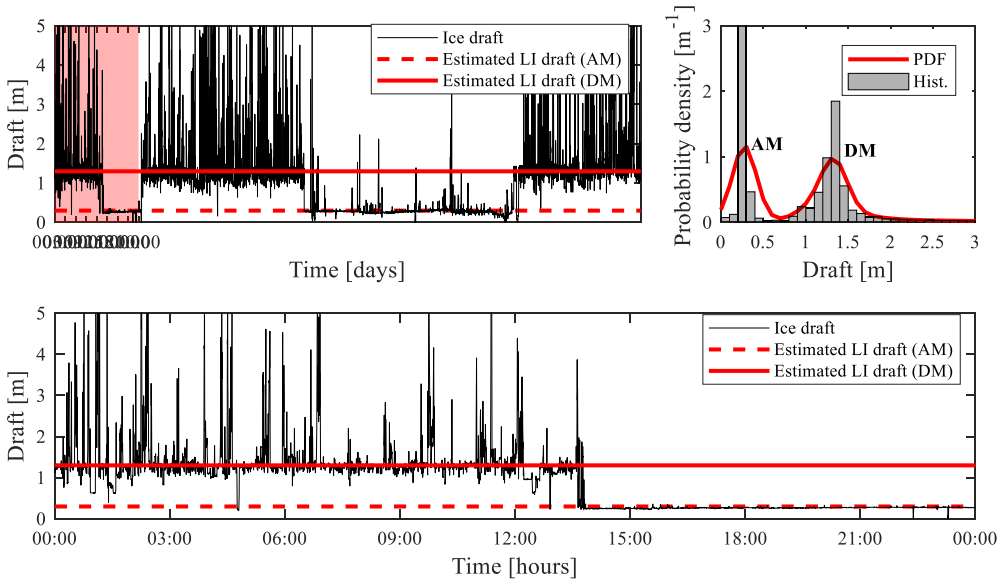

Figure 3. Example of level ice estimation for a weeklong draft record in FYI environment with a multimodal ice draft distribution. Two modes are identified. Absolute mode (AM) is the mode with the highest probability density. Deepest mode (DM) is the mode with the deepest draft. Panel description same as described in Figure 2 caption.

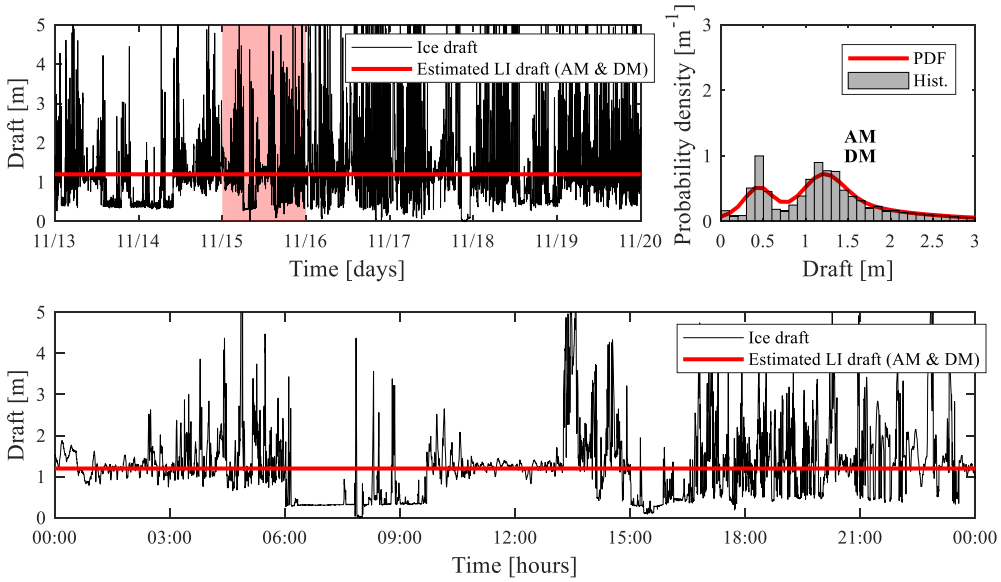

Figure 4. Example of level ice estimation for a weeklong draft record in MYI environment with multimodal ice draft distribution. In this case, AM and DM are in the same location. Panel description same as described in Figure 2 caption.

CORRELATION BETWEEN LEVEL ICE DRAFT AND RIDGE KEEL DRAFT

To analyze the correlation between level ice draft and ridge keel draft, we subsample the data in weekly subsets. We chose this approach in contrast to analyzing transects with a fixed length (e.g., 50 km) because this sampling resembles the situation of an offshore structure with a fixed location interacting with the incoming ice. For each subset, the level ice draft is identified, and the maximum keel draft is recorded. This results in 1461 data points. As mentioned in the previous section, in most cases identification of the mode that indicates the LI draft was unambiguous. This is obvious for unimodal distributions and for cases when AM and DM have identical location in a distribution. In cases when AM and DM are not located identically, there is a question whether AM or DM is representative of the LI draft. To answer this question, one must keep in mind that the primary goal of our research is to establish a formulation for quantifying the relationship between LI draft and ridge keel draft for use in a probabilistic assessment of ridge loads. As discussed in the introduction, LI draft (thickness) is relevant for the evaluation of the limit force. Therefore, it would be sensible to pick a conservative option. That would be the DM, being always the thicker ice and thereby causing a higher force. Furthermore, this approach has proven to be more practical and results in a better correlation of LI draft and keel draft (DM has a better predictive capability of the extreme keel draft).

Let us now compare two alternatives for choosing the representative mode, explain the differences and quantify to what extent the results are changing. Two panels of Figure 5 illustrate the correlation between the surrounding LI draft and the draft of the weekly deepest keel. The left panel uses the absolute mode with the highest probability density for estimating the surrounding level ice draft. The right panel uses the deepest mode in case of multimodal draft distributions. AM option suffers a drawback that it is often indicating to the shallower mode in the multimodal distributions. This happens when leads open and new ice is formed that is relatively uniform in comparison to the deeper mode and therefore has a narrower mode with a higher peak. This explains the occurrence of points in the top-left corner (shallow LI and deep keels) of the left panel diagram. DM option takes this into account and picks the deepest of the multiple modes. It can be seen in the right panel that the points in the top-left corner have mostly disappeared. However, due to this overall trend of rightwards shift of points towards the deeper draft, we can see occurrence of points in the bottom right corner (deep LI and shallow keels) of the right panel.

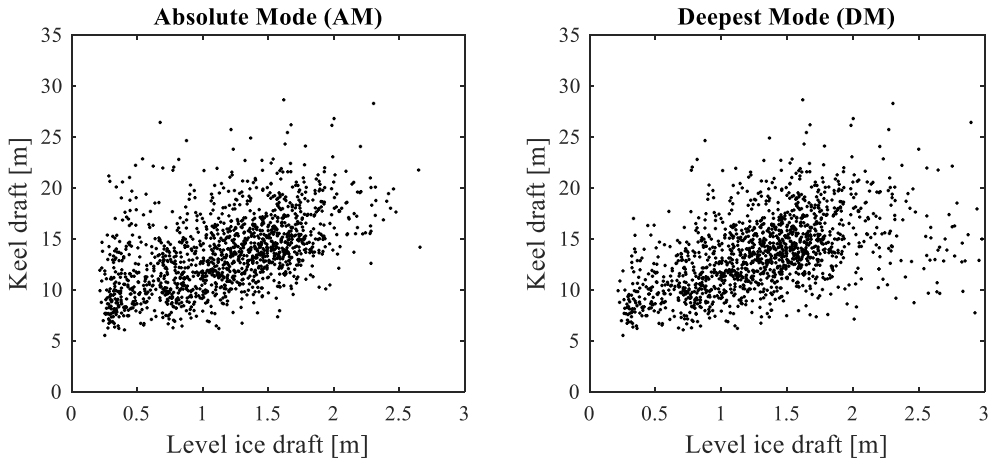

Figure 5. Correlation between the surrounding level ice draft and the draft of the weekly deepest keel. Keel draft represents the weekly maximum keel draft in both panels. The left panel used AM and the right panel used DM for estimating the level ice draft.

A closer inspection of all points revealed that the outlier points in the bottom right corner of the right panel diagram were in fact false identification induced by spurious modes. By looking at the draft distribution, time series of the draft and the drift speed of the ice (measured by acoustic Doppler current profilers), it can be seen that on some occasions ice movement would stop for a prolonged period. ULS would then record the same ice surface for hours or even days. This means that one of the histogram bins would excessively rise and therefore cause the occurrence of spurious modes that do not represent LI. Upon closer inspection of all points, we were able to manually correct these errors. Some of the points (60 out of 1461) had to be removed altogether because the draft distribution was corrupted to an extent that there were no modes that could be reliably identified as LI. For some of the points (58 out of remaining 1401), it was possible to manually identify the mode representing the LI. The described procedure resulted in a cloud of points that were obtained by DM criterion and subsequent manual correction. This cloud of points (Figure 6) is used for further analysis. Note that the weeks with LI draft lower than 0.2 m were not analyzed because LI draft identification was not reliable in this case. Furthermore, keel draft and LI draft are rather shallow in this case and would not cause extreme ridge load events, making this part of data non-relevant for the scope of probabilistic ridge load assessment.

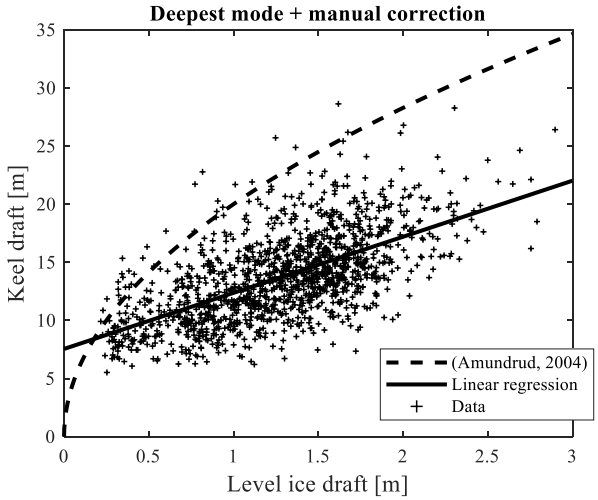

Figure 6. Correlation between the surrounding level ice draft and the draft of the weekly deepest keel. Curve proposed by Amundrud et al. (2004) represents truncation of keel development at a draft of $20h^{1/2}$ m. Linear regression (solid line) is obtained using the least-squares fit technique and has an intercept of 7.55 and a slope of 4.83.

It can be observed in Figure 6 that the overall correlation between the LI draft and keel draft exhibits a linear trend. However, the upper limit of the keel draft can be described with a square root function with respect to the LI draft. This is in good agreement with similar truncation curves as proposed by Hibler (1980), Hopkins (1994, 1998) and more recently by Amundrud et al. (2004). Amundrud et al. (2004) propose a truncation curve in form of square root function defined as $20h^{1/2}$ m, where h is the draft of the adjacent LI. We have plotted this curve in Figure 6 and only a few data points lie above the truncation curve (2.2% of all data points). This is similar to 4% reported by (Amundrud et al., 2004).

The most prominent difference of our result to the findings by Amundrud et al. (2004) is that in our study the cloud of points follows a linear trend, rather than an overall trend that looks like the upper limit with the shape of a square root function. The explanation for this difference is twofold. The first explanation is that Amundrud et al. (2004) consider the LI draft adjacent to the deepest ridge of the 50 km transect. Our LI draft represents the deepest prominent LI found in the weeklong transect of ice over the same location. This means that our LI draft is most often the upper bound of the LI draft that can be found in the ice field and this would simply mean that our data points tend to move rightwards. The second explanation is that we take the deepest ridge during a weeklong transect and not a fixed 50 km transect. Although ADCP measurements of ice drift were not always available, we were able to have an insight into the length of our weeklong transects. No detailed analysis of the influence of the weekly transect lengths was undertaken and we only report that for 30% of cases the weekly transect lengths were shorter than 50 km. This means that for these points there was a smaller probability of encountering extreme ridges and thus bringing some of the data points downwards. However, for the rest of the points that had weekly transect lengths higher than 50 km, the probability of encountering deeper ridges should be increased. Without knowing if there is some relationship between LI draft and weekly average drift speed (thus weekly transect lengths), we cannot conclude what was the overall influence on the keel depth (vertical location of data points in Figure 6).

In the remaining part of this section, we will propose a probabilistic simulation technique for replicating the cloud of points as illustrated in Figure 6. The solid line in this figure represents a result of linear regression using the method of least squares. The regression line has an intercept of 7.55 and a slope of 4.83. We can now define a ratio $R_i\left(h_i\right)$ that is defined as a ratio between the keel draft of individual points D_i and the linear regression line $D\left(h_i\right)$:

$$R_i\left(h_i\right) = D_i / D\left(h_i\right) \tag{4}$$

This ratio is calculated for all data points and illustrated with respect to the LI draft in the left panel of Figure 7. The right panel of the same figure illustrates the distribution of the ratio by means of a histogram and fitted lognormal (LN) probability distribution function. Figure 8 shows Q-Q plots (Wilk and Gnanadesikan, 1968) for lognormal and generalized extreme value (GEV) distributions applied to the ratio R_i. This is a graphical method for studying the distribution of data. If data is distributed according to the tested PDF, the points should lie on a straight line with slope 1. Both lognormal and GEV distributions have exceptionally good agreement with the empirical distribution of the ratio R_i. For further use in this paper, we have chosen the lognormal distribution with mean 1.00 and standard deviation 0.2161.

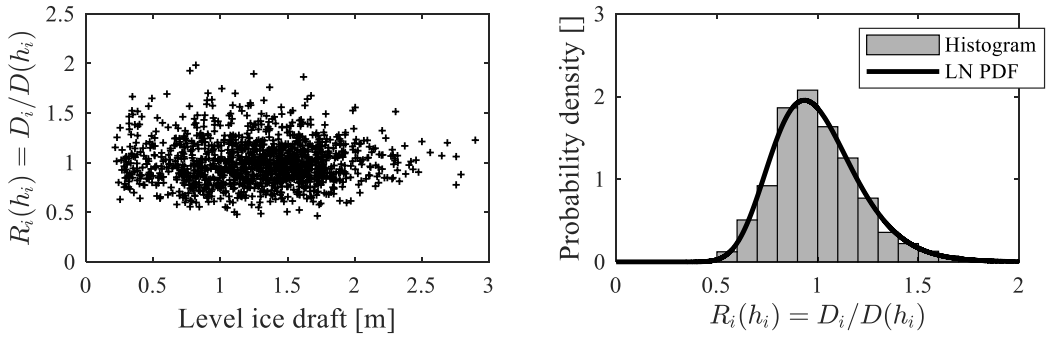

Figure 7. The left panel shows the ratio as defined by Eq. (4) in relation to the level ice draft. The right panel shows the distribution of the ratio represented with a histogram and a fitted PDF using the lognormal (LN) probability distribution function with mean 1.00 and standard deviation 0.2161.

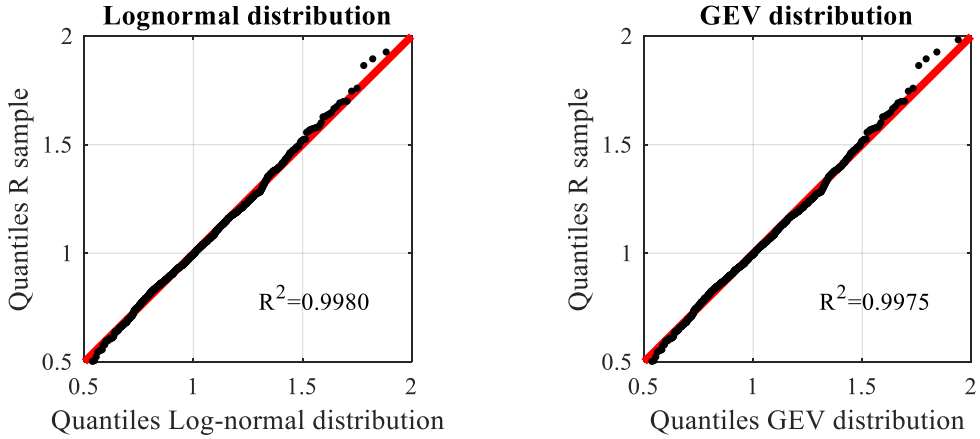

Figure 8: Comparison of the Q-Q plots for the log-normal and generalized extreme value (GEV) distributions applied to the ratio R_i as defined in Eq. (4). R^2 is the coefficient of determination that indicates how well the data aligns with the proposed PDF.

The linear regression line from Figure 6 is giving the information about the general trend of correlation between the LI draft and the keel draft. The ratio given by Eq. (4) is giving us the information about the variation of the keel draft with respect to the general trend. Given that we have a sample of level ice draft, the above two information is enough for simulating the keel draft, while keeping the statistical properties of the keel draft and the correlation properties to the LI draft. The simulation can be summarized with the following expression:

$$D_i = \left(a + b \cdot h_i\right) \cdot R_i \quad , \tag{5}$$

where D_i is the simulated keel draft, a and b are intercept and slope of the linear regression line from Figure 6, R_i is a Monte Carlo sampled ratio that follows the lognormal distribution derived earlier in this paper. Commonly, in a Monte Carlo probabilistic simulation of the ice environment, the LI draft and ridge keel draft are sampled independently according to their respective unconditional (marginal) distributions. In the approach presented here, we keep the conditionality (correlation) of the two variables. In an actual probabilistic simulation, one would simulate the LI draft according to its PDF that considers seasonal and intraseasonal variabilities (e.g., Samardžija et al., 2018). To compare the simulated data and the field data, in our simulation, we use the deterministic sample of LI draft that was obtained in the field. In other words, we use the Eq. (5), with coefficients a and b as determined earlier, sample the ratio R_i, and take a deterministic sample of LI draft h_i. An example cloud of data for one such simulation is shown in Figure 9.

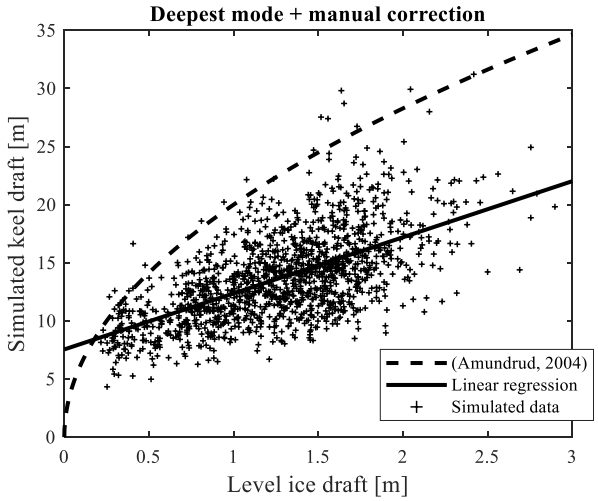

Figure 9. Correlation between the surrounding level ice draft and the simulated draft of the weekly deepest keel. In comparison to Figure 6, the LI draft (horizontal coordinates) is the same and the keel draft (vertical coordinates) is simulated. The linear regression line is the same as in Figure 6 obtained from field data and shown here for a better visual comparison of the field data and the simulated data.

To analyze how well the simulated data is predicting the extreme keel drafts, we show the exceedance probability plot of the keel draft in the left panel of Figure 10. We have repeated simulation 1000 times to get a better representation of the tail of the simulated data distribution. It this way we can see that the marginal distribution of the keel draft is replicated well in the simulated data. We should sound a note of caution in interpreting these results for two reasons. The first reason is that the data does not represent the distribution for one location, but multiple locations. The second reason is that the LI draft variability is not extrapolated but repeated from the actual data (LI draft obtains maximum as given in field data, whereas it could be larger during the longer simulated period). We perform this simulation for the mere purpose of comparing the field data and simulated data. In addition, the Q-Q plot is given in the right panel of Figure 10. This plot indicates that there is a slight overestimate in the tail of the simulated keel draft.

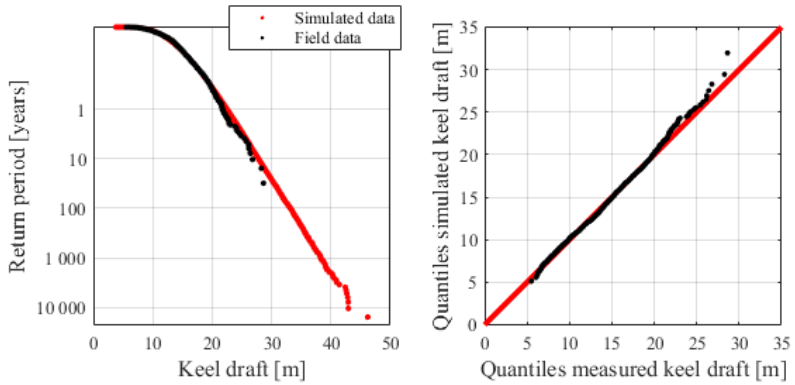

Figure 10. Left panel: Exceedance probability plot for the filed data and simulated data. Right panel: Q-Q plot of the measured keel draft and simulated keel draft.

DISCUSSION

The findings of this paper reinforce the existence of a positive correlation between level ice draft and ridge keel draft. This is in good agreement with previous studies that show similar results, such as reported in work by Amundrud et al. (2004). However, our study shows an overall linear trend in the correlation between the two variables and an upper limit that can be

described with a square root function. This is in contrast with findings where both the overall trend and the upper limit have a shape of square root function. The discrepancy can be explained by the difference in sampling technique (temporal vs spatial). We used a fixed temporal frame (1 week), while earlier studies were more focused on fixed topographic transects (e.g., 50 km). This difference is a significant finding because it shows an example of how a subtle detail in data sampling can have implications on the statistical interpretation of the data. Due attention to this kind of details must be exercised when performing a probabilistic simulation of ice environment. Sampling technique and the simulation technique should have the same nature and if this is not possible, a transformation of the distribution with respect to the ice drift data should be performed.

It is interesting to note that the deepest mode (DM) had the best correlation to the weekly extreme keel draft. Further studies should be performed to make a solid conclusion on the influence of different modes of the LI draft to the keel draft. Nevertheless, we give some of our observations in the following lines. Note that the correlation between LI draft and keel draft presented in this paper does not directly imply the correlation between LI draft and *creation* of deep keels. It is expected that thicker LI will produce deeper ridges (explained by the mechanical principles of ridge building processes). However, it is also true that thicker LI is present towards the end of the winter season and this means that there was more time for deep ridges to be created. Therefore, it is important to note that our study indicates a correlation between the LI draft and the *presence* of deep keels, rather than a correlation between LI draft and *creation* of deeps keels. Also note that the presence of deep LI draft modes early in the winter season (typically modes caused by MYI) was accompanied by many deep ridges. We conclude that in cases with multimodal distributions of LI draft, presence of shallow LI modes had minimal effect on limiting the extreme keel draft and presence of deep LI modes was accompanied with the presence of deep keels.

The simulation technique of the keel draft for a given sample of LI draft proposed in this paper maintained the qualitative properties found in field data. These properties are the overall linear trend of the correlation an upper limit that can be described with a square root function. Closer inspection of the marginal distribution of keel draft by means of exceedance probability plot indicates that the simulated distribution replicates well the field data distribution. However, the Q-Q plot indicates that there is a slight overestimation of the keel draft in the simulated data. The reason for this can be found in the left panel of Figure 7. There is an indication that the ratio R_i converges towards 1 for higher LI draft. Due to the small sample of data points in the extreme domain, it is not possible to conclude whether this is a coincidence or a natural phenomenon. In our simulation, the ratio R_i is independent of LI draft and thereby this ratio can sample higher values in combination with deep LI draft, which in turn results in deep keels.

Given that our findings are based on location-specific data, the results from such analyses are not directly transferable and applicable to other locations. Effects such as different ice drift patterns and boundary conditions could alter the correlation properties between LI draft and keel draft. If a probabilistic assessment of ice ridge loads is undertaken in a design process of an offshore structure, similar data from the location of interest should be available to perform analysis and simulation suggested in this paper. This is a major drawback since similar data is rarely available. Future studies will investigate possibilities of making general conclusions about the correlation between the LI draft and keel draft. If this proves to be possible, it should be possible to get at least a first estimate about the ridge keel statistics for a location where only LI draft (thickness) data is available (field measurements, remote sensing or simulations of ice growth). Such studies will require more detailed analysis of the ridge statistics that will consider all of the ridges and not only the weekly deepest ridges. Due attention will have to be paid to the ridge frequency and ice drift properties to make conclusions scalable to other locations of interest.

Ideally, we should be able to simulate all ridges incoming to the location of interest and not only the weekly deepest. The approach described in this paper focuses only on weekly deepest ridges. These ridges are not necessarily causing the maximum loads. It means that if our approach is used, one must make conservative assumptions about the consolidated layer. It is important to note that the consolidated layer thickness is possibly even more important geometrical parameter that the keel draft. Probabilistic simulation of consolidated layer thickness is a topic reserved for future work. The key issue here will be to answer the question of correlation between the keel draft and the consolidated layer thickness. It is expected that this study will show that the relatively shallow ridges formed at the beginning of winter season grow a thick consolidated layer towards the end of winter season and that the relatively deep ridges formed towards the end of winter season have a thin consolidated layer. This would mean that the consolidated layer thickness and keel draft are negatively correlated.

CONCLUSIONS

Our analysis of ice draft data from the Beaufort Sea suggests that there is a positive linear correlation between level ice draft and presence of deep ridge keels. We have presented an improved method for identifying the level ice draft from ice draft distributions using a non-parametric approximation of ice draft probability distributions. In case of multimodal distributions, the deepest mode shows the best correlation to the keel draft. Our method for analyzing level ice draft and keel draft could be applied for other locations of interest. Simulation technique presented here could then be utilized for probabilistic assessment of ice loads where the surrounding level ice thickness and the keel draft would be properly correlated. This would result in more realistic calculations of limit force. Future work will concentrate on more detailed analysis of ridge statistics that would ideally result in generalized findings about correlation between level ice thickness and ridge keel draft. This would enable us to scale the correlation to other locations and make estimates about ridge statistics based only on level ice thickness. Furthermore, future work should also investigate the correlation between consolidated layer thickness and ridge keel draft.

ACKNOWLEDGMENTS

The authors wish to acknowledge the support of the Research Council of Norway through the Centre of Research-based Innovation, SAMCoT, and the support of the SAMCoT partners. This work has been carried out within the NTNU Oceans Pilot project "Risk, reliability and ice data in arctic marine environment". The ice draft data were collected and made available by the Beaufort Gyre Exploration Program based at the Woods Hole Oceanographic Institution (http://www.whoi.edu/beaufortgyre) in collaboration with researchers from Fisheries and Oceans Canada at the Institute of Ocean Sciences. We gratefully acknowledge their effort in collecting this data and making it publicly available.

REFERENCES

Amundrud, T. L., Melling, H. & Ingram, R. G. 2004. Geometrical constraints on the evolution of ridged sea ice. *Journal of Geophysical Research,* 109**,** 12 pp.

Bowman, A. W. & Azzalini, A. 1997. *Applied smoothing techniques for data analysis: the kernel approach with S-Plus illustrations,* OUP Oxford.

Charlebois, L., Frederking, R., Timco, G. W., Watson, D. & Richard, M. 2018. Evaluation of pack ice pressure approaches and engineering implications for offshore structure design. *Cold Regions Science and Technology,* 149**,** 71-82.

Croasdale, K. R. The limiting driving force approach to ice loads. 16th Annual Offshore Technology Conference, OTC 1984, May 7, 1984 - May 9, 1984, 1984 Houston, TX,

United states. Offshore Technology Conference, 57-64.
Croasdale, K. R. Limit force ice loads - An update. 20th International Conference on Port and Ocean Engineering under Arctic Conditions, POAC, 2009 Lulea, Sweden. Lulea University of Technology, 230-239.
Croasdale, K. R. Ice ridging forces, ice rubble, and other neglected topics in ice-structure interaction. 10th International Conference and Exhibition on Performance of Ships and Structures in Ice 2012, ICETECH 2012, September 17, 2012 - September 20, 2012, 2012a Banff, AB, Canada. Society of Naval Architects and Marine Engineers, 1-6.
Croasdale, K. R. 2012b. Ice rubbling and ice interaction with offshore facilities. *Cold Regions Science and Technology*, 76-77**,** 37-43.
Haas, C. 2010. Dynamics Versus Thermodynamics: The Sea Ice Thickness Distribution. *Sea Ice: Second Edition.* Wiley-Blackwell.
Hibler , W. D. 1980. Modeling a variable thickness sea ice cover. *Monthly Weather Review,* 108**,** 1943-1973.
Hopkins, M. A. 1994. On the ridging of intact lead ice. *Journal of Geophysical Research,* 99**,** 16351-60.
Hopkins, M. A. 1998. Four stages of pressure ridging. *Journal of Geophysical Research,* 103**,** 21883-91.
ISO 19906 2010. Petroleum and natural gas industries - Arctic offshore structures.
Krishfield, R. A., Proshutinsky, A., Tateyama, K., Williams, W. J., Carmack, E. C., McLaughlin, F. A. & Timmermans, M. L. 2014. Deterioration of perennial sea ice in the Beaufort Gyre from 2003 to 2012 and its impact on the oceanic freshwater cycle. *Journal of Geophysical Research: Oceans,* 119**,** 1271-305.
Melling, H. & Riedel, D. A. 1996. Development of seasonal pack ice in the Beaufort Sea during the winter of 1991-1992: a view from below. *Journal of Geophysical Research,* 101**,** 11975-91.
Mudge, T. D., Ross, E., Fissel, D. B. & Marko, J. R. Further improvements to understandings of extreme arctic sea ice thickness derived from upward looking sonar ice data. 22nd International Conference on Port and Ocean Engineering under Arctic Conditions, POAC 2013, 2013 Espoo. Lulea University of Technology.
Parmerter, R. R. & Coon, M. D. 1972. Model of pressure ridge formation in sea ice. *Journal of Geophysical Research,* 77**,** 6565-75.
Ross, E., Fissel, D., Marko, J. & Reitsma, J. An improved method of extremal value analysis of arctic sea ice thickness derived from upward looking sonar ice data. Arctic Technology Conference 2012, December 3, 2012 - December 5, 2012, 2012 Houston, TX, United states. Society of Petroleum Engineers, 879-886.
Samardžija, I., Høyland, K. V., Leira, B. J. & Næss, A. 2018. Probabilistic Assessment of Ice Environment and Ridge Loads for the Norströmsgrund Lighthouse. *24rd IAHR Symposium on Ice.* Vladivostok, Russia.
Silverman, B. 1986. Density Estimation for Statistics and Data Analysis.
Timco, G. W., Sudom, D., Frederking, R., Barker, A. & Wright, B. D. 2017. A critical review of Arctic pack ice driving forces: New sources of data. *Cold Regions Science and Technology,* 138**,** 1-17.
Tuhkuri, J. & Lensu, M. 2002. Laboratory tests on ridging and rafting of ice sheets. *Journal of Geophysical Research,* 107**,** 8-1.
Wilk, M. B. & Gnanadesikan, R. 1968. Probability Plotting Methods for the Analysis of Data. *Biometrika,* 55**,** 1-17.

A.3 Paper 3

Paper 3:

Samardžija, I., & Høyland, K. V. (2023). Analysis of the relationship between level ice draft, ridge frequency and ridge keel draft for use in the probabilistic assessment of ice ridge loads on offshore structures. *Ocean Engineering*, *270*, 113593. https://doi.org/10.1016/j.oceaneng.2022.113593

Ocean Engineering 270 (2023) 113593

Contents lists available at ScienceDirect

Ocean Engineering

journal homepage: www.elsevier.com/locate/oceaneng

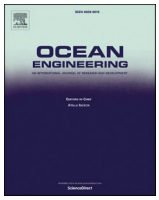

Analysis of the relationship between level ice draft, ridge frequency and ridge keel draft for use in the probabilistic assessment of ice ridge loads on offshore structures

Ilija Samardžija *, Knut V. Høyland

Norwegian University of Science and Technology, Trondheim, Norway

ARTICLE INFO

Handling Editor: Prof. A.I. Incecik

Keywords:
Ice profiling sonar
Ice ridge draft
Ice ridge frequency
Level ice draft
Probabilistic design

ABSTRACT

Level ice draft, ice ridge keel draft and ridge frequency are important variables in the probabilistic assessment of ice ridge loads on offshore structures. We use ice profiling sonar (IPS) measurements of ice draft from the Beaufort Sea to analyse the relationship between these three variables. We propose a probabilistic simulation technique of ridge keel drafts. Two examples of simulations are given. The first example simulates the weekly deepest ridges. The simulated distribution of the weekly deepest ridge keel draft agrees with the measured data. The second example simulates all ridges deeper than 5 m. This simulation results in overestimation of the ridge keel draft in the tail section of the distribution. For both simulations, with the relationships established in this paper, the only needed input is level ice draft. Future studies should investigate whether the relationships found in the Beaufort Sea are valid in other areas or if there is a possibility of scaling the correlations. If the correlations prove predictably scalable for other locations, it could be possible to estimate the ridge keel draft distribution and ridge frequency by knowing only the level ice draft (thickness) statistics. This study is our first endeavour in this direction.

1. Introduction

Structures in Arctic offshore regions must be designed to withstand ice loads. In regions where icebergs are not present or can be managed, ice ridges are the most common extreme load scenarios. Ridges form in dynamic events when sea ice is moved by water currents and, more commonly, wind; internal pressures are developed, and ridges are formed in compressive and shearing events of ice failure.

The design of offshore structures has to include considerations of uncertainty. Probabilistic methods for estimating wave loads are well established and use wave spectrums. A few wave spectra are used world-wide even though the wave environment vary substantially. The calculation of loads on offshore structures from first-year ice ridges requires inputs such as level ice thickness, consolidated layer thickness, ridge keel draft and the mechanical properties of ice and ice rubble (ISO 19906, 2019). The most important parameters are the thickness of the consolidated layer, the keel draft and the empirical coefficient C_R. Estimating extreme loads on structures in a deterministic approach requires conservative estimates for the input variables. This can be done based on available data or an analysis of physical phenomena (e.g., limited natural growth of level ice). However, in a probabilistic approach, long-term data are normally required to describe statistical distributions of input variables, and it is preferable to understand and include the correlations between these variables. The main motivation behind our study is assessing the difficulties in performing accurate probabilistic simulations of ice ridge loads for fixed offshore structures. Samardžija et al. (2018) explored the limitations in performing such an analysis and identified several shortcomings. Two of these are addressed here. The first is how to quantify the correlation between the level ice thickness and the ridge keel draft. The second is how to adequately quantify the ridge frequency throughout the autumn and winter and into summer. To answer these questions, we analyse ice draft data from the pack ice zone of the Beaufort Sea.

There is considerable evidence of the positive correlation between level ice thickness and ridge keel draft (Parmerter and Coon, 1972; Timco and Sayed, 1986; Hopkins, 1998; Tuhkuri and Lensu, 2002; Amundrud et al., 2004). Previous research also indicates that a ridge can obtain its maximum draft only if several conditions are met. First, there needs to be enough material provided by level ice for creation of the ridge. Second, internal pressure in the pack ice caused by wind and

* Corresponding author.
E-mail address: ilija.samardzija@ntnu.no (I. Samardžija).

https://doi.org/10.1016/j.oceaneng.2022.113593
Received 29 March 2022; Received in revised form 18 November 2022; Accepted 29 December 2022
Available online 12 January 2023

current needs to be high enough to create the ridge. Third, this critical internal pressure needs to last long enough to complete the creation of the ridge. Given that these conditions are fulfilled, a ridge will reach a certain maximum draft and subsequently start growing in width. This was observed in laboratory tests with scaled ridging experiments (Timco and Sayed, 1986; Tuhkuri and Lensu, 2002). Numerical models also suggest that ridges grow only to a limited draft (Hopkins, 1998; Parmerter and Coon, 1972). Amundrud et al. (2004) analysed ice profiling sonar (IPS) data from the Beaufort Sea and suggested an empirical relationship between the maximum keel and nearby level ice draft. They proposed an upper bound function of the maximum ridge keel draft as a function of the adjacent level ice draft ($20\,h^{1/2}$, where h is in m). These relationships are similar to those in our findings in many aspects. The difference is that we are focused on correlating level ice thickness with the statistical distribution of keel draft (maximum of a single ridge) in a way that is optimized for probabilistic ridge load calculations rather than only focusing on finding the upper bound of the ridge keel draft. We should add that the observed level ice next to a ridge does not have to be the ice from which the ridge was formed. It can be both thicker and thinner. If the ridge is formed by closing a refrozen lead the surrounding level ice may be thicker than the ice that formed the ridge. But if the ice cover diverges after a ridging event creating open water next to the ridge, new ice may form and the observed level ice will be thinner than the ice from which the ridge was formed.

The interaction rate (number of ridge impacts per unit of time) is an important parameter that needs to be connected with the adopted statistical distributions of input variables. This is the same as the temporal ridge frequency (ridges/week) that is analysed in this paper. Ridges form in periodic events throughout the winter, but do not disappear before summer melt. In other words, it is reasonable to assume that the number of ridges will increase as the winter progresses and the level ice grows. The interaction rate considers the exposure of a structure that can be expressed in various ways, and in general terms, it is a way to account for the harshness of a particular ice environment (Jordaan et al., 2010).

We have chosen to quantify the ridge frequency in temporal reference (number ridges per week) because this is the parameter needed in probabilistic simulation of ridge loads. The measured ice draft data is also given in time. It is of course possible to quantify ridge frequency in spatial reference (e.g., number of ridges per kilometer). However, in probabilistic simulation of ridge loads, one would eventually need to transfer the spatial ridge frequency into the temporal ridge frequency because simulation is performed in time domain. This implies involving ice drift speed and concentration in the simulation. This would be an unnecessary complication that, in our experience, only reduces the accuracy of the relationship between the variables that are vital for ridge load calculation and ultimately undermines the reliability of the estimated loads. To discuss this issue in more tangible manner, we present the flowchart of our simulation approach (Fig. 1), and a flowchart of possible simulation approach where spatial ridge frequency is used (Fig. 2). Our simulation approach is intentionally simplistic and only the parameters needed for ridge load estimation as given in the ISO 19906 are simulated (level ice draft, mean ridge keel draft and temporal ridge frequency). In case shown in Fig. 2, one needs to simulate ice concentration and ice drift speed in order to transfer spatial ridge frequency into temporal ridge frequency. Furthermore, starting with level ice drift,

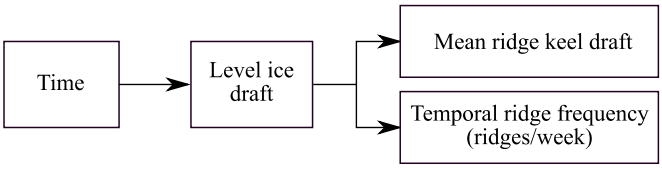

Fig. 1. Flowchart of the probabilistic simulation of variables needed for ridge load calculation that is proposed in this paper.

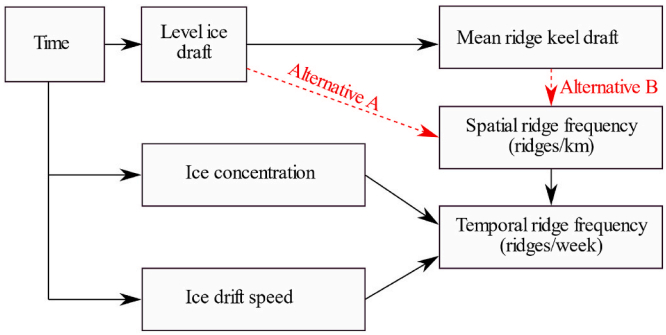

Fig. 2. Flowchart of a possible probabilistic simulation approach where spatial ridge frequency is included.

one needs to make two or three steps (depending on whether alternative A or B is chosen) to simulate the temporal ridge frequency. While making these steps errors are inevitably made and error propagation causes the relationship between level ice draft and temporal ridge frequency to be less accurate. In Figs. 1 and 2 the arrow indicate transformation by statistical simulation, and the more simulation steps the higher inaccuracy. In addition, we have experienced that with this approach the seasonality of the temporal ridge frequency is also impaired. This makes this approach unsuitable for probabilistic analysis of seasonal ridge loads (which is one of the goals for our future research).

Our findings regarding the relationship between ridge keel draft, ridge frequency, and level ice draft is our first step towards developing an approach where probabilistic assessments of ice ridge loads can be performed with limited ridge statistics data. Using level ice thickness data (measured or simulated) and our findings, one should be able to obtain a preliminary estimate of the ridge statistics (i.e., expected drafts and ridge frequency). This would simplify the probabilistic assessment of ice ridge loads because level ice thickness has a clear seasonal trend and is easier to measure and predict.

Relationships quantified in this paper, such as correlation between level ice draft and weekly number of ridge encounters, are location specific. It is expected that the relationships will quantitatively change with change in boundary conditions (e.g., ice drift speed, ice concentration, proximity of land or marginal ice zone). Therefore, due caution is required if findings from this paper are used to simulate ridge statistics for locations other than the Beaufort Sea. Simulation results for other locations would be questionable without an analysis of location specific data and recalibration of the relationships.

Our study has a main focus on quantification of the relationships that are important for probabilistic assessment of ridge loads. The analysis is optimized for accuracy and practicality in probabilistic prediction of ride loads. Causality of the relationships and analysis of the physical phenomena lying behind them is thereby only briefly commented. This, however, limits the widespread use of the approach presented in this paper. Analysis about utility of our approach in other locations is reserved for future research.

2. Data

The pack ice in the Beaufort Sea offers good opportunities for the study of sea ice using IPS data. During the summer, the area can become ice-free (depending on the latitude and ice conditions of a particular year). Due to the Beaufort Gyre circulation, the pack ice is in almost constant motion. This moves enough ice above the sonar array to craft reliable statistical conclusions (Fig. 5), while the time frames for data subsets can be kept small enough that statistical stationarity can be assumed. We use weekly subsets of data for our analysis as a practical compromise between having enough data to make reliable statistical calculations and not seeing excessive change in ridge statistics and the

level ice thickness during that time.

The data were obtained within the Beaufort Gyre Exploration Project, which had a main purpose of investigating basin-scale mechanisms regulating anomalies in freshwater content in the Beaufort Gyre (Proshutinsky et al., 2009). The large volume (continuous measurement for 15 years) and excellent resolution (IPS sampling rate of 1 or 2 s) of the data offer an excellent opportunity to analyse ice ridge properties relevant for engineering. Specific details about the instrumentation and data specifications are described here. Further details can be found on the Beaufort Gyre Exploration Project website http://www.whoi.edu/website/beaufortgyre/home and the publications listed there.

Among the instruments that were deployed on bottom-tethered moorings, ice profiling sonars, and acoustic Doppler current profilers (ADCPs) are relevant for our study. IPS instruments measure ice draft by measuring the return period of acoustic signals emitted from the instrument as they reflect from the bottom surface of the ice. The corresponding distance is calculated using the speed of sound in the water above the instrument. The distance to the water surface is measured by pressure sensors. Ice draft is the difference between the distance to the water surface and the distance to the ice bottom surface. IPS models IPS4 and IPS5, manufactured by ASL Environmental Sciences, were deployed on either three or four (depending on the year) bottom-tethered moorings in the Beaufort Sea (Fig. 3). Listed in Table 1 are the location and deployment year of the moorings used in this study. Beam width of the IPS is 1.8°, sampling a footprint of about 2 m from around 50 m below the bottom surface of the ice. The accuracy of the individual draft measurements is ± 10 cm (Proshutinsky et al., 2009).

2.1. Ice drift data

The ADCP measured the water column current profile and ice velocity. It works on the principle of the Doppler effect by emitting acoustic signals at a fixed frequency and registering the reflected signal with a shifted frequency that is proportional to the velocity of the moving object (ice bottom surface). ADCP instrument was typically instrumented only on one mooring per year. This limits the usage of ice drift measurement in our analysis. Furthermore, ice drift data were flawed with measurement errors. Spurious unnatural peaks in ice drift speed occurred when open water segments were present (Fig. 4). These errors are most obvious during the summer months. After several attempts, we have not managed to filter out these errors and excluding weeks with flawed data would impose unwanted bias in our analysis.

We have resorted to use reanalysis data for ice drift speed provided

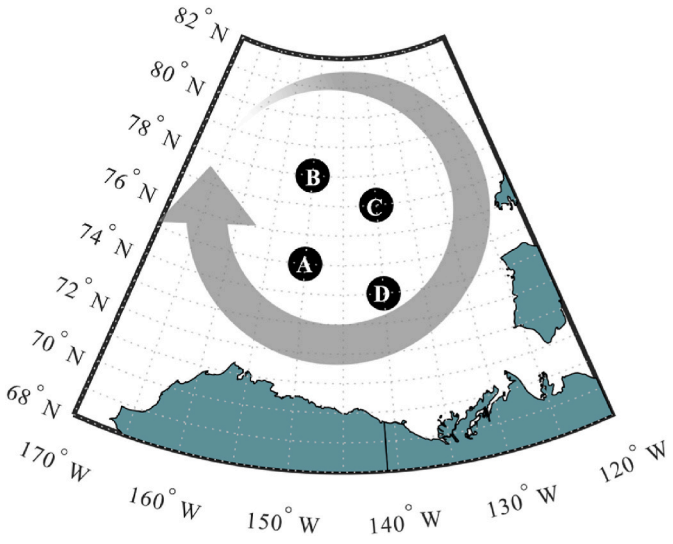

Fig. 3. Locations of bottom-tethered moorings with IPSs. The arrow broadly represents the mean sea ice circulation of the Beaufort Gyre.

Table 1
Location and years of the moorings.

Station	Latitude	Longitude	Water depth (m)	Years
A	75N	150°W	3825	2003–2017
B	78°N	150°W	3821	2003–2004, 2006, 2008–2010, 2012–2013, 2015–2017
C	77° N	140°W	3722	2003–2005, 2007 2018
D	74°N	140°W	3521	2006–2008, 2010, 2012–2014, 2016–2017

by TOPAZ4 system (Xie et al., 2017). This dataset provides daily mean ice drift velocity, as well as the daily ice concentration. Values are given for grid cells with spatial resolution of 12.5 km × 12.5 km. Due to the concerns about the accuracy and difference in resolution of this dataset to our main data (IPS draft measurements), we are not using this data for the main analysis of this paper. The results given in this subsection are only designed to be supplementary.

Using the daily mean ice drift speed and concentration we are able to estimate the weekly ice transect length by making a weekly sum of multiplication of the two parameters. Fig. 5 illustrates the seasonal development for this parameter, as well as the overall distribution. Note that only those weeks that were included in analysis are considered here (e.g., weeks with fewer than 15 ridges are excluded). These weeks are excluded because statistical conclusions with low amount of sample ridges is not reliable. Further, these weeks occurred mainly early in the season and this part of the season is less important for the ridge load estimation as ice is not that severe in this part of the season.

Note the overall decreasing trend in the weekly ice transect length over the season. The reason for this is most probably the gradual slowdown in ice drift as the ice field gets more compact and the more abrupt decrease in the ice concentration during the summer months. Also, seasonal variation of the wind speed is a probable cause for the observed trend. Since we analyse temporally referenced number of ridges (weekly number of ridges) later in the text, we can say that decrease in the weekly ice transect length is suppressing the positive correlation between the level ice draft and weekly number of ridges.

3. Level ice draft identification

IPS measurements cannot directly differentiate between undeformed level ice and deformed ice features such as rafted ice or ice ridges. If an ice draft histogram is made, in most cases, one or two distinct modes are present that indicate the most frequently occurring draft classes. Typically, these modes reflect the undeformed level ice draft (Haas, 2010).

In this section, we describe our approach for finding modal level ice drafts, that is the mode of the probability density function. First, we show two examples that provide details about the approach. We use these examples to define and illustrate the absolute mode (AM) and the deepest mode (DM) of ice draft distributions. The absolute mode is the mode with the highest probability density value, and the deepest mode is the mode with the deepest draft value. Then, we describe the misidentification of modes and the procedure for identifying the same.

Fig. 6 illustrates example **E1**, where the ice environment consists of what is most likely first-year ice (FYI). We can see in Fig. 8 that the preceding summer was ice-free, and the measured ice represents newly formed ice. This example represents a simple case where AM and DM are in the same location and there is no ambiguity in finding the level ice draft. Fig. 7 illustrates example **E2**, where the ice environment seems to be consisted of both FYI and old ice. The draft distribution is bimodal, and the deeper draft is too deep for month of November to be FYI. We can trace the origin of these examples in Fig. 8.

To gain further confidence in our level ice draft identification, we analyse the seasonal development of level ice draft. First, an estimate is made of the level ice draft in 1-h intervals by calculating the absolute mode for 1-h-long data subsets. This gives us a reasonable estimate of

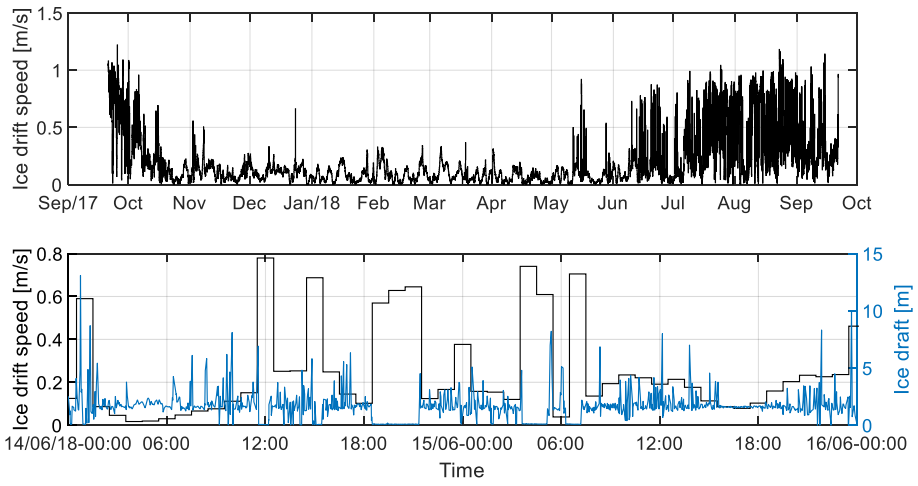

Fig. 4. Example of ADCP ice drift speed data for mooring at location B for year 2017. Bottom panel illustrates unnatural peaks in ice drift speed measurements when open water segments occurs.

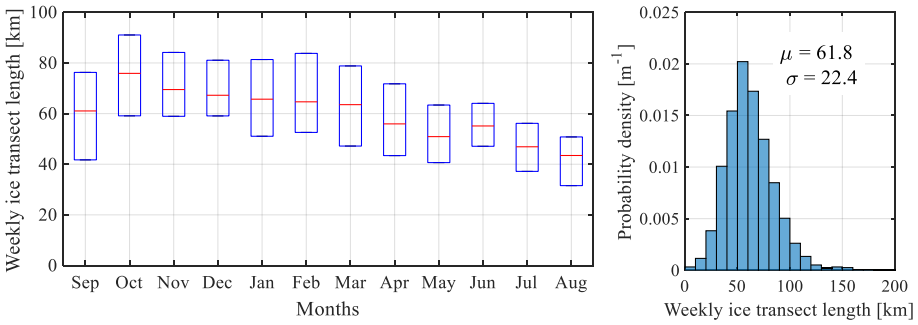

Fig. 5. Seasonal development (left) and overall distribution (right) of the weekly ice transect length – all data. Monthly median is indicated with the central mark in each box and the 25th and 75th percentiles indicated with the bottom and top edges of each box, respectively.

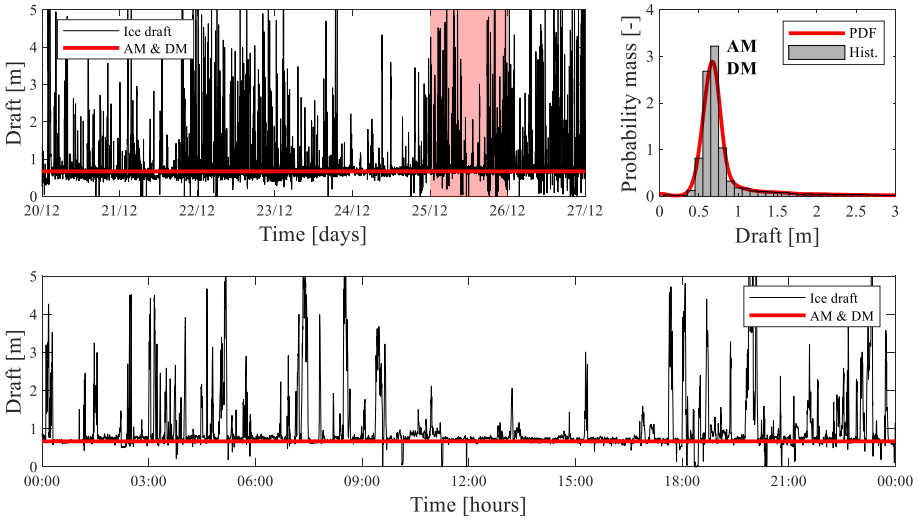

Fig. 6. Example E1 (2012–2013, location B, see Fig. 8) illustrates a unimodal ice draft distribution where AM and DM are in the same location.

the instantaneous level ice draft. Using this instantaneous level ice draft estimates we can make weekly histograms of level ice draft. The evolution of these weekly histograms can be traced by representing weekly histograms with vertical slices aligned horizontally in a time reference and with the frequency of ice draft class represented with a colour map (Fig. 8).

Fig. 8 shows the evolution of the level ice draft distribution for two seasons (2012–2013 and 2013–2014) at location "B". These two seasons illustrate an example of first-year ice that survives the summer season and becomes second-year ice. We use this plot to examine the performance of AM and DM mode identification. On three occasions (January 2013 - E4, February 2013 and February 2014), DM identification estimated level ice draft that is higher than the pronounced deepest mode. On closer inspection of these points, we observed that this was caused by

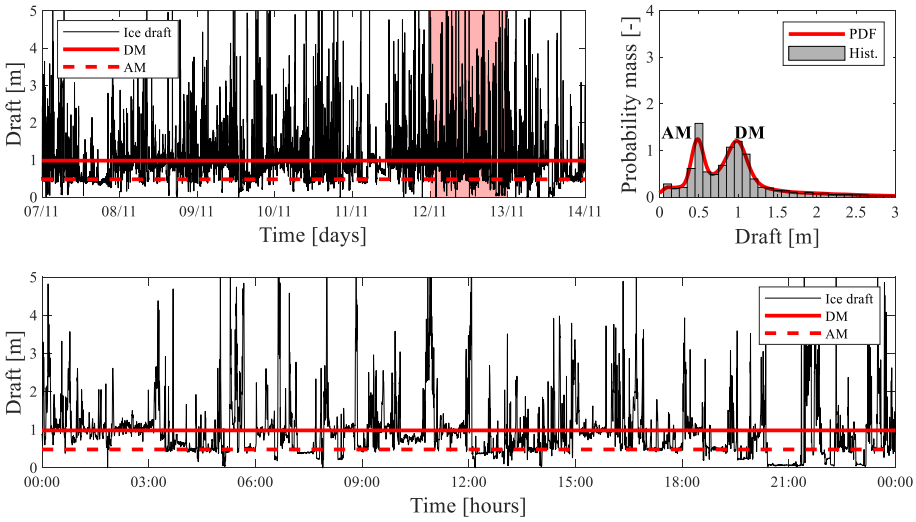

Fig. 7. Example E2 (2013–2014, location B, see Fig. 8) illustrates a bimodal ice draft distribution where AM and DM are not in the same location.

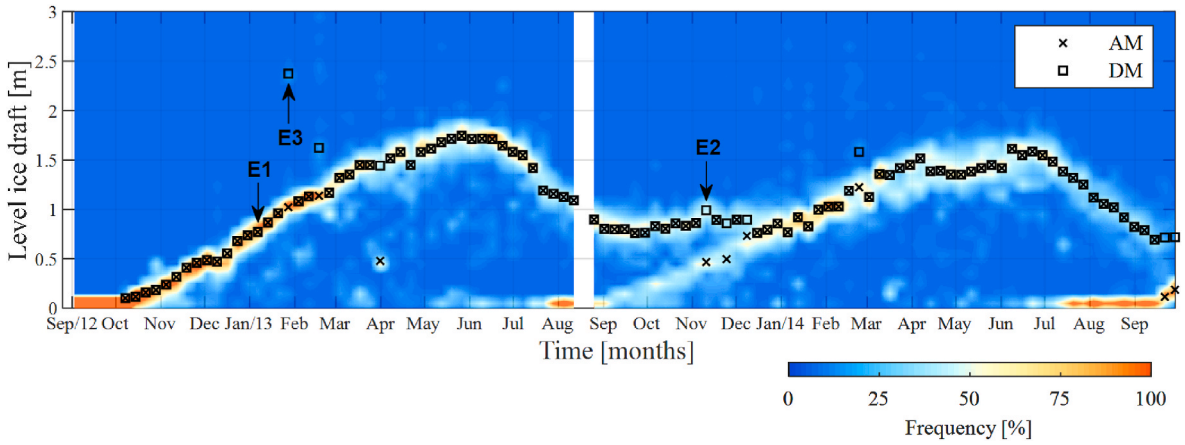

Fig. 8. Evolution of the level ice distribution during the 2012–2013 and 2013–2014 seasons at location "B". The weekly estimate of level ice draft using the absolute mode (AM) is depicted with crosses, and the deepest mode (DM) is depicted with rectangles. Arrows and text annotations mark examples used for illustrating specific cases of level ice draft identification.

"stagnant ice events". Week from January 2013 is a good example of one such event (marked as E3 in Fig. 8). Ice slows down or completely stops, and the IPS instrument continuously detects ice draft from a single ice feature for a prolonged time. The draft of this feature appears as a small (but still detectable) mode in the ice draft distribution. These events cause misidentification of the level ice draft in the automated procedure and produce outliers. We inspected all automatically identified level ice draft data points and manually corrected the misidentifications.

Note that the level ice identification procedure is switching between FYI (First-Year Ice) and MYI (Multi-year Ice). Early in the season, the procedure favours MYI (if present), and FYI later in the season when the two modes merge. Level ice that is identified this way is rather unpractical for analysis of the physical nature of ridge creation processes. However, it is practical in the sense that it has shown to have a reasonably good predictive capability of ridge statistics. As we show later in the text, this mode can be correlated with weekly mean ridge keel draft and number of ridges and these correlations can be used for probabilistic simulation of ridge statistics based on known level ice draft. Furthermore, it represents a conservative higher value of the surrounding level ice that is used for estimating the limit force in ridge load calculation. This is a favourable choice in ridge load calculation.

4. Ridge statistics

A ridge system can be described in one dimension by the number of ridges (per unit time or unit length) and the mean ridge draft (Hibler et al., 1972). In this section, we show the seasonal development of the two variables and the relationship between them. The first step in this analysis is to identify and count individual ice ridges from IPS ice draft measurements. In the second step, we divide the ridges into weekly subsets, and for each subset, we count the weekly number of ridges and calculate the mean ridge keel draft. Using the mean ridge keel draft and the negative exponential distribution, we effectively describe the weekly ridge keel draft probability distribution. A total of 199128 ridges deeper than 5 m were identified from the IPS draft measurements in the Beaufort Sea. The measurements spanned a period of 15 seasons with multiple instrumented locations, and in total, 37 season locations were available for analysis.

In this paper, all analyses were conducted on the entire set of data. Some analysis was performed for the data grouped by different mooring deployment sites and compared (not reported in the paper). Although there were small statistical differences, the conclusions made in this paper would not change significantly if a single mooring site data was used. In order to ensure a more robust basis for analysis, it was decided to use the entire data set.

Independent keels are identified using the Rayleigh criterion, which is extensively used for identifying ridges from both the bottom and surface profiles of ice (Wadhams and Horne, 1980; Williams et al., 1975). Keels are initially identified as local maxima with a draft deeper than 5.0 m. This limit is required to ensure that the majority of the identified features are mechanically grown features. Subsequently, the criterion ensures that wide keels with multiple local maxima are counted as one independent keel. The criterion removes keels with a trough (on either side of the point of local maximum) that does not rise halfway towards the level ice surface, in our case fixed arbitrarily as a draft of 2.5 m. This value should reflect the local level ice, and although the level ice draft is smaller in most cases, we retain the 2.5 m threshold in order to have compatible results with earlier studies. We note that using a 2.0 m threshold did not change the results significantly.

There is considerable evidence that the distribution of keel draft of individual ridges identified by the Rayleigh criterion obeys a negative exponential type (Ekeberg et al., 2013; McLaren et al., 1984; Wadhams and Horne, 1980). Once the Rayleigh parameters are allocated and fixed, the ridge keel draft distribution is described with only one parameter (the mean). This is convenient, as we can analyse the relationship between level ice and ridge draft by analysing the relationship between weekly level ice draft and weekly mean keel draft. However, we must bear in mind that ridge statistics are not completely described only with the mean; we must also include the number of ridges to obtain a complete description.

A total of 1697 individual weeks are analysed. For each week, a certain number of individual ridges are identified, and the mean ridge keel draft is calculated. Fig. 9 shows the development of the number of ridges per week. Fig. 10 shows the development of the weekly mean ridge keel draft. A certain seasonal regularity with some variability can be observed. At the beginning of the season, we can observe a larger scatter of the mean keel draft and outliers with a large number of ridges. This is caused by seasons where multiyear ice is present in the early part of the ice growth season. Presence of old also causes occasional large number of ridges early in the season.

5. Relationship of ridge statistics and level ice draft

5.1. Filtering of data based on number of ridges per week

We ignored weeks with fewer than 15 ridges. This occurs more often in the early part of an ice growth season because ridges have not yet developed (Fig. 11). We ruled out 113 out of a total of 1697 weeks (including all years and all sites), leaving 1584 weeks for further analysis. Fig. 11 shows the probability of having fewer than 15 ridges during a week with respect to level ice draft. This was done because statistics are not reliable when having low number of ridges.

It is important to remember that there can be weeks with few ridges when performing a probabilistic simulation where level ice is also simulated. This can be considered by using the fitted function from Fig. 11. In our simulations in Section 6, we do not consider this because our simulation is based on measured level ice draft data, where weeks with a low number of ridges are already ruled out. However, in our future work, where we plan to simulate level ice draft, we will need to consider weeks without ridges. For this, we will use the fitted function shown in Fig. 11.

5.2. Weekly deepest ridge keel draft versus level ice draft

For the forthcoming analysis, we use the level ice draft estimated using the DM identification procedure with subsequent manual correction of misidentification. The main result is that we have found a positive relationship between level ice and weekly deepest keel draft that can be described with an linear regression (Fig. 12). Using a regression obtained by least squares approximation, we can describe the general linear relationship with the following function: $D = 8.63 + 3.99\,h$, where D is the weekly deepest keel draft and h is the weekly level ice draft. It is important to note that we do not try to explain the causal relationship between the two variables and the natural phenomenon lying behind the relationship, but only try to capture the correlation for engineering purposes. As we will show in Section 6, the linear regression is very useful for the probabilistic simulation of the weekly deepest keel draft.

Note that ridges with keels shallower than 5 m are not identified and that weeks with less than 15 ridges are not considered in our analysis. This removes many of the data points with a shallower level ice draft. If the relationship is to be analysed for shallower level ice draft, one should use an alternative ridge identification that would not disregard shallow ridges. With this in mind, it is recommended that the relationship for shallower level ice needs to be interpreted with caution. Also note that in cases with shallower level ice drafts, deep ridges are often old ridges from the previous season.

5.3. Weekly mean ridge keel draft versus level ice draft

The relationship between level ice and weekly mean keel draft is shown in Fig. 13. An obvious positive correlation can be observed. Using a regression obtained by least squares approximation, we can describe the general linear relationship with the following function: $\overline{D} = 6.03 + 0.51\,h$, where $\overline{D}$ is the weekly mean keel draft and h is the level ice draft.

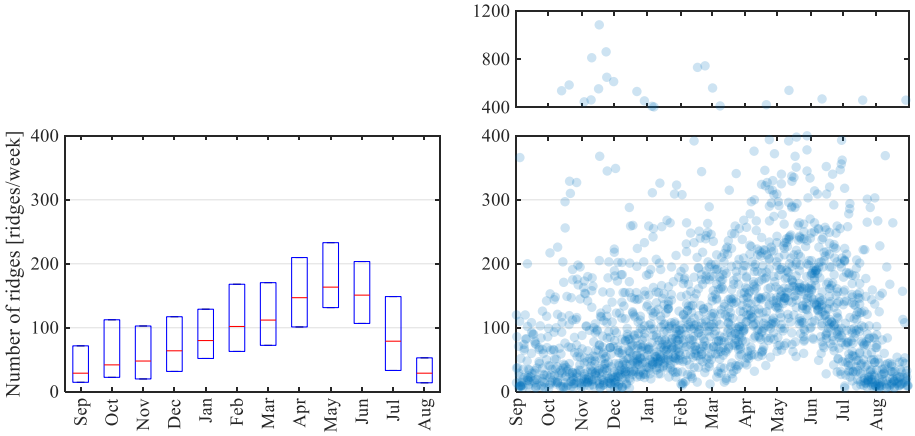

Fig. 9. Seasonal development of weekly number of ridges. Left panel: Monthly median indicated with red lines with 25th and 75th percentile indicated with bottom and top edges of the boxes, respectively. The right panel shows a scatter plot where each analysed week is represented with an individual circle. The right panel is divided in two parts such that the seasonal development can be inspected more carefully.

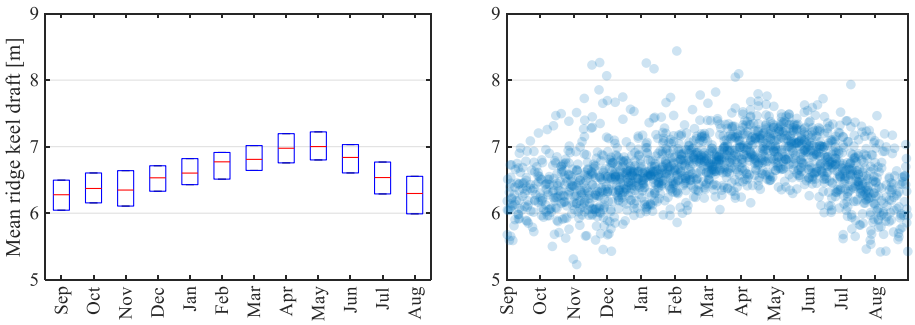

Fig. 10. Seasonal development of weekly mean keel draft. Left panel: Monthly median indicated with red lines with 25th and 75th percentile indicated with bottom and top edges of the boxes, respectively. The right panel shows a scatter plot where each analysed week is represented with an individual circle.

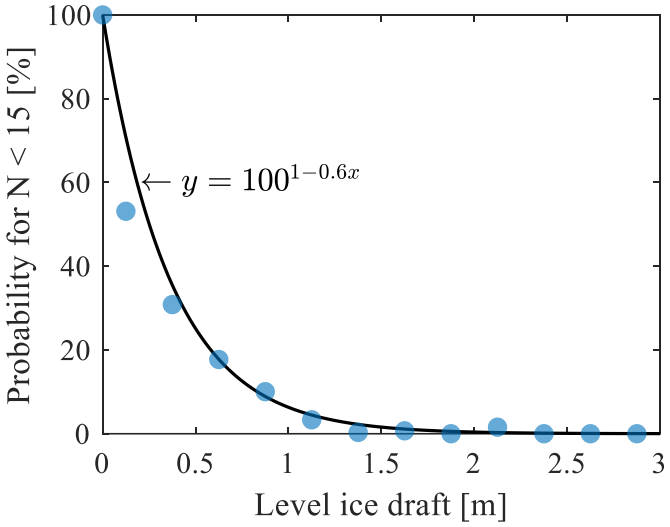

Fig. 11. Probability of having a week with fewer than 15 ridges with respect to level ice draft.

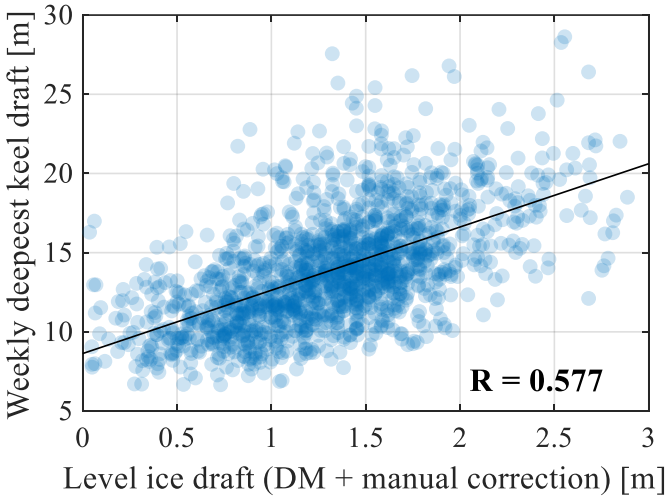

Fig. 12. Relationship between level ice and weekly deepest keel draft. The solid line represents a regression obtained by least-squares approximation (intercept $a_1 = 8.63$; slope $b_1 = 3.99$). R is the Pearson correlation coefficient for the two parameters.

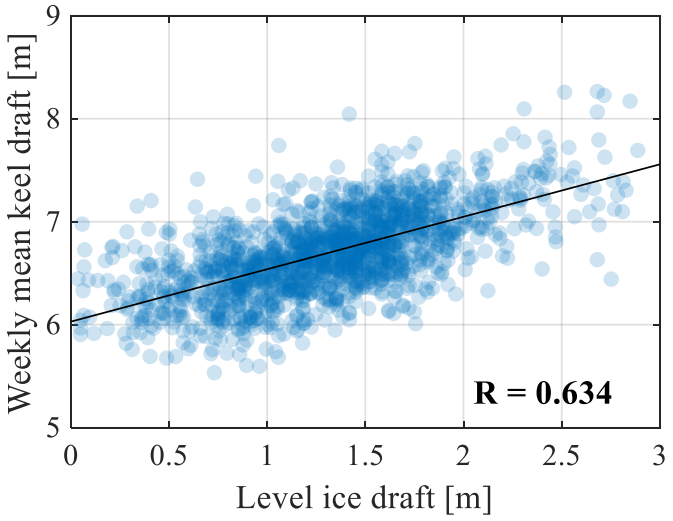

Fig. 13. Relationship between level ice and weekly mean keel draft. The solid line represents a linear regression obtained by least-squares approximation (intercept $a_2 = 6.03$; slope $b_2 = 0.51$). R is the Pearson correlation coefficient for the two parameters.

This function is later used in Section 6 for a probabilistic simulation of the weekly mean keel draft.

5.4. Ridge frequency versus level ice draft

In this subsection we analyse the relationship between level ice draft and ridge frequency given both in temporal reference (ridges per week) and spatial reference (ridges per kilometer).

The relationship between the level ice draft and the weekly number of ridges is illustrated in Fig. 14. We can see that a higher number of ridges is associated with a deeper level ice draft. The reasons for this can be attributed to several factors. Time is one of these factors. As the level ice grows during a season, more time has passed, and more ridging events have occurred; therefore, more ridges accumulate in the ice field. Using a regression obtained by least squares approximation, we fit the following power function to the data: $N = 84.69 \cdot h^{1.318}$. This function is later used in Section 6 for a probabilistic simulation of the weekly number of ridges.

The relationship between the level ice draft and the spatial ridge frequency is illustrated in Fig. 15. We can see that the relationship is similar as the relationship shown in Fig. 14. In order to analyse the relationship between the temporal and spatial ridge frequency, we present the relationship of the two variables in Fig. 16. We can see that the two variables are linearly correlated with a scatter around the linear relationship that is explained by the variability in ice drift speed and concentration.

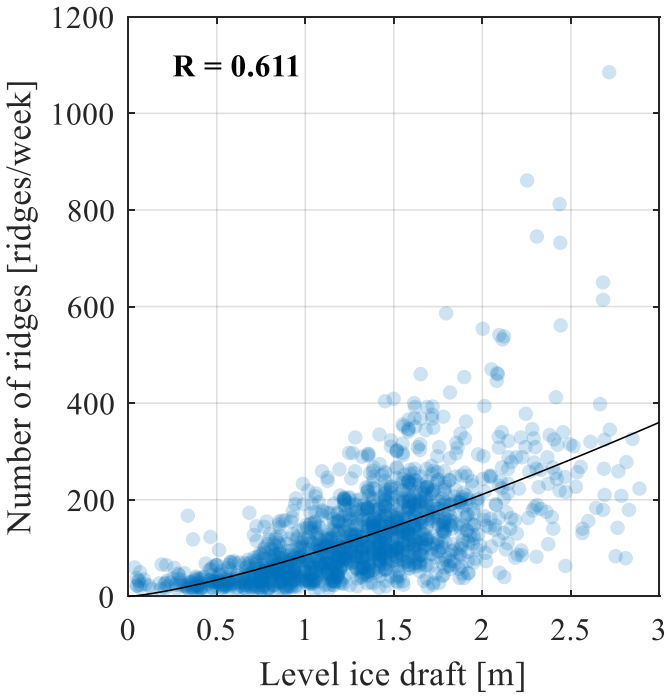

Fig. 14. Relationship between level ice draft and the weekly number of ridges. The solid line is a fitted power function of the type $y = a_3 \cdot x^{b_3}$ ($a_3 = 84.69$; $b_3 = 1.318$). R is the Pearson correlation coefficient for the two parameters.

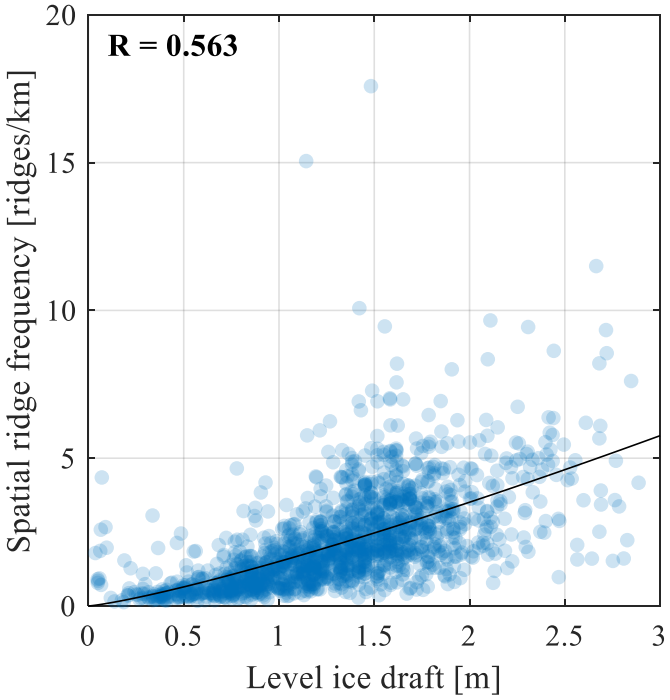

Fig. 15. Relationship between level ice draft and the spatial ridge frequency. R is the Pearson correlation coefficient for the two parameters.

6. Probabilistic simulation of ridge keel draft

6.1. Introduction to simulations

In this section, we utilize our findings of the relationship between level ice and ridge statistics and propose two approaches for probabilistic simulation of the ridge keel draft. The traditional way to simulate ridge keels is to fit a negative exponential distribution to keel draft data and use this distribution in a Monte Carlo simulation. However, this approach disregards the relationship of keel to level ice draft. In our approach, we preserve this relationship. In addition, our approach can be used for simulating the seasonality of ridge statistics. This can be used for a probabilistic analysis of the seasonal evolution of ridge loads on offshore structures.

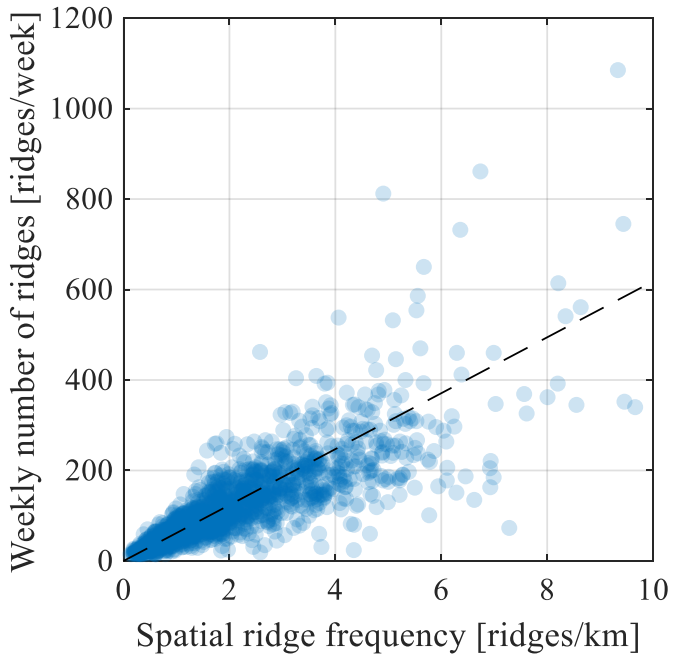

Fig. 16. Relationship of ridge frequency in spatial and temporal reference. Dashed line is a linear function of spatial ridge frequency multiplied by the mean weekly ice transect length ($y = 61.8\ x$).

Depending on the need, one can choose to simulate only weekly deepest keels or all keels (deeper than 5 m). We will describe approaches for both alternatives in two separate subsections. For both alternatives, the first step is to simulate the level ice draft according to its independent statistical distribution. This can be done by accounting for the interseasonal variability of level ice draft (Samardžija et al., 2018). Then, ridge keels can be simulated according to the relationship to the level ice draft that we presented in this paper. In the examples given in this section, we skip the first step for level ice draft simulation and instead use the dataset of measured level ice draft presented earlier in this paper. We do this to analyse the effectiveness of our approach in simulating the keel draft while maintaining the relationship to level ice draft. In this way, the simulated keel draft data will be directly comparable to the field data.

The statistical analysis in the previous section is done on the complete available dataset. In this section, the probabilistic simulations are based on the complete dataset and the results are compared with the complete dataset. This is done to mimic a real case scenario where probabilistic load model is based on the available data and simulation is done to extend the load estimates to extreme load values such as 100-year return period and 10,000-year return period. To further examine the predictability performance of our proposed model, we present a cross-validation analysis in the Appendix. Half of the dataset is randomly selected as a training dataset the simulation input and the results are compared to the remaining validation dataset.

6.2. Simulation of weekly deepest ridges

The relationship of keel to level ice draft can be decomposed into two components. The first component is the general linear relationship, and

the second component is the variability around the linear relationship. As shown in the previous section (Fig. 12), the linear relationship can be quantified using a linear function. The variability around this linear relationship can be quantified by the following ratio:

$$R_i(h_i) = D_i / D(h_i) \quad (1)$$

where index i indicates that the ratio is calculated for the individual i-th point (week number i), h_i is the level ice draft, D_i is the weekly deepest ridge keel draft and $D(h_i) = a + b \cdot h_i$ is the value of the linear regression line for the given level ice draft h_i (parameters a and b are given in the caption of Fig. 12). The ratio indicates how much the keel draft deviates from the linear regression line. We refer to this ratio as "normalized weekly deepest keel draft" (i.e., normalized to the linear regression line).

We want to use a probability distribution for the simulation of this ratio. Fig. 17-a shows the distribution of the normalized weekly deepest keel draft. A log-normal distribution fits the data reasonably well (mean of logarithmic values: -0.0204; standard deviation of logarithmic values: 0.2024). This can be observed by visual comparison of the histogram to the fitted distribution (Fig. 17-a) and using a Q-Q plot (Fig. 17-b).

We are now ready to make a probabilistic simulation of the weekly deepest keel draft for a given level ice draft. We simulated 1584 points with level ice drafts from the earlier section that were estimated using the DM identification procedure with subsequent manual correction. The simulation technique can be summarized with the following expression:

$$D_i = (a_1 + b_1 \cdot h_i) \cdot R_i \quad (2)$$

where D_i is the simulated weekly deepest keel draft, a_1 and b_1 are the intercept and the slope of the linear regression line from Fig. 12, and R_i is the normalized weekly deepest keel draft ratio that is sampled according to the fitted log-normal distribution shown in Fig. 17. In other words, for a given level ice draft, we first estimate what would be the expected keel draft according to the linear regression and then multiply it with a factor to account for the variability around the general linear relationship. We repeat this calculation for all 1584 points. An example of one simulation run is given in Fig. 18. Visual observation indicates a good qualitative replication of the correlation and the Pearson correlation coefficient indicates a good quantitative replication.

We use an exceedance probability plot of the weekly deepest keel draft to compare the distributions of the simulated and observed data (Fig. 19). Since the distribution of the simulated data can vary between multiple simulations (especially in the tail section of the distribution), we repeat the simulation 100,000 times and make the best estimate by calculating the 50th percentile exceedance probability curve. Additionally, we estimated 90% and 98% confidence intervals. The high number of simulations was chosen by trial and error approach with a goal to get reproducible and smooth 98% confidence interval. The simulated best estimate is in good agreement with the observed data.

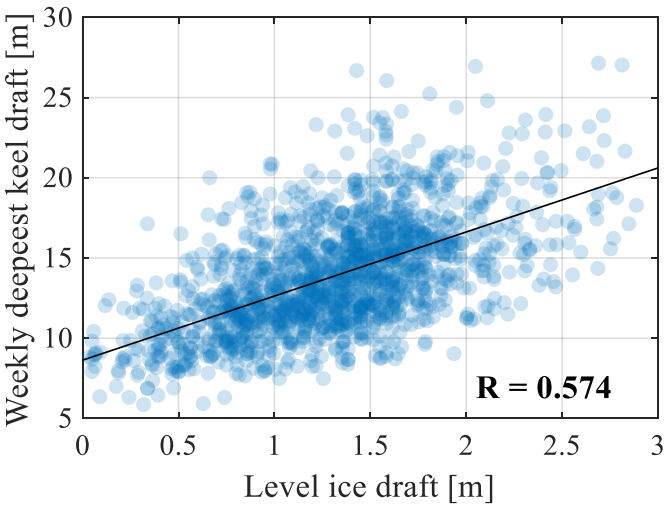

Fig. 18. Surrounding level ice versus the simulated weekly deepest keel draft. The solid line is the linear regression from Fig. 12 (not a new linear regression with respect to the simulated data). This line is replotted to provide a reference for comparing the simulated data from this figure to the observed data shown in Fig. 12. R is the Pearson correlation coefficient for the two parameters.

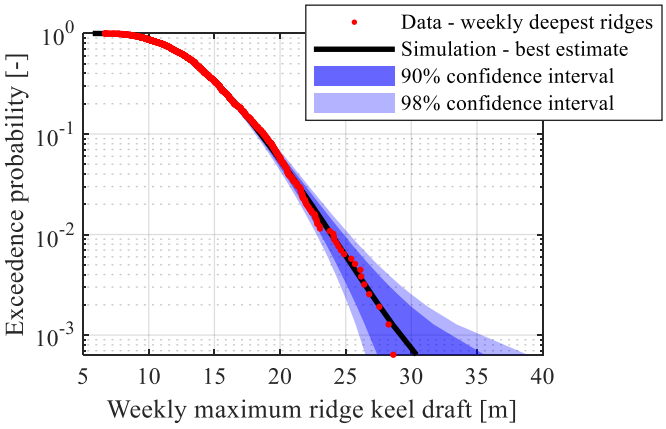

Fig. 19. Comparison of the simulated weekly maximum ridge keel draft to the observed data.

6.3. Simulation of all ridges (deeper than 5 m)

We will now describe a procedure for the simulation of all ridges deeper than 5 m. The simulation is based on the established relationship

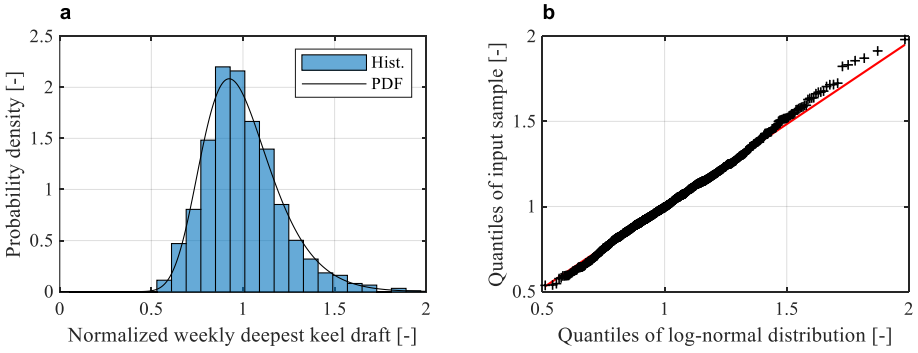

Fig. 17. (a) Distribution of the normalized weekly deepest keel draft (all data). The fitted probability density function (PDF) is a log-normal function (mean of logarithmic values: -0.0204; standard deviation of logarithmic values: 0.2024). (b) Q-Q plot comparing the fitted log-normal distribution to the input sample with normalized weekly deepest keel draft data.

between the level ice draft and weekly mean keel draft (Fig. 13), as well as the relationship between the level ice draft and the weekly number of ridges (Fig. 14). The procedure can be divided into the following steps:

1. Establish a dataset for the level ice draft. This can be either a measured or a simulated dataset. In our example, we use the measured ice draft dataset.
2. Simulate the weekly mean keel draft for a given level ice draft according to the relationship established between the level ice draft and the weekly mean keel draft.
3. Simulate the weekly number of ridges for a given level ice draft according to the relationship between the level ice draft and the weekly number of ridges.
4. Using the simulated weekly mean keel draft ($\overline{D}$) and the weekly number of ridges (N) for a given week, simulate N ridges according to the given weekly mean keel draft and the negative exponential distribution. This step is repeated for all weeks.

The second step of the simulation is performed in an analogous way to the simulation of the weekly deepest keel draft for a given level ice draft, with a difference that now we simulate the mean ridge keel draft based on level ice draft.

The third step of the simulation, where we generate weekly numbers of ridges for a given weekly level ice draft, is performed in a similar manner to the simulation of weekly mean keel draft and simulation of deepest keel draft. In this step, we need to reproduce the relationship between the weekly level ice draft and the weekly number of ridges shown in Fig. 14. We can decompose this relationship also into two components (general relationship and the variability around the general relationship). However, the general relationship component is now described with a power function (solid line in Fig. 14).

Once we have simulated the weekly mean keel drafts and the weekly number of ridges for all weeks, for each i-th week, we can simulate N_i number of ridges according to a negative exponential distribution with mean parameter $\overline{D}_i$. We repeat the simulation 1000 times and make the best estimate by calculating the 50th percentile exceedance probability curve. The exceedance probability plot comparing the observed and simulated data is given in Fig. 20. The estimated 90% and 98% confidence intervals are also shown. The observed data do not align perfectly with the best estimated simulated distribution. The tail of the simulated distribution is heavier, and it gives deeper keels than the observed distribution. It can be said that the observed data lie around the lower 5th percentile curve. This means that the probability for the simulation to produce the observed distribution is approximately 5%.

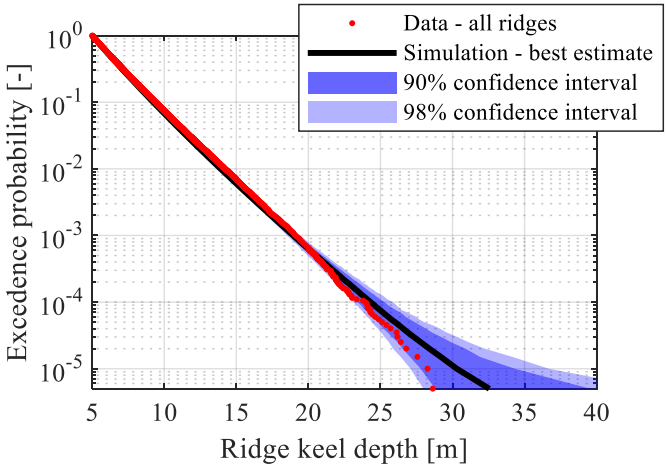

Fig. 20. Comparison of all simulated ridges to the observed data.

7. Discussion

The presence of multiple level ice draft classes with diverse drafts in ice fields is common. The goal was to find the level ice draft class that has the best predictive capability with regard to ridge keel draft. Our analysis revealed that this is the deepest level ice draft class indicated by the deepest mode. The fact that our level ice draft detection is identifying both FYI and MYI is limiting the analysis of the phenomenological nature of the correlations shown in this paper. We must remember that the primary motivation of this paper was to establish a relationship between level ice and ridge keel draft for use in the probabilistic assessment of ridge loads on offshore structures. Level ice thickness is needed in these calculations for estimating the limit force. The limit force is the maximum force that the surrounding ice can exert upon a structure indirectly through a ridge in front of the structure. It is thereby sensible to use the thickest level ice present in the field because it is a conservative approach.

The relationship between level ice and ridge keel draft presented in this paper does not directly imply a causal relationship between thick level ice and the *creation* of deep ridges. Although it is expected that thicker level ice will produce deeper ridges (explained by the mechanical principles of ridge building processes), it is also true that level ice is thicker towards the end of the ice growth (spring/summer) when more time has passed for deep ridges to be created. Therefore, our study indicates a relationship between thick level ice and the *presence* of deep ridges.

We analysed the relationship between level ice draft and weekly deepest ridge keel draft. As the word "weekly" indicates, we used a temporal sampling technique, where each data point represents a subsample determined by a temporal unit (week-long subsamples). Our approach is different from what is typically found in the literature, where the spatial subsampling technique is more common (each data point represents a subsample defined by a spatial unit, e.g., 50 km long profiles). The difference in sampling technique makes subtle qualitative differences in the relationship between level ice and deepest ridge keel draft. One such difference is that the general relationship of maximum keel draft and surrounding level ice thickness with a spatial sampling technique has a square root shape ($h_k < 20\sqrt{h_i}$ (h_k in meters) Amundrud et al., 2004), whereas with a temporal sampling technique (our approach), the general relationship between mean keel draft and surrounding level ice thickness has a linear shape (Fig. 13). This is important to have in mind when performing probabilistic simulation of ridge keel draft where correlation to the level ice draft is maintained. Due caution needs to be exercised in interpretation of the established correlation and in translation of the same into the probabilistic simulation.

Using the established relationship between level ice and the weekly deepest ridge keel draft, we were able to replicate the weekly deepest ridge keel draft distribution in a probabilistic simulation. The simulation takes level ice draft as an input and produces weekly deepest keel drafts. The simulated distribution fits almost perfectly to the measured data, and the relationship between the two variables is well preserved. This type of simulation is useful if we are interested only in the deep ridges. For example, this is the case in the probabilistic assessment of ridge scouring of seabed pipelines.

In probabilistic assessments of ridge loads on an offshore structure, we are interested in all ridges that arrive at the structure of interest. This is because it is not necessarily the deepest ridges that cause the highest loads. Therefore, we had to establish an approach where all ridges are simulated. We started from a standpoint where we can divide the simulation into weekly steps. For any week, to simulate all the week's ridges, we need the mean ridge keel draft and the number of ridges. For this reason, we have analysed the relationship between level ice draft and weekly mean ridge keel draft, as well as the relationship between the level ice draft and the weekly number of ridges.

We have shown an example of the simulation of all ridges where we

used the measured level ice draft as the input. The resulting simulated distribution of ridge keel draft was somewhat more conservative than the measured distribution. A larger part of the simulated ridges aligns with the measured distribution, but the tail section of the simulated distribution overestimates the draft. This is not surprising since the simulated distribution is influenced by the large weight of many shallower ridges. We can see in Fig. 20 that the measured distribution starts to deviate from the simulated distribution for ridges deeper than 20 m. Note that there were only 128 out of 199,128 measured ridges that were deeper than 20 m. It is possible that this deviation is due to chance. In fact, we have estimated that there is a roughly 5% probability that the simulation will produce a distribution similar to the measured one.

We will conclude this section with a comparison of the two simulations and the measured distribution. To have these distributions directly comparable, we need to transfer all the distributions to terms of return period and plot them on an exceedance probability plot. We advise caution when interpreting the return periods from this plot. The measurements are taken at multiple locations, and in our transformation, each year's location is considered an independent year of measurements. This is not the case in reality because the measurements at two locations during the same year are not fully independent. We make this transformation only with the intention of having the distributions directly comparable. Transfer of a distribution to terms of a return period is a process of transferring a parent distribution to an annual maximum distribution (Jordaan, 2005). The transformed distributions are illustrated in Fig. 21 by means of the exceedance probability plot. Note that this type of visual assessment is, in fact, analysing the tail of the distributions. Fig. 22 illustrates the cumulative distribution functions, where more details are visible for shallower drafts.

The simulation of the weekly deepest ridges results in an almost perfect fit with the measured data, whereas the simulation of all ridges results in deeper ridges than the measured ridges in the tail section of the distribution. We can see in Fig. 22 that the measured data initially align with the simulated distribution of all ridges, but when moving towards a deeper draft, it aligns with the simulated distribution of weekly deepest ridges (transition of the orange line from the blue line towards the black line). We cannot draw final conclusions on which of the two approaches gives a better prediction of extreme ridges. However, we can provide some indications about why this difference occurs. In the simulation of weekly deepest ridges, we prepared the inputs by fitting the tail of the distribution by considering only the extreme (weekly deepest) ridges. In the simulation of all ridges, we prepared the inputs by considering all measured ridges. One simulation is optimized for the tail of the distribution, and the other simulation is optimized for the overall distribution of the keel draft. Considering the measured ridges, the shape of the distribution in the shallow draft section indicates that extreme ridges should be slightly deeper than the measured extreme ridges. On the other hand, the shape of the distribution in the deeper draft section indicates a possibility that there is some limiting factor to the draft of

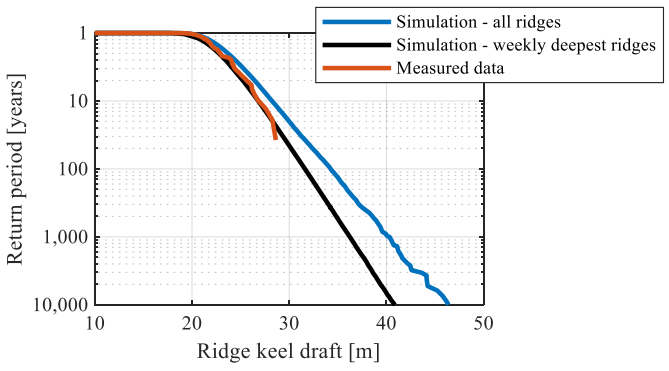

Fig. 21. Exceedance probability plot of the measured and simulated ridge keel drafts with probabilities given in terms of the return period.

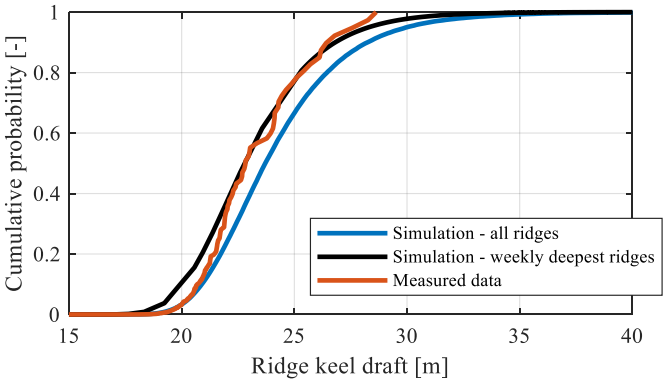

Fig. 22. Cumulative distribution function plot of the measured and simulated ridge keel drafts.

extreme ridges and that the tail of the distribution is tapering off. This reasoning is supported by the findings of Melling and Riedel (1996), who observed truncation of the exponential distribution for a deep ridge keel draft. They ascribed the truncation to the finite strength of the level ice from which the ridges are created.

Based on our analysis, we cannot say with confidence whether the limited draft of extreme ridges is due to chance or due to some natural limiting mechanism. However, we can offer an intuitive explanation of the natural phenomena behind the ridge creation processes that lead to the limited draft of extreme ridges. The maximum ridge keel draft is limited by four boundary conditions: (a) level ice thickness, (b) wind forcing, (c) wind (storm) duration, and (d) quantity of ridge building material (ice). If conditions (b), (c) and (d) are fulfilled, the thickness of the level that is governing the strength of the level ice will limit the maximum draft of the created ridge. This will often be the case early in the season when level ice is thin. Wind forcing is large and long enough, and there is enough level ice to build a ridge with a maximum draft limited by level ice thickness. Later in the season, when level ice is thick, it is less likely that the wind forcing will be strong and long enough to build a ridge with a maximum draft limited by level ice thickness. Therefore, we can hypothesize that the growth of ridge keels is limited by level ice thickness early in the season and is limited by wind forcing later in the season.

Since the ridge keel draft is not the only factor governing the ridge loads on offshore structures, we recommend the use of simulation of all ridges for use in the probabilistic assessment of ridge loads. With this approach, the relationship with the surrounding level ice thickness is maintained. This is more important than the overestimation of extreme ridge drafts. If the keel draft is the main factor in the design, we recommend a simulation of weekly deepest ridges. An example of this would be the design of the seabed pipeline burial depth.

8. Conclusions

A total of 199128 ridges deeper than 5 m were identified from the IPS draft measurements in the Beaufort Sea. The measurements spanned a period of 15 seasons with multiple instrumented locations, and in total, 37 season locations were available for analysis. On average, 5381 ridges were identified for one season location. We divided the data into weekly subsamples. For each week, we identified level ice draft, maximum ridge keel draft, mean ridge keel draft and the number of ridges. The following relationships were analysed: level ice and ridge keel draft; level ice draft and ridge frequency. The analysis was optimized for a probabilistic assessment of ridge loads on offshore installations. The evidence from this study suggests that the deepest mode of the ice draft distribution (thickness level ice class) has the a solid correlation and a useful predictive capability of the ridge keel draft.

We have shown two examples of how our findings can be utilized in

probabilistic simulations of ridge keel draft where the correlation to the level ice draft is preserved. The first example simulated only the weekly deepest ridges, and the second example simulated all ridges deeper than 5 m. Together with correlations established in this paper, level ice draft data is the only input needed for these simulations. Relative to ridge data, level ice data are better known, have clear seasonal trends and are easier to measure and simulate. This gives us an opportunity to investigate ridge statistics in areas where ridge draft measurements are not available. In addition, our approach can be used for the assessment of climate change effects on ridge statistics and, indirectly, the effects on risks for offshore installations in Arctic regions. This can be done by simulating the input level ice draft with a certain climate change scenario taken into account. However, our method needs further validation. Future studies need to consider other locations to investigate whether the correlations from this study are universal and whether the relationships are predictable (e.g., using boundary conditions such as shore vicinity and drift speed).

The thickness of the consolidated layer (the fully frozen layer in the waterline area of the ridge) is possibly the most important geometrical parameter for ridge load calculations on offshore structures. We have not considered this parameter in this paper, and further study is needed to establish a complete framework for a probabilistic simulation of ridge geometrical properties. We are currently in the process of investigating options for a combined probabilistic-physical simulation of consolidated layer thickness. The aim is to simulate ridges using the approach described in this paper and then probabilistically estimate the ridge creation time and consolidated layer thickness using a physical formulation of consolidated layer growth.

The main finding of our study is that ridge statistics described by mean ridge keel draft and ridge frequency are clearly coupled with level ice draft statistics. The ice data needed for Arctic offshore projects are typically sparse, and probabilistic assessments of ridge loads on offshore structures are often performed using a combination of limited and incompatible data sources. Our study provides a simplified framework for probabilistic ridge load assessment where the only met-ocean input is the level ice thickness statistics. We hope that our research will be valuable in solving the difficulty of structural reliability calculations for offshore structures in Arctic regions with little data.

CRediT authorship contribution statement

Ilija Samardžija: Conceptualization, Data curation, Formal analysis, Investigation, Methodology, Software, Validation, Visualization, Writing – original draft. **Knut V. Høyland:** Funding acquisition, Supervision, Writing – review & editing.

Declaration of competing interest

The authors declare that they have no known competing financial interests or personal relationships that could have appeared to influence the work reported in this paper.

Data availability

https://www2.whoi.edu/site/beaufortgyre/data/mooring-data/

Acknowledgements

The data were collected and made available by the Beaufort Gyre Exploration Program based at the Woods Hole Oceanographic Institution (http://www.whoi.edu/beaufortgyre) in collaboration with researchers from Fisheries and Oceans Canada at the Institute of Ocean Sciences. The authors wish to acknowledge the support of the Research Council of Norway through the Centre of Research-based Innovation, SAMCoT, and the support of the SAMCoT partners. This work has been carried out within the NTNU Oceans Pilot project "Risk, Reliability and Ice Data in Arctic Marine Environment".

Appendix

This appendix is showing the results of the cross-validation analysis of the model. In the main part of the paper, complete dataset was used for calibration of the parameters and the simulated data was compared to the same complete dataset. In practice, one would use collected data to learn and train the model and new data would be simulated with the trained model (e.g., to make an estimate of extreme values with a 100-year return period). The cross-validation in this appendix analyses the capability of the model to predict new data. It is worth noting that this validation does not prove the capability of the model to simulate data for other geographical locations.

Half of the complete dataset (training dataset) is taken for establishing the correlations needed for the simulation and the other half (validation dataset) is reserved for validation of the simulated data. Training dataset is selected by randomly taking individual year-long measurements. The validation is done by repeating the cross-validation procedure nine times and comparing the simulated results with the validation dataset by means of q-q plots (nine plots in Figs. 23 and 24). Q-Q plots are used to compare the distributions of the training and validation datasets. Simulated distribution in each of the nine plots represents an average of 100 simulations. This was necessary in order to get a better representation of the tail.

Fig. 23 shows the validation for the simulation of weekly deepest ridges. Visual observation of the q-q plots reveals that the validation dataset and the simulation dataset are well aligned with the linear function $y = x$ and thus confirms that the two datasets have the same distribution. This confirms that the model has a good prediction performance in practice when independent data is used for calibrating the model.

Fig. 24 show the validation for the simulation of all ridges deeper than 5 m. Here as well, the validation dataset and the simulation dataset are reasonably aligned with the linear function $y = x$, with an exception that the model tends to overestimate the draft of the deeper ridges. This overestimation is discussed in the earlier sections of this paper.

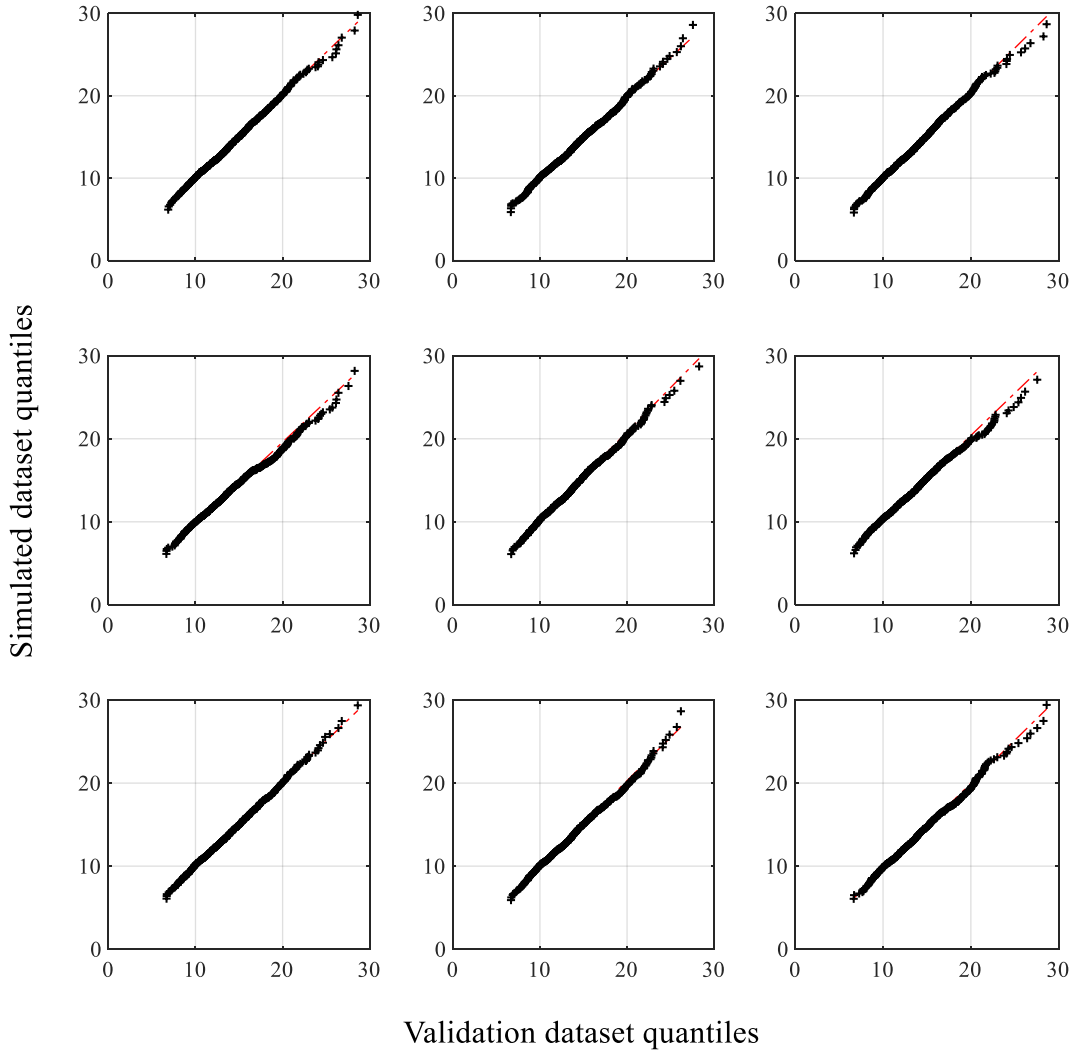

Fig. 23. Comparison of the simulated weekly deepest ridges keel drafts (m) to the validation dataset by means of q-q plots. Dashed line is a linear function x = y.

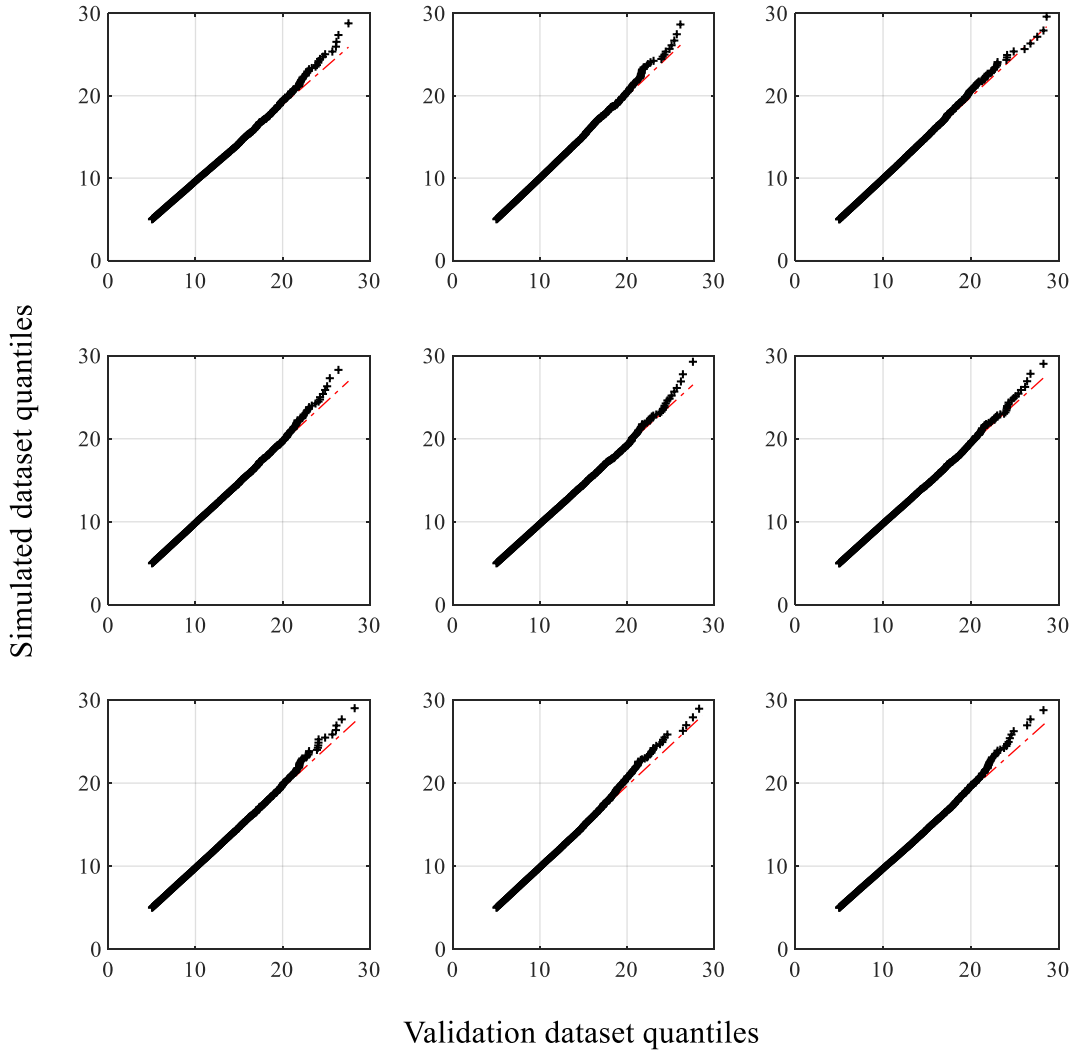

Fig. 24. Comparison of the simulated all ridge keel drafts (m)to the validation dataset by means of q-q plots. Dashed line is a linear function x = y.

References

Amundrud, T.L., Melling, H., Ingram, R.G., 2004. Geometrical constraints on the evolution of ridged sea ice. J. Geophys. Res. 109 (C6), 12.

Ekeberg, O.-C., Hoyland, K., Hansen, E., 2013. Extreme keel drafts in the fram Strait 2006-2011. In: Proc. 22nd International Conference on Port and Ocean Engineering under Arctic Conditions, POAC 2013, June 9, 2013 - June 13, 2013, Espoo, Finland.

Haas, C., 2010. Dynamics versus thermodynamics: the sea ice thickness distribution. In: Sea Ice, second ed. Wiley-Blackwell, pp. 113–151.

Hibler, W., Weeks, W., Mock, S., 1972. Statistical aspects of sea-ice ridge distributions. J. Geophys. Res. 77 (30), 5954–5970.

Hopkins, M.A., 1998. Four stages of pressure ridging. J. Geophys. Res. 103 (C10), 21883–21891.

ISO 19906, 2019. Petroleum and Natural Gas Industries - Arctic Offshore Structures.

Jordaan, I., 2005. Decisions under Uncertainty: Probabilistic Analysis for Engineering Decisions. Cambridge University Press.

Jordaan, I., Bruce, J., Masterson, D., Frederking, R., 2010. Local ice pressures for multiyear ice accounting for exposure. Cold Reg. Sci. Technol. 61 (2–3), 97–106.

McLaren, A.S., Wadhams, P., Weintraub, R., 1984. The sea ice topography of M'Clure Strait in winter and summer of 1960 from submarine profiles. Arctic 110–120.

Melling, H., Riedel, D.A., 1996. Development of seasonal pack ice in the Beaufort Sea during the winter of 1991-1992: a view from below. J. Geophys. Res. 101 (C5), 11975–11991.

Parmerter, R.R., Coon, M.D., 1972. Model of pressure ridge formation in sea ice. J. Geophys. Res. 77 (33), 6565–6575.

Proshutinsky, Andrey, et al., 2009. Beaufort Gyre freshwater reservoir: state and variability from observations. J. Geophys. Res.: Oceans 114, C1.

Samardžija, I., Høyland, K.V., Leira, B.J., Næss, A., 2018. Probabilistic assessment of ice environment and ridge loads for the norströmsgrund lighthouse. In: Proc. 24rd IAHR Symposium on Ice, Vladivostok, Russia.

Timco, G., Sayed, M., 1986. Model tests of the ridge-building process in ice. In: Proc. 8th IAHR Symposium on Ice, Iowa City, Iowa.

Tuhkuri, J., Lensu, M., 2002. Laboratory tests on ridging and rafting of ice sheets. J. Geophys. Res. 107 (C9), 8, 1.

Wadhams, P., Horne, R.J., 1980. An analysis of ice profiles obtained by submarine sonar in the Beaufort Sea. J. Glaciol. 25 (93), 401–424.

Williams, E., Swithinbank, C., R, G. De Q., 1975. A submarine sonar study of arctic pack ice. J. Glaciol. 15 (73), 349–362.

Xie, J., Bertino, L., Knut, L., Sakov, P., 2017. Quality assessment of the TOPAZ4 reanalysis in the Arctic over the period 1991-2013. Ocean Sci. 13 (1), 123–144.

A.4 Paper 4

Paper 4:

Samardžija, I., Høyland, K. V., Leira, B. J., & Næss, A. (2023a). Consolidated layer thickness in probabilistic simulation of first-year ice ridges. *Cold Regions Science and Technology*. https://doi.org/10.1016/j.coldregions.2023.104021

Cold Regions Science and Technology 216 (2023) 104021

Contents lists available at ScienceDirect

Cold Regions Science and Technology

journal homepage: www.elsevier.com/locate/coldregions

Consolidated layer thickness in probabilistic simulation of first-year ice ridges

Ilija Samardžija [a,*], Knut V. Høyland [a], Bernt J. Leira [b], Arvid Naess [c]

[a] Department of Civil and Environmental Engineering, Norwegian University of Science and Technology, Trondheim, Norway
[b] Department of Marine Technology, Norwegian University of Science and Technology, Trondheim, Norway
[c] Department of Mathematical Sciences, Norwegian University of Science and Technology, Trondheim, Norway

ARTICLE INFO

Keywords:
Consolidated ice ridge layer
Ice ridge load
Probabilistic design

ABSTRACT

This research study focuses on resolving the issue of sparse data and information required for the probabilistic assessment of ice ridge loads in offshore structures in Arctic regions. The study introduces the consolidated layer thickness into the simulation of ice ridge loads. Through the analysis of seasonal development of level ice draft, ridge keel draft, and ridge frequency, conclusions were drawn on the timing of ridge creation. The data used for this analysis was obtained from ice profiling sonars located in the Beaufort Sea. An analytical approach was established to estimate the probability density function of ridge formation timing, which was then used to simulate ridge age, determine an analytical formulation for consolidated layer growth, and investigate its thickness properties. The study found a negative correlation between consolidated layer thickness and ridge keel draft, which contradicts the previously held assumption in the literature that these variables are not related. This research establishes a framework for probabilistic simulation of ice ridge systems characterized by certain parameters, such as ridge keel draft, level ice draft, ridge frequency, and consolidated layer thickness, which facilitates maintaining the correlations between the parameters in the simulation.

1. Introduction

When designing structures in waters with sea ice but no icebergs, or in waters where icebergs can be managed, the primary concern is how to withstand the extreme loads caused by sea ice ridges. Internal ice pressure, caused by sea currents and, more importantly, wind, can break the level ice surface and push the individual ice floes together, creating pressure ridges or inducing the floes to slide past each other, forming shear ridges. Initially, a ridge comprises loosely packed ice pieces. During the remaining part of the winter season, the layer in the vicinity of the water surface consolidates, as the water between the ice blocks freezes. This solid part of the ice is called the consolidated layer. The ridge keel is composed of a consolidated layer and the loose rubble below it, while the part above the consolidated layer is referred to as the sail.

Ridge loads are calculated conventionally by separating the total load into individual components belonging to the individual parts of the ridge (sail, consolidated layer, keel rubble). The sail component is often neglected, as it is considered not to contribute significantly to the total load. The load component contributed by the consolidated layer is calculated by estimating the force required for breaking of the solid ice, for which the main parameters are the thickness and mechanical properties of the consolidated layer. The rubble component is often calculated using the mathematical formulation of the passive failure mode of granular materials that is common in soil modeling. Here, the rubble thickness (ridge keel draft reduced by the thickness of the consolidated layer) and the mechanical properties, such as apparent rubble cohesion and the angle of internal friction, are of interest.

Ridge loads can be estimated using deterministic or probabilistic approaches. A deterministic approach requires estimates of the input parameters for use in the load formulation. It is unclear which type of combination of return periods should be applied for individual parameters when this approach is used. Often, the only viable option is to use extreme input values for the main parameters (e.g. 100-year consolidated thickness and 100-year ridge keel draft). This approach regularly overestimates the load and, as a rule, a fully probabilistic approach predicts less conservative magnitudes for the loads (Løset et al., 2006, p. 116).

A probabilistic approach is based on characterisation of the input parameters employing probability density functions (PDFs). The Monte

* Corresponding author.
E-mail address: ilija.samardzija@ntnu.no (I. Samardžija).

https://doi.org/10.1016/j.coldregions.2023.104021
Received 4 March 2023; Received in revised form 15 August 2023; Accepted 18 September 2023
Available online 19 September 2023

Carlo simulation technique is conventionally applied for simulation of ridge loads. However, the disadvantage of using a probabilistic approach is that the data required for establishing the input PDFs are sparse and, in certain geographical locations, even completely non-existent. Further, the input parameters are typically correlated to some extent, but the correlations are still not fully understood.

An important correlation is that between the level ice thickness (or draft) and the ridge keel draft. Positive correlation between these two parameters is well recognised and, to some extent, quantified (Amundrud et al., 2004; Hopkins, 1998; Parmerter and Coon, 1972; Timco and Sayed, 1986). In our previous study, this relationship is quantified in a manner optimised for use in probabilistic simulation of ridge loads, and we proposed a framework for the simulation (Samardžija and Høyland, 2023). Here, we present a continuation of the study.

Data on consolidated layer thickness is scarce due to costly and challenging field measurements. Current data is limited to specific locations, usually measured at the end of the season, and likely biased towards older and larger ridges. This paper aims to develop a method to add consolidated layer thickness as output in the probabilistic simulation framework of ice ridges established in Samardžija and Høyland (2023) in a predominantly first-year environment, assuming that winter consolidation dominates (Leppäranta et al., 1995; Høyland, 2002). The primary objective of this study was to investigate the potential correlation between consolidated layer thickness and ridge keel draft, as these two parameters have hitherto been considered independent of one another. (ISO 19906, 2019, p. 217; Løset et al., 2006, p. 115: Timco and Burden, 1997).

Our investigation focused only on FY ice ridges, as the physical description and mathematical formulation of the consolidation of old ridges are more complicated compared with those for FY ice ridges. The reason for this is that the processes during the decay phase when a FY ridge transforms into a second-year ridge are still not fully understood (Shestov et al., 2018; Shestov and Marchenko, 2016).

2. Data

The analysis presented in this paper is based on ice draft data obtained using ice-profiling sonars during the period of 2003–2017. The sonars were deployed on bottom-tethered moorings beneath the Arctic ice pack in the Beaufort Sea. The moorings were recovered and data retrieved annually during Joint Ocean Ice Study cruises between July and October. The moorings were anchored in water deeper than 3500 m, and the sonars were positioned in the top flotation sphere between 20 and 85 m beneath the ice cover, depending on the mooring length and deployment depth. The locations of the moorings are approximately 75°N, 150°W; 78°N, 150°W; 76°N, 140°W; 74°N, 140°W. The data was collected as part of the Beaufort Gyre Exploration Project (Proshutinsky et al., 2010). The IPS has a beam width of 1.8°, which allows for the measurement with a 2-m footprint at a nominal depth of 50 m beneath the bottom surface of ice. The accuracy of each draft measurement obtained using this method is approximately ±10 cm, as stated in a study by Proshutinsky et al. (2010).

The study in this paper examines previously reported variables and correlations from Samardžija and Høyland (2023) instead of conducting an analysis on the raw sonar data. The previous study evaluated statistical quantities and seasonality for level ice draft, ridge keel draft, and ridge occurrence frequency. Please note that in Samardžija and Høyland (2023) sea ice in some seasons compromise of both first-year and multi-year ice. In this paper, we have analysed only the subset of data that was characterized by first-year ice. These were the winter seasons with preceding ice-free summer seasons and where no distinct modes with values higher than first-year level ice draft were present. These high modes are typically seen when multi-year ice is present in a significant amount.

In addition to the ice draft data from ice-profiling sonars, this paper also utilizes level ice thickness data obtained from papers by Ronkainen et al. (2018), Saloranta (2000), Samardžija and Høyland (2023), Johnston and Timco (2004) and Melling (2002).

3. Methods

We studied seasonal level ice growth and ridge keel statistics (draft and count). Our analysis revealed ridge formation processes. In the first subsection, we introduced the ridging likelihood function, which calculates ridge formation timing. Using the ridge formation time, we calculated the ridge age. In section two, we present a Monte Carlo simulation of ridge systems, including parameters such as level ice thickness, ridge keel draft, ridge frequency, and consolidated layer thickness.

3.1. Analytical derivation of the ridging likelihood function

Our analysis focused on the ice growth period, typically from October to June, and excluded the melting season as it was assumed that ridge formation was not significant during that time. Analytical functions were established for the seasonal development of level ice thickness, mean ridge keel draft, and weekly number of ridges. The analytical function for level ice is based on curve fitting to measured data. The functions for the mean ridge keel draft and weekly number of ridges are analytically derived using the level ice thickness function and correlations of these two variables with the level ice thickness. All functions are given with respect to the normalised season time, where $\widetilde{t} = 0$ is the start of the ice growth season and $\widetilde{t} = 1$ is the end (i.e. start of the ice melt season). We first established a function for the level ice thickness and, subsequently, using correlations from Samardžija and Høyland (2023), we established functions for the mean ridge keel draft and ridge number. Finally, these functions were employed to derive the ridging likelihood function.

The normalised level ice thickness as a function of normalised season time is described by:

$$\widetilde{h}_i = \widetilde{t}^{(1-i)}, \tag{1}$$

where $\widetilde{h}_i$ is the normalised level ice thickness averaged over seasons and $\widetilde{t}$ is the normalised season time. The level ice thickness is normalised against the maximum thickness attained during each season. This expression describes the typical shape of seasonal level ice growth and captures the constant ice growth rate early in the season, as well as the typical decrease of the ice growth rate towards the end of the season. The expression is based on several data sources for level ice growth and is illustrated in Fig. 1. Note that data from Samardžija and Høyland (2023) is representing only one season and not a mean of all season regarded in the paper.

Curve modelled using Eq. (1) does not provide an adequate fit for all locations, with the most significant difference observed for the pack ice data from the Baltic Sea (yellow stars in Fig. 1). This dataset presents a line representing the daily level ice thickness averaged over 14 seasons for the period 2003–2016. The daily level ice thickness data were gathered based on ice chart information. Pack ice usually comprises multiple-level ice thickness classes produced by lead opening and refreezing events. This could mean that the level ice thickness detected in pack ice is equal to or smaller than the thickest (and oldest) ice class that has been growing since the beginning of the season. However, this may not be the case for landfast ice. Landfast ice comprises only one ice thickness class that can be considered the upper limit of the thickness classes in the nearby pack ice. This factor could explain why the curve that describes the average pack ice growth is lying below the curves that describe the landfast ice growth. When detecting level ice thickness in pack ice, thinner thickness classes (created in refreezing events) are detected occasionally. Data points representing such occurrences could cause the lowering of the averaged level ice thickness curve in

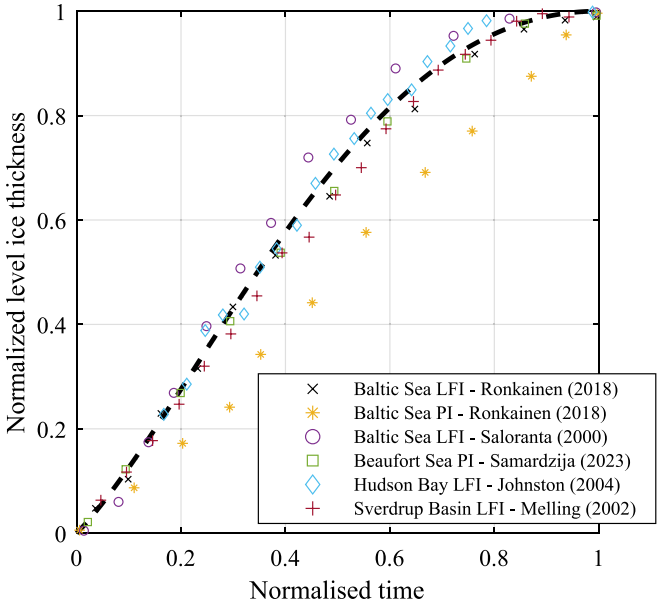

Fig. 1. Comparison of the normalised level ice thickness curve given by Eq. (1) – $h_i = t^{(1-t)}$ (dashed line) with examples of measured level ice growth for various locations (PI is pack ice and LFI is landfast ice).

comparison with the nearby landfast ice. There may be other factor that contribute to the discrepancy observed in the pack ice data from the Baltic Sea that we are not aware of. Irrespective of whether our hypothesis for this phenomenon is correct, this observation indicates the importance of using the highest mode of the level ice thickness (representing the ice growing from the start of the season) for the model presented in this paper in order to mirror the same level ice thickness that was considered in Samardžija and Høyland (2023).

Fig. 1 shows the level ice growth curve for the pack ice from the Beaufort Sea (green squares). This dataset was obtained from Samardžija and Høyland (2023). The authors identified the level ice thickness using upward-looking sonar (ULS) data. As shown, this curve does not have a linear shape in contrast with that for the pack ice from the Baltic Sea. This may be due to the fact that Samardžija and Høyland (2023) reported the deepest level ice draft as the representative value for each week, which was the draft class that had grown from the beginning of the season. This selection process could have produced values that were comparable to those of landfast ice. For a certain year, normalised level ice thickness is transferred into the level ice thickness function by multiplying Eq. (1) by the maximum level ice thickness of that year $h_{i,AM}$. In our analytical analysis, we used $h_{i,AM} = 1,8\ m$ for explanatory purpose. This value is reflecting a typical season in the Beaufort Sea. When performing simulation for a specific location, level ice thickness data can be used. In absence of such data, level ice thickness can be estimated using the empirical Zubov (1943) expression as suggested in Li et al. (2016).

$$h_i = \widetilde{h}_i \cdot h_{i,AM}. \tag{2}$$

Samardžija and Høyland (2023) reported a linear relationship between the level ice draft and mean keel draft that is described in terms of an intercept of 6.03 and slope of 0.51. Using this relation, the level thickness growth curve can be transformed to a curve that describes the seasonal development of the mean ridge keel draft, as illustrated in Fig. 2(b), and the linear function is expressed as:

$$\overline{D} = a_2 + b_2 \cdot \frac{\rho_i}{\rho_w} \cdot h_i, \tag{3}$$

where a_2 and b_2 are the intercept and slope, respectively, h_i is the level ice thickness,ρ_i and ρ_w are the sea ice and water densities, respectively.

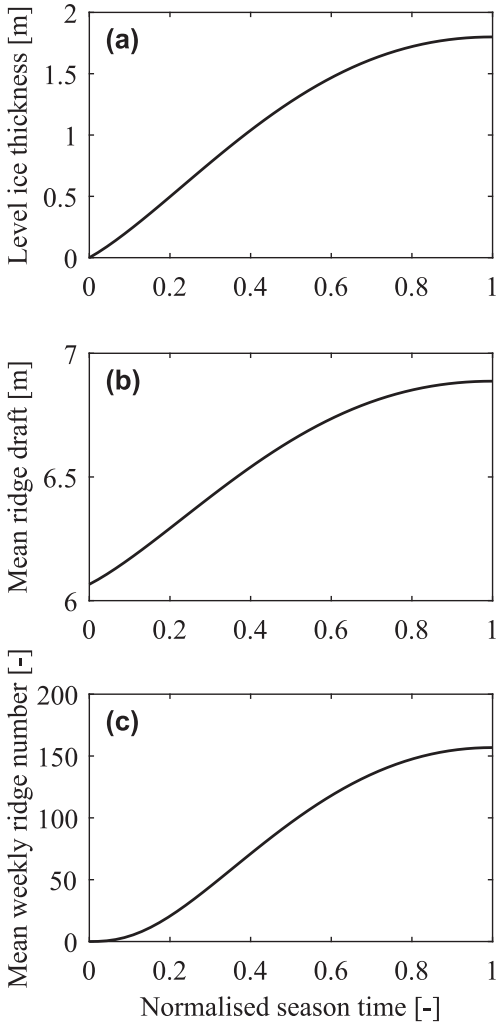

Fig. 2. (a) Seasonal development of the level ice thickness based on data fitting to measured values, described by Eq. (2). (b) Seasonal development of the mean ridge draft derived as a linear transformation from the level ice thickness curve, described by Eq. (3). (c) Seasonal development of the weekly mean number of ridges derived as a non-linear transformation from the level ice thickness curve, described by Eq. (5).

We used $\rho_i = 917\ \frac{kg}{m^3}$ and $\rho_w = 1025\ \frac{kg}{m^3}$. The ratio of ice and water densities was introduced for transforming from level ice thickness to level ice draft based on isostatic equilibrium. We did not consider the effect of snow on isostatic equilibrium in our analysis due to the lack of accurate snow thickness information. Including it would likely have a small impact on level ice thickness accuracy.

A transformation can also be constructed from level ice thickness to the weekly number of ridges. This number describes how many ridges (deeper than 5 m) pass the location of interest during a single week. The transformation is made based on the relationship reported in Samardžija and Høyland (2023). The correlation is described in terms of a power function. The weekly number of ridges is expressed as:

$$N = a_3 \cdot \left(\frac{\rho_i}{\rho_w} \cdot h_i\right)^{b_3}, \tag{4}$$

where $a_3 = 84.69$ and $b_3 = 1.318$. When the correlation was analysed and quantified in Samardžija and Høyland (2023), data points (i.e. weeks) with less than 15 ridges were not considered, which occurred more often in the early part of the season when the ridge field had not developed yet. In Samardžija and Høyland (2023), the probability of

having weeks with less than 15 ridges was quantified as a function of level ice draft (i.e., $p = 100^{1-0.6h_i}$, given in percentage). The function can be used to improve the accuracy of Eq. (4), as is done in Eq. (5), with the result shown in Fig. 2(c). Eq. (4) was multiplied by the probability of having a week with more than 15 ridges.

$$N = a_3 \cdot \left(\frac{\rho_i}{\rho_w} h_i\right)^{b_3} \cdot \left(1 - \frac{100^{1-0.6h_i}}{100}\right). \quad (5)$$

In Fig. 3, these functions were validated with the data points representing individual weeks. The data points originate from Samardžija and Høyland (2023). Note that only seasons with predominantly FYI environment are considered here. The black lines correspond to the analytical functions from Fig. 2. The red lines represent a moving average over a sliding window of 50 data points. As shown, the chosen functions (Eq. (1) and Eq. (2)) for describing the level ice growth are a good fit for the data. A discrepancy seen early in the season could be ascribed to many points that had to be removed in this part. The points in question refer to data points that were associated with relatively low values of level ice thickness. If these points were included in the analysis, they would be mostly located below the analytical curve due to their low values. Another potential explanation for the discrepancy is the presence of old ice from previous seasons. Despite our analysis being limited to seasons with preceding ice-free summers, it is most likely that some old ice may have drifted to the location and contributed to the discrepancy discussed.

In the remaining part of this subsection, the above established functions are used to derive the PDF for the timing of ridge formation. It was observed that for the data used, the average length of the portion of the season from the start to the peak in level ice growth was approximately 35 weeks. By computing the time derivative and knowing the duration of the ice growth part of the season, the weekly ridge production rate could be estimated (Fig. 4).

Fig. 2(b) describes the mean ridge keel draft of the ridges present in the ice field at the given time in the season. However, this is different from the mean ridge keel draft of the created ridges at the given time in the season. During a single week, a certain number of ridges are created, and the mean keel draft increases. As the number of new ridges is usually small in comparison with the number of ridges already present, the mean keel draft of the newly created ridges must be higher compared with the already present ridges. Negative exponential distribution is well suited for describing the distribution of ridge keel draft (Ekeberg et al., 2013; McLaren et al., 1984; Wadhams and Horne, 1980). We assumed that the distribution of newly created ridges also followed this type. The following expression facilitates deriving the mean ridge keel draft of the created ridges during a given week:

$$D_n = pD_c + (1-p)D_{n-1}. \quad (6)$$

The expression was taken from Everitt (2014), and it describes the mean of an exponential distribution comprising a mixture of two exponential distributions with weights p and $1-p$. In our context, D_n is the mean ridge keel draft for a certain week in a season, D_{n-1} is the mean ridge keel draft of the preceding week, and D_c is the mean ridge keel draft of the created ridges during the present week. Weeks are indexed by $n = 0,1,2\cdots n_s$, where n_s is the number of weeks during the ice growth part of the season (35 in this case). $D_0 = 0$ is the week preceding the first week with ridges detected. The parameter p is defined as:

$$p = \frac{N_c}{N_{n-1}}, \quad (7)$$

where N_c is the number of ridges created in a given week (Fig. 4) and N_{n-1} is the accumulated number of ridges up to the end of the preceding week (Fig. 2(c)). By rearranging Eq. (6), we obtained an expression for the mean ridge keel draft of the created ridges (Eq. (8)). The resulting seasonal development of the mean ridge keel draft of the created ridges is illustrated in Fig. 5.

$$D_c = \frac{D_n - (1-p)D_{n-1}}{p}. \quad (8)$$

We simulated the age of a ridge with a given keel draft and arrival time. The probability for formation of a ridge (ridging) with a draft $D_0 \pm \Delta D$ at any point in a season can be calculated by:

$$P(\tilde{t}) = \int_{\overline{D}_0-\Delta D}^{\overline{D}_0+\Delta D} \lambda(\tilde{t}) e^{-\lambda(\tilde{t})x} dx = \lambda(\tilde{t}) \bullet e^{-\lambda(\tilde{t})\overline{D}_0} \bullet e^{\lambda(\tilde{t})\Delta D} \bullet \left(1 - e^{-1}\right), \quad (9)$$

where $\lambda(\tilde{t})$ is an "intensity" parameter that describes the negative exponential distribution of created ridges throughout a season and is

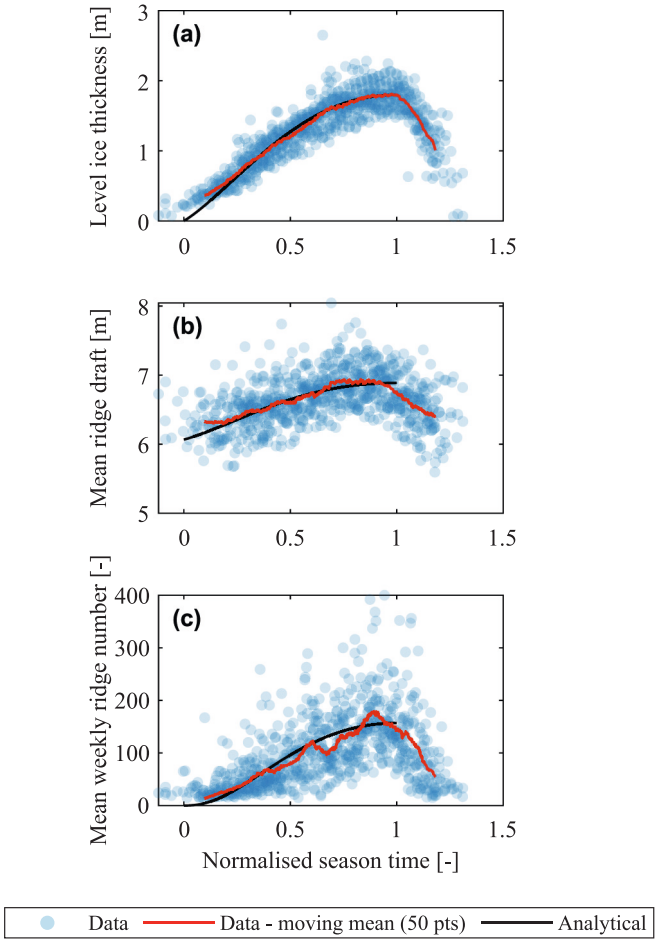

Fig. 3. Comparison of the analytical functions (black lines) presented in Fig. 2 with the measured data. Each point represents one week of measurement.

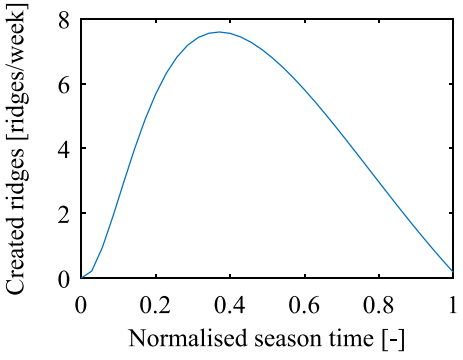

Fig. 4. Seasonal development of the weekly ridge creation rate, calculated as a time derivative from the seasonal variation of the mean weekly ridge number.

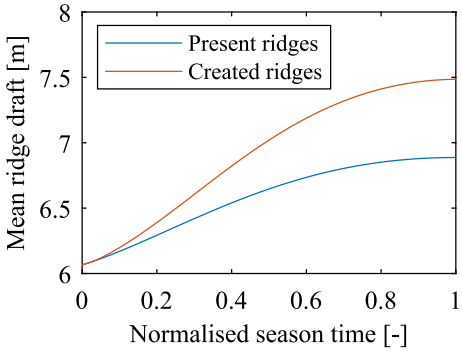

Fig. 5. Comparison of the seasonal development of the mean ridge keel draft of ridges present in the ice field and the newly created ridges for one week.

given as: $\lambda(\tilde{t}) = \frac{1}{D_c(\tilde{t})-5}$. Subtraction by 5 in the denominator is because the negative exponential distribution is shifted by 5 units relative to the origin (dictated by the Rayleigh criterion threshold parameter). Note that the subtraction is done for parameter $\overline{D}_0 = D_0 - 5$. This function has a certain maximum during a season $P(\tilde{t})_{max}$. By dividing Eq. (9) with $P(\tilde{t})_{max}$ the normalised probability function of ridging is obtained:

$$P_n(\tilde{t}) = \frac{P(\tilde{t})}{P(\tilde{t})_{max}} = \frac{\lambda(\tilde{t}) \bullet e^{-\lambda(\tilde{t})\overline{D}_0} \bullet e^{\lambda(\tilde{t})\Delta D} \bullet (1 - e^{-1})}{\left[\lambda(\tilde{t}) \bullet e^{-\lambda(\tilde{t})\overline{D}_0} \bullet e^{\lambda(\tilde{t})\Delta D} \bullet (1 - e^{-1})\right]_{max}}. \tag{10}$$

If ΔD becomes infinitesimally small, the normalised likelihood function of ridging is obtained:

$$P_n(\tilde{t}) = \lim_{\Delta D \to 0} \frac{\lambda(\tilde{t}) e^{-\lambda(\tilde{t})\overline{D}_0} \bullet e^{\lambda(\tilde{t})\Delta D}(1 - e^{-1})}{\left[\lambda(\tilde{t}) e^{-\lambda(\tilde{t})\overline{D}_0} \bullet e^{\lambda(\tilde{t})\Delta D}(1 - e^{-1})\right]_{max}} = \frac{\lambda(\tilde{t}) \bullet e^{-\lambda(\tilde{t})\overline{D}_0}}{\left[\lambda(\tilde{t}) \bullet e^{-\lambda(\tilde{t})\overline{D}_0}\right]_{max}} \tag{11}$$

With the focus on the numerator in Eq. (11), clearly, it has the form of a negative exponential distribution (i.e. $\lambda e^{-\lambda x}$). This shows that Eq. (11) produces the likelihood of a ridge with draft D_0 to be created at time $\tilde{t}$ divided by the seasonal peak value. We used the term *likelihood* instead of *probability* because, in this function, the parameter describing the distribution $\lambda(\tilde{t})$ varies with time and parameter $\overline{D}_0$ is constant (it is the opposite case for PDFs) (Edwards, 1984). Another difference compared with PDFs is that the likelihood function does not integrate to one.

The ridge creation rate varies throughout a season (Fig. 4). The ridging likelihood increases linearly with an increase in the ridge production rate. This is accounted for by adding the term $dN(\tilde{t})$ in both the numerator and denominator of eq. (11). The relative likelihood function of ridging is then defined as:

$$P_r(\tilde{t}) = \frac{P(\tilde{t})dN(\tilde{t})}{\left[P(\tilde{t})dN(\tilde{t})\right]_{max}} = \frac{\lambda(\tilde{t}) \bullet e^{-\lambda(\tilde{t})\overline{D}_0} \bullet dN(\tilde{t})}{\left[\lambda(\tilde{t}) \bullet e^{-\lambda(\tilde{t})\overline{D}_0} \bullet dN(\tilde{t})\right]_{max}} \tag{12}$$

Fig. 6 illustrates the relative ridging likelihood for five ridges arriving at time $t_a = 1$, with drafts $D_0 = 5m, 8m, 12m, 20m, 30m$. The likelihood for the creation of shallow ridges is higher early in the season, whereas, for deeper ridges, it is higher towards the end of the season. This is expected, as thin level ice is less likely to produce deep ridges. The positive correlation between level ice thickness and ridge keel draft has been previously established by Samardžija and Høyland (2023). As demonstrated in the current paper, it can also be observed that the mean ridge keel draft of produced ridges increases over the course of a season, as illustrated in Fig. 5. Accordingly, there is a positive correlation between level ice thickness and mean ridge keel draft of created ridges. Please note that we are not pointing to a causal relationship between level ice thickness and ridge draft, but rather to the presence of a positive correlation between the two variables.

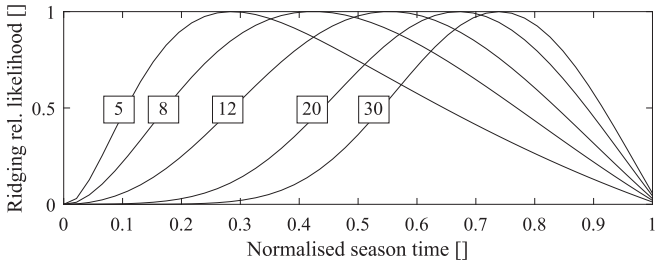

Fig. 6. Relative ridging likelihood functions for five ridges that arrive to a structure at time $t_a = 1$ (peak of the ice growth). Ridge drafts are indicated by the numbers in the squares. The plot demonstrates a pattern where ridges with shallower keels at season's end are more likely to have originated from the early parts of the season, while ridges with deeper keels are more probable to have developed during the latter segments of the season.

In the next subsection we show how this function can be used to construct probabilistic simulation of ridging timing, ridge age, and consolidated layer thickness.

3.2. Probabilistic simulation of ridge systems

A ridge system can be characterized by the number of ridges (ridge frequency) and mean ridge keel draft (Hibler et al., 1972). In Samardžija and Høyland (2023), a probabilistic framework is described for simulating such ridge systems using a Monte Carlo technique. The input data for the simulation are level ice draft or thickness. Here, we describe how consolidated layer thickness can be added to the simulation. Further, in the previous study (Samardžija and Høyland, 2023), we used measured data for the input level ice thickness and here we demonstrate how this input can be simulated.

In order to simulate level ice thickness, we aimed to replicate the data presented in Fig. 3(a). To achieve this, both interannual and seasonal variability were taken into consideration. Interannual variability was simulated by generating an annual maximum level ice thickness from a normal distribution with a mean of 1.8 m and a standard deviation of 0.2 m. The number of weeks during a single season was also considered as a random variable, with a positive correlation to the annual maximum level ice thickness (correlation coefficient of 0.55). A uniform distribution with limits of 31 and 39 was used to simulate the number of weeks during a single season. A copula was utilized to simulate the two dependent variables. Seasonal variability was simulated using the standardised level ice growth curve given by Eq. (2), however, in reality, the level ice does not strictly follow this smooth curve. To account for this, a small, normally distributed random noise was added to each data point, with a mean of zero and a standard deviation of 5% of the given weekly level ice thickness value. Additionally, a certain number of weeks were excluded in proportion to the number of weeks when the number of ridges was virtually zero, as proposed in Samardžija and Høyland (2023) with empirical expression for the probability of having a week without ridges as a function of level ice thickness ($p = 100^{1-0.6h_i}$, expressed in percentage).

For direct comparison of the simulation results with the measured data, we conducted a simulation for 19 seasons and a comparison with the 19 measured season locations (Fig. 7). As shown, there are discrepancies in the early phase of ice growth. The measured data show that the ice growth started somewhat earlier in comparison with the simulated data. One possible explanation for the observed discrepancy may be attributed to the lack of congruence between the fitted ice growth curve and the measured data as depicted in Fig. 3(a). An alternate explanation could be the presence of residual ice that has persisted through the preceding melt season. The simulated data matches the measured data well in the later part of the season. To further analyse the performance of the simulated level ice thickness distribution, we conducted a simulation with 10,000 seasons. The mode of the distribution,

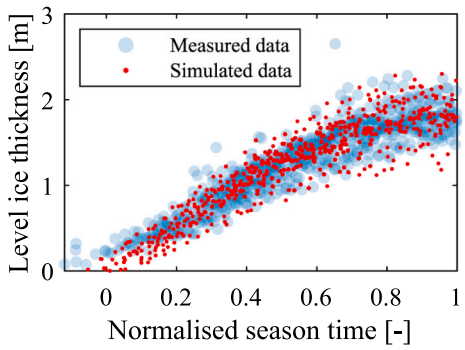

Fig. 7. Comparison of measured and simulated weekly level ice thickness.

corresponding to the ice thickness class of 1.50–1.75, indicates a point of diminishing ice growth and a resultant stabilization at a relatively consistent value over an extended period. The comparison between the simulated and measured data is shown in Fig. 8. The simulation replicated the measured data well, with an exception being the thinnest level ice class. In the histogram, the first bin (0–0.25 m) of the simulated data showed higher probability than the measured data. This is most probably because about 66% of the measured data points were removed for the points with level ice thickness class 0–0.25 m. We deemed further efforts to improve agreement for this ice class unnecessary, as the class is not important in simulating ridge loads.

The next step was simulating the weekly number of ridges and the weekly mean keel draft, which was done using the established procedure in Samardžija and Høyland (2023). For a given level ice thickness h_i, the weekly mean keel draft can be simulated by:

$$\overline{D}_i = a_2 + b_2 \cdot \frac{\rho_i}{\rho_w} \cdot h_i \cdot \overline{R}_i, \tag{13}$$

where index i indicates the individual i-th point (week), $a_2 = 6.03$ and $b_2 = 0.51$ are the intercept and the slope of the linear regression stemming from the analysis of the relationship between the two parameters. $\overline{R}_i$ is a random number sampled from the normal distribution, with a mean value of 1.00 and standard deviation of 0.00471. Using the previously simulated level ice thickness as input (Fig. 8), the weekly mean ridge keel draft was simulated. The results of the simulation are presented in Fig. 9(a).

For a given level ice thickness h_i, the weekly number of ridges could be simulated by:

$$N_i = a_3 \cdot \left(\frac{\rho_i}{\rho_w} h_i \right)^{b_3} \cdot R_{N,i}, \tag{14}$$

where $a_3 = 84.69$ and $b_3 = 1.318$ are coefficients stemming from the analysis of the relationship between the two parameters. $R_{N,i}$ is a random number sampled from the gamma distribution, with scale parameter 0.2832 and shape parameter 3.5251. The simulated weekly number of ridges versus the level ice thickness are illustrated in Fig. 9(b).

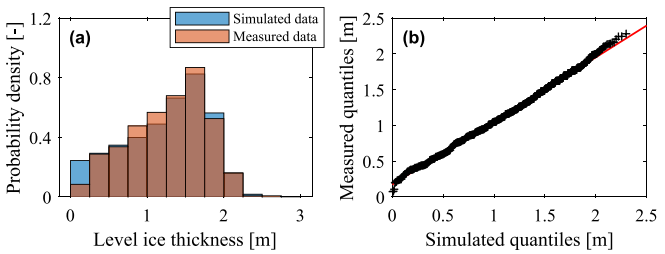

Fig. 8. Comparison of measured versus simulated weekly level ice thickness across 10,000 simulated seasons, depicted via a histogram (a) and a Quantile-Quantile (Q-Q) plot (b).

The individual ridges for all weeks could be simulated with the weekly mean ridge keel draft and number of ridges. For each week, N_i number of ridges was simulated according to a negative exponential distribution with mean parameter $\overline{D}_i$. The distribution of the simulated ridge keel drafts is illustrated in Fig. 10 by means of a probability exceedance plot. For the simulated 10,000 seasons there was a total of 30,375,508 ridges. This amounted to 3737 ridges per season. Note that the drafts are not comparable to the drafts in the Beaufort Sea and are somewhat shallower than the drafts presented in Samardžija and Høyland (2023) because only the ridges formed in predominantly FYI environments were considered in this paper.

In the remaining part of this subsection, we present a procedure for simulating the consolidated layer thickness. The inputs required for simulation of each individual ridge are ridge arrival time t_a and ridge keel draft D_0. For any ridge, a relative likelihood function of ridging could be established (Eq. (12); Fig. 6). This function was used to simulate the time of ridging. The technique can be demonstrated by two examples. Ridges in these examples have keel drafts of 20 m and 8 m and arrival times of 1.0 and 0.7, respectively. Inverse transform sampling is a common technique used in Monte Carlo simulation to obtain random numbers (Gentle, 2006). However, the technique requires a cumulative distribution function (CDF) as input. Alternatively, a PDF can be used to compute CDF. A relative likelihood function of ridging can be transformed into a PDF by scaling the function. The scaling is done by solving Eq. (15) with respect to C. In this way, a PDF is obtained as given by Eq. (16), where the integral over the entire domain of definition for the function is equal to 1. The PDFs for the two examples are shown in Fig. 11. In practice, the inverse transform sampling technique can be applied directly on the relative likelihood functions. However, we chose to use PDFs to satisfy mathematical rigour. A ridging PDF can be established for any ridge with a given draft and arrival time. It is unique for each ridge.

$$C \int_{\tilde{t}=0}^{\tilde{t}=1} P_r(\tilde{t})\, d\tilde{t} = 1, \tag{15}$$

$$f_r(\tilde{t}) = C\, P_r(\tilde{t}), \tag{16}$$

Once the ridge creation time t_c is simulated using the ridging PDF, the age of a ridge could be calculated by:

$$t_{ra} = t_a - t_c. \tag{17}$$

The ridge age variable was used to estimate the thickness of the consolidated layer. For illustration, a simplistic consolidated layer growth model was used, assuming that the consolidated layer grew at double the rate of the level ice. Therefore, the same equations as for the level ice (Eq. (1) and Eq. (2)) were used, with ridge creation time as the input variable and the thickness multiplied by two (Eq. (18)).

$$h_c = 2 \cdot {t_{ra}}^{(1-t_{ra})} \cdot h_{i,AM} \tag{18}$$

Multiplication by two is taken as the upper limit of the reported ratio of the consolidated layer and level ice growth rates (Høyland, 2002; Leppäranta and Hakala, 1992; Timco and Goodrich, 1988). A more advanced consolidated layer growth model could be used, but this would not change the main conclusions of our study presented in this paper.

4. Results and discussion

In this section, several aspects of the simulation results are discussed, with a focus on the consolidated layer thickness and correlation to other variables. First, we conducted a comparison of the distributions of the level ice thickness and the consolidated layer thickness (Fig. 12). Note that the distributions represent thicknesses for a given ridge (i.e. thickness of the consolidated layers of ridges that arrive at the location of interest and the corresponding surrounding level ice thickness). This

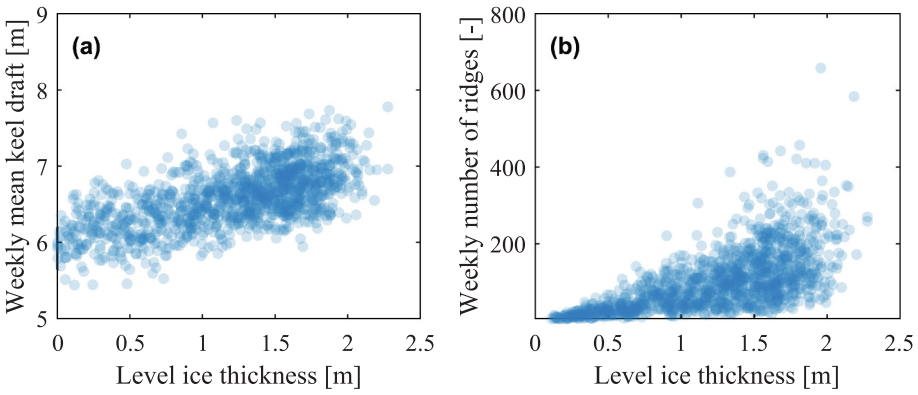

Fig. 9. Simulated weekly mean keel draft (a) and number of ridges (b) with respect to the level ice thickness. The illustration represents a subsample of 40 simulated seasons.

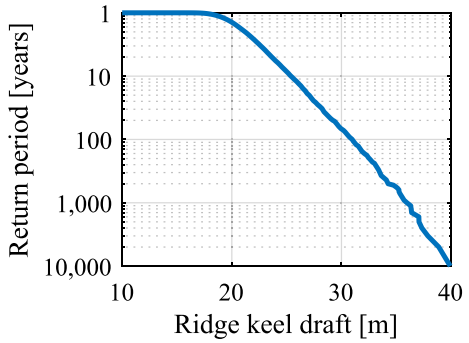

Fig. 10. Plot of exceedance of probability for the simulated ridge keel drafts.

differs from the level ice thickness distribution shown in Fig. 8, where the distribution represents the thickness for a given week. Level ice thickness has a relatively small value of the probability density for the thin ice classes, as more ridges are present in the ice field towards the end of the season when the level ice is thicker. This is not the case for the consolidated layer because more ridges are formed later in the season, therefore, these ridges have a relatively thin consolidated layer.

The correlation between consolidated layer thickness and ridge keel draft was analysed utilizing a bivariate plot as depicted in Fig. 13. The results of the analysis indicated a negative correlation between the two variables, as an increase in consolidated layer thickness corresponded to a decrease in ridge keel draft. The shallow ridges formed earlier in the season have more time to form a consolidated layer, while deep ridges formed later in the season may not have enough time to do so, which could explain the negative correlation. This reasoning is similar to that by Brown et al. (2001), with these authors concluding that there are two "typical" categories of extreme ridges, namely deep keels associated with a relatively thin consolidated layer and shallow keels with a relatively thick consolidated layer.

To better illustrate the possible explanation for the negative correlation between consolidated layer thickness and keel draft, we present two ridges in Fig. 14. Ridge "A" is formed early in the season and has a shallow keel due to the positive correlation between surrounding level ice thickness and mean ridge keel draft of formed ridges. However, by the end of the season, it has a thick consolidated layer due to its early formation. Ridge "B" is formed mid-season and has a deeper keel due to thicker surrounding level ice. But it has a thinner consolidated layer than Ridge "A" because it was formed later and did not have enough time to develop a thicker consolidated layer. It is important to note the following detail here. Averaged over all ridges late in the season the consolidated layer is at its maximum. Also, averaged over all ridges late in the season the keel draft is on its maximum. However, when individual ridges are considered, deeper drafts are associated with thinner consolidated layer.

In Fig. 15 we present the consolidated layer thickness with respect to normalised season time and the surrounding level ice thickness.

The joint variation of consolidated layer thickness and ridge keel draft was further examined using environmental contour lines. This method predicts estimates of extremes with a certain return period and is shown in Fig. 16. The contour lines were constructed using the numerical method by Huseby et al. (2013).

Our assumption that the ridge keel draft remains unchanged post-formation is a significant caveat in this study. Ridge keel draft may alter after its initial formation due to several phenomena.

The first of these is re-ridging, where the keel subsequently increases in depth. Current literature lacks adequate information about this

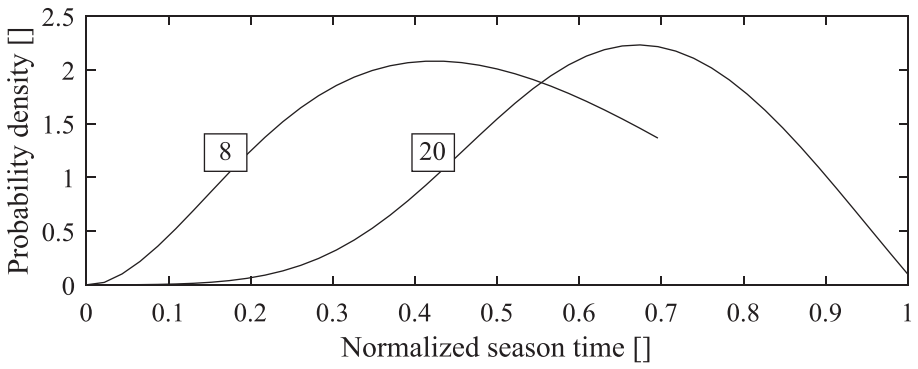

Fig. 11. Probability density functions for creation of ridges with keel drafts of 8 m and 20 m, arriving at normalised season times of 0.7 and 1.0, respectively. These functions serve as a tool to simulate the time of ridge creation on a probabilistic basis.

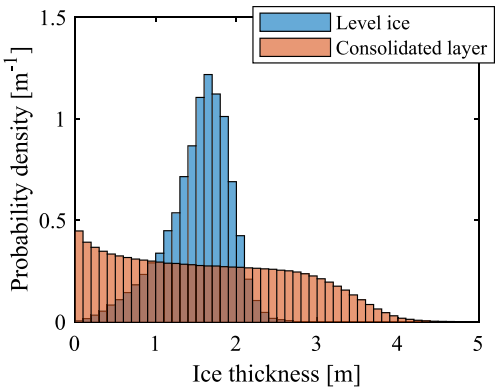

Fig. 12. Distribution of the simulated level ice and consolidated layer thickness.

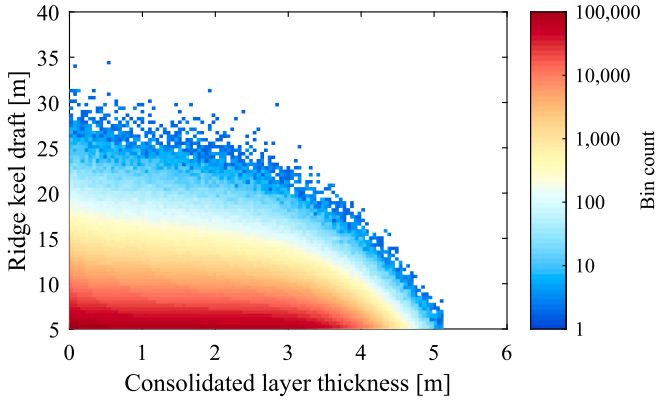

Fig. 13. Bivariate intensity plot illustrating the relationship between consolidated layer thickness. Please note that the ridges considered in this plot encompass all simulated ridges that reach a specified location throughout the entirety of the simulated winter seasons.

process, with uncertainties persisting on the frequency of such events and the degree of depth increase following re-ridging. If frequent, re-ridging could potentially weaken the negative correlation between the consolidated layer thickness and the ridge keel draft. An illustrative life story of a deep ridge could be its initial formation as a shallow ridge at the season's onset, followed by significant consolidated layer development. Towards the end of the season, a re-ridging event could occur, leading to a deeper ridge keel. This possibility could accommodate the existence of deep ridges with a thick consolidated layer.

The second phenomenon is the decrease of the ridge keel draft due to thermal degradation due to oceanic heat flux, rubble packing and mechanical decomposition of the rubble (Ervik et al., 2018; M. Leppäranta et al., 1995. An increased oceanic heat flux could potentially speed up the thermal degradation process, particularly in regions with warmer ocean temperatures or increased ocean warming due to climate change. This phenomenon is better reported in the literature, and it would be reasonable to incorporate it into the simulation. This inclusion would strengthen the negative correlation between the consolidated layer thickness and the ridge keel draft, as a deep ridge arriving late in the season would be even less likely to have formed early in the season. Furthermore, it is worth mentioning that an increased heat flux could affect freeze bonding between ice blocks, potentially reducing the stability of the ice ridges and influencing the ridge loads.

In the light of these complexities and uncertainties, future work should aim at refining our understanding of these phenomena, allowing for improved modeling of ridge keel drafts under different climate scenarios and geographical regions.

To analyse the effect of the decreasing keel during a season, we repeated the simulation with the inclusion of a decreasing keel draft. This was done by substituting a changing keel draft $\overline{D}_0(\tilde{t})$ in Eq. (12) for a constant keel draft $\overline{D}_0$. For example, for a ridge with a keel draft of 20 m that arrived at the normalised season time $\tilde{t} = 1$, we calculated what the keel draft could be at any time during the season. As the ice growing part of the season is roughly eight months, one such ridge should have a draft of 27.2 m ($20m + 0.03\frac{m}{\text{day}} \cdot 240\text{days} = 27.2m$) if it had formed at the beginning of the season and with a keel draft reduction rate of 3 cm/day (this exemplary value is adopted from Ervik et al. (2018)). To improve understanding of the effect of a reducing keel draft on the simulation, we constructed a figure similar to Fig. 6, with the difference being that we considered only one draft and several ridge keel reduction rates (Fig. 17). We found that with an increase in the magnitude of the ridge keel draft reduction rate, the relative probability of ridge formation was more compressed towards the time of ridge arrival. This means that, on average, with this effect included, ridges were younger, and the negative correlation with the consolidated layer thickness was strengthened.

Fig. 18 shows a bivariate histogram of the consolidated layer thickness and the ridge keel draft, where an average ridge keel decrease rate of 3 cm/day was applied in the simulation. We observed a strengthened negative correlation between the two parameters in comparison with the base case simulation shown in Fig. 13. To show the impact on the simulation results, we compared the base case (where the decrease in keel was not considered) with two other cases where the keel decrease was included. This comparison is shown using contour lines in Fig. 19.

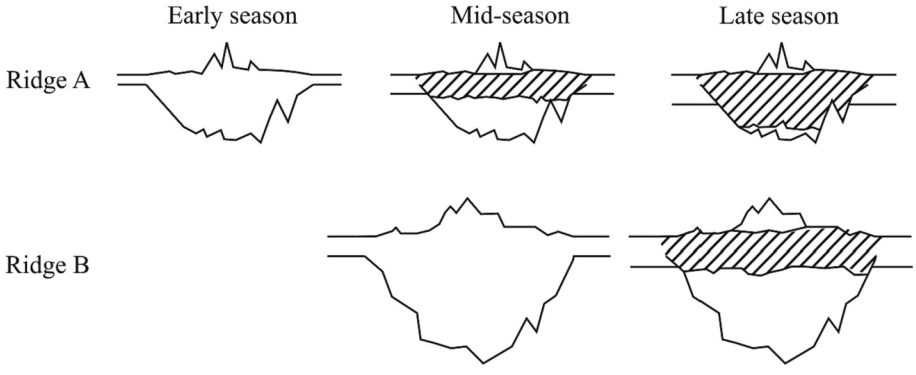

Fig. 14. Comparison of ridges formed at different points in the season: early (Ridge A) versus mid-season (Ridge B). The hatched area signifies the consolidated layer. Ridge A is representative of an older first-year ridge characterized by a substantial consolidated layer and a shallow keel, whereas Ridge B exemplifies a younger first-year ridge with a comparatively thinner consolidated layer and a deeper keel.

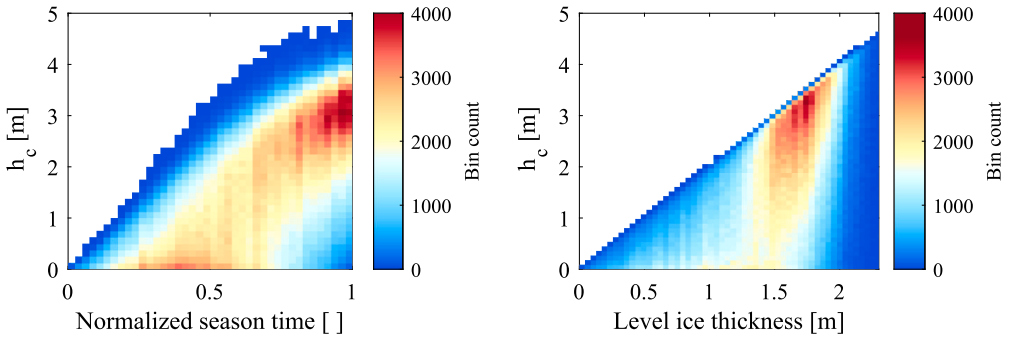

Fig. 15. Comparison of consolidated layer thickness to the normalised season time (left) and the surrounding level ice thickness (right).

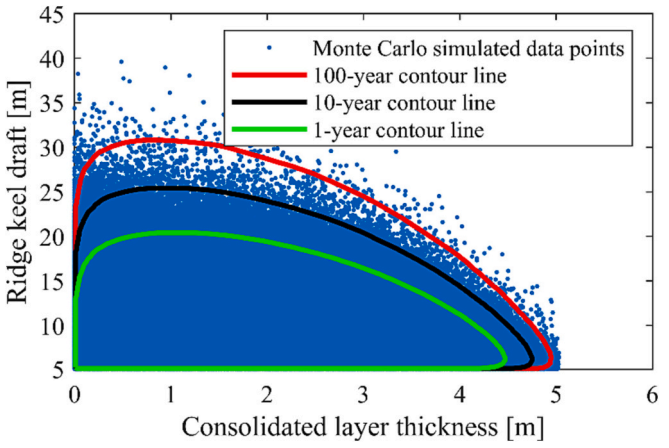

Fig. 16. Environmental contour lines for 1-, 10-, and 100-year return periods. Each point represents a single ridge from the simulation. The contour lines illustrate the likely values of the ridge parameters for each return period.

5. Conclusions

We analysed the consolidated layer thickness based on the observation of ridge formation timing, as inferred from the seasonal development of ridge statistics (i.e. mean ridge keel draft and number of ridges). We proposed a new technique for simulating the consolidated layer thickness based on a Monte Carlo probabilistic simulation. Our results indicated that the consolidated layer thickness and the ridge keel draft were correlated negatively.

In combination with our previous work, we were able to conduct a holistic probabilistic simulation of the key geometrical parameters required for ridge load calculations (level ice thickness, consolidated layer thickness, and ridge keel draft). Further, we addressed the problem of estimating ridge frequency. The main contribution of this study is that the simulation methodology incorporates the crucial relationships between the relevant parameters. The resulting consolidated layer thickness values require further validation. However, large-scale measurements of consolidated layer thickness for such validation are not available. We hope that future novel techniques, such as remote sensing measurements, could produce such datasets. In the meantime, our technique can be validated only partially by employing expert judgement. Our study provides valuable insight into the complexity of ridge parameters that are interconnected in multiple ways and change constantly throughout a season.

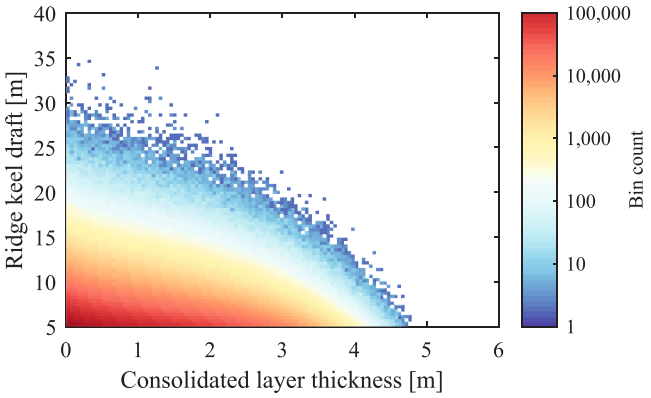

Fig. 18. Level plot of bivariate histogram of the consolidated layer thickness and keel draft for a simulation where a decreasing ridge keel draft rate of 3 cm/day is applied.

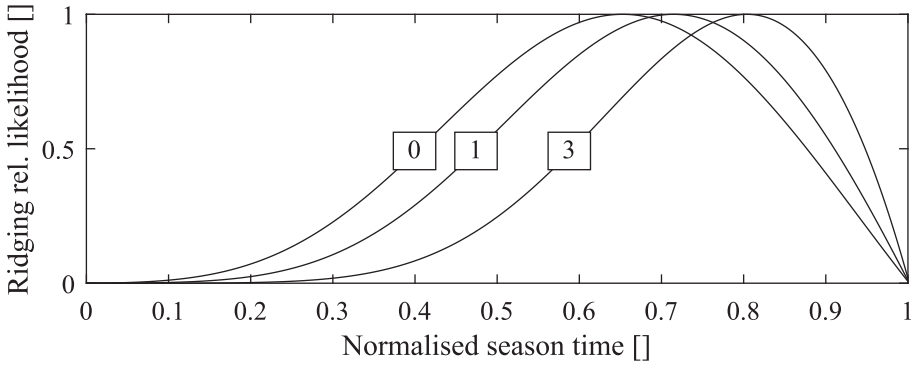

Fig. 17. Ridging relative likelihood functions for a ridge with a draft of 20 m that arrives at time $t_a = 1$ (peak of the ice growth). Each of the three lines has a different ridge keel reduction rate, indicated by the numbers in the squares (0, 1, and 3 cm/day). The different rates could simulate variations in the oceanic heat flux, with higher rates potentially representing higher heat flux conditions.

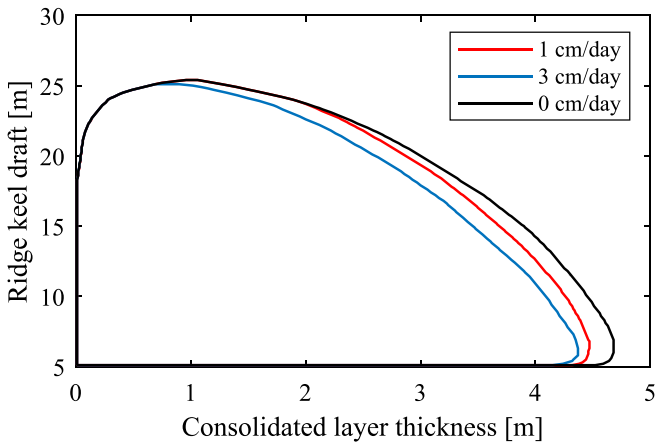

Fig. 19. Environmental contour lines for a 100-year return period and different rates of ridge keel decrease. The decrease rates of ridge keel draft are indicated in the legend. The different rates could simulate variations in the oceanic heat flux, with higher rates potentially representing higher heat flux conditions. Conclusions

CRediT authorship contribution statement

Ilija Samardžija: Conceptualization, Methodology, Software, Formal analysis, Investigation, Data curation, Writing – original draft, Writing – review & editing, Visualization. **Knut V. Høyland:** Methodology, Writing – review & editing, Supervision, Project administration, Funding acquisition, Resources. **Bernt J. Leira:** Supervision, Writing – review & editing. **Arvid Næss:** Supervision, Writing – review & editing.

Declaration of Competing Interest

The authors declare that they have no known competing financial interests or personal relationships that could have appeared to influence the work reported in this paper.

Data availability

https://www2.whoi.edu/site/beaufortgyre/data/mooring-data/

Acknowledgements

The data were collected and made available by the Beaufort Gyre Exploration Program based at the Woods Hole Oceanographic Institution (http://www.whoi.edu/beaufortgyre) in collaboration with researchers from Fisheries and Oceans Canada at the Institute of Ocean Sciences. The authors wish to acknowledge the support of the Research Council of Norway through the Centre of Research-based Innovation, SAMCoT, and the support of the SAMCoT partners. This work was conducted under the NTNU Oceans Pilot project *Risk, Reliability and Ice Data in Arctic Marine Environment*. This work has been supported by the NFR sponsored project 326834: *Risk of sea ice and icebergs for field development in the Southwestern Barents Sea (RareIce)*.

References

Amundrud, T.L., Melling, H., Ingram, R.G., 2004. Geometrical constraints on the evolution of ridged sea ice. J. Geophys. Res. 109 (C6) https://doi.org/10.1029/2003JC002251, 12 pp.

Brown, T.G., Jordaan, I.J., Croasdale, K.R., 2001. A probabilistic approach to analysis of ice loads for the Confederation Bridge. Can. J. Civ. Eng. 28 (4), 562–573. https://doi.org/10.1139/cjce-28-4-562.

Edwards, A.W.F., 1984. *Likelihood*: CUP Archive.

Ekeberg, O.-C., Hoyland, K., Hansen, E., 2013. Extreme keel drafts in the Fram Strait 2006-2011. In: Proc. 22nd International Conference on Port and Ocean Engineering under Arctic Conditions, POAC 2013, Espoo, Finland.

Ervik, Å., Høyland, K.V., Shestov, A., Nord, T.S., 2018. On the decay of first-year ice ridges: Measurements and evolution of rubble macroporosity, ridge drilling resistance and consolidated layer strength. Cold Reg. Sci. Technol. 151, 196–207. https://doi.org/10.1016/j.coldregions.2018.03.024.

Everitt, B.S., 2014. Finite mixture distributions. In: Wiley StatsRef: Statistics Reference Online.

Gentle, J.E., 2006. Random Number Generation and Monte Carlo Methods. Springer Science & Business Media.

Hibler, Weeks, W.F., Mock, S.J., 1972. Statistical aspects of sea-ice ridge distributions. J. Geophys. Res. 77 (30), 5954–5970. https://doi.org/10.1029/JC077i030p05954.

Hopkins, M.A., 1998. Four stages of pressure ridging. J. Geophys. Res. 103 (C10), 21883–21891. https://doi.org/10.1029/98JC01257.

Høyland, K.V., 2002. Consolidation of first-year sea ice ridges. J. Geophys. Res. 107 (C6) https://doi.org/10.1029/2000JC000526, 15–11.

Huseby, A.B., Vanem, E., Natvig, B., 2013. A new approach to environmental contours for ocean engineering applications based on direct Monte Carlo simulations. Ocean Eng. 60, 124–135. https://doi.org/10.1016/j.oceaneng.2012.12.034.

ISO 19906, 2019. Petroleum and Natural Gas Industries - Arctic Offshore Structures.

Johnston, M., Timco, G., 2004. Developing an Ice Strength Algorithm for SubArctic Regions. Report CHC-TR-023 submitted to Canadian Ice Service, by Canadian Hydraulics Centre, March, 2004, 28 pp. doi:10.4224/12329076.

Leppäranta, M., Hakala, R., 1992. Structure and strength of first-year ice ridges in the Baltic Sea. Cold Reg. Sci. Technol. 20 (3), 295–311. https://doi.org/10.1016/0165-232X(92)90036-T.

Leppäranta, M., Lensu, M., Kosloff, P., Veitch, B., 1995. The life story of a first-year sea ice ridge. Cold Reg. Sci. Technol. 23 (3), 279–290. https://doi.org/10.1016/0165-232x(94)00019-t.

Li, H., Bjerkås, M., Høyland, K.V., Nord, T.S., 2016. Panel loads and weather conditions at Norströmsgrund lighthouse 2000-2003. In: Proc. 23 rd IAHR Symposium on Ice, Ann Arbor, Michigan, USA.

Løset, S., Shkhinek, K.N., Gudmestad, O.T., Høyland, K.V., 2006. Actions from Ice on Arctic Offshore and Coastal Structures. LAN, St. Petersburg, Russia.

Melling, H., 2002. Sea ice of the northern Canadian Arctic Archipelago. J. Geophys. Res. Oceans 107 (C11). https://doi.org/10.1029/2001JC001102, 2-1.

McLaren, A.S., Wadhams, P., Weintraub, R., 1984. The sea ice topography of M'Clure Strait in winter and summer of 1960 from submarine profiles. Arctic 110–120.

Parmerter, R.R., Coon, M.D., 1972. Model of pressure ridge formation in sea ice. J. Geophys. Res. 77 (33), 6565–6575.

Proshutinsky, A., Krishfield, R., Timmermans, M.L., Toole, J., Carmack, E., McLaughlin, F., Williams, W.J., Zimmermann, S., Itoh, M., Shimada, K., 2010. Beaufort Gyre freshwater reservoir: State and variability from observations. J. Geophys. Res. - Part C - Oceans 115 (C1), 00–10. https://doi.org/10.1029/2008JC005104.

Ronkainen, I., Lehtiranta, J., Lensu, M., Rinne, E., Haapala, J., Haas, C., 2018. Interannual Sea ice thickness variability in the Bay of Bothnia. Cryosphere 12 (11), 3459–3476. https://doi.org/10.5194/tc-12-3459-2018.

Saloranta, T.M., 2000. Modeling the evolution of snow, snow ice and ice in the Baltic Sea. Tellus A: Dynamic Meteorology and Oceanography 52 (1), 93–108. https://doi.org/10.1034/j.1600-0870.2000.520107.x.

Samardžija, I., Høyland, K.V., 2023. Analysis of the relationship between level ice draft, ridge frequency and ridge keel draft for use in the probabilistic assessment of ice ridge loads on offshore structures. Ocean Eng. 270, 113593. https://doi.org/10.1016/j.oceaneng.2022.113593.

Shestov, A., Marchenko, A., 2016. Thermodynamic consolidation of ice ridge keels in water at varying freezing points. Cold Reg. Sci. Technol. 121, 1–10. https://doi.org/10.1016/j.coldregions.2015.09.015.

Shestov, A., Høyland, K., Ervik, Å., 2018. Decay phase thermodynamics of ice ridges in the Arctic Ocean. Cold Reg. Sci. Technol. 152, 23–34. https://doi.org/10.1016/j.coldregions.2018.04.005.

Timco, G., Burden, R., 1997. An analysis of the shapes of sea ice ridges. Cold Reg. Sci. Technol. 25 (1), 65–77. https://doi.org/10.1016/S0165-232X(96)00017-1.

Timco, G., Goodrich, L.E., 1988. Ice rubble consolidation. In: Proc. 9th IAHR Symposium on Ice, Sapporo, Japan.

Timco, G., Sayed, M., 1986. Model tests of the ridge-building process in ice. In: Proc. 8th IAHR Symposium on Ice, Iowa City, Iowa.

Wadhams, P., Horne, R.J., 1980. An Analysis of Ice Profiles Obtained by Submarine Sonar in the Beaufort Sea. J. Glaciol. 25 (93), 401–424. https://doi.org/10.3189/s0022143000015264.

Zubov, N., 1943. Arctic Ice. Izdatel'stvo Glavsevmorputi, Moscow, Russia.

A.5 Paper 5

Paper 5:

Samardžija, I., Høyland, K. V., Leira, B. J., & Næss, A. (2023b). Probabilistic assessment of first-year ice ridge action on offshore structures. *Cold Regions Science and Technology*. [Paper under peer review]

This paper is awaiting publication and is not included in NTNU Open